

# **Synthesis and Transformation of Cyclic Nitrones: New Candidates for the Inhibition of $\alpha$ -L-Fucosidases**

Von der Fakultät Chemie der Universität Stuttgart

zur Erlangung der Würde eines

Doktors der Naturwissenschaften

(Dr. rer. nat.)

genehmigte Abhandlung

vorgelegt von

James Leo Redcliffe

aus

St. Helens,

England

Hauptberichter: Prof. Dr. V. Jäger

Mitberichter: Prof. Dr. S. Hashmi

Tag der mündlichen Prüfung: 2.3.2011

Institut für Organische Chemie

der Universität Stuttgart

2011



## Some parts of this work have been published and/or presented

### Publications

W. Frey, V. Jäger, J. L. Redcliffe: „Crystal structure of (3S,4R,5S)-5-bromomethyl-3,4-isopropylidenedioxy-3,4-dihydro-5H-pyrrole-1-oxid, C<sub>8</sub>H<sub>12</sub>BrNO<sub>3</sub>”; *Z. Kristallogr. NCS* **2003**, *218*, 109-110.

Gulla, M.; Bierer, L.; Redcliffe, L.; Schmidt, S.; Jäger, V. “Synthesis of Cyclic Nitrones by Bromocyclization of Unsaturated Oximes”, *ARKIVOC* **2006**, 76-88.

Gulla, M.; Bierer, L.; Schmidt, S.; Redcliffe, L.; Jäger, V. “Bromocyclization of Unsaturated Oximes. Synthesis of Five-Membered Cyclic Nitron (Pyrroline N-Oxides)”, *Z. Naturforsch.* **2006**, *61b*, 471-485.

### Presentations

“Transformation of Cyclic Nitrones from Bromocyclization of Unsaturated Oximes: A New Route to Potent Inhibitors of  $\alpha$ -L-Fucosidases”; N,O-Heterocycles and More – 1<sup>st</sup> BBS-Symposium on Organic Chemistry, April 7<sup>th</sup> – 10<sup>th</sup>, 2005, Bratislava, Slovak Republic.

“Synthese und Transformationen cyclischer Nitron: Ein Weg zur Herstellung hochwirksamer Inhibitoren von  $\alpha$ -L-Fucosidasen”; Tag der Organischen Chemie der Universität Stuttgart (TOCUS), 12<sup>th</sup> October, 2005.

### Poster contributions

“Synthesis and transformation of cyclic Nitrones -A route to potent glycosidase inhibitors”; 2<sup>nd</sup> 2002 Younger European Chemists' Conference, Heidelberg, 30. 9 – 2.10. 2002.

“Transformation of Cyclic Nitrones from Bromocyclisation of Unsaturated Oximes: A Route to Potent Inhibitors of  $\alpha$ -L-Fucosidases”; ORCHEM, September 9<sup>th</sup> – 11<sup>th</sup>, 2004, Bad Nauheim.

*In loving memory...*

ERIC REDCLIFFE

10.4.1947 – 20.7.2010

<b>1</b>	<b>Introduction .....</b>	<b>1</b>
1.1	Opening Remarks.....	1
1.2	Glycosidases and Glycosylation .....	2
1.3	Glycosylation and Disease .....	4
1.3.1	Oncology.....	4
1.3.2	Storage diseases.....	7
1.3.3	Antiviral agents .....	10
1.4	$\alpha$ -L-Fucosidase Inhibitors as Therapeutic Agents? .....	13
1.5	Aims of Dissertation.....	16
<b>2</b>	<b>Synthesis of Cyclic Nitrones.....</b>	<b>19</b>
2.1	Synthesis of Cyclic Nitrones by Electrophilic Cyclisation of Unsaturated Oximes .....	19
2.1.1	Seminal work by Grigg <i>et al.</i> ....	19
2.1.2	Electrophilic cyclisations of oximes by Jäger and co-workers .....	20
2.1.3	General and miscellaneous examples of nitrone syntheses.....	24
2.1.4	Synthesis of cyclic nitrones by intramolecular <i>N</i> -alkylation ( $S_N2$ -type) of oximes .....	26
2.1.5	Synthesis of cyclic nitrones by epoxide opening .....	27
2.2	Results and Discussion .....	30
2.2.1	Synthesis of cyclic nitrones, <i>L-lyxo</i> <b>5</b> and <i>D-ribo</i> <b>6</b> .....	30
2.2.1.1	Synthesis of the unsaturated pentenose oxime <b>4</b> from D-ribose .....	30
2.2.1.2	Bromocyclisation of pentenose oxime <b>4</b> .....	31
2.2.1.3	Reaction pathway of the bromocyclisation of oxime <b>4</b> .....	32
2.2.1.4	NMR and solid state properties of <i>D-ribo</i> -nitrone <b>6</b> .....	34
2.2.2	Synthesis of <i>L-fuco</i> -nitrones <b>27</b> , <b>28</b> , and <i>D-altro</i> -nitrone <b>29</b> .....	36
2.2.2.1	Initial investigations with non-carbohydrate-derived precursors .....	36
2.2.2.2	Use of L-galactose as a carbohydrate starting material precursor? .....	38
2.2.2.3	Synthesis of <i>D-arabino</i> hexenose oximes <b>18</b> and <b>22</b> from D-lyxose .....	40
2.2.2.4	Attempted synthesis of a TES-protected <i>D-arabino</i> -hexenose oxime .....	45
2.2.2.5	Stability of acetonide <b>11</b> under acidic conditions.....	46
2.2.2.6	Bromocyclisation of hexenose oximes <b>18</b> and <b>22</b> .....	48
2.2.2.7	NMR and conformational analysis of the <i>L-fuco</i> -nitrones <b>27</b> , <b>28</b> , and <i>D-altro</i> -nitrone <b>29</b> .....	50
<b>3</b>	<b>Reactions of Cyclic Nitrones.....</b>	<b>55</b>
3.1	General Introduction .....	55
3.1.1	Quick overview of common nitrone reactions .....	56
3.2	Own Results .....	61
3.2.1	Chemoselective reduction of <i>L-lyxo</i> -nitrone <b>5</b> and <i>D-ribo</i> -nitrone <b>6</b> .....	61
3.2.2	Addition of Grignard reagents to nitrones <i>L-lyxo</i> <b>5</b> and <i>D-ribo</i> <b>6</b> .....	62
3.2.2.1	Configuration and conformational analysis of addition products <b>34-51</b> according to NMR spectroscopic data and comparison with the X-ray structures of pyrrolidines <b>41</b> and <b>51</b> .....	64
3.2.3	Grignard addition to TIPS-protected <i>L-fuco</i> -nitrone <b>28</b> .....	78
<b>4</b>	<b>Oxidation of <i>N</i>-Hydroxypyrrolidines.....</b>	<b>85</b>
4.1	Introduction .....	85

4.2	Regioselectivity of Oxidation.....	86
4.2.1	Oxidation of <i>N</i> -hydroxypiperidines. Earlier work of Thesing, Ali, Tufariello, and Pothier and Jäger.....	86
4.2.2	Oxidation of <i>N</i> -hydroxypyrrolidines. Electronic effects and mechanism .....	90
4.3	Own Results .....	94
4.3.1	General notes .....	94
4.3.2	Oxidation of 2-methyl <i>N</i> -hydroxypyrrolidines <b>31</b> and <b>33</b> .....	94
4.3.3	Influence of bromine substituent. Oxidation of 2-bromomethyl <i>N</i> -hydroxypyrrolidines <b>30</b> and <b>32</b> .....	96
4.3.4	<i>Cis</i> or <i>trans</i> proton abstraction? Oxidation of 2,5-disubstituted <i>N</i> -hydroxypyrrolidines <b>34</b> and <b>68</b> .....	99
4.3.5	Role of conjugation in the oxidation of 5-anisyl-substituted <i>N</i> -hydroxypyrrolidines <b>41</b> and <b>71</b> .....	101
4.4	Reactions of Bromomethyl-Ketonitrones .....	103
4.4.1	1,3-Dipolar cycloaddition of 2-anisyl-substituted-bromomethyl nitrene <b>63</b> .....	103
4.4.2	Generation and reactions of cyclic vinylnitrosonium cations from bromomethylnitrones .....	103
4.4.2.1	Background of $\alpha$ -chloronitrones from Eschenmoser, Kempe <i>et al.</i> .....	103
4.4.2.2	Own results: Treatment of bromomethyl-ketonitrone <b>57</b> with AgBF <sub>4</sub> .....	107
<b>5</b>	<b>Synthesis of <math>\alpha</math>-L-Fucosidase Inhibitors .....</b>	<b>109</b>
5.1	Own Results .....	109
5.1.1	Lithium aluminium hydride reduction of the bromomethyl group .....	109
5.1.2	Concomitant reduction of C—Br and N—O bonds .....	110
5.1.3	Synthesis of <i>N</i> -hydroxypyrrolidinetriols.....	113
5.1.4	N—O bond cleavage of <i>N</i> -hydroxypyrrolidines with zinc/acetic acid or with samarium(II) diiodide.....	114
5.1.5	Deprotection of cyclic amines and synthesis of pyrrolidinediols with 2-aryl side-chains.....	115
5.1.6	Catalytic hydrogenation followed by deprotection to yield pyrrolidinediol hydrobromides.....	117
5.1.7	X-Ray crystal structures of selected pyrrolidinediols .....	118
5.1.7.1	General remarks .....	118
5.1.7.2	Discussion of the X-ray crystal structure of the <i>p</i> -methoxyphenyl-substituted pyrrolidinediol <b>96·HCl</b> .....	119
5.1.7.3	Discussion of 2-([1,1'-biphenyl]-4-yl)-substituted pyrrolidinediol <b>97·HCl</b> .....	120
5.1.8	Synthesis of deoxyfuconojirimycin derivatives.....	123
<b>6</b>	<b>Glycosidase Mechanism and <i>In Vitro</i> Tests .....</b>	<b>127</b>
6.1	General Remarks.....	127
6.2	Mechanism of Glycosidase Hydrolysis .....	128
6.3	Enzymatic Inhibition from Iminopolyols.....	133
6.4	Fucosidase Inhibition .....	139
6.4.1	Structure activity relationships .....	140
6.4.1.1	General notes .....	140
6.4.1.2	Aminocyclopentanetriols and derivatives thereof .....	142
6.4.1.3	$\beta$ -Amido L-fucosyl-nojirimycin C-glycosides .....	145
6.4.1.4	Derivatives of 3,4-dihydroxy-5-methylpyrrolidines .....	151
6.4.2	Fucosidase Mechanism .....	153
6.5	Own Results – In Vitro Tests .....	155
6.5.1	Test Methodology .....	155

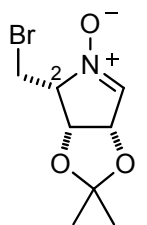
6.5.2	Tables of the biological results .....	156
6.5.3	Discussion of structure-activity relationships .....	165
<b>7</b>	<b>Summary .....</b>	<b>171</b>
7.1	Bromocyclisations and Synthesis of Fucosidase Inhibitors .....	171
7.2	Oxidation of <i>N</i> -Hydroxypyrrolidines .....	174
7.3	Outlook .....	177
<b>8</b>	<b>Experimental.....</b>	<b>179</b>
8.1	General .....	179
8.1.1	Separation und purification .....	180
8.1.2	Analytic .....	181
8.2	Experiments Relating to Chapter 2 .....	184
8.2.1	Preparation of cyclic nitrones from D-ribose .....	184
8.2.2	Preparation of cyclic nitrones from D-lyxose .....	190
8.3	Experiments Relating to Chapter 3 .....	219
8.3.1	Chemoselective reduction of L- <i>lyxo</i> -nitronone <b>5</b> and D- <i>ribo</i> -nitronone <b>6</b> .....	219
8.3.2	Addition of C-nucleophiles to L- <i>lyxo</i> -nitronone <b>5</b> and D- <i>ribo</i> -nitronone <b>6</b> .....	223
8.3.3	Nucleophilic addition to the TIPS-protected L- <i>fuco</i> -nitronone <b>28</b> .....	236
8.4	Experiments Relating to Chapter 4 .....	239
8.4.1	Oxidation of 2-substituted <i>N</i> -hydroxypyrrolidines .....	239
8.4.2	Oxidation of 2,5-disubstituted <i>N</i> -hydroxypyrrolidines .....	248
8.4.3	Reactions of the bromomethyl-ketonitrones <b>57</b> and <b>63</b> .....	258
8.5	Experiments Relating to Chapter 5 .....	262
8.5.1	Lithium aluminium reduction of the bromomethyl group .....	262
8.5.2	Attempts at the concomitant reduction of C—Br and N—O bonds .....	274
8.5.3	Reduction by catalytic hydrogenation .....	279
8.5.4	N—O bond cleavage of the <i>N</i> -hydroxypyrrolidines using zinc .....	282
8.5.5	N—O bond cleavage of <i>N</i> -hydroxypyrrolidines with samarium diiodide .....	289
8.5.6	Synthesis of pyrrolidinetriols .....	291
8.5.7	Synthesis of pyrrolidinediols .....	294
8.5.8	Synthesis of 2-([1,1'-biphenyl]-4-yl)-deoxyfuconojirimycin <b>115·HCl</b> .....	313
<b>9</b>	<b>X-Ray Crystal Structure Data .....</b>	<b>317</b>
9.1	(2 <i>S</i> ,3 <i>R</i> ,4 <i>S</i> )-2-Bromomethyl-3,4-dihydroxy-3,4- <i>O</i> -isopropylidene-3,4-dihydro-2 <i>H</i> -pyrrole-1-oxide ( <b>6</b> ) .....	317
9.2	4- <i>O</i> - <i>tert</i> -Butyldimethylsilyl-2,3- <i>O</i> -isopropylidene-D-lyxopyranose ( <b>10</b> ) .....	321
9.3	(2 <i>R</i> ,3 <i>R</i> ,4 <i>S</i> ,5 <i>S</i> )-2-Bromomethyl-1,3,4-trihydroxy-3,4- <i>O</i> -isopropylidene-5-(4-methoxyphenyl)-pyrrolidine ( <b>41</b> ) .....	325
9.4	(2 <i>R</i> ,3 <i>R</i> ,4 <i>S</i> ,5 <i>S</i> )-2-Bromomethyl-5-(4-bromophenyl)-1,3,4-trihydroxy-3,4- <i>O</i> -isopropylidene-pyrrolidine ( <b>45</b> ) .....	331
9.5	(2 <i>R</i> ,3 <i>R</i> ,4 <i>S</i> ,5 <i>S</i> )-2-Bromomethyl-1,3,4-trihydroxy-3,4- <i>O</i> -isopropylidene-5-(4-phenoxyphenyl)-pyrrolidine ( <b>47</b> ) .....	337
9.6	(2 <i>S</i> ,3 <i>R</i> ,4 <i>S</i> ,5 <i>S</i> )-2-Bromomethyl-5-(4- <i>N,N</i> -dimethylanilino)-1,3,4-trihydroxy-3,4- <i>O</i> -isopropylidene-pyrrolidine ( <b>51</b> ) .....	343
9.7	(2 <i>R</i> ,3 <i>R</i> ,4 <i>R</i> ,5 <i>R</i> ,6 <i>S</i> )-6-([1,1'-Biphenyl]-4-yl)-2-bromomethyl-3,4,5-trihydroxy-3,4- <i>O</i> -isopropylidene-5-triisopropylsilyloxy-piperidine ( <b>52</b> ) .....	348
9.8	(2 <i>S</i> ,3 <i>R</i> ,4 <i>S</i> )-5-Bromomethyl-3,4-dihydroxy-3,4- <i>O</i> -isopropylidene-2-(4-methoxyphenyl)-3,4-dihydro-2 <i>H</i> -pyrrole-1-oxide ( <b>63</b> ) .....	353

9.9	(1 <i>R</i> ,2 <i>S</i> ,4 <i>aS</i> ,8 <i>aS</i> ,9 <i>aR</i> )-1,2-Dihydroxy- <i>O</i> -1,2-isopropylidene-octahydro-4-oxa-3 <i>a</i> -aza-cyclopenta[ <i>b</i> ]naphthalene-9 <i>a</i> -carbonitrile ( <b>67</b> )	357
9.10	(2 <i>S</i> ,3 <i>S</i> ,4 <i>R</i> ,5 <i>S</i> )-1,3,4-Trihydroxy-2-isopropyl-3,4- <i>O</i> -isopropylidene-5-methyl-pyrrolidine ( <b>69</b> )	361
9.11	(2 <i>R</i> ,3 <i>S</i> ,4 <i>R</i> )-3,4-Dihydroxy-3,4- <i>O</i> -isopropylidene-5-methyl-2-phenyl-2 <i>H</i> -pyrrole-1-oxide ( <b>82</b> )	366
9.12	(2 <i>S</i> ,3 <i>S</i> ,4 <i>R</i> ,5 <i>S</i> )-3,4-Dihydroxy-2-(4-methoxyphenyl)-5-methylpyrrolidine hydrochloride ( <b>96·HCl·CH<sub>3</sub>OH</b> )	369
9.13	(2 <i>S</i> ,3 <i>S</i> ,4 <i>R</i> ,5 <i>S</i> )-2-([1,1'-Biphenyl]-4-yl)-3,4-dihydroxy-5-methylpyrrolidine hydrochloride ( <b>97·HCl·CH<sub>3</sub>OH</b> )	373
9.14	(2 <i>S</i> ,3 <i>S</i> ,4 <i>R</i> ,5 <i>S</i> )-2-(4-Chlorophenyl)-3,4-dihydroxy-5-methylpyrrolidine hydrochloride ( <b>99·HCl·CH<sub>3</sub>OH</b> )	377
9.15	(2 <i>S</i> ,3 <i>S</i> ,4 <i>R</i> ,5 <i>S</i> )-2-(4-Bromophenyl)-3,4-dihydroxy-5-methylpyrrolidine hydrochloride ( <b>100·HCl</b> )	380
9.16	(2 <i>S</i> ,3 <i>S</i> ,4 <i>R</i> ,5 <i>S</i> )-3,4-Dihydroxy-5-methyl-2-(4-methylthiophenyl)-pyrrolidine hydrochloride ( <b>101·HCl·CH<sub>3</sub>OH</b> )	384
9.17	(2 <i>S</i> ,3 <i>S</i> ,4 <i>R</i> ,5 <i>S</i> )-3,4-Dihydroxy-5-methyl-2-(4-phenoxyphenyl)-pyrrolidine hydrochloride ( <b>102·HCl</b> )	388
9.18	(2 <i>S</i> ,3 <i>S</i> ,4 <i>R</i> ,5 <i>S</i> )-3,4-Dihydroxy-5-methyl-2-(4-phenoxyphenyl)-pyrrolidine hydrochloride ( <b>102·HBr</b> )	394
9.19	(2 <i>S</i> ,3 <i>S</i> ,4 <i>R</i> ,5 <i>S</i> )-3,4-Dihydroxy-2-(4- <i>N,N</i> -dimethylanilino)-5-methylpyrrolidine dihydrochloride ( <b>104·2HCl</b> )	400
9.20	(2 <i>S</i> ,3 <i>S</i> ,4 <i>R</i> ,5 <i>S</i> )-2- <i>tert</i> -Butyl-3,4-dihydroxy-5-methyl-pyrrolidine hydrobromide ( <b>110·HBr</b> )	403
<b>10</b>	<b>Acknowledgments</b>	<b>407</b>
<b>11</b>	<b>Curriculum Vitae</b>	<b>409</b>
<b>12</b>	<b>Formula Register</b>	<b>411</b>
<b>13</b>	<b>Literature</b>	<b>415</b>



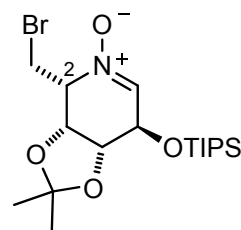
## Preliminary remarks and nomenclature

Literature citations, schemes, diagrams, tables and equations were numbered consecutively, as were all of the compounds prepared during this work (i.e. **1**, **2**, **3** etc.). A formula register is presented at the end (Section 12). The remaining structures shown in this work are labelled in boldface capitals, i.e. **A**, **B**, ..., **Z**, **AA**, **AB**, etc. The compounds were named according to the IUPAC guidelines for heterocyclic compounds, particularly those with partial saturation, in accordance with the “added hydrogen rule”.<sup>[†]</sup> In some instances, as shown below, the carbohydrate configuration, i.e. *L-xylo*, *D-ribo*, *L-fuco* etc., is given next to the structure number to add emphasis to the text. Pertinent examples include:



**5** *L-lyxo*

"...2-bromomethyl....-3,4-dihydro-2*H*-...  
pyrrole-1-oxide"

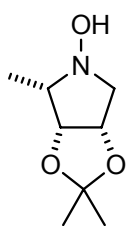


**28** *L-fuco*

"...2-bromomethyl....-2,3,4,5-tetrahydro...  
pyridine-1-oxide"

**not:** "*5-bromomethyl....-5*H*-pyrrole-1-oxide...*  
or: "*...1-pyrroline-*N*-oxide*"

The IUPAC guidelines for saturated heterocyclic systems were also taken to name all “imino” analogues of carbohydrate derivatives. The alternative carbohydrate nomenclature for the compounds – though widely used – was not employed in this work. For example:

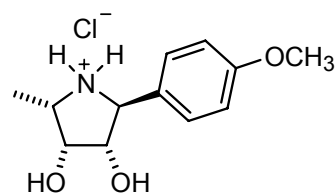


**31**

"1,3,4-trihydroxy....2-methylpyrrolidine"

**carbohydrate:**

"1,4,5-trideoxy-....1,4-hydroxyimino-*L*-lyxitol"



**96·HCl**

"3,4-dihydroxy-2-(*p*-methoxyphenyl)-  
5-methylpyrrolidine hydrochloride"

**carbohydrate:**

"1,4,5-trideoxy-1-*C*-(*p*-methoxyphenyl)-  
1,4-imino- $\alpha$ -*L*-lyxitol..."

[†] Refer to Bünzli-Trepp, U, “Handbuch für die systematische Nomenklatur der Organischen Chemie, Metallorganischen Chemie und Koordinationschemie – Chemical-Abstracts-Richtlinien mit IUPAC-Empfehlungen und vielen Trivialnamen”, Logos Verlag Berlin, 2001.

## Abbreviations

Å	Angstrom ( $10^{-10}$ m)	$\Delta H^\ddagger$	activation enthalpy	Neu	neuraminic acid
Ac	acetyl	HIV	human immune-deficiency virus	Nu	nucleophile
AIDS	acquired immune deficiency syndrome	HPLC	high pressure liquid chromatography	$\tilde{\nu}$	wave number
aq.	aqueous	Hz	Hertz	<i>o</i>	<i>ortho</i>
Asn	asparagine	HRMS	high resolution mass spectroscopy	<i>p</i>	<i>para</i>
$[\alpha]$	optical rotation	i-	(a) iso-; (b) <i>ipso</i>	p.	page
Bn	benzyl	IC <sub>50</sub>	inhibition constant for 50 % remaining enzyme activity	PE	petrol ether
<i>c</i>	concentration	Ion.	ionisation	Ph	phenyl
calc.	calculated	IR	infrared	ppm	parts per million ( $10^{-6}$ )
cat.	catalytic	% I	procent inhibited	py	pyridine
CI	chemical impact	<i>J</i>	NMR coupling constant (Hz)	quant.	quantitative
cm	centimeter	<i>K</i>	Kelvin	<i>R</i>	<i>rectus</i>
conc.	concentrated	<i>K<sub>i</sub></i>	inhibition constant for 50 % remaining enzyme activity	R	(a) organic rest; (b) universal gas constant
°C	degree(s) Celsius	<i>K<sub>m</sub></i>	Michaelis-constant	ref.	reference
d	(a) deuterated; (b) day(s);	kcal	kilocalorie	RP	reverse phase
D	(a) deuterium; (b) D-series (Emil Fischer); (c) spectral line of Na at 589 nm	L	L-series (E. Fischer)	r. t.	room temperature
decomp.	decomposition	lit.	literature reference	r. r.	regioisomeric ratio
DFJ	deoxyfuconojirimycin	$\lambda$	wave length (nm)	<i>S</i>	<i>sinister</i>
DMSO	dimethylsulfoxide	M	molarity	<i>S</i>	substrate
DMP	dimethoxypropane	M <sup>+</sup>	molecular ion	Ser	serine
DNJ	deoxynojirimycin	<i>m</i> -	<i>meta</i>	SiO <sub>2</sub>	silica gel
d. r.	diastereoisomeric ratio	Man	mannose	$\Delta S^\ddagger$	activation entropy
$\delta$	NMR chemical shift	mbar	millibar	<i>t</i>	<i>tertiary</i>
<i>E</i>	<i>Entgegen</i> ( <i>trans</i> )	Me	methyl	TBAF	tetrabutyl-ammonium fluoride
E	experiment	MeOH	methanol	TBS	<i>tert</i> -butyldimethylsilyl
EC	enzyme class	MHz	mega Hertz ( $10^6$ Hz)	TBDMS	<i>tert</i> -butyl-dimethylsilyl
EE	ethyl acetate	min	minute(s)	TES	triethylsilyl
EI	electron impact	ml	millilitre	THF	tetrahydrofuran
Eq.	equivalent	mmol	millimole ( $10^{-3}$ mol)	Thr	threonine
ES	enzyme substrate complex	mM	millimolar	TIPS	triisopropylsilyl
Et	ethyl	mol	mole	TLC	thin layer chromatography
Et <sub>2</sub> O	diethyl ether	m. p.	melting point	TLP	typical laboratory procedure
EtOH	ethanol	nm	nanometer ( $10^{-9}$ m)	TMS	(a) trimethylsilyl; (b) tetramethylsilyl (NMR spectroscopy)
eV	electron volt	MPLC	medium pressure liquid chromatography	Ts	tosyl
FAB	fast atom bombardment	Ms	mesylate	UV	ultraviolet (spectroscopy)
Fuc	fucose	MS	mass spectrometry	vit.	vitamin
$\Delta G^\ddagger$	Gibbs free energy of activation	$\mu$ M	micromolar ( $10^{-6}$ mol)	Z	<i>Zusammen</i> ( <i>cis</i> )
Gal	galactose	N	normality		
<i>gem</i>	geminal	nM	nanomolar ( $10^{-9}$ mol)		
Glc	glucose				
h	hour(s)				

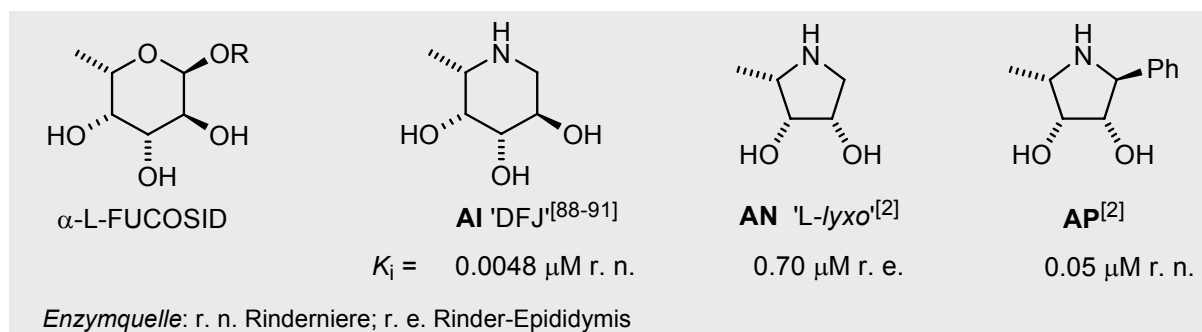
# Zusammenfassung

## Synthese und Transformationen von cyclischen Nitronen – ein Weg zu neuen Strukturen mit $\alpha$ -L-Fucosidase-Hemmaktivität

### Zielsetzung der Dissertation

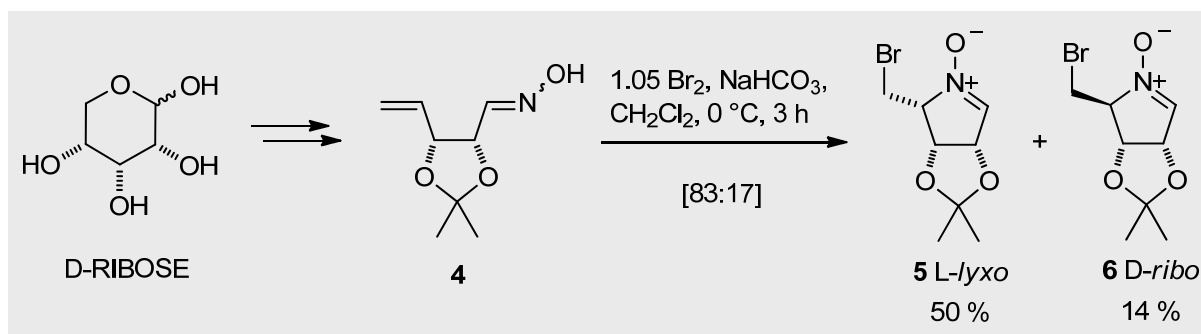
Das Ziel der vorliegenden Arbeit bestand darin, die Entwicklung neuer Glycosidase Inhibitoren zu synthetisieren. Glycosidasen katalysieren den Abbau von glycosidischen Bindungen und spielen eine wichtige Rolle bei der Herstellung von N-Glykoproteinen. Solche Proteine sind an einer Vielzahl biologisch relevanter Prozesse und krankhafter Veränderungen beteiligt. Aufgrund dieser Eigenschaften sind diese Verbindungen möglicherweise zur Behandlung von Krankheiten geeignet. In dieser Arbeit wurden gezielt neue Kandidaten für die Hemmung von  $\alpha$ -L-Fucosidasen ins Visier genommen. 1-Desoxy-L-fuconojirimycin (DFJ, **AI**) und Pyrrolidindiol (**AN**) gehören zu den bereits literatur-bekanntesten  $\alpha$ -L-Fucosidase-Inhibitoren (Abbildung I). Im Laufe der Doktorarbeit von L. Bierer<sup>[2]</sup> entpuppte sich das Pyrrolidin **AP** als starker Inhibitor von  $\alpha$ -L-Fucosidasen und zugleich als neue Leitstruktur, die einen lipophilen Rest mit  $\pi$ -System aufweist. Es lag nun nahe, den Effekt der C-2-Seitenkette systematisch zu untersuchen.

### Abbildung I



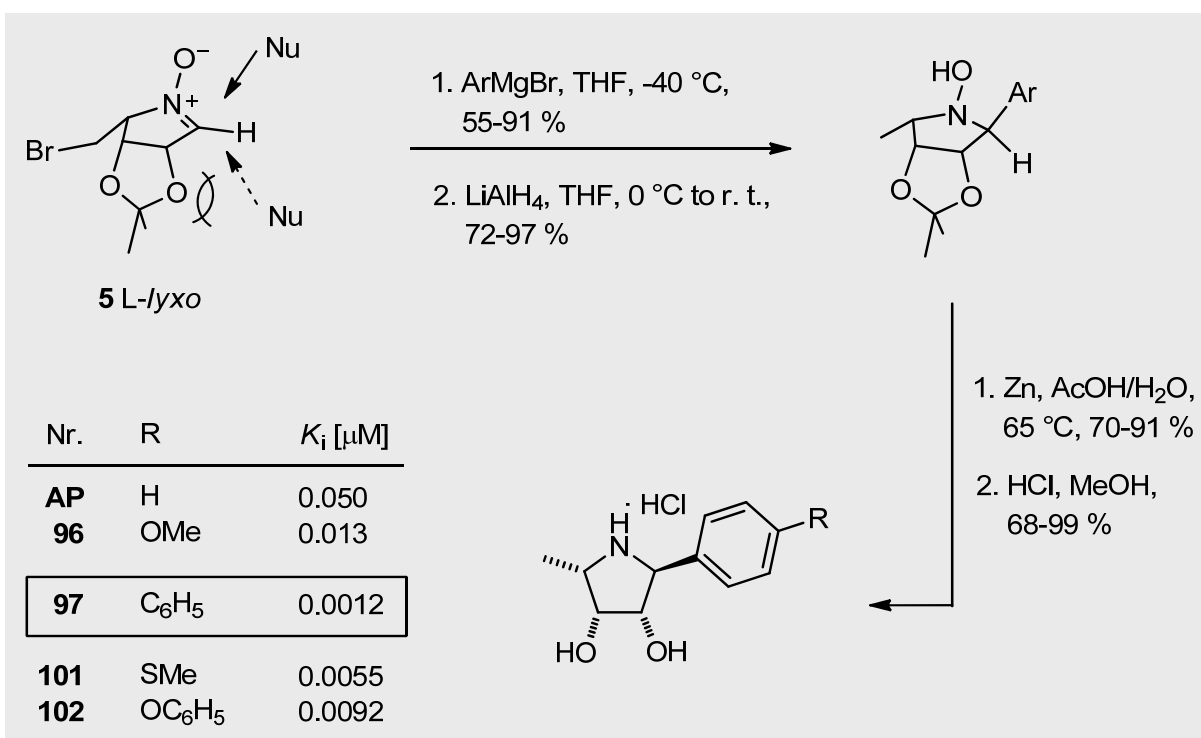
Der Weg zu diesen diastereo- und enantiomerenreinen, hochfunktionalisierten Pyrrolidinen war möglich durch brom-induzierte Cyclisierung des Pentenoseoxims **4**, ausgehend von D-Ribose. Die elektrophile Cyclisierung des Oxims **4** stellte den Schlüsselschritt dar und führte zu den cyclischen Nitronen **5** und **6**, bei denen das Pyrrol-1-oxid **5** als Synthesebaustein mit L-lyxo-Konfiguration bevorzugt gebildet wurde (Schema I).

### Schema I



In vorherigen Arbeiten (vgl. Lit.<sup>[2,4,117-118,177]</sup>) hatte sich Nitron als vielseitige Bausteine erwiesen. Die Addition von Grignard-Reagenzien an das L-lyxo-Nitron **5** verlief hochdiastereoselektiv und lieferte in meist sehr guten Ausbeuten die tetrasubstituierten *N*-Hydroxypyrrolidine. Bei der Einführung der neuer Seitenkette wurde bewusst eine Entscheidung getroffen, nur die *para*-Stellung des Aromaten-Substituenten zu variieren. Durch einfache zweistufige Reduktion und Schutzgruppen-Abspaltung konnten die neuen Pyrrolidin-Polyole erhalten werden, deren biologische Aktivität in Enzymtests evaluiert werden sollte (Schema II). Auf Grund dieser Ergebnisse sollten Struktur-Wirkungsbeziehungen insbesondere im Hinblick auf Fucosidase-Inhibition formuliert werden.

### Schema II



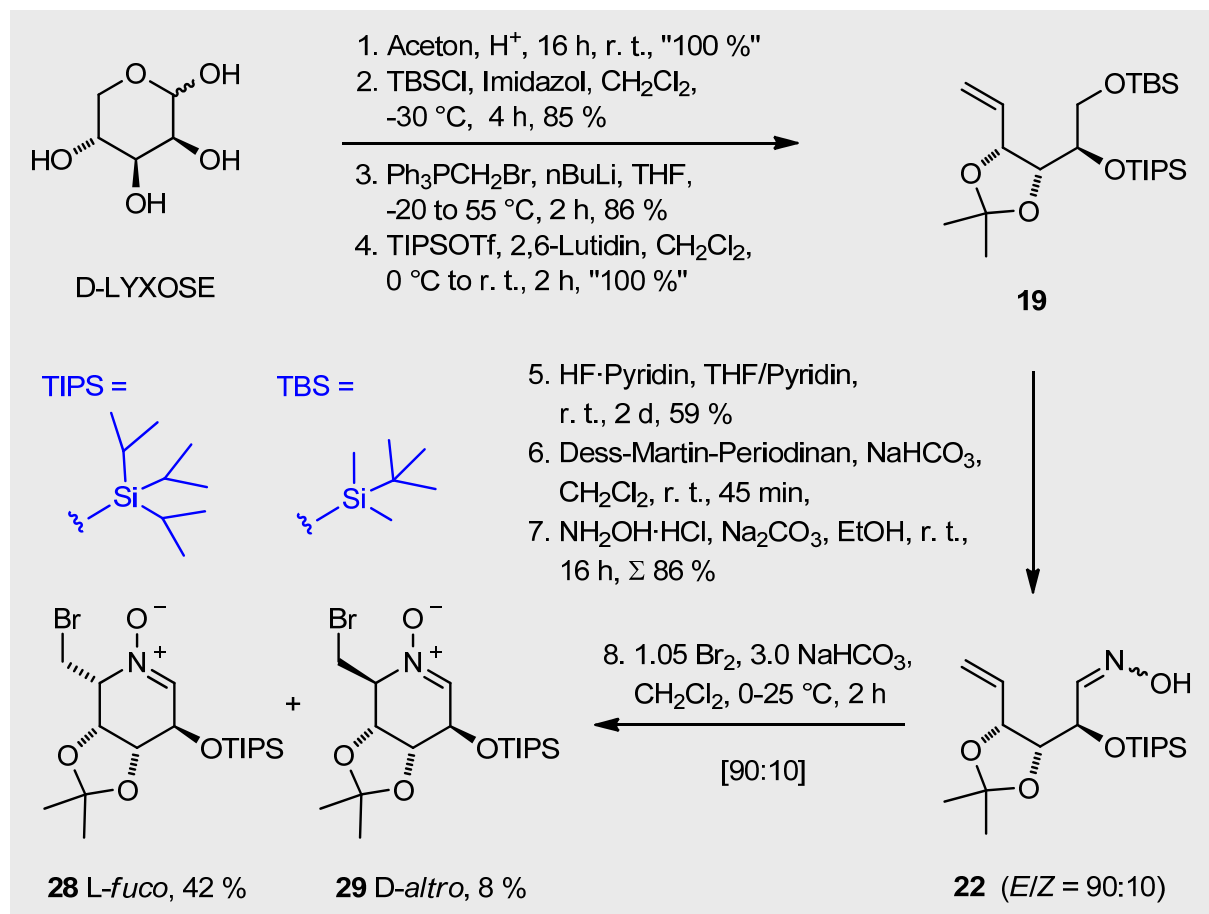
Alle untersuchten Pyrrolidin-Polyole mit *para*-Substituenten am Phenyl-Ring zeigten erhöhte Aktivität gegenüber  $\alpha$ -L-Fucosidasen im Vergleich zum Stamm-Pyrrolidin **AP**. Für die Stärke der Inhibition ist der Charakter des *para*-Substituenten von großer Bedeutung. Erstaunlich war die gute „Toleranz“ der  $\alpha$ -L-Fucosidase gegenüber unterschiedlich großen, lipophilen bzw. hydrophilen Funktionalitäten in *para*-Stellung des Aromats. Im allgemeinen stellte sich heraus, dass Pyrrolidine mit zunehmender Größe der 2-Seitenkette stärkere Hemmwirkung aufwiesen. Die stärkste Inhibition im Nanomolar-Bereich wurde mit dem Biphenyl-substituierten Pyrrolidin **97·HCl** ( $K_i = 0.0012 \mu\text{M}$ ) erzielt. Dieser Wert liegt deutlich unter dem bislang besten mit Fünf-Ringen erreichten Inhibitionswert für  $\alpha$ -L-Fucosidasen ( $0.050 \mu\text{M}$  für das Stamm-Pyrrolidin **AP**, *Rinder-Nieren*). Zudem liegt dieser Wert auf vergleichbarem Niveau mit den stärksten bei Sechs-Ringen erreichten Hemmwirkungen z. B. mit 1-Desoxy-L-fuconojirimycin (DFJ, **AI**).

Bezogen auf Inhibitoren mit Phenyl und Biphenyl-Seitenketten (**AP** bzw. **97·HCl**) entspricht die Änderung von  $K_i$  um 1.6 logarithmische Einheiten eine Senkung der freien Bindungsenthalpie ( $\Delta G^\circ$ ) um 9.3 kJ/mol bzw. 2.3 kcal/mol. Dieser Beitrag zur Senkung von  $\Delta G^\circ$  geht vermutlich auf Kosten von Wasserstoffbrücken mit geordneten Wassermolekülen, welche beim Andocken der lipophilen Seitenkette verdrängt werden. Die erhöhte Bewegungsfreiheit der Wassermoleküle erhöht den Entropieanteil und senkt damit die freie Bindungsenthalpie. Zudem belegen die oben gezeigten Ergebnisse die Hypothese, dass, erstens, in der Bindungstasche der  $\alpha$ -L-Fucosidase im Bereich der Substituenten an C-2 relativ viel Raum vorhanden ist und, zweitens, die Möglichkeit für eine stärkeren Inhibition durch  $\pi$ -Elektronen-(lipophile)-Wechselwirkungen besteht.

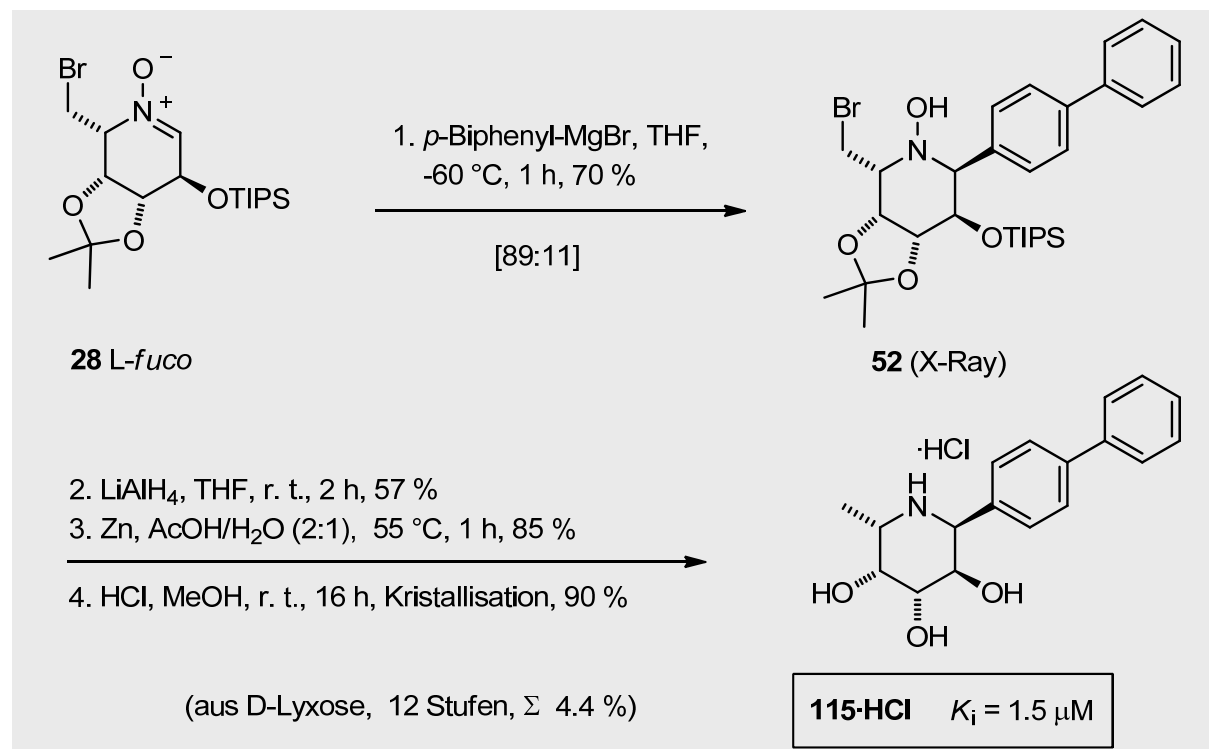
Ein weiterer Teil dieser Arbeit befasst sich mit der stereoselektiven Synthese von substituierten Piperidinen. In folgenden wurde das benötigte L-*fuco*-konfigurierte Nitron **28** über eine Bromcyclisierung des Triisopropylsilyl-geschützten Hexenoseoxims **22** dargestellt. Das ungesättigte Oxim war aus D-Lyxose in 8 Schritten gut zugänglich (Schema III).

Wie bereits bei den Pyrrolidinen oben dargestellt, wurde an das L-*fuco*-Nitron **28** eine „Biphenyl“-Seitenkette eingeführt. Für die Addition des Nucleophils wurde aus den  $^{13}\text{C}$ -NMR-spektroskopischen Daten eine recht gute Diastereoselektivität (d. r. = 89:11) beobachtet. Die Reduktion des Additionsprodukts **52** mit Lithiumaluminiumhydrid bzw. mit aktiviertem Zink-Staub und die Abspaltung der Acetonid-Schutzgruppe mit Salzsäure ergab nach Kristallisation das  $\alpha$ -L-*fuco*-konfigurierte Piperidin-Hydrochlorid **115·HCl** (Schema IV; 12 Stufen, 4.4 % Gesamtausbeute).

## Schema III



## Schema IV



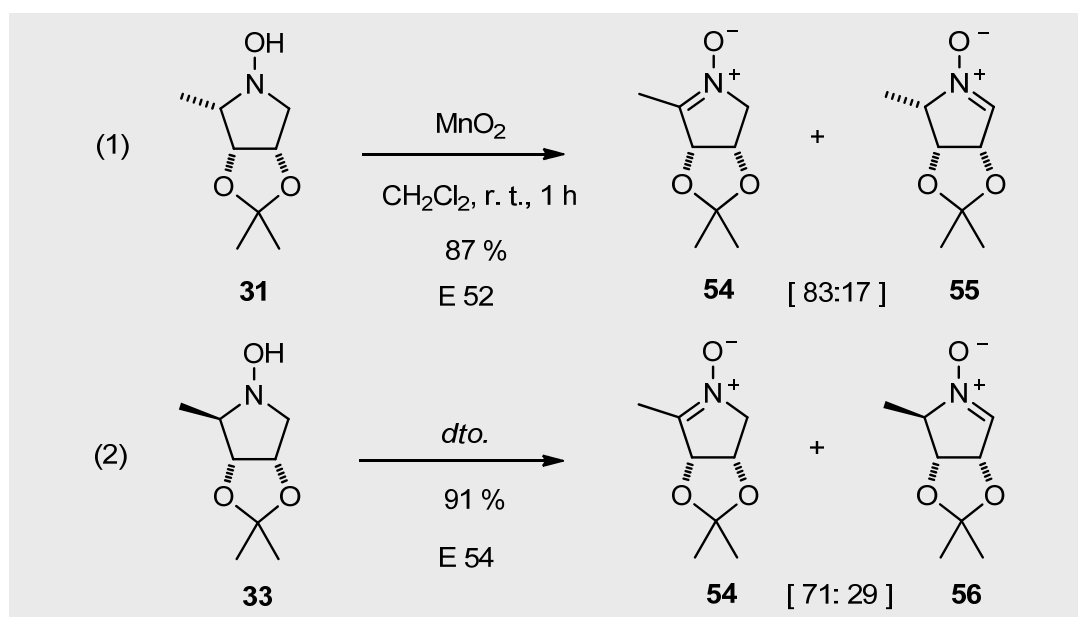
Leider erwies sich das Triol-Hydrochlorid **115·HCl** als vergleichsweise 1000-fach schwächerer Inhibitor von *Rinder-Nieren* Fucosidasen. Offenbar muss bei dieser Verbindungsklasse – wie für die Pyrrolidin-Diole beschrieben – weiterhin die Auslegung der Seitenkette mit der in der hydrophoben Tasche des Enzyms weitgehend übereinstimmen bzw. hineinpassen. Hierbei könnte die Konformationänderung des Piperidin-Rings eine entscheidende Rolle bei der Herabsetzung der Hemmwirkung gespielt haben. Wie aus den  $^1\text{H}$ - bzw.  $^{13}\text{C}$  NMR-spektroskopischen Daten ersichtlich, lag eine  $^1\text{C}_4$  und nicht, wie üblich bei dieser Substanzklasse, die  $^4\text{C}_1$ -Konformation vor.

### Oxidation von *N*-Hydroxypyrrolidinen

Die Oxidation von tri- bzw. tetra-substituierten *N*-Hydroxypyrrolidinen wurde mit Mangan(IV)-oxid und Quecksilber(I)-oxid als Oxidations-Reagenzien untersucht. Auf Grundlage der erhaltenen Ergebnisse können folgende Befunde erörtert werden:

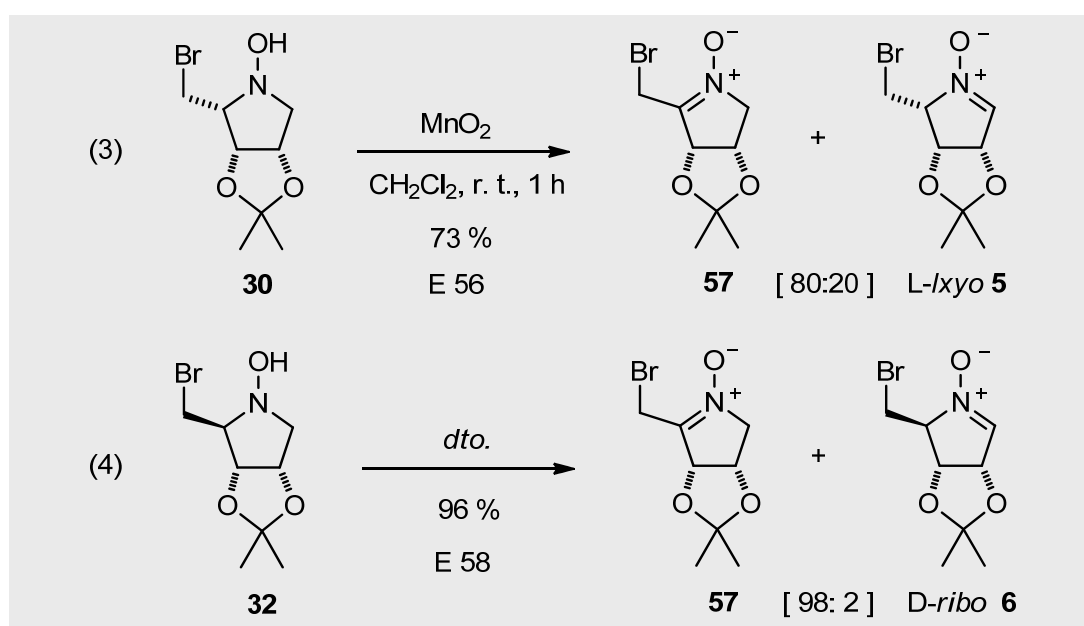
- (a) Die Oxidation von 2-Methyl-*N*-hydroxypyrrolidinen **31** und **33** lieferte die regioisomeren Nitrone **54** und **55** (Gl. 1) bzw. **54** und **56** (Gl. 2) in einem ca. 4:1-Verhältnis (Schema V). Die Wahl des Oxidationsmittels beeinflusste die Regioselektivität der Reaktion nicht. Als bevorzugtes Regioisomer wurde stets das „Ketonitron“-Produkt gebildet (vgl. Kapitel 4.2).

### Schema V



- (a) Wie oben abgebildet, wurde bei der Oxidation von *N*-Hydroxypyrrolidinen **31** und **33** nur eine sehr geringe Bevorzugung der Abspaltung des zum Alkoxy-Substituent an C-3 *trans*-ständigen 2-H-Atoms (Gl. 1) gegenüber der Abspaltung des entsprechenden *cis*-ständigen 2-H-Atoms (Gl. 2) festgestellt. Hierbei hing offensichtlich das Beobachtete Diastereomerenverhältnis von den Sterischeinflüsse zur Proton-Abspaltung nicht ab.
- (b) Dagegen wurden bei der Oxidation von 2-Brommethyl-substituierten *N*-Hydroxypyrrolidinen sehr unterschiedliche Regioselektivitäten beobachtet (Schema VI). In diesem Falle machte sich das Auftreten eines stereoelektronischen Effekts bemerkbar, wie sich aus die große Spannweite der Regioselektivität von 80:20 bis zu >98:2 für die Oxidation von den *L*-lyxo- (Gl. 3) bzw. *D*-ribo-konfigurierten Pyrrolidinen (Gl. 4) interpretieren lässt.

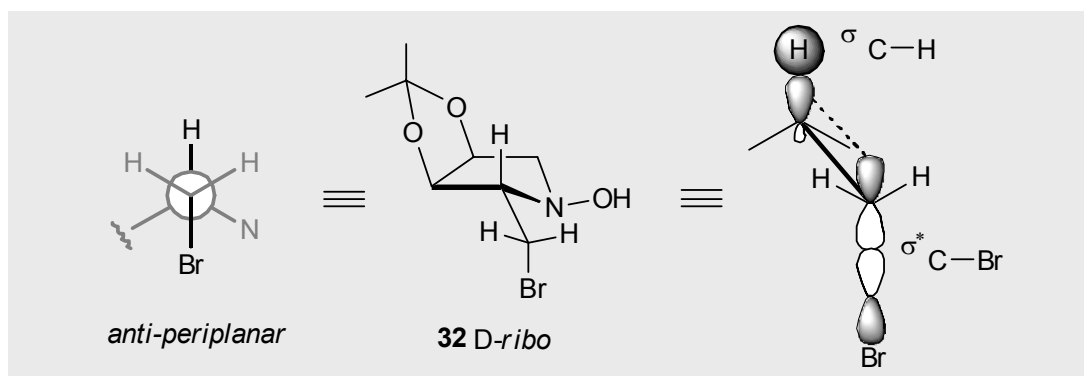
### Schema VI



Energetisch betrachtet ist  $\Delta\Delta G^\ddagger$  zur Abspaltung des 2-H-Atoms im *D*-ribo-Pyrrolidin **32** nun ca. 1.50 kcal/mol niedriger als für 2-H im *L*-lyxo-Pyrrolidin **30**. Eine mögliche Erklärung dieses Befundes geht auf die Molekülorbitalwechselwirkungen zurück (Abbildung II). Betrachtet man diese Wechselwirkung in Sinne von bindenden  $\sigma_{\text{C-H}}$  mit dem antibindenden  $\sigma_{\text{C-Br}}^*$ -Molekülorbital, so kann diese nur wirksam sein, wenn das Br-Atom und das 2-H *anti* zueinander stehen.



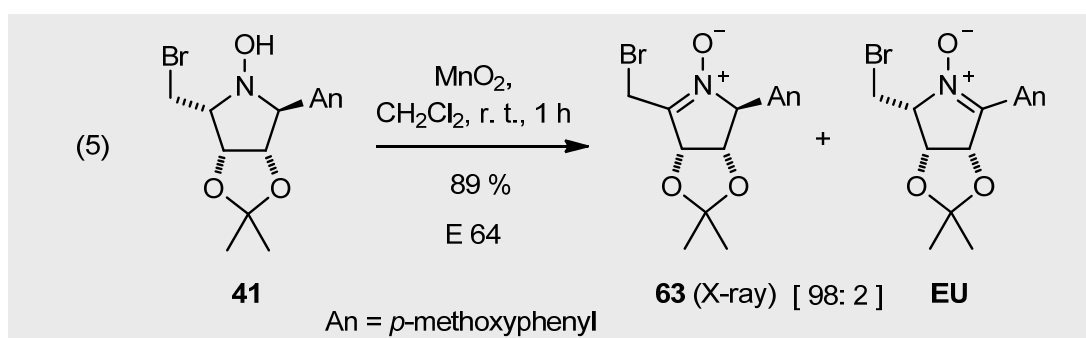
Abbildung II



Im (letzten) Deprotonierungsschritt der Oxidation zum Nitron kann diese Wechselwirkung jetzt die entstehende negative Ladung am  $\alpha$ -C-Atom stabilisieren (vgl. Kapitel 4.2.2 und Lit.<sup>[303,308b,313]</sup>). Die Anordnung der Brommethyl-Gruppe in L-lyxo Pyrrolidin **30** ist so, dass das Bromatom *syn-klinal* zum 2-H steht. Wie zu erwarten, wirkt sich diese Tatsache auf die Regioselektivität nicht aus, wie die im Vergleich erreichte Regioselektivität der Oxidation des „brom-freien“ L-lyxo-Pyrrolidins **31**, die nahezu unverändert bleibt, bestätigt.

- (c) Die Rolle der Konjugation wurde ebenfalls untersucht. Hierbei konnte gezeigt werden, dass ein möglicher Ausbau des konjugierten Systems mit der C=N-Doppelbindung im Sinn einer bevorzugten Abspaltung des zum Aromaten benachbarten 5-H-Atoms praktisch gar nicht erfolgte wurde (vgl. Sektion 4.3.5). Stattdessen belegen die Ergebnisse das erneute Auftreten eines stereoelektronischen Effekts (Schema VII). Dieser bevorzugte die Abspaltung des 2-H-Atoms, das in *trans*-Anordnung sprich *anti-periplanar* zum Alkoxy-Substituent am C-3-Atom steht. Demzufolge wurde für das 2-(*p*-Anisyl)-5-brommethyl-1-hydroxypyrrolidin **41** (Gl. 5) eine selektive Oxidation (d. r. > 98:2) beobachtet. Von Brommethyl-nitron **63** wurde eine Kristallstrukturanalyse als ein weiterer Strukturbeleg erhalten (vgl. Kapitel 9.8).

Schema VII



## Resumee und Ausblick

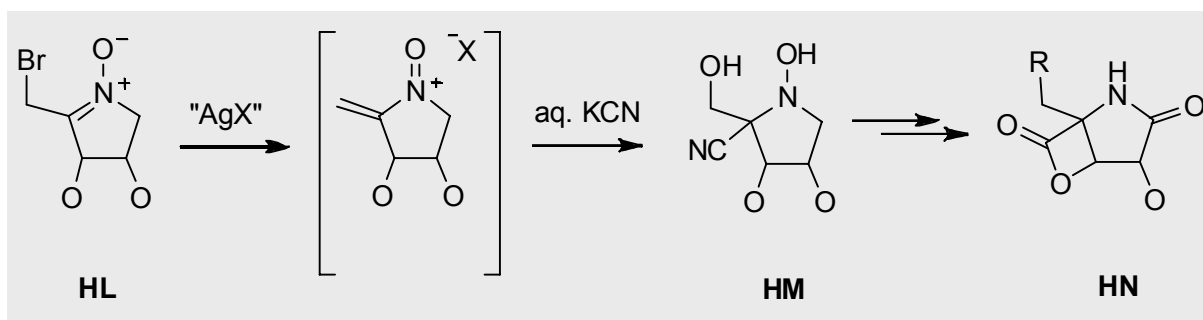
Die herausragenden Ergebnisse dieser Arbeit wurden oben in Kürze diskutiert. Die Brom-Cyclisierung  $\gamma,\delta$ - bzw.  $\delta,\varepsilon$ -ungesättigter Oxime lieferte die entsprechende Dihydro-pyrrol- bzw. Trihydro-pyridin-1-oxide, welche eine Route zur Darstellung von hochsubstituierten Pyrrolidinen bzw. Piperidinen mit L-Fucose-ähnlicher Konfiguration ermöglichen. Es wurden verschiedene, unterschiedlich funktionalisierte Pyrrolidinpolyole dargestellt, die meist eine sehr starke Hemmwirkung gegenüber  $\alpha$ -L-Fucosidasen zeigten. Darüber hinaus wurde die Oxidation von tri- und tetra-substituierten *N*-Hydroxypyrrolidinen systematisch untersucht. Daraus ist eine neue Klasse von Brommethyl-ketonitronen entstanden, die sich vermutlich als Synthesebausteine verwenden lassen.

Unter Anwendung der im Rahmen dieser Arbeit entwickelte Synthese-Route zu *D-arabino*-konfigurierten Hexenoseoximen (wie z. B. **22**) verläuft die anschließende Bromcyclisierung meist mit nur zufriedenstellenden Ausbeuten. Die Bereitstellung von weiteren Oximderivaten könnte sich als sehr nützlich erweisen und könnte eine positive Auswirkung auf die Ausbeute des Cyclisierungs-Schritts haben. Zum Beispiel stehen andere Silyl-Gruppen als Schutzgruppen zur Wahl, z. B. *tert*-Butyldiphenylsilyl. Daneben sollten auch die Reaktionsbedingungen ausgiebig und systematisch untersucht werden. Auf diesem Gebiet wurden bereits Untersuchungen, in erster Linie von Wallasch<sup>[121]</sup> und Krenz<sup>[122]</sup> aus der Arbeitsgruppe Jäger, begonnen.

Im Kapitel 4.4.2.2 wurde auf den Strukturtyp von Brommethyl-ketonitronen **57** kurz hingewiesen und gezeigt, dass diese Verbindungen präparatives Interesse besitzen. In Anlehnung an einen Heterodien-Typ, den der *N*-Vinyl-*N*-cyclohexyl-nitrosonium-Ionen, welche von Eschenmoser et al.<sup>[100,330-331,335]</sup> in die präparative Chemie eingeführt worden sind, erhält man durch  $\text{Ag}^+$ -induzierte Bromid-Eliminierung die cyclischen Heterodiene vom Typus **HL**. Eine Palette von Reaktionen stehen solchen Vinylnitrosonium-Ionen zur Verfügung. Wie im Kapitel 4.2.2 gezeigt wurde, reagiert ein solches Heterodien mit Olefinen im Sinne einer [4 + 2]-Cycloaddition, so dass sich anschliessend in Cyanid-Adukte vom Typus **66/67** bei der Behandlung mit KCN erhalten lassen (vgl. Schema 44, s. 105-106). Es soll hier jedoch deutlich gemacht werden, dass diese Untersuchungen sich sehr in der Anfangsphase befinden. Die Darstellung cyclischer Vinylnitrosonium-Ionen bzw. entsprechender Cyanid-Adukte ausgehend vom Brommethyl-ketonitron **57** gelang bis jetzt lediglich in nur niedrigen Ausbeuten. Eine genauere Untersuchung über das Verhalten weiterer Modellolefine unter dem Einfluss von Silber-Salzen mit Brommethyl-ketonitronen

steht noch an. Die Behandlung von Heterodienen (abgeleitet vom Nitron **HL**) direkt mit einer wässrigen KCN-Lösung bietet möglicherweise einen Zugang zu neuartigen  $\beta$ -Cyanhydrinen, z. B. von **HM** (vgl. Holzapfel et al., Lit.<sup>[336b]</sup>), welche anschliessend in biologisch-relevanten „Omuralid“-ähnliche Systeme **HN** überführt werden können (vgl. Feng Li, *Dissertation*, Lit.<sup>[189a]</sup>) (Schema VIII).

### Schema VIII





# 1 Introduction

## 1.1 Opening Remarks

Iminosugars<sup>[1]</sup> such as polyhydroxylated pyrrolidines (1,4-iminoglycitols) can function as strong and specific glycosidase inhibitors, acting as a barrier to the enzymatic degradation of oligosaccharides and polysaccharides.<sup>[2,3,4,5]</sup> The attributable explanation for this is the mimicry of an *exo*-protonated glycoside **A**, or of the purported *endo*-protonated flattened-chair pyranosyl cationic intermediate **B**, postulated to arise during the transition state of the natural substrate **C** during hydrolysis (Diagram 1).<sup>[6]</sup> The main thrust of the work presented here dealt with the synthesis of 2,5-disubstituted polyhydroxylated pyrrolidines **D** (protonated), which, although having no obvious direct resemblance to a flattened-chair pyranosyl cation, are quite capable of eliciting strong inhibition against particular hydrolytic enzymes. The tight binding of these iminosugars may, however, be due to other less-quantifiable factors such as non-directional Coulombic forces, directional hydrogen bonding, and also the interaction of C-glycosides with the aglycon enzyme pocket.<sup>[7]</sup> The results in this thesis reflect a particular emphasis on an investigation of the latter and confirm that pyrrolidines which have extended, flat anomeric substituents, i.e. at position R in **D**, are best-equipped to inhibit  $\alpha$ -L-fucosidases in a very potent and selective fashion.

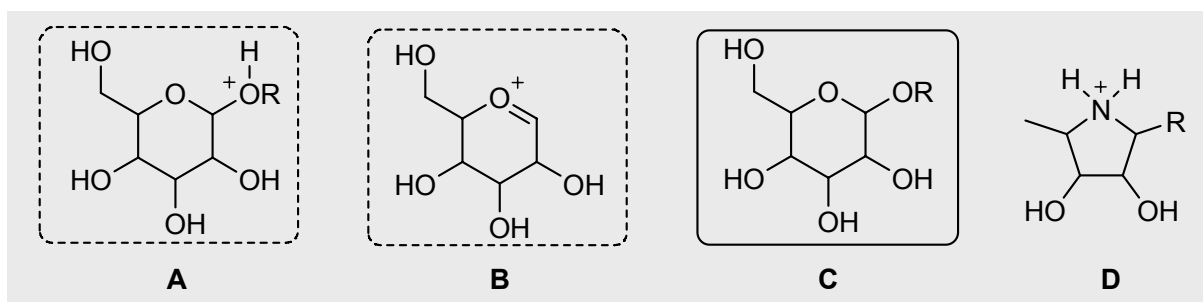


Diagram 1: Natural substrate **C**; natural substrate C-glycoside mimic **D**.

## 1.2 Glycosidases and Glycosylation

Glycosidases are enzymes that are integral to the secretory pathway of N-linked glycoproteins. This pathway ensures that the necessary quality control steps lead to the expression of correctly folded and assembled glycoconjugates.<sup>[8,9]</sup> This process, otherwise known as post-translational protein quality control, consists of a number of very orderly occurring molecular interactions between newly synthesised membrane and secretory glycoproteins and a multicomponent control machinery which takes place in the endoplasmic reticulum and Golgi compartments of the cell. This machinery, in essence, begins with the cotranslational transfer of the parent oligosaccharide,  $\text{Glc}_3\text{Man}_9\text{GlcNAc}_2$ , linked to a dolichol carrier, onto the asparagine residue of an Asn-X-Ser/Thr glycosylation sequon of the protein. A 'cocktail' of glucosidases and mannosidases proceeds to 'trim' the terminal glucose and mannose residues in a programmed way (Diagram 2). The parent N-linked oligosaccharide thus forms part of a biological 'conveyer belt' which traffics the processed oligosaccharide to various destinations so that further trimming events can take place. This trafficking is often portrayed as a terminal and irreversible post-translational modification. However, these glycans are repeatedly modified and serve as handles for sorting events within cells.

One of these sorting events, as mentioned above, is associated with protein folding, and is portrayed in Diagram 3. In this example, a particular enzyme,  $\alpha$ -glucosidase II, has trimmed the last of the outer 1,2-linked glucose units and the glycan that results,  $\text{Man}_9\text{GlcNAc}_2$ , interacts with another enzyme called UDP-Glc:glycoprotein glucosyltransferase. This enzyme functions as a folding sensor and can ascertain whether the polypeptide chain of the glycoprotein is correctly folded, and if so, gives a green light for onward transport to the Golgi apparatus for further processing. However, if the polypeptide is only partially folded, a transient reglucosylation occurs by this glucosyltransferase, making it a substrate for two very important lectins.<sup>[10]</sup> These lectins, calreticulin and calnexin, are proteins which possess discrete domains, so-called carbohydrate-recognition domains (CRDs), and display an acute binding for monoglucosylated N-linked oligosaccharides. They, in effect, 'escort' the partially unfolded polypeptide chain to a luminal protein, ERp57. For their supervisory capacity, such lectins have acquired the moniker, 'molecular chaperons' (*vide infra*). ERp57 is a member of the protein disulphide isomerase family which builds disulphide bonds within the polypeptide chain and as such can assist in the correct folding of N-glycoproteins. As can be seen, dissociation of the calnexin substrate complex is mediated by deglucosylation through glucosidase II. Depending upon the folding state of the released glycoprotein, it may undergo further processing and export from the ER in case a native conformation was achieved or it may be retained in the ER for a further round of binding, if still misfolded.

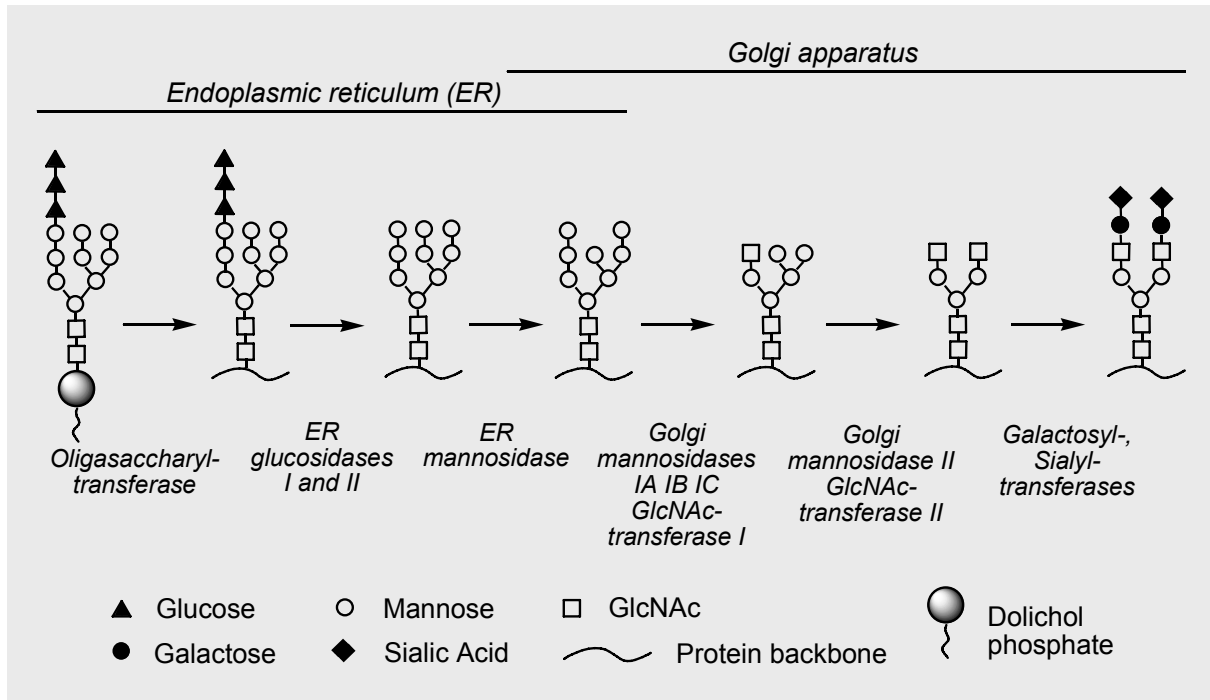


Diagram 2: Schematic representation of N-linked oligosaccharide processing of exportable glycoproteins (“trimming process”) leading to complex N-linked glycans.

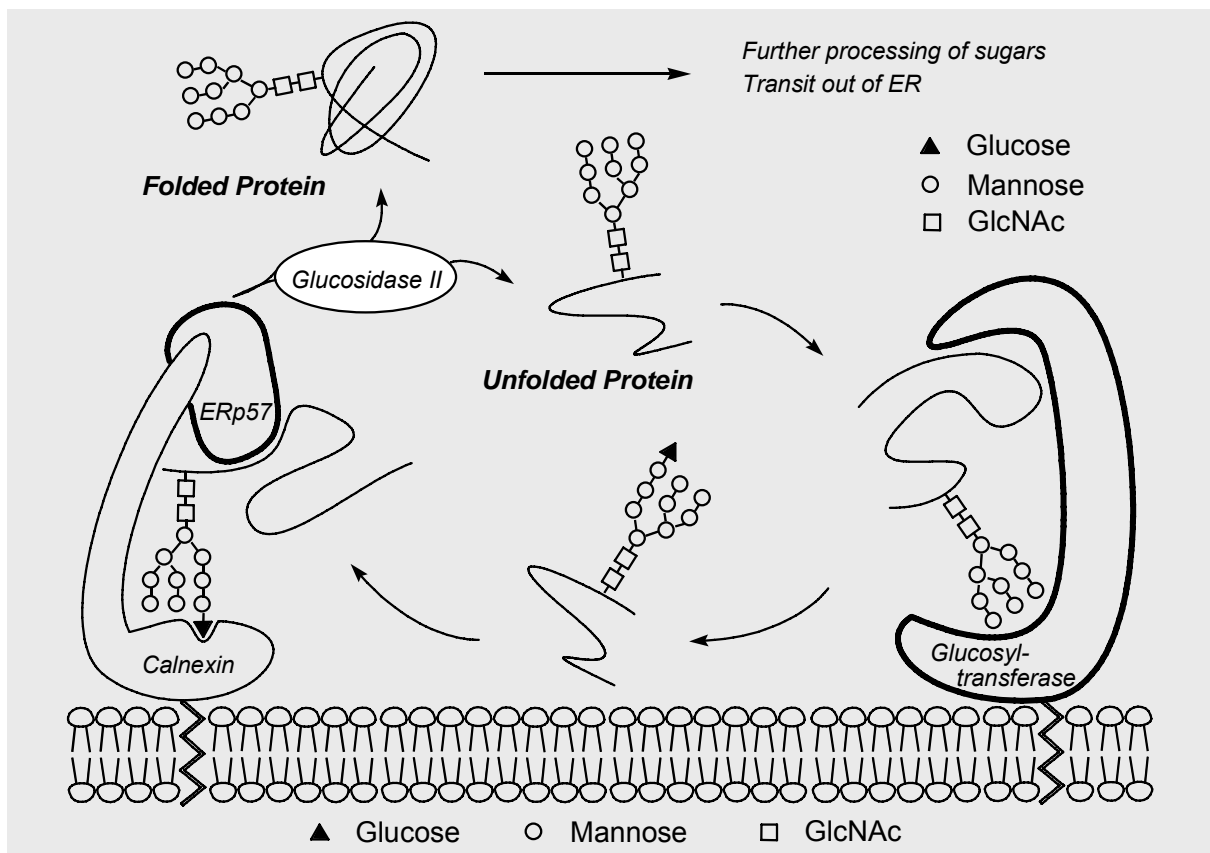


Diagram 3: The calnexin/calreticulin cycle, a sorting event, in which glucose is re-attached to misfolded glycoproteins which are retained in the endoplasmic reticulum.

The opposing functions of glucosidase II and glucosyltransferase provide the basis for an intriguing on-and-off cycle, while it is clear that these interactions cannot persist indefinitely! Although a highly regulated trafficking of exportable glycoproteins has evolved, many obstacles must be overcome so that a high-fraction of newly synthesised secretory and plasma membrane proteins can be exported by the cell to their correct destinations. Perturbations to this process, more often than not due to subtle mutations in the coding sequences of polypeptide precursors, can lead to defective protein trafficking and can cause the disease phenotype. Since glycosidases and glucosyltransferases are themselves proteins, changes to their morphology, activity or prevalence can elicit an incorrect glycosylation pattern, the aspects of which are far reaching and are detailed below.

## 1.3 Glycosylation and Disease

### 1.3.1 Oncology

The glycosylation pattern of cells expressing glycoproteins has been known to alter in disease.<sup>[11]</sup> The underlying reason for this is the addition or deletion of a specific glycosidase or glucosyltransferase to a biological system which then invokes a change to the glycosylation phenotype of the cell. The primary destinations of glycoproteins are the outer, or endothelium region, of mammalian cells and tissues and accordingly the sugar epitopes of these glycoconjugates are thought to play a crucial role in various biological processes including cell adhesion,<sup>[12,13]</sup> cell-cell recognition,<sup>[14]</sup> immune defense and inflammation,<sup>[9]</sup> cell growth,<sup>[15]</sup> as well as fertilisation and virus replication.<sup>[16]</sup> In 1987, a breakthrough from Dennis<sup>[17]</sup> first disclosed a direct-link between cells expressing a “false glycosylation pattern” and the detrimental consequences for the host associated with malignant or metastatic progression. This could be correlated to an up-regulation of *N*-acetylglucosaminyltransferase V (GNT-V) (catalyses formation of GlcNAc $\beta$ 1-6Man linkages) and subsequent production of tetra-antennary oligosaccharides, in which two branches extend from the 1,6 arm of the core rather than the 1,3 arm.<sup>[16,18]</sup> This 1,6-branching facilitates an increase in ‘global-sialylation’ through the attachment of terminal sialic acid (‘NeuAc’) units to the growing polylactosamine backbone and, although not completely understood, for additional adhesion of selectins to heavily sialylated N-glycans (Diagram 4). Likewise, aggregation of internal sialyl Lewis<sup>x</sup> /Lewis<sup>a</sup> epitopes (cf. Diagram 9) is found extensively in colorectal cancer cells due to the action of sialyl- and fucosyltransferases.<sup>[19]</sup> The transfected cells are antigenic for E-selectin



which is recruited to the surface of endothelial cells during malignant progression. Because cancer cells expressing such carbohydrate epitopes may become highly motile after adherence to E-selectin, there is a strong link between selectin-binding and systemic migration and intravasation.<sup>[12,13,18a,19,20]</sup> Spurred on by this, substantial effort has gone into designing 'carbohydrate-based vaccines'. One route, publicised by Danishefsky,<sup>[21]</sup> takes advantage of the adhesive properties of selectins to cancer cells by employing oligosaccharide-conjugates that mimic the tumour-associated antigens (e.g. Lewis-type, Globo-H, GM2 etc.) linked to an immunogenic carrier protein, keyhole limpet haemocyanin ('KLH'-conjugates).<sup>[21]</sup> The peptide portion contains the required antigens required for T-cell help to register an immunological response (i.e. generation of antibodies).<sup>[13,21]</sup> Indeed, this and other 'magic bullet' approaches, including monoclonal antibodies, antibody-directed enzyme prodrug therapy ('ADEPT'), are all reliant on the 'glycocode' for their function.<sup>[22]</sup>

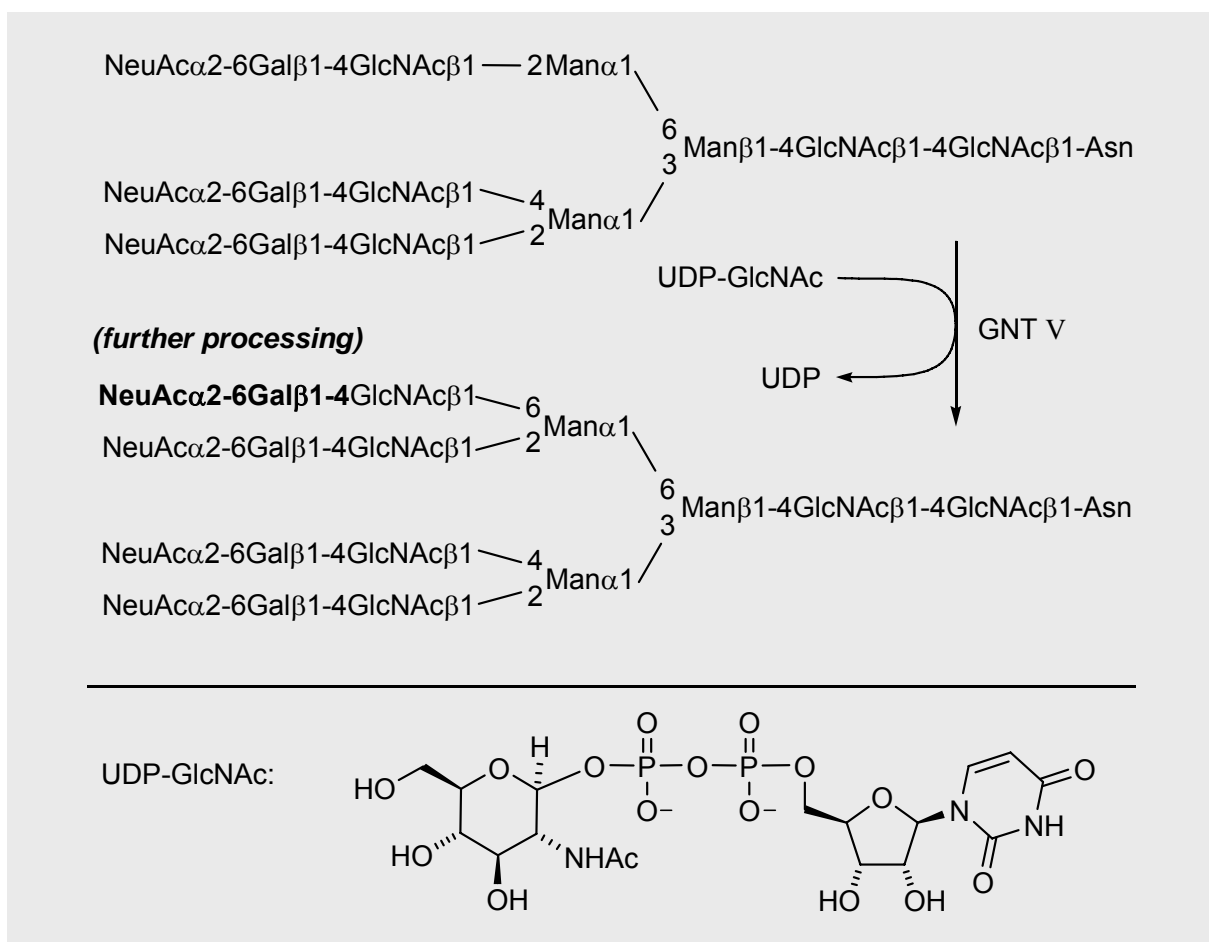


Diagram 4: Formation of branched  $\beta$ 1-6 N-linked oligosaccharides. UDP-GlcNAc:*N*-acetylglucosaminyltransferase V (GNT-V) transfers GlcNAc leading to the  $\beta$ 1-6-branching phenotype. This carbohydrate epitope is associated with malignancy and metastasis progression in certain human cancers.<sup>[17,18]</sup>

As alluded to above, the ability to prevent metastasis is another arm of drug therapy and one that has a chance of success. Here, a number of glycosidase inhibitors have emerged as potential anti-metastasis drug candidates. They are largely based on mannosidase inhibitors like deoxymannonojirimycin (DMJ) **E**, DIM **F** or swainsonine **G**. In particular, indolizidine **G**, first isolated from *Swainsona canescens* by Huxtable in 1979,<sup>[23]</sup> is a potent inhibitor of mammalian Golgi  $\alpha$ -mannosidase II (GMII) ( $IC_{50} = 0.04 \mu\text{M}$ ) and jack bean  $\alpha$ -mannosidase ( $IC_{50} = 0.4 \mu\text{M}$ ).<sup>[24]</sup> Swainsonine can inhibit formation of sarcoma lung metastases<sup>[24a]</sup> and haematological malignancies.<sup>[24b]</sup> It works by blocking N-glycoprotein processing prior to the addition of the  $\beta$ 1-6 antennae and thus prevents further downstream modifications by glycosyltransferases (e.g. GNT-V, *vide supra*). Due to a high degree of homology between GMII and lysosomal mannosidases, swainsonine is known to cross-inhibit both and induces the undesirable build-up of mannose-rich lysosomal oligosaccharides leading to storage disease symptoms ('swainsonine-induced mannosidosis').

Pearson attempted to address this problem by designing the swainsonine derivative **H** that on account of its extended aglycon side chain should be better positioned to mimic the outer mannose-sites of the natural substrate (GlcNAcMan<sub>5</sub>GlcNAc<sub>2</sub>-Asn-X) which are hydrolysed sequentially by GMII (cf. Diagram 2).<sup>[25]</sup> Although indolizidine **H** inhibited jack bean  $\alpha$ -mannosidase ( $IC_{50} = 0.05 \mu\text{M}$ ) stronger than swainsonine **G** ( $IC_{50} = 0.4 \mu\text{M}$ ), this result cannot be used as a reliable criterion for selectivity, since comparative data for competing inhibition of mammalian lysosomal  $\alpha$ -mannosidase has yet to be published.<sup>[25a]</sup> However, GMII has been recently expressed and cloned into *Drosophila melanogaster* cells and the resulting enzyme's ('dGMII') X-ray structure determined with swainsonine **G** and DMJ **E**.<sup>[26]</sup> Interestingly, the active site cavity of GMII and dGMII is highly conserved; each is lined by aromatic residues that are involved in sizable hydrogen bond and hydrophilic binding contributions to the inhibitors which, themselves, are anchored in place by an active site Zn cation.<sup>[26,27]</sup> In light of this, Pearson's compound **H** is presumably a better inhibitor on account of its lateral, lipophilic side chain that is able to 'squeeze-out' aggregate water molecules which have been revealed to reside in a cavity on the open side of the active site.<sup>[26]</sup> As discussed later (see Section 6), the displacement of structured water molecules can have positive implications for inhibitor-substrate binding ('entropic gains'<sup>[28]</sup>).

Likewise, structurally simpler polyhydroxylated pyrrolidines **I** ( $IC_{50} = 6.2 \mu\text{M}$ )<sup>[29]</sup> and **J** ( $IC_{50} = 0.7 \mu\text{M}$ ),<sup>[30]</sup> reported by Vogel and Juillerat-Jeanneret, potently inhibit  $\alpha$ -mannosidase (jack bean). In particular, the diamine **J**, once esterified, prevents the proliferation of glioblastoma and melanoma cells even though a trade-off in the inhibition potency towards  $\alpha$ -mannosidases is observed.<sup>[30b,31]</sup>

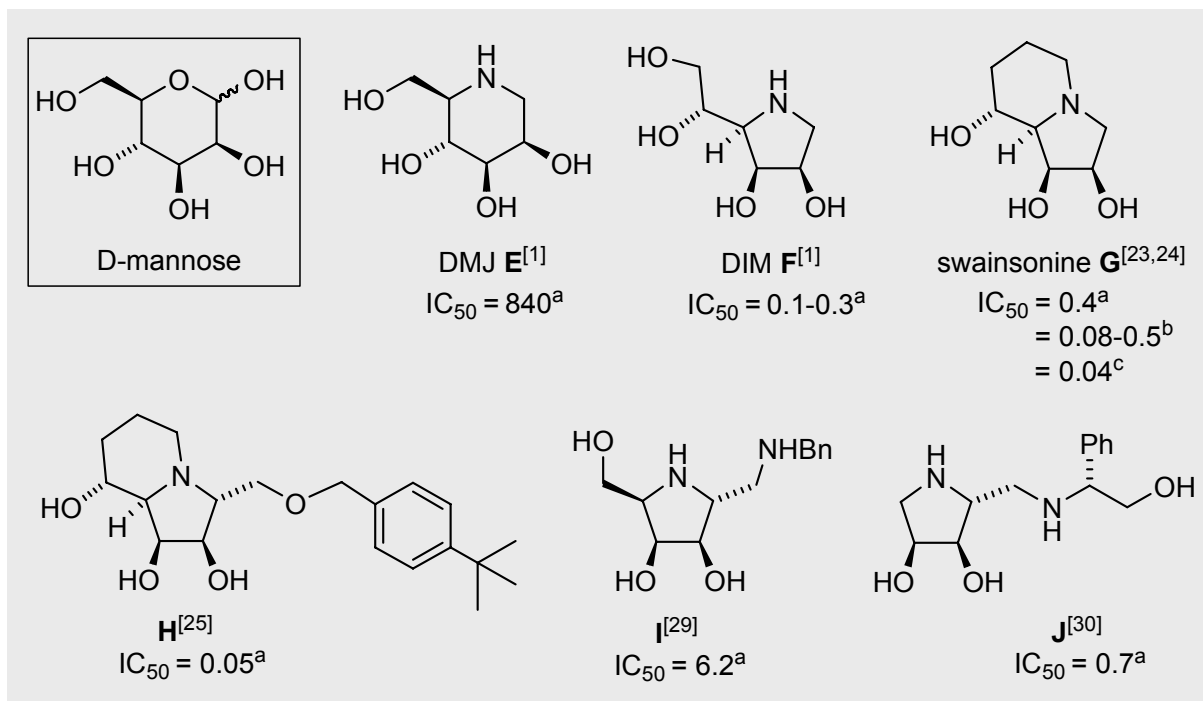


Diagram 5: Mannosidase inhibitors as potential anti-cancer agents. DMJ = *manno*-deoxynojirimycin **E**<sup>[1]</sup>; DIM = 1,4-dideoxy-1,4-imino-D-mannitol **F**<sup>[1]</sup>;  $\alpha$ -mannosidase source: a = jack bean; b = lysosomal (mammalian); c = Golgi ('GMII', mammalian) (concentration values in  $\mu$ M).

### 1.3.2 Storage diseases

Interest in lysosomal storage diseases has increased significantly.<sup>[32]</sup> Although overlooked by most pharmaceutical companies ("orphan diseases"), such disorders present attractive opportunities for clinical development due to their well-understood pathology, straightforward path of intervention (i.e. enzyme replacement) and a price premium for treatment (ca. \$170,000 per patient per annum).<sup>[32]</sup> Around two-dozen rare carbohydrate metabolism disorders are known of which two conditions in particular, Gaucher's and Fabry's disease, are best documented, each afflicting around 5000 patients worldwide.<sup>[32]</sup> Gaucher's disease, caused by insufficient lysosomal glucocerebrosidase (GCCase; otherwise known as ceramide  $\beta$ -glucosidase; EC 3.2.1.45), leads to the accumulation of glucosylceramide **K**, a precursor in the biosynthesis of complex glycosphingolipids.<sup>[33]</sup> Over 200 gene mutations are known to afflict GCCase that, to varying extents, contribute to an abolishment of catalytic activity and reduced stability by causing the glycoprotein to miss-fold.<sup>[34,35]</sup> Perhaps not surprisingly, the mutated protein is not secreted by the cell but instead becomes an easy target for the quality

control machinery of the endoplasmic reticulum (ER) (cf. Section 1.2) and is quickly banished to the ER-associated degradation ('ERAD')/ubiquitin proteasome pathway.<sup>[16,36]</sup> The most prevalent mutations, however, to GCCase (N370S and G202R) which cause the type I clinical phenotype of Gaucher's disease, leave the catalytic site intact and are amenable to molecular chaperon therapy. Glucosidase inhibitors such as (*gluco*)-deoxynojirimycin **L** (DNJ), 1,5-dideoxy-1,5-imino-D-xylitol **M** and nortropane derivate **N** (calystegine B<sub>2</sub>) can increase the residual activity of GCCase by binding strongly to the native conformation of the enzyme in the endoplasmic reticulum (Diagram 6). Put simply, this can impart folding stability to the defective glycoprotein allowing the GCCase variants to 'escape' from the ER (thus avoiding degradation) to allow trafficking to the lysosome to take place.<sup>[35,37]</sup> The level of improvement in residual activity of GCCase in treated fibroblast cells from Gaucher patients with the N370S mutation correlates well to the progressively lower IC<sub>50</sub> values of the inhibitors **L**, **M** and **N** (i.e. 240, 2.3, 1.0 μM, respectively). This could be a consequence of the greater cellular permeability of the inhibitors due to marginal increases in lipophilicity.<sup>[35]</sup> On the other hand, isofagomine **O**, a traditionally strong β-glucosidase inhibitor (e.g. K<sub>i</sub> = 0.11 μM; sweet almonds),<sup>[1]</sup> where the nitrogen is relocated to the anomeric position, is a substantially better substrate for GCCase (IC<sub>50</sub> = 0.04 μM).<sup>[35]</sup> Several mechanisms have been proposed to explain the marked efficacy of isofagomine **O**.<sup>[38]</sup>

Along with enzyme replacement and chaperon therapy, a further alternative is to reduce the influx of substrate to the lysosome by inhibiting the biosynthesis of glycosphingolipids. This strategy has been termed substrate deprivation.<sup>[33]</sup> The aim is to inhibit glucosylceramide transferase ('GCT'; EC 2.4.1.80) which catalyses the condensation of UDP-glucose with ceramide to produce glucosylceramide **K** (Diagram 6). Lead compounds include the FDA-approved *N*-butyl-deoxynojirimycin **P** (Zavesca<sup>TM</sup>; Actelion) for Gaucher patients who are not suited to enzyme replacement therapy.<sup>[39]</sup> Shown to be a moderate inhibitor of GCT *in vivo* (IC<sub>50</sub> = 50 μM), Zavesca **P** has clinical drawbacks because of co-inhibition of lysosomal α-glucosidase and intestinal sucrase and maltase.<sup>[40]</sup> Overkleeft has described *N*-alkyl<sup>[41,42]</sup> and, more recently, C-alkylated<sup>[42]</sup> derivatives of **P** bearing extended lipophilic substituents. While Overkleeft's *N*-alkylated derivative **Q** proved a superior substrate for GCT (IC<sub>50</sub> = 0.2 μM) compared to the marketed compound **P**, co-inhibition of intestinal enzymes remained an issue. In comparison, C-glycoside derivative **R**, albeit a weaker inhibitor of GCT (IC<sub>50</sub> = 9 μM) compared to **P**, did not, importantly, inhibit intestinal glycosidases and may be suitable for clinical development.<sup>[42]</sup> In a similar vein, α-galactosidase inhibitors including *galacto*-deoxynojirimycin **S**, *N*-alkylated substrate **T** and α-homomethyl derivative **U**, have been investigated as chemical chaperons for the treatment of Fabry's disease (deficiency of α-galactosidase).<sup>[32]</sup>

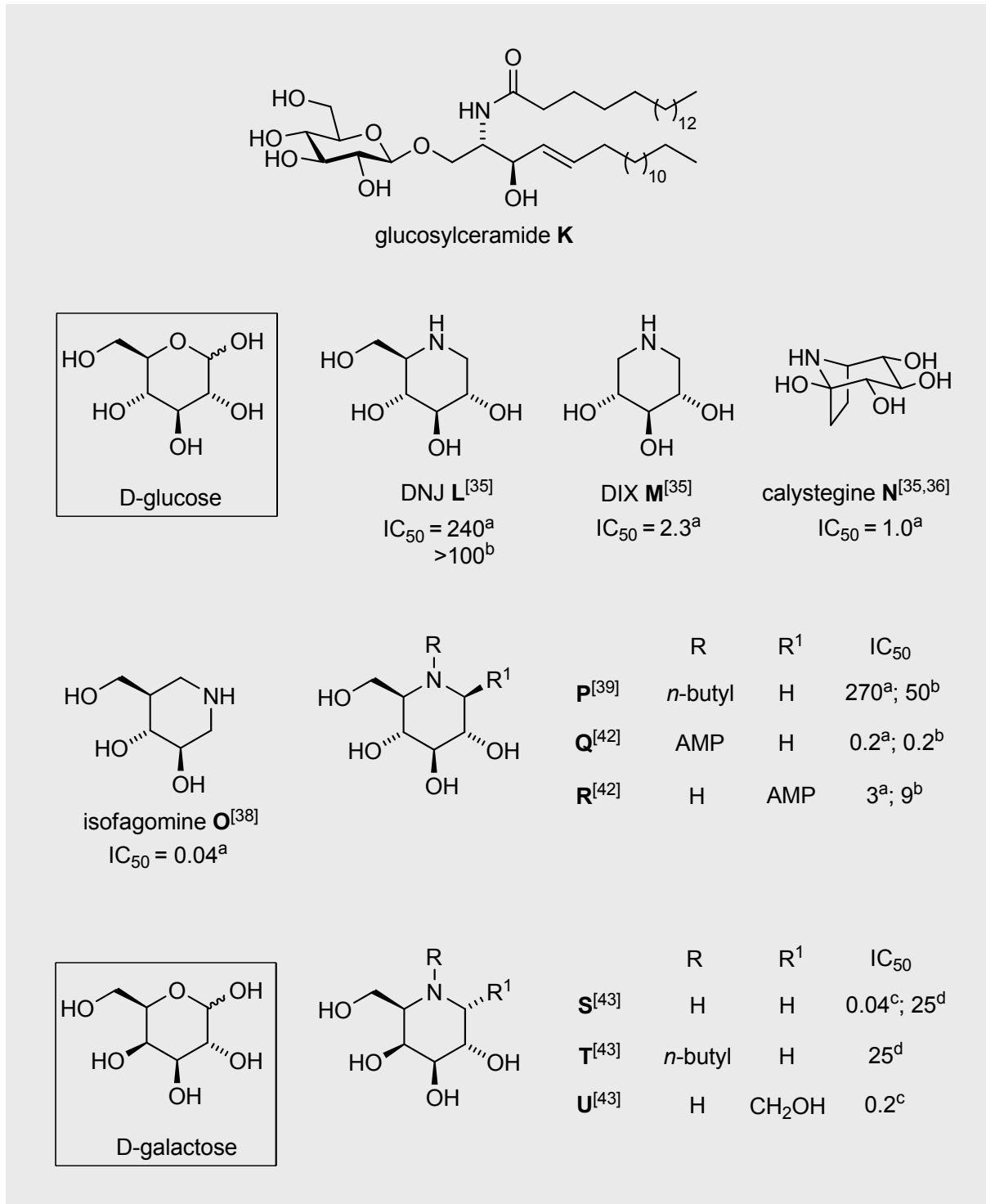


Diagram 6: Selected glucosidase and galactosidase inhibitors with clinical application in the treatment of lysosomal storage disorders.<sup>[32-44]</sup> DNJ = *gluco*-deoxynojirimycin **L**<sup>[35]</sup>; DIX = 1,5-dideoxy-1,5-imino-D-xylitol **M**<sup>[35]</sup>; **P** = Zavesca<sup>TM</sup> (Miglustat)<sup>[39,40]</sup>; **S** = *galacto*-deoxynojirimycin (DGJ),<sup>[43]</sup> AMP = 5-(adamantan-1-yl-methoxy)-pentyl.<sup>[42]</sup> Enzyme source: a = human glucocerebrosidase; b = glucosylceramide synthase; c =  $\alpha$ -galactosidase A (Fabry; human mutation R301Q); d = jack bean  $\alpha$ -galactosidase (concentration values in  $\mu$ M).

In 2001, the European Union approved Fabrazyme™ (developed by Genzyme) as an enzyme replacement therapy treatment for Fabry's disease. Concurrently, Fan et al.<sup>[43]</sup> demonstrated that compounds **S** to **U**, inhibitors of human  $\alpha$ -galactosidase A ( $IC_{50}$  = 0.04, 16, 0.2  $\mu$ M, respectively), were able to correct abnormal protein folding, thereby effectively enhancing the mutant enzyme activity in lymphoblasts from Fabry patients with the clinical phenotype mutation, R301Q. Interestingly, DGJ **S** is a non-selective inhibitor of several mammalian (e.g. human lysosomal  $\alpha$ -galactosidase  $IC_{50}$  = 25  $\mu$ M) and non-mammalian glucosidases (e.g. coffee bean  $\alpha$ -galactosidase  $IC_{50}$  = 0.003  $\mu$ M), although this has evidently not dented its progress in ongoing clinical trials in the United States (currently phase II)<sup>[44]</sup> as an orally available treatment for Fabry's disease.

### 1.3.3 Antiviral agents

Since 1981, the human immunodeficiency virus (HIV) has killed around 20 million people worldwide, with approximately 40 million people living with the disease at the end of 2004.<sup>[45,46,47]</sup> No vaccine is available for HIV and modern chemotherapy relies on optimising the synergistic effects of drug combinations to elicit a highly active antiretroviral response.<sup>[46]</sup> From the FDA-approved drug classes that combat HIV infection, nucleoside reverse transcriptase inhibitors, such as azidothymidine (AZT **V**; Diagram 7),<sup>[46]</sup> and protease inhibitors (e.g. indinavir,<sup>[46]</sup> tipranavir<sup>[48]</sup>) have been the main stay for drug combination therapy. To date, the FDA has licensed eight protease inhibitors which, when taking 1981 as a bench mark for HIV infection, equates on average to a new drug every ca. 3 years. This statistic, in other words, depicts a pharmaceutical industry that is merely playing 'catch-up' to combat drug resistance caused by a gradually mutating HIV virus. The future, however, looks rosy, and alternative therapies that target the prevention of viral entry offer promise.<sup>[49]</sup> The entry of HIV<sup>[22,46,49,50,51]</sup> is initiated by the binding of the viral glycoprotein gp120 to the cellular CD4 receptor on T lymphocytes or macrophages, followed by subsequent interaction with chemokine co-receptors CCR5 (on macrophages) or CXCR4 on T lymphocytes. Following binding, extensive conformational changes occur in gp120 involving "hypervariable loops". These "loops" become moved to a position which trigger a second trimeric viral protein, gp41, to come "crashing" down upon the host membrane leading to fusion of the virus with the host cell. Around 1988, Sunkara,<sup>[52]</sup> Fleet and Dwek<sup>[53]</sup> and others<sup>[54,55]</sup> reported that  $\alpha$ -glucosidase I inhibitors, *N*-butyl-deoxynojirimycin (NB-DNJ, **P**) (cf. Diagram 6), castanospermine **X** and an esterified derivative, the 6-O-butanoyl castanospermine ('BuCast', **Y**), exhibited anti-HIV activity (Diagram 8).

Initially, castanospermine was thought to be a potential antiviral treatment, especially after it had show synergistic effects with AZT **V**.<sup>[56]</sup> 6-O-Butanoylcastanospermine **Y**,<sup>[55]</sup> on the other hand, was significantly more anti-HIV active, despite being a 10-fold weaker inhibitor of  $\alpha$ -glucosidase I (i.e.  $IC_{50}$  1.27  $\mu$ M vs. 0.12  $\mu$ M, Diagram 8). The explanation of this paradox is that 'BuCast' **Y** is taken up by cells and absorbed in the bloodstream quicker, before subsequently being hydrolysed to castanospermine **X** – i.e. it is a prodrug. The antiretroviral properties of iminosugars **P**, **X** and **Y** are due to their interference with the correct glycosylation pattern of the viral glycoprotein, gp120.<sup>[46,51,52,53b,54-56]</sup> Perturbation of the viral envelope glycoprotein by removing glucose residues does not, however, lead to weakened gp120-CD4 binding.<sup>[57]</sup> Instead, the entry of HIV at the level of post gp120/CD4 binding is compromised,<sup>[58]</sup> NB-DNJ **P** was shown to affect the conformation of the hypervariable loops of gp120, thereby obstructing downstream binding of the transmembrane viral glycoprotein, gp 41, to the host cell. Despite the known efficacy of these compounds, the market for iminosugar-based antiretroviral agents disappeared rapidly following the subsequent discovery of the chemokine HIV co-receptors, CCR5 and CXCR4.<sup>[59,60]</sup> These receptors can be envisaged as being the “doorway” which gp120 uses, after binding to the CD4 receptor on T-lymphocytes, to trigger the transmembrane viral protein, gp 41. Ironically, with the advent of Pfizer's CCR5 receptor-blocker Maraviroc **W**,<sup>[61]</sup> (Diagram 7) interest in iminosugars as potential HIV-entry inhibitors may, at some point, see a resurgence: it itself is an *N*-alkylated nortropane derivative, similar to the calystegines (cf. calystegine B<sub>2</sub> **N**, Diagram 6).

Apart for HIV infection, studies have shown that  $\alpha$ -glucosidase I inhibitors, including castanospermine **X**, NB-DNJ **P** and other *N*-alkylated derivatives, are potentially useful in the treatment of several other human diseases including: hepatitis B,<sup>[62]</sup> bovine viral diarrhea virus (a tissue culture model for hepatitis C),<sup>[63]</sup> dengue<sup>[64]</sup> and herpes simplex virus type 2<sup>[65]</sup> (reviewed in lit.<sup>[66]</sup>). During a screening of substances as agents against the human coronavirus (causes severe acute respiratory syndrome, 'SARS'), lipid-like O-benzyl-protected deoxynojirimycin derivate **Z** was discovered.<sup>[67]</sup> Wong<sup>[68,69]</sup> has recently published a combinatorial study starting with the 1-amino-1,2,5-dideoxy-2,5-imino-D-mannitol core **AA**, to synthesise numerous amides at C—1 to produce substances with a 2000-fold improvement in  $\alpha$ -glucosidase inhibition (i.e. C-glycoside **AB**;  $IC_{50}$  0.015  $\mu$ M) compared to the parent compound (**AA**;  $IC_{50}$  30  $\mu$ M, Diagram 8). *N*-Alkylated pyrrolidine **AC** was also identified as an antiviral agent against Japanese encephalitis virus and dengue virus serotype 2, although having a considerably weaker  $\alpha$ -glucosidase inhibition profile (*vide supra*).

Of current interest are antiviral agents that hinder the replication of human influenza virus.<sup>[66]</sup> Unlike HIV, the coat of the influenza A and B virus strains is highly conserved, exhibiting trimeric haemagglutinin and tetrameric neuraminidase.; the latter of which targets host-lectins

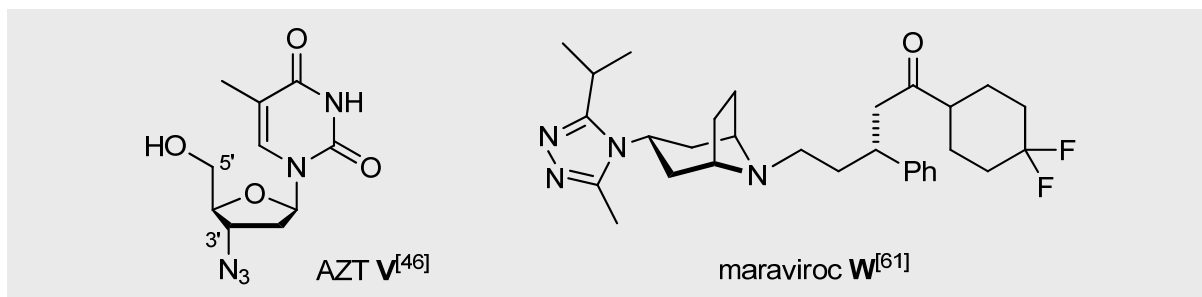


Diagram 7: FDA approved HIV-antiretroviral treatment azidothymidine (AZT, **V**)<sup>[46]</sup> and Pfizer's HIV entry inhibitor (CCR5 antagonist) maraviroc (**W**).<sup>[61]</sup>

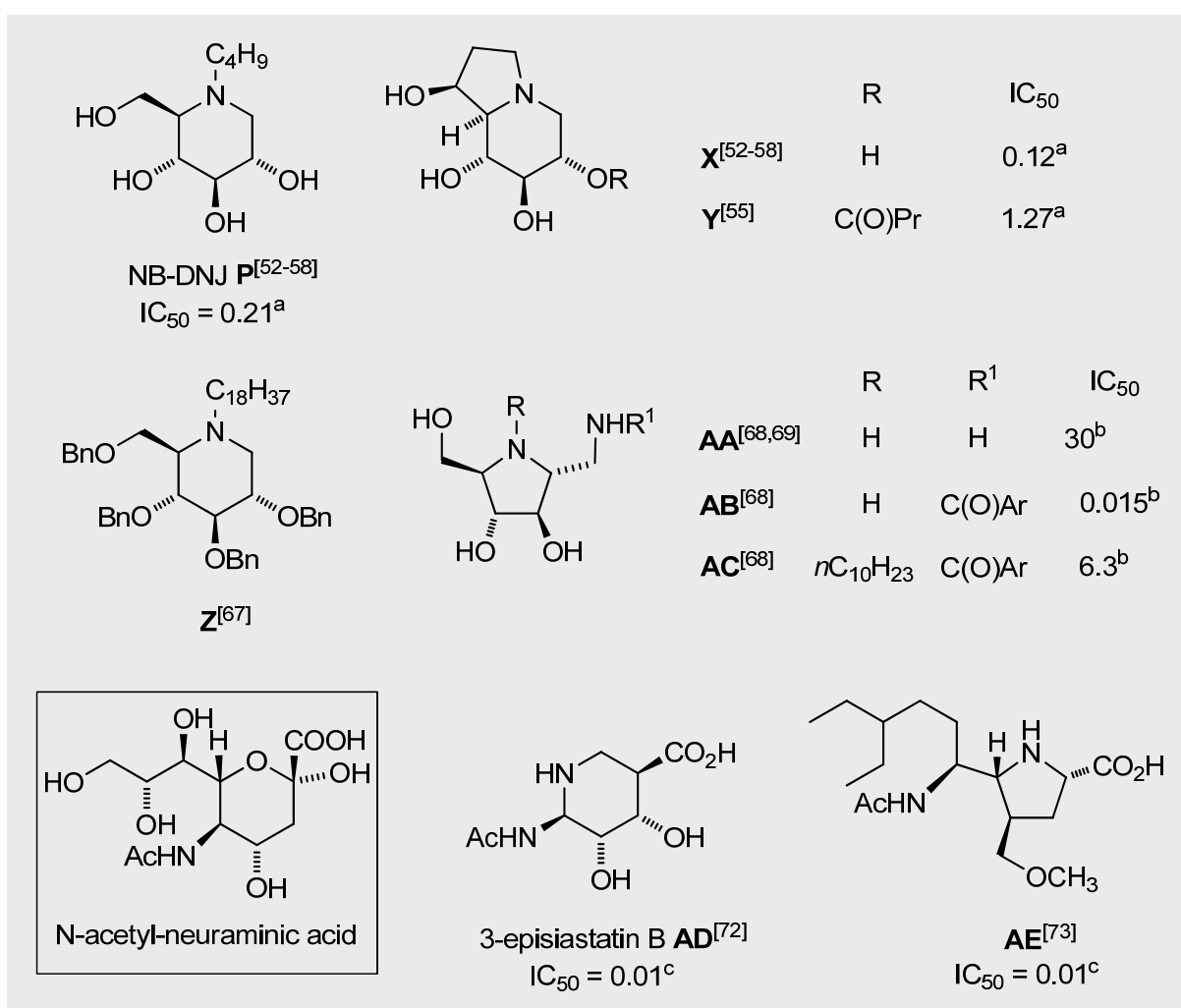


Diagram 8: Literature examples of *N*- and *C*-alkylated glycosidase inhibitors with antiviral properties.<sup>[52-58,62-73]</sup> Active against (a) HIV-entry (**P**; castanospermine **X**; 'BuCast' **Y**);<sup>[52-58]</sup> (b) SARS, human coronavirus (**Z**);<sup>[67]</sup> (c) influenza mimics of *N*-acetyl-neuraminic acid (**AD, AE**).<sup>[70-73]</sup> Ar = 1,2-dihydrocyclobutabenzene.<sup>[68]</sup> Enzyme source: a =  $\alpha$ -glucosidase I, pig kidney; b =  $\alpha$ -glucosidase, bakers' yeast; c = human influenza virus *N*-acetyl-neuraminidase (concentrations in  $\mu$ M).



bearing sialic acid (*N*-acetyl-neuraminic acid) residues.<sup>[16]</sup> Neuraminidase activity is essential for influenza virus replication and activity. Inhibitors of *N*-acetyl-neuraminidases mimic the natural substrate, *N*-acetyl-neuraminic acid, and include FDA-licensed substances such as Zanamivir (Relenza™),<sup>[70]</sup> a 4-guanidino analogue of 2,3-dehydro-2-deoxy-*N*-acetylneuraminic acid, and Oseltamivir (Tamiflu™),<sup>[71]</sup> a carbocyclic *N*-acetyl-neuraminic acid mimetic (not shown). Derivatives of naturally occurring iminosugars such as the 3-epimer of siastatin B, piperidine **AD**, have good activity against the influenza virus (IC<sub>50</sub> 0.01 μM)<sup>[72]</sup> as does the rationally designed synthetic pyrrolidine **AE** (IC<sub>50</sub> 0.01 μM),<sup>[73]</sup> thus rivalling the anti-influenza activities of the commercial products (Diagram 8).

## 1.4 α-L-Fucosidase Inhibitors as Therapeutic Agents?

α-L-Fucosidase (EC 3.2.1.51) is a ubiquitous lysosomal glycosidase which has been widely isolated and studied.<sup>[74,75]</sup> This ubiquity is due to the presence of a diverse and widespread group of hydrophilic and hydrophobic fucose-containing glycoconjugates (e.g. oligosaccharides, glycoproteins and glycolipids).<sup>[76]</sup> The ability of α-L-fucosidase to catalyse the removal of α-1,2, α-1,3, α-1,4, or α-1,6 residues implies that such fucose-containing glycans are not linear in nature, but mostly branched glycans of very diverse composition and, accordingly, biological function (reviewed by Lowe in lit.<sup>[77]</sup>). The best examples of fucosylated glycans with biological significance are those concerning the *ABO* blood group antigens (i.e. α-1,3-fucosylated glycans), which are made after the *ABO* locus has encoded a particular glycosyltransferase to further modify the H antigen **AF** (Diagram 9).<sup>[16]</sup> Recently, fucose-α-1,2-galactose (Fucα1-2Gal) **AG** has been implicated in long-time memory and other cognitive processes. For example, preventing formation of Fucα1-2Gal linkages by incorporation of 2-deoxy-D-galactose into glycan chains has been shown to cause irreversible amnesia in animals.<sup>[78]</sup> In rat models, it appears that the level of fucosylation of proteins at the synapse is linked to neuronal development, although little is known about the mechanisms of communication involving Fucα1-2Gal sugars.<sup>[79]</sup> Fucose is also an essential component of the pseudo-tetrasaccharide, sialyl Lewis X (sLe<sup>x</sup>; NeuAcα2-3Galβ(1-4)[Fucα1-3]GlcNAc) **AH** and its [Fucα1-4]-isomer, sialyl Lewis a (sLe<sup>a</sup>; not shown), which are known ligands for selectins and are regarded as tumour-associated antigens.<sup>[80,81]</sup> As mentioned already in Section 1.3.1, the number of sLe<sup>x</sup> and sLe<sup>a</sup> structures is increased in carcinoma cells and this is thought to contribute to the metastatic dissemination of tumour cells.<sup>[13,19]</sup>

It should be noted that the increased occurrence of sLe<sup>x</sup> and sLe<sup>a</sup> structures has been linked to the up-regulation of  $\alpha$ -L-fucosidases, which liberate fucose from glycoproteins and glycolipids in the lysosomal compartment of the cell. Fucose liberated this way can be transported across the lysosomal membrane to the cytosol to be converted into its active form, GDP-L-fucose (*via* the 'fucose-salvage pathway').<sup>[77,82]</sup> This nucleotide must enter the Golgi apparatus where it serves as a substrate in the synthesis of fucosylated glycoconjugates by fucosyltransferases.<sup>[74,77]</sup> In cancer therapy, the monitoring of levels of serum  $\alpha$ -L-fucosidases as a 'biochemical marker' is an important criterion for the (early) diagnosis and progress of several cancers and has found extensive publication.<sup>[83]</sup> However, it is not clearly understood whether changes of the level of  $\alpha$ -L-fucosidase are linked to the onset of pathological manifestation, or merely represent a secondary consequence related to the up-regulation of the fucosylation machinery. Such is the diversity of fucose-containing glycoconjugates, it is likely, however, that many additional functions of fucosylated glycans remain to be uncovered. For example: Although the increased expression of fucosylated glycans in rheumatoid arthritis<sup>[84]</sup> and cystic fibrosis<sup>[85]</sup> is known to occur, it remains to be determined if there are casual relationships or direct links between glycan aberration and pathogenesis.

It would seem that inhibitors of  $\alpha$ -L-fucosidases – when not currently foreseeable as therapeutic agents – may be of some use as 'biological terrorists' to assist in assessing the function of fucosylated glycans. A large number of  $\alpha$ -L-fucosidase inhibitors exist which, not surprisingly, share the same hydroxyl group topography as the parent sugar, L-fucose (itself a moderate inhibitor; IC<sub>50</sub> = 0.6 mM, bovine kidney<sup>[86]</sup>, Diagram 9). The synthetic deoxyfuconojirimycin (**AI**, DFJ) is considered the paradigmatic  $\alpha$ -L-fucosidase inhibitor ( $K_i$ 's between 0.001-0.006  $\mu$ M)<sup>[87,88,89,90,91]</sup> and was first synthesised by Fleet and co-workers.<sup>[92]</sup> Compound **AI** was, along with *N*-butyl nojirimycin **P** and castanospermine derivatives, **X** and **Y** (*vide supra*), implicated as a lead compound with anti-HIV activity.<sup>[53]</sup> The HIV-2 envelope glycoprotein has since been found to be heavily core-fucosylated (elucidated by Liedtke through enzymatic digestion/MALDI-TOF analysis),<sup>[93]</sup> and the efficacy of **AI** is probably linked to changes in core fucosylation induced by DFJ. An interesting characteristic of  $\alpha$ -L-fucosidase is its insensitivity to anomeric substituents – even those with the wrong anomeric configuration. The inhibition values of  $\alpha$ - (i.e. above) and  $\beta$ - (i.e. below) homomethyl-deoxyfuconojirimycin ( $\alpha/\beta$ -HFJ, **AJ** & **AK**, respectively) are, for example, essentially the same ( $K_i$  = 0.0053-0.0058  $\mu$ M).<sup>[90,94]</sup> Experience has shown, however, that the inhibition of  $\alpha$ -L-fucosidases is crucially dependent on the preservation of ring configuration. Thus, the introduction of the 4-methyl appendage in Fleet's DFJ derivative **AL** led to extremely compromised inhibition towards  $\alpha$ -L-fucosidase (IC<sub>50</sub> = 0.50  $\mu$ M, human placenta).<sup>[95]</sup>

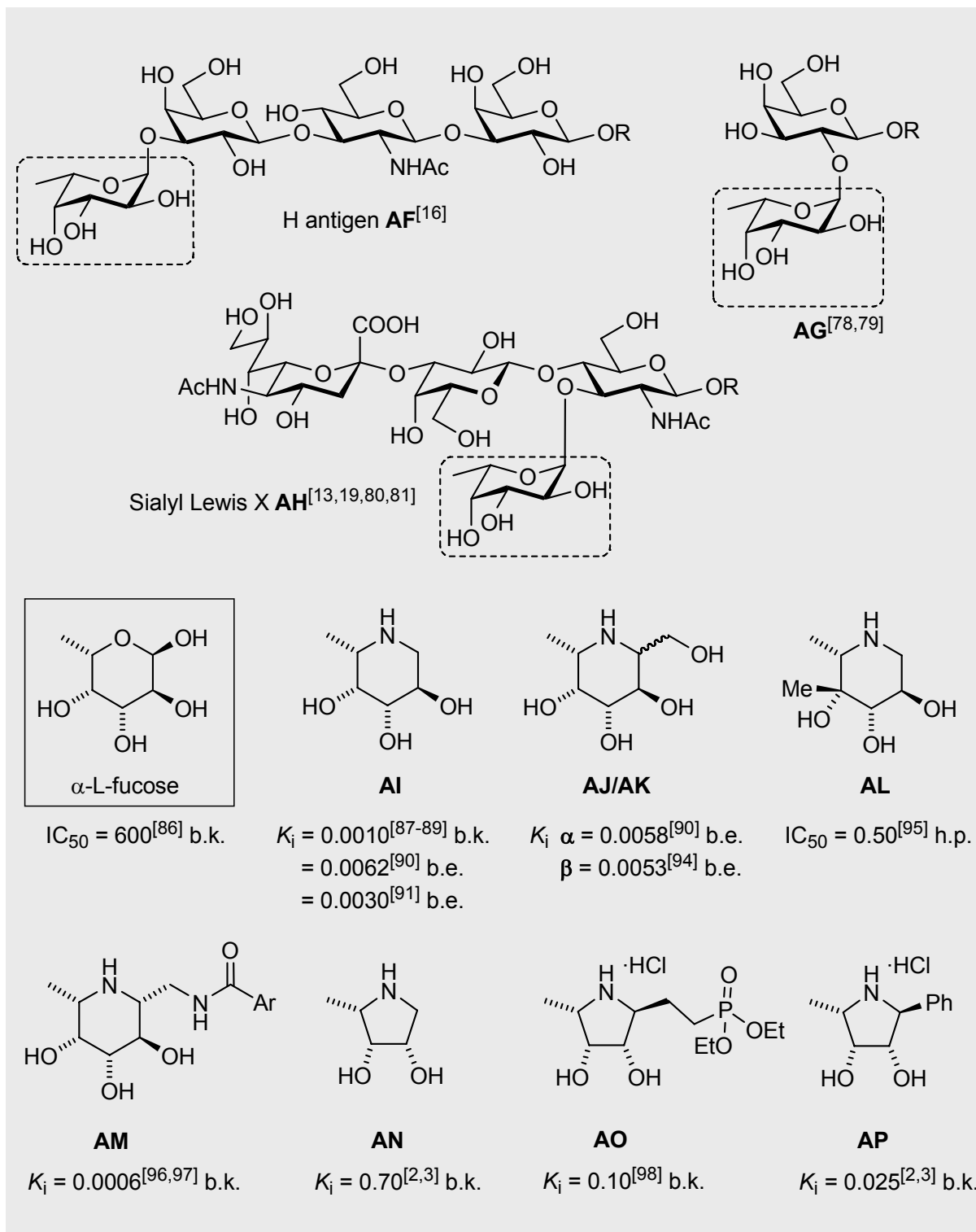


Diagram 9: Fucosylated glycoconjugates with biological significance (**AF**, **AG**, **AH**) and a selection of piperidine- and pyrrolidine-based  $\alpha$ -L-fucosidase inhibitors (**AI–AP**). Ar in **AM** = 5-fluoro-1*H*-indole.<sup>[96,97]</sup> **AI** = deoxyfuconojirimycin (DFJ); **AJ**, **AK** =  $\alpha$ - and  $\beta$ -homomethylfuconojirimycin, respectively ( $\alpha/\beta$  HFJ); enzyme source =  $\alpha$ -L-fucosidase, b.k. *bovine kidney*; b.e. *bovine epididymis*; h.p. *human placenta*. ( $IC_{50}/K_i$  inhibition concentrations in  $\mu$ M)

In comparison, substitution at C-2 with a large “amido-aromatic” side chain, as reported by Wong and co-workers, led to sub-nanomolar inhibitor **AM**.<sup>[96,97]</sup> To be discussed later in Section 6,  $\alpha$ -L-fucosidase can tolerate substrates with substitution at C-2. Likewise, polyhydroxylated pyrrolidines – generally thought to be poorer inhibitors of  $\alpha$ -L-fucosidase – perform better in the form of their C-2 substituted analogues (e.g. Defoin’s phosphonate derivative **AO**,<sup>[98]</sup>  $K_i = 0.10 \mu\text{M}$ , or, better still, Bierer and Jäger’s 2-phenyl derivative **AP**,<sup>[2,3]</sup>  $K_i = 0.025 \mu\text{M}$ ) compared to the ‘parent’ pyrrolidine **AN**<sup>[2,3]</sup> ( $K_i = 0.70 \mu\text{M}$ ; Diagram 9).

## 1.5 Aims of Dissertation

The main aim of this work entailed the synthesis of new inhibitors of  $\alpha$ -L-fucosidases by transforming L-lyxo nitron **5**, using a well-defined pathway according to Bierer,<sup>[2,3]</sup> into highly substituted polyhydroxylated pyrrolidines (see from Section 3 onwards). Bierer in his dissertation was fortunate enough to unearth 2-phenyl-substituted pyrrolidine **AP** (see Diagram 9, above) as one of the two (the other: 2-ester) new lead compounds in terms of inhibition potency towards  $\alpha$ -L-fucosidase from bovine epididymis ( $K_i = 0.05 \mu\text{M}$ ) and bovine kidney ( $K_i = 0.04 \mu\text{M}$ ). This was an unexpected result in relation to the body of literature known at that time (i.e. up until 1999) and compared to the activity of unsubstituted pyrrolidine diol **AN** ( $K_i = 0.70 \mu\text{M}$ , cf. Diagram 9). This result threw up the idea that other aromatic substrates might also show similar or even improved activity towards the target enzyme. Thus, it was envisaged that the phenyl side-chain in Bierer’s lead compound **AP** should be modified to give an indication of structure-activity relationships. To narrow down the range of possible target structures, an arbitrary decision was taken to synthesise several pyrrolidines with para-substituted aryl substituents only (Diagram 10). The biological results of these new fucosidase inhibitors are discussed from Section 6 onwards.

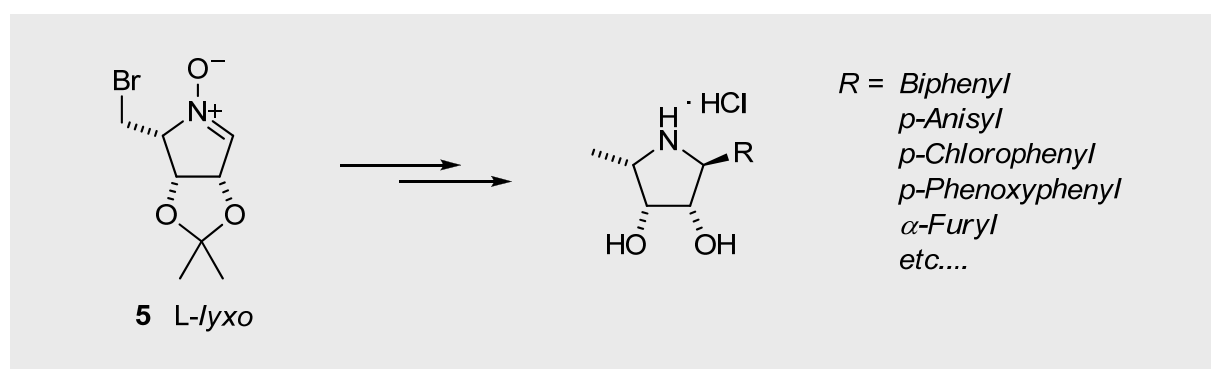


Diagram 10: Planned target structures from L-lyxo-nitron **5**

One other topic of this dissertation concerned the chemistry of *N*-hydroxypyrrolidines. After addition of Grignard nucleophiles to the *L*-lyxo-nitrone **5**, the resulting *N*-hydroxypyrrolidines are usually reduced further. One aim here was to investigate the opposite reaction, i.e. the oxidation of *N*-hydroxypyrrolidines to obtain new cyclic nitronone building blocks (from Section 4). Two precedents exist from Pothier<sup>[99]</sup> and Palmer,<sup>[4]</sup> previous members of the Jäger group, for the oxidation of *N*-hydroxypiperidines and *N*-hydroxypyrrolidines. Oxidation of *N*-hydroxypyrrolidines, shown in Diagram 11, can lead to nitrones of type **AQ** which are potentially useful in subsequent [3 + 2] cycloadditions (Section 4.3). Bromomethyl nitrones of type **AR** could also be useful for the synthesis of cyclic vinylnitrosonium cations (**AS**) – a reaction in direct parallel to the the silver ion-induced dehalogenation of  $\alpha$ -chloroaldonitrone **AT**, developed by Eschenmoser and colleagues<sup>[100]</sup> (see Section 4.4.). The enophile **AS** should undergo [4 + 2] cycloadditions (Section 4.5).

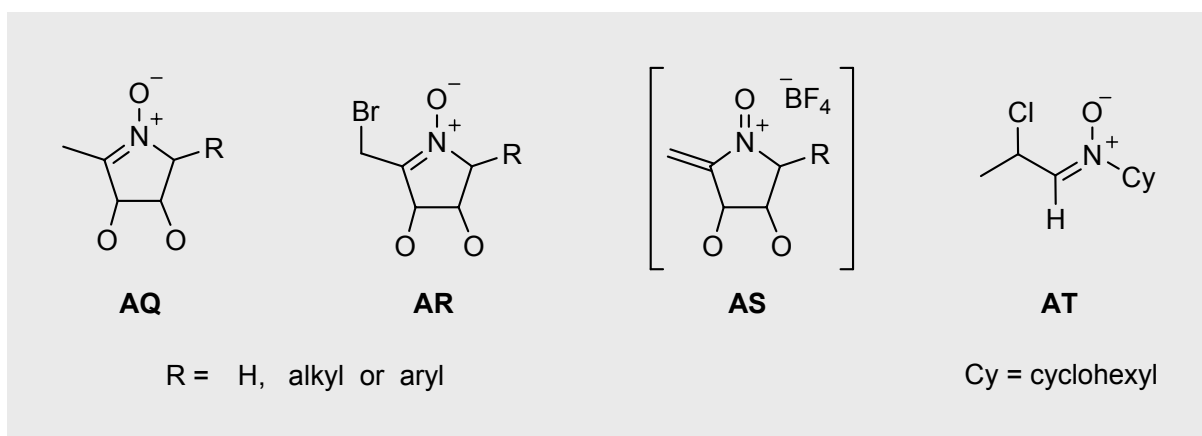


Diagram 11: Planned synthesis of nitrones **AQ** and **AR** through oxidation of *N*-hydroxypyrrolidines. The bromomethylnitrone **AR** should undergo silver ion-induced dehalogenation to provide vinylnitrosonium cation **AS**. For comparison, dehalogenation of  $\alpha$ -chloroaldonitrone **AT**, introduced by Eschenmoser,<sup>[100]</sup> is a facile process.



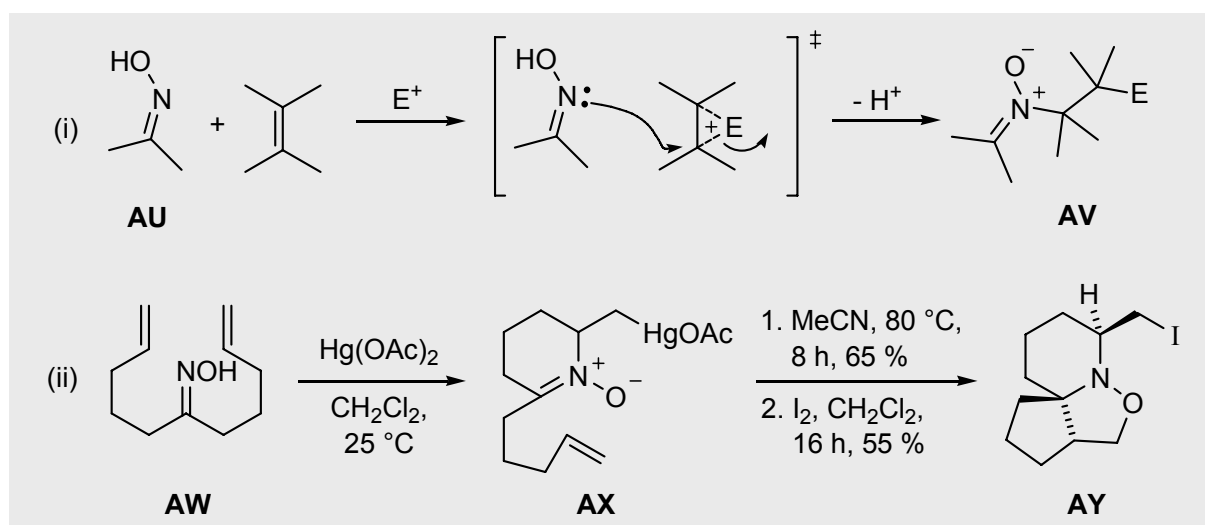
# 2

## Synthesis of Cyclic Nitrones

### 2.1 Synthesis of Cyclic Nitrones by Electrophilic Cyclisation of Unsaturated Oximes

#### 2.1.1 Seminal work by Grigg *et al.*

Since 1994, the group of V. Jäger has been engaged in the synthesis of  $\alpha$ -L-fucosidase inhibitors.<sup>[2,3,4,101]</sup> The entry to these compounds, due to failure with cyclopentane derivatives to obtain good fucosidase inhibition (J. Greul, lit.<sup>[102]</sup>), relies on the electrophile-induced cyclisation of sugar-derived  $\omega$ -unsaturated oximes, forming cyclic nitrones. The approach involves the cyclisation of an oxime, *via* nitrogen to a  $\pi$ -bond that has been activated by an appropriate electrophile. This process was in essence developed by Grigg *et al.*, who treated oximes (**AU**) with olefins to provide nitrones of type **AV** [case (i), Scheme 1]. The reaction is amenable to the use of a range of electrophiles such as palladium(II) chloride,<sup>[103]</sup> phenylseleninyl bromide,<sup>[104]</sup> mercury(II) acetate,<sup>[105]</sup> *N*-bromo-succinimide and (mediocre) iodine.<sup>[106]</sup>



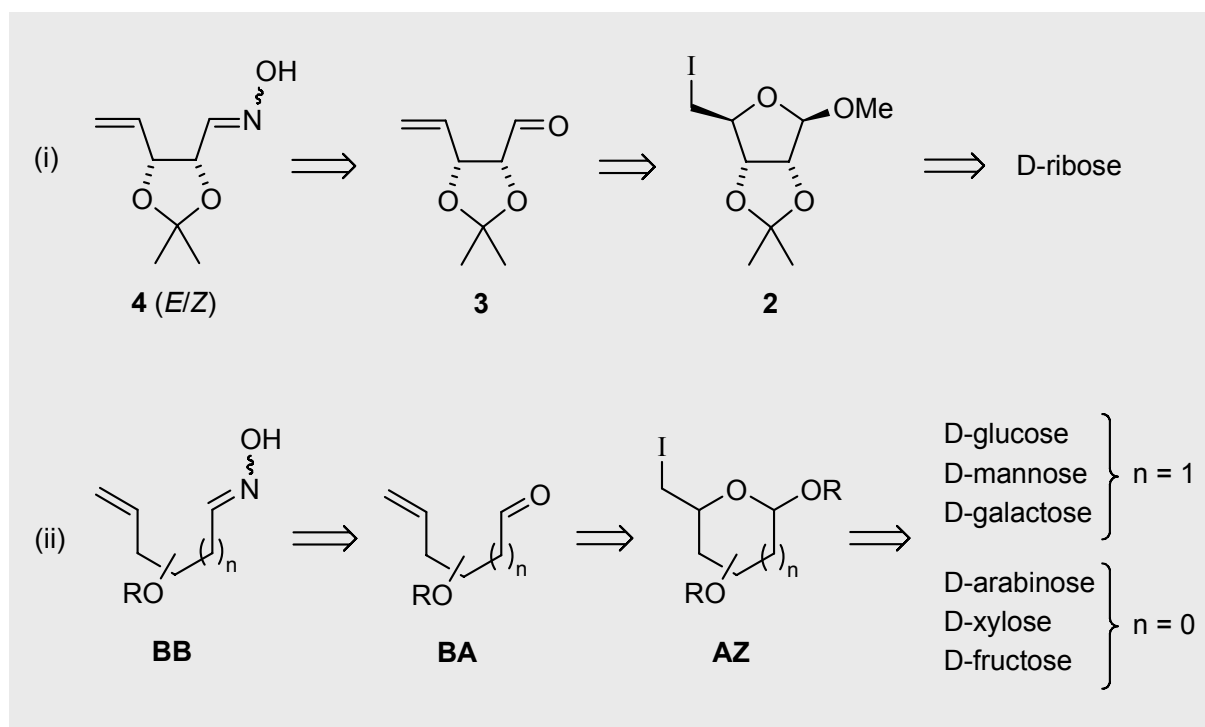
Scheme 1: Examples of Grigg's electrophile-induced cyclisation of unsaturated oximes<sup>[106]</sup>

In the case of palladium salts, Grigg employed O-allylated oximes to effect the known [2,3]-sigmatropic rearrangement for inter- and intramolecular trapping with dipolarophiles.<sup>[103,107]</sup> Grigg's next development constituted the intramolecular reaction of oximes bearing  $\gamma$ - or  $\delta$ -alkenyl substituents which upon treatment with various electrophiles provided five- and six-membered cyclic nitrones, respectively. Complexation, for example, of Hg(II) to bis- $\delta$ -alkenyl-substituted oxime **AW** gave the intermediate nitrone **AX** followed by a concomitant intramolecular cycloaddition to yield the tricyclic isoxazolidine derivative **AY**, as a single diastereoisomer [case (ii), Scheme 1]. This reaction class is neither restricted to the reaction of oximes with alkenes, nor to the use of electrophiles, listed above. Gallagher and co-workers<sup>[108]</sup> have demonstrated that allenes can be used as the acceptor in the Ag(I)-catalysed oxime-allene cyclisation for the preparation of five and six-membered nitrones. The product distribution of this transformation – i.e. nitrone *versus* oxazine formation – depended heavily on the oxime geometry.

### 2.1.2 Electrophilic cyclisations of oximes by Jäger and co-workers

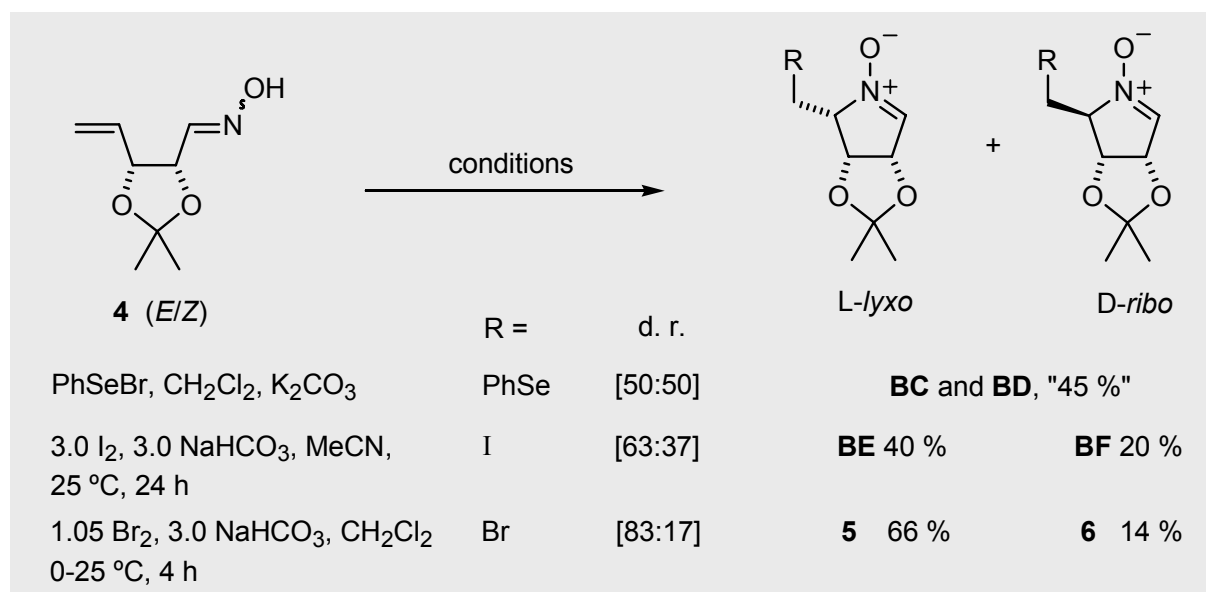
In 1994, Shaw and Jäger<sup>[109a]</sup> investigated the scope of electrophile-induced cyclisations applied to unsaturated oximes of 'chiral pool' origin. The chosen sugar, D-ribose, can be converted into the unsaturated oxime **4** *via* the aldehyde precursor **3**, using the 5-deoxy-5-iodo sugar **2** as the key intermediate. This disconnection is modelled heavily on the Vasella and Burnett<sup>[110]</sup>, and later Ganem<sup>[111]</sup>, approach to the reductive fragmentation of 6-bromo-6-deoxy pyranosides **AZ** with zinc, which leads to 5,6-dideoxy-5-hexenoses **BA** and, correspondingly, the incumbent oximes **BB**. Although, it should be noted that Jäger and Grund at the same time as Vasella could show that the synthesis of unsaturated oximes – both  $\alpha,\beta$  and  $\beta,\gamma$  " $\alpha$ -enoximes" – through the base-induced ring cleavage of 2-isoxazolines was possible.<sup>[109b]</sup> Interestingly, the fragmentation under Vasella's conditions has recently been demonstrated with 5-deoxy-5-iodo sugars derived from D-arabinose,<sup>[112]</sup> D-xylose<sup>[113]</sup> and D-fructose<sup>[114]</sup> (cf. Section 2.2.1.1). Mechanistically, the reaction has older routes, and is reminiscent of the synthesis of terminal olefins from ethers *via*  $\beta$ -alkoxyhaloalkanes through elimination with magnesium under mild conditions (a la Boord)<sup>[115]</sup> Shaw's variation was to conduct elimination of 5-deoxy-5-iodo sugar **2** with n-BuLi at -78 °C. Under these conditions a probable intermediary lithium hemi-acetal is generated at low temperature, which collapses cleanly upon warming and work-up with the expulsion of methanol to furnish the unsaturated pentenose **3**. This indeed turned out to be the case and, following oximation, the unsaturated pentenose oxime **4** was envisaged to be a good substrate for electrophile-induced cyclisation. The experimental description is contained in Section 2.2.1.2 and in Scheme 14.





Scheme 2: (i) Pathway to D-ribose-derived oxime **4** via fragmentation of 5-deoxy-5-iodo sugar **2**<sup>[2,3,109]</sup> and, (ii) literature-known unsaturated oximes derived from the fragmentation of several other 6-<sup>[110,111]</sup> and 5-iodo-deoxy sugars.<sup>[112-114]</sup>

Wightman et al.<sup>[116]</sup> applied Grigg's methodology to effect cyclisation of the oxime **4** with phenyl-selenium bromide yielding L-lyxo- and D-ribo-configured nitrones, **BC** and **BD**, respectively. The reaction proceeded in moderate yield ( $\Sigma$  50 %) and abysmal selectivity (d. r. **BC:BD** = 1:1). The iodocyclisation of Shaw and Jäger<sup>[3,109]</sup> led to improved yield and, importantly, gave moderate preference for L-lyxo-configured idonitronone **BE**. The iodocyclisation was further studied by Bierer,<sup>[2,3]</sup> who investigated several other iodine reagents (e.g.  $KI_3$ , N-iodosuccinamide) under basic conditions. The best results, nonetheless, were observed with iodine and sodium hydrogencarbonate in acetonitrile (d.r. **BE:BF** = 67:33); the idonitrones exhibited, however, a propensity to decompose (even at -20 °C) which precluded the measurement of correct elemental analysis. These foregoing trends were not observed in the case of the bromocyclisation of oxime **4** by Bierer.<sup>[2,3]</sup> This cyclisation afforded the two diastomeric nitrones, L-lyxo **5** and D-ribo **6** in a combined yield of up to 80 % (25 mmol scale), with very good selectivity towards the desired L-lyxo nitronone **5** (d. r. **5:6** = 83:17) (Scheme 3). The five synthetic steps from D-ribose culminated in a total yield of 37 % for nitrones L-lyxo **5** and 7.9 % for D-ribo **6**. Crucially, these nitrones, both crystalline (cf. Section 2.2.1.4 and lit.<sup>[182,186]</sup>) could also be handled at room temperature with all but any detectable decomposition.



Scheme 3: Electrophile cyclisation of oxime **4** with phenylselenium bromide from Wightman<sup>[116]</sup> and improved iodo- and bromocyclisation by Jäger, Shaw<sup>[3,109]</sup> and Bierer<sup>[2,3]</sup> resulted in the key building-block *L*-lyxo nitronium **5**.

With the *L*-lyxo-bromomethylnitronium secured, Gulla set about the systematic exploration of the scope of the enoxime bromocyclisation.<sup>[117,118]</sup> Several  $\gamma,\delta$ -unsaturated oximes were prepared which led to the respective bromomethyl-cyclic nitroniums. Yields varied from 23 to 87 %, depending on the structural features (Diagram 12).

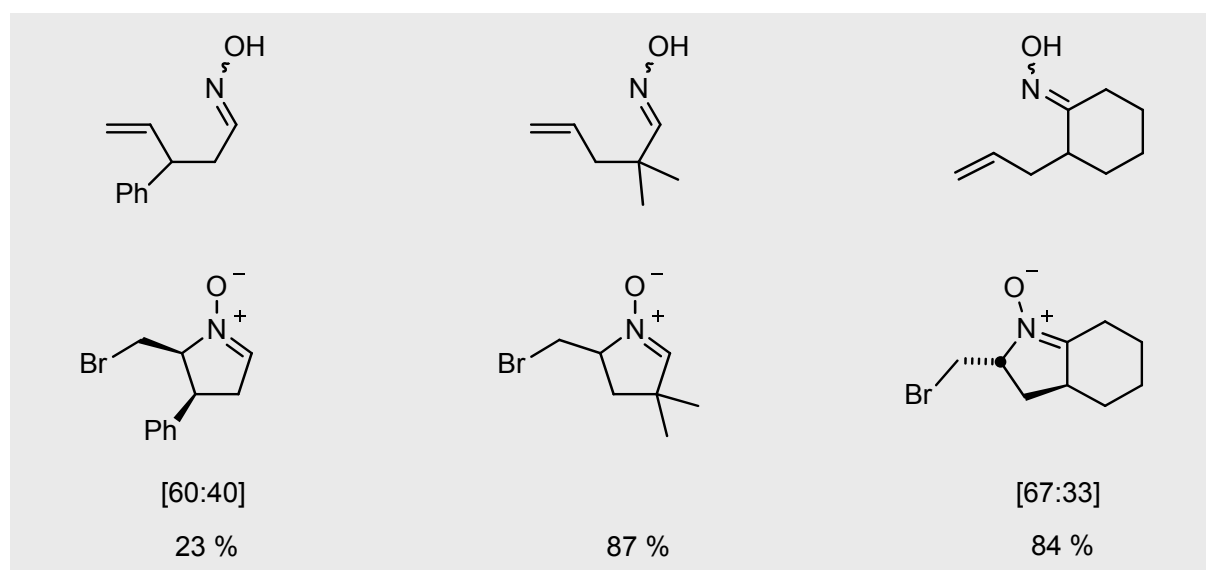
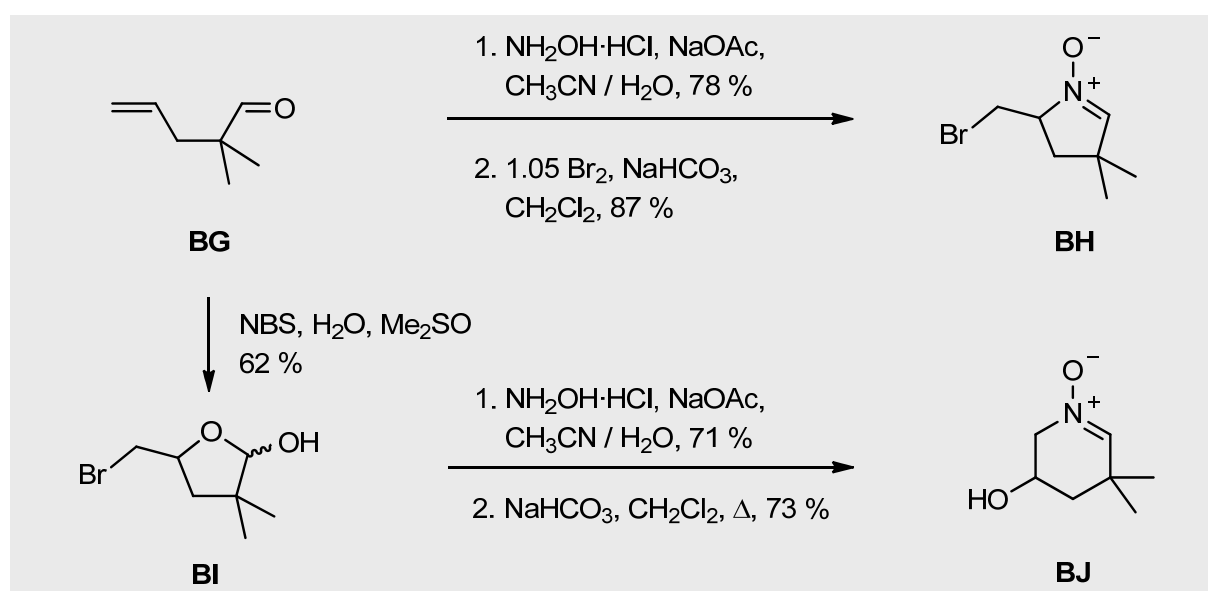


Diagram 12: Further unsaturated oximes used for bromocyclisation under standard conditions, i. e. 1.05 Eq. Br<sub>2</sub>, 3.0 Eq. NaHCO<sub>3</sub>, CH<sub>2</sub>Cl<sub>2</sub>. Adopted from lit.<sup>[117]</sup> (M. Gulla). In case of diastereoisomeric mixtures, only the major one is depicted.

Up until now, cyclisations of  $\gamma,\delta$ -unsaturated oximes induced by electrophiles led to 5-membered nitrones, observing the *exo*-cyclisation mode without exception – in accordance with entropy and with Baldwin's empirical rules for ring-closures.<sup>[119]</sup> The latter also applied to  $\delta,\epsilon$ -enoximes where trihydro-pyridine-1-oxides are formed (cf. Scheme 5). Gulla, however, demonstrated the possibility of *endo*-cyclisation with  $\gamma,\delta$ -unsaturated oximes. Recourse to 3,3-dimethyl-4-butenal **BG** illustrates this point (Scheme 4): its oxime led to a high yield of the bromomethyl-nitronone **BH**, whereas treatment of the aldehyde with *N*-bromosuccinimide in DMSO/water afforded the bromohydrin **BI** (present as the hemiacetal). After transformation to the oxime followed by heating at reflux in  $\text{CH}_2\text{Cl}_2$ , the six-membered nitronone **BJ** was secured in 73 %.

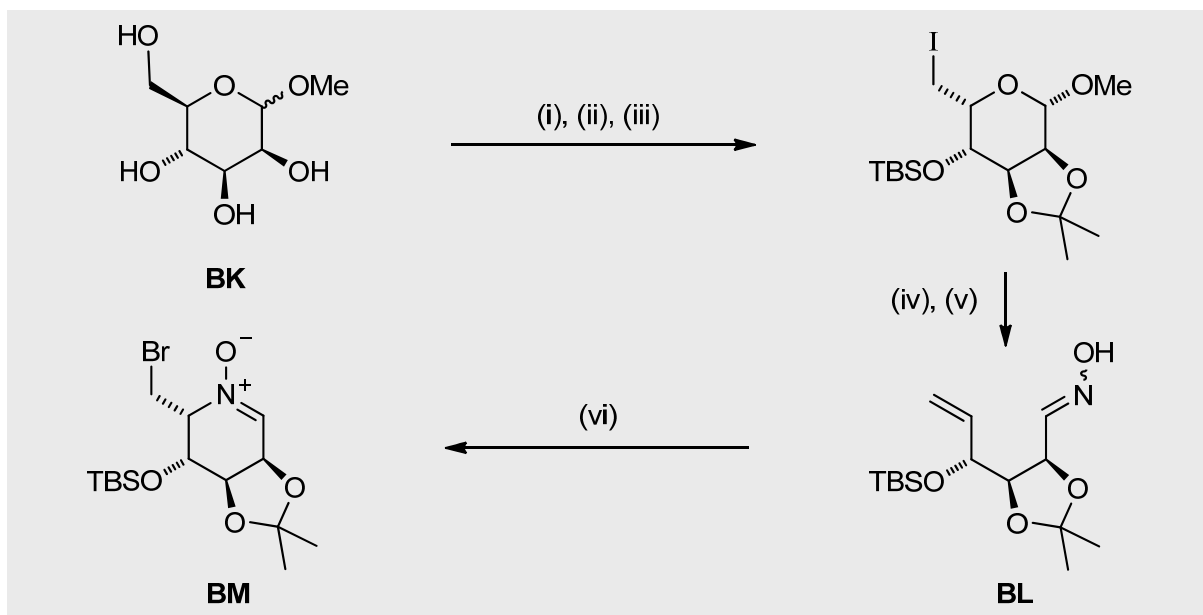


Scheme 4: *Exo*- and *endo*-cyclisation modes from aldehyde substrate **BG**. Adopted from lit.<sup>[117]</sup> (M. Gulla and Jäger).

The “bromohydrin route” has been extended by Castiglia.<sup>[101]</sup> This investigation, which employs D-ribose-derived pentenose **3** as starting material, can ostensibly be described as “work in progress” and will therefore not be discussed here further.

The bromocyclisation has seen application with the oximes of sugar-derived 5,6-dideoxy-5-hexenoses (i.e. of type **BB**, see Scheme 2).<sup>[120,121]</sup> Unlike the bromocyclisation of Bierer's pentenose oxime **4**, or the majority of those featured in Gulla's work, the bromine-induced cyclisation of 5-hexenose oximes has been met with mixed results. Yields are typically lower, possibly due to competing pathways (i.e. isoxazoline formation), and the incompatibility of certain protecting groups to the conditions of cyclisation.<sup>[120]</sup> The bromocyclisation of 5-

hexenose oxime **BL** by Hahn<sup>[120]</sup> and Wallasch<sup>[121]</sup> represents the current ‘best case’ result. The oxime **BL** was prepared from methyl  $\alpha$ -D-mannopyranoside **BK** according to the route outlined in Scheme 5 (5 steps, 28 % overall yield), and subjected to ‘standard’ cyclisation conditions to yield the 6-membered nitrone **BM** as a single diastereoisomer in 45 % yield. No discussion of possible decomposition or co-products is given.<sup>[121]</sup> Further investigation, however, in this area is currently underway by J. Heller (Dissertation).<sup>[122]</sup>



Scheme 5: Synthesis of the six-membered nitrone **BM** from Wallasch:<sup>[121]</sup> (i) pTsOH, acetone, DMP, r. t., 13 h, 70 %; (ii) I<sub>2</sub>, PPh<sub>3</sub>, imidazole, toluene, 80 °C, 2 h, 90 %; (iii) tBuMe<sub>2</sub>SiOTf, CH<sub>2</sub>Cl<sub>2</sub>, r. t., 2 h, 95 %; (iv) Zn, NH<sub>4</sub>Cl, vit. B<sub>12</sub> (cat.), 21 h, r. t., MeOH; (v) NH<sub>2</sub>OH·HCl, pyridine, r. t., 20 h,  $\Sigma$  54 % (2 steps); (vi) Br<sub>2</sub>, NaHCO<sub>3</sub>, CH<sub>2</sub>Cl<sub>2</sub>, 0 – 25 °C, 45 %.

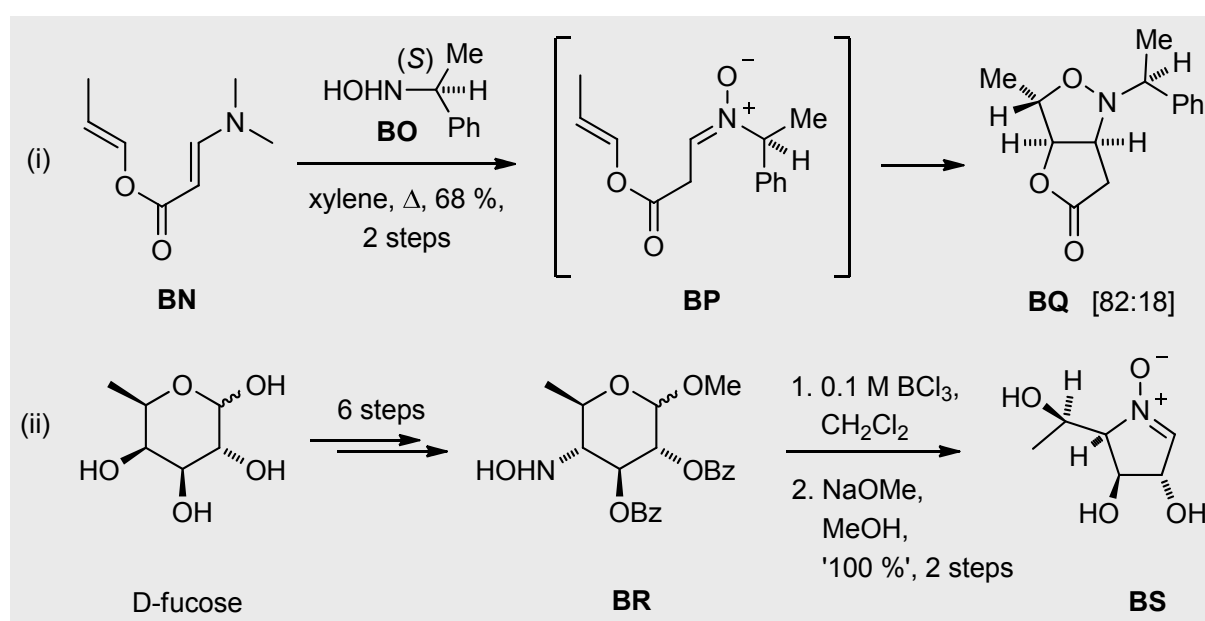
### 2.1.3 General and miscellaneous examples of nitrone syntheses

Nitrones are easily accessible synthetic intermediates and very useful tools in the construction of complex molecules and biologically active, nitrogen-containing compounds. Review articles by Döpp and Döpp (*Houben-Weyl*)<sup>[123]</sup> and Merino (*Science of Synthesis*)<sup>[124]</sup> address general aspects of nitrone synthesis while a more recent review by Brandi<sup>[125]</sup> and co-workers considers the synthesis of enantiopure cyclic nitrones; the review is conveniently organized according to the size of the nitrone ring. Nitrone syntheses which are of general utility involve the condensation of N-monosubstituted hydroxylamines with carbonyl compounds (for aldonitrones),<sup>[123,124,126]</sup> or the zinc-mediated reduction of  $\gamma$ -nitro-aldehydes and ketones (for ketonitrones), as has been reported by Todd<sup>[127]</sup> and Black.<sup>[128]</sup>

Nitrones are also accessible through the oxidation of secondary amines. Generally, a suitable metal catalyst, such as selenium dioxide,<sup>[129]</sup> sodium tungstate<sup>[130]</sup> or methyltrioxorhenium,<sup>[131]</sup> is mixed with 30 % aqueous hydrogen peroxide. A safer variation has been reported by Shibata<sup>[132]</sup> and Goti and co-workers,<sup>[133]</sup> which uses a hydrogen peroxide-urea complex in combination with methyltrioxorhenium. In addition, Davis' reagent [(phenylsulfonyl)-3-phenyloxaziridine]<sup>[134]</sup> and dimethyldioxirane (DMDO)<sup>[135]</sup> are also known oxidants for the transformation of secondary amines to nitrones.

For the oxidation of *N,N*-disubstituted hydroxylamines, several reagents are known. This will be, however, discussed later in Section 4 (onwards) along with experimental results of the oxidation of 2- and 2,5-disubstituted *N*-hydroxypyrrolidines.

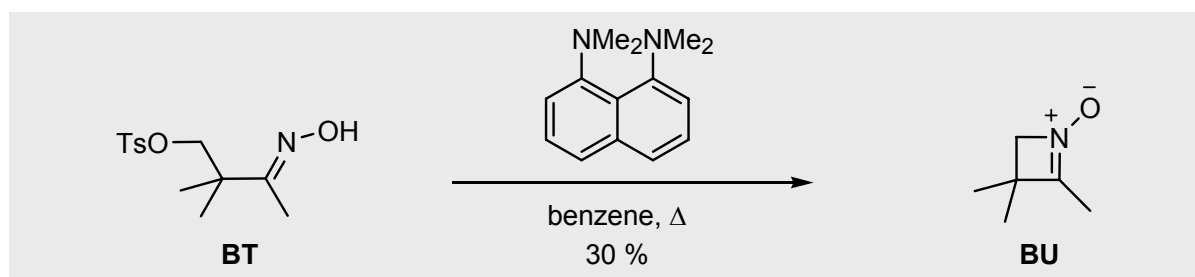
The methods of nitrone synthesis described so far are relatively well-established procedures. It is worth noting some less common methods that offer entry to a wider choice of nitrone derivatives. For example, the chiral nitrone **BP** was obtained by treating the enamine **BN** with the oxalate salt of *N*-[(*S*)-1-phenylethyl]-hydroxylamine **BO**. Concomitant enantioselective [3 + 2] cycloaddition afforded the isoxazolidine **BQ** [case (i), Scheme 6], which constitutes a precursor to acosamine (i.e. the sugar fragment of an anthracycline-based antibiotic).<sup>[136]</sup> In another interesting example, Golik and co-workers<sup>[137]</sup> synthesised the D-fucose-derived hydroxy amino sugar **BR** in 6 steps. Spontaneous nitrone formation during 'demethylation' with 0.1 M BCl<sub>3</sub> at -78 °C and hydrolysis of the benzoate groups led to the required cyclic nitrone **BS**, which proved of use for determining the configuration of the four asymmetric centres of the hydroxy amino sugar fragment of esperamicin A<sub>1</sub> [case (ii), Scheme 6].



Scheme 6: Nitron syntheses from (i) Wovkulich<sup>[136]</sup> and (ii) Golik<sup>[137]</sup>

### 2.1.4 Synthesis of cyclic nitrones by intramolecular *N*-alkylation ( $S_N2$ -type) of oximes

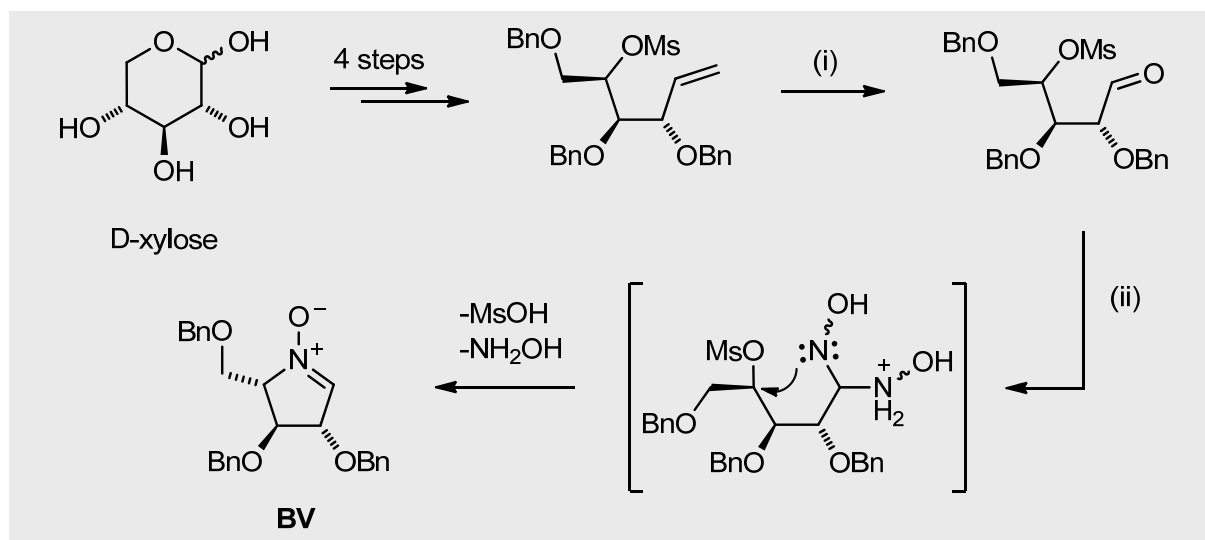
The *N*-alkylation of oximes is a valuable tool for the synthesis of cyclic nitrones. Generally, the intramolecular variant of this reaction can be initiated when suitable leaving groups are situated at  $\beta$ -,  $\gamma$ - or  $\delta$ -position to an (*E*)-oxime, leading to 4-, 5- or 6-membered cyclic nitrones, respectively, whereas the corresponding (*Z*)-oximes are preferentially *O*-alkylated. The presence of certain substituents can favour the formation of conformationally strained nitrones. For example, taking the oxime **BT** with naphthalene-1,8-diamine ('proton sponge') provided 2,3,3-trimethyl-3,4-dihydroazet-1-oxide **BU** in 30 % yield (Scheme 7).<sup>[138]</sup> The oxime **BT** bears a *gem*-dimethyl moiety and is assisted in the cyclisation by the Thorpe-Ingold effect<sup>[139]</sup> to counteract the energy barrier of forming disfavoured strained cyclobutene rings (ca. 30 kcal/mole).<sup>[140]</sup>



Scheme 7: Black's synthesis of the novel four-membered nitrone **BU**<sup>[138]</sup>

Tamura's<sup>[141]</sup> method for the selective *N*-alkylation of *O*-silylated  $\gamma$ -mesyloxy oximes has become popular. The prerequisite silylated oximes are obtainable from sugar-derived lactols in expedient fashion. After oximation, the unmasked  $\gamma$ -hydroxyl group is transformed into a leaving group (usually mesylate, but not always) to give *O*-silylated  $\gamma$ -mesyloxy-oximes. Upon desilylation with 'non-basic' fluoride ion (tetrabutylammonium triphenyldifluorosilinate 'TBAT') (to avoid competing  $\beta$ -elimination of the mesyloxy group), cyclisation proceeds spontaneously to afford cyclic 5-membered nitrones (4 examples, lit.<sup>[141]</sup>). Reproducibility problems using TBAT have, however, been recently reported.<sup>[142]</sup> *O*-Silylation is necessary to obviate the problem of the competing *O*-alkylation of (*E*)-oximes (which would lead to 1,2-oxazines).<sup>[123]</sup> Tamura himself was probably inspired by the seminal work of LeBel and Balasubramanian<sup>[143]</sup> which dealt with the *N*-alkylation of *O*-trimethylsilyloximes with trialkyloxonium tetrafluoroborates (*viz.* Meerwein's reagent). An alternative is to first treat sugar-derived lactols with Wittig reagents (i.e. Ph<sub>3</sub>P=CH<sub>2</sub>), followed by mesylation and ozonolysis. The resulting aldehydes are allowed to react with a moderate excess of

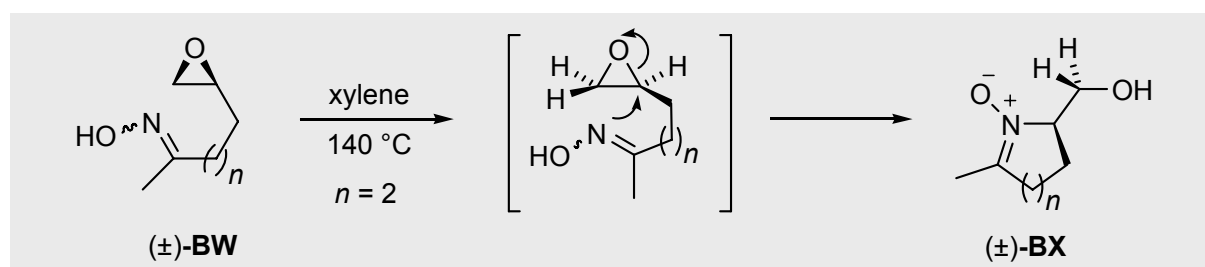
hydroxylamine (usually 2 equivalents) to afford cyclic nitrones. Examples of this strategy have been published by Wightman<sup>[144]</sup> and more recently by Huang and Yu.<sup>[145]</sup> Taking Huang's report as a representative example, the cyclic nitrone **BV** could be obtained from D-xylose in 8 steps and ca. 21 % overall yield (Scheme 8).



Scheme 8: D-Xylose-derived synthesis of nitrone **BV** by Huang and Yu: (i)  $O_3/O_2$ ,  $CH_2Cl_2$ ,  $-40$  °C, (ii) 2 Eq.  $NH_2OH \cdot HCl$ ,  $Et_3N$ ,  $H_2O$ - $MeOH$ , r.t. to  $60$  °C (D-xylose, 8 steps,  $\Sigma$  ca. 21 %).

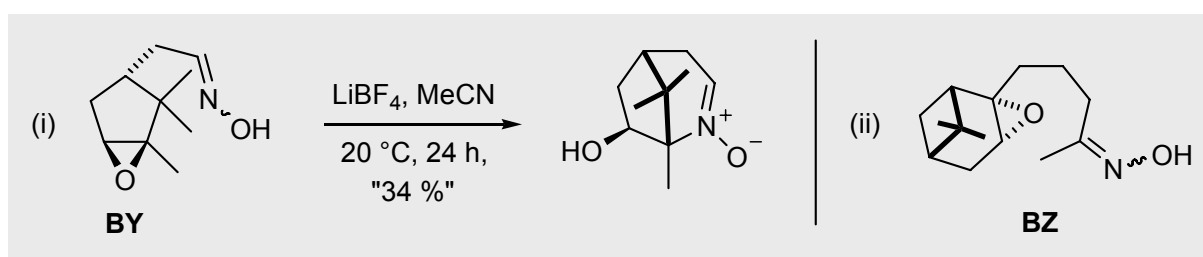
### 2.1.5 Synthesis of cyclic nitrones by epoxide opening

This variation of cyclic nitrone synthesis by *N*-alkylation of oximes *via* epoxide-opening was first demonstrated by Grigg et al. in 1989.<sup>[146]</sup> The intramolecular variation can be considered analogous to the internal oxirane ring-opening with epoxy alcohols to generate tetrahydrofurans and -pyrans.<sup>[147]</sup> For example, Grigg reported the reaction of the  $\delta$ -epoxyheptanone oxime **BW** which underwent thermal 6-*exo*-tet ring-closure to yield a 6-membered cyclic nitrone **BX** (Scheme 9).<sup>[148]</sup> No competing 1,2-oxazepine formation nor 7-*endo*-tet ring-opening were observed (thus obeying Baldwin's rules for ring-closure).<sup>[119]</sup>



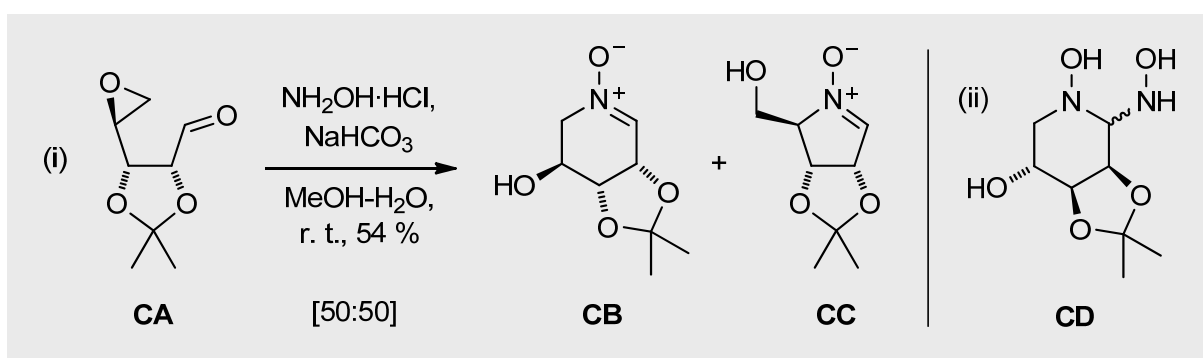
Scheme 9: Six-membered cyclic nitrone synthesis through epoxide opening<sup>[148]</sup>

The facility of this process requires the geometry of the attacking nucleophile and the breaking oxirane C-O bond to be co-linear (i.e.  $S_N2$ -like). Grigg has, in relation to this, pointed out that longer reaction times and forcing conditions were required for test substrates with steric encumbrance. For example, cajoling epoxycampholenal oxime **BY** into a facially selective 6-*exo*-tet cyclisation was only possible after epoxide activation with  $\text{LiBF}_4$  (30 mol %, 34 % yield) [case (i), Scheme 10].<sup>[149]</sup> Lithium chloride as ‘activator’ was also used, although this was accompanied by competing chlorohydrin formation, which led to poorer yields.<sup>[148]</sup> In comparison, the  $\alpha$ -pinene derived oxime **BZ** was disinclined to react – even under forcing conditions [case (ii), Scheme 10]. Grigg attributed the non-reactivity to the  $\text{C}(\text{CH}_3)_2$  moiety, which is purported to shield the epoxide from ‘back-side’ cleavage by the internal oxime nucleophile in either 6-*exo*-tet or, alternatively, 7-*endo*-tet manner.



Scheme 10: Troublesome reactivity of sterically encumbered epoxyoximes<sup>[148,149]</sup>

Elsewhere, the reaction of the D-ribose-derived epoxyaldehyde **CA**<sup>[150]</sup> with hydroxylamine led to a non-regioselective 1:1 mixture of six- and five-membered nitrones, **CB** and **CC**, respectively [case (i), Scheme 11].<sup>[151]</sup> However, the chosen conditions were probably not forcing enough to drive the reaction to completion, which explains why the isolation of a related co-product, the cyclic bis-hydroxylamine **CD** (from experiments in the opposite enantiomeric series) was possible [case (ii), Scheme 11]. That the cyclisation may occur through the intermediacy of a geminal bis(hydroxylamine) is also of no exception: Vasella has reported similar intermediates from a cyclisation which produced a nitronium related to L-fucose.<sup>[152]</sup>

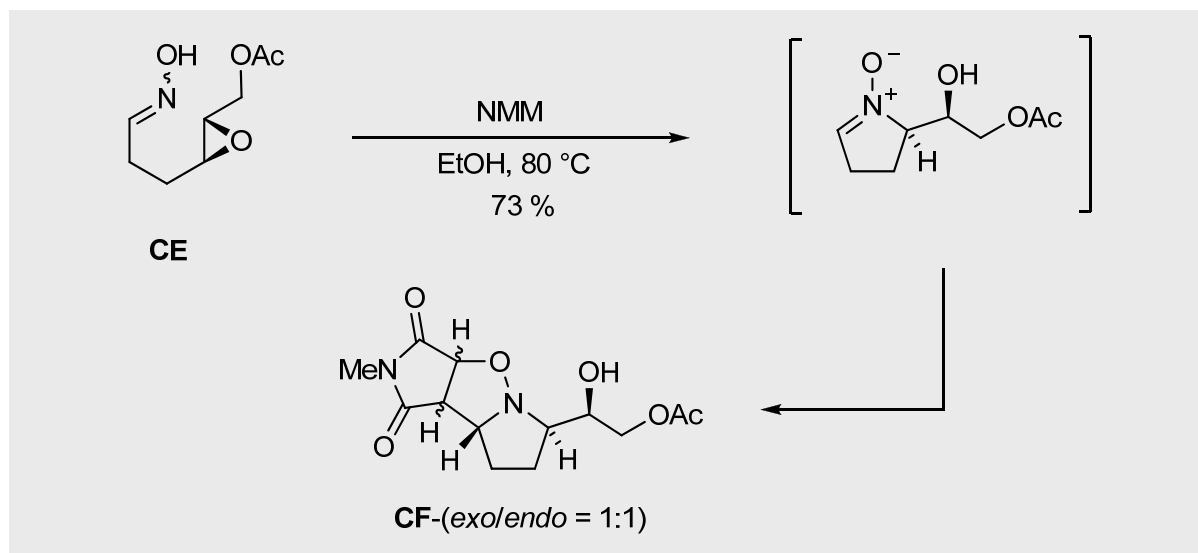


Scheme 11: Non-regioselective epoxide opening from Wightman<sup>[151]</sup>



Ring-closure of terminally *unsubstituted*  $\gamma$ -epoxyoximes may intrinsically be beleaguered by regioselectivity issues, irrespective of whether actual oximes or geminal bis(hydroxylamine)s are the alkylating species involved. It is particularly interesting to note that in this respect Grigg and co-workers divulge no findings to suggest the contrary. Among the assortment of epoxyoximes tested in Grigg's work, no report of the reactivity of 5,6-epoxy-2-hexanone oxime [i.e. the  $n = 1$  analogue of the epoxyoxime ( $\pm$ )-**BW**, see Scheme 9] is given, and so a comparison between the cyclisation of *unsubstituted*  $\gamma$ - and  $\delta$ -epoxyoximes unfortunately is not possible.<sup>[146,148,149]</sup>

From Grigg's work, the only class of  $\gamma$ -epoxyoximes that undergo regioselective 5-*exo* cyclisation are those where a substituent is present at the distal end of the epoxide. The reaction of Grigg's  $\gamma$ -epoxyester oxime **CE** is representative (Scheme 12): The structures of the nitrones were determined after the attendant [3 + 2]-cycloaddition with *N*-methylmaleimide ('NMM') in which two products **CF** arose by a facially selective cycloaddition to the nitron C=N part *anti* to the bulky CH(OH)CH<sub>2</sub>OAc substituent.<sup>[149]</sup> Incidentally, oxiranyl esters are themselves noted for their reactivity; rearrangements involving neighbouring group participation and/or orthoester formation have literature precedents.<sup>[153,154]</sup>



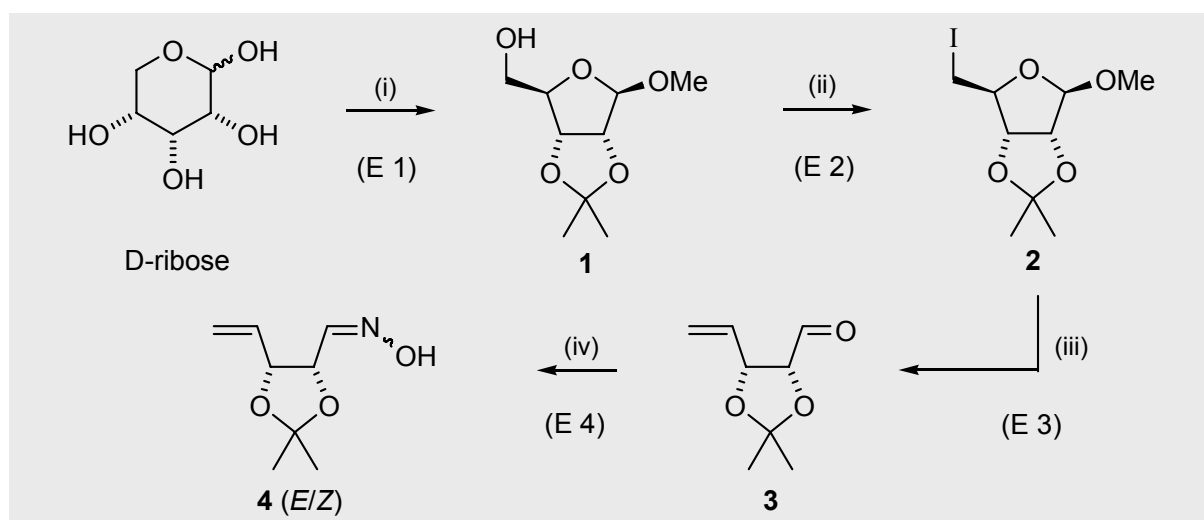
Scheme 12: Selectivity for 5-*exo* cyclisation reflects the use of terminally substituted epoxides which provided the 5-membered nitron intermediate.<sup>[149]</sup>

## 2.2 Results and Discussion

### 2.2.1 Synthesis of cyclic nitrones, L-lyxo 5 and D-ribo 6

#### 2.2.1.1 Synthesis of the unsaturated pentenose oxime 4 from D-ribose

As the reader may already have gathered (see Section 2.1.2.), pentenose oxime **4** is obtainable from D-ribose in 4 efficient steps.<sup>[2,3,4,109]</sup> The route has been developed extensively and used by Bierer.<sup>[2]</sup> However, the method to introduce the 1,3-dioxolane system<sup>[155]</sup> to afford protected D-ribose derivative **1** needed to be improved. Using a modified transacetalation procedure of van Tilberg and co-workers,<sup>[156]</sup> by employing HCl gas for the acid-catalysed isopropylideneation of D-ribose, shorter reaction times (4 h) and improved yields (91 %; cf. lit.<sup>2,157</sup> ca. 70 %) were obtained. In comparison, Leonard and Carraway's<sup>[157]</sup> method for D-ribose protection is afflicted by variable yields and significant side-product formation, invariably due to the protracted reaction length and slow onset of monoacetone-1,5-anhydroribofuranose.<sup>[158]</sup> The 5-hydroxyl group was then smoothly substituted according to a standard procedure<sup>[159,160]</sup> in excellent yield (84 %; cf. lit.<sup>2,159</sup> ca. 90 %) to provide the 5-deoxy-5-iodosugar **2**. Very recently, milder reaction conditions for iodination, perhaps better suited for larger experiments (e.g. dichloromethane at room temperature) have been published,<sup>[161]</sup> although no evaluation of these conditions was undertaken in this Thesis.

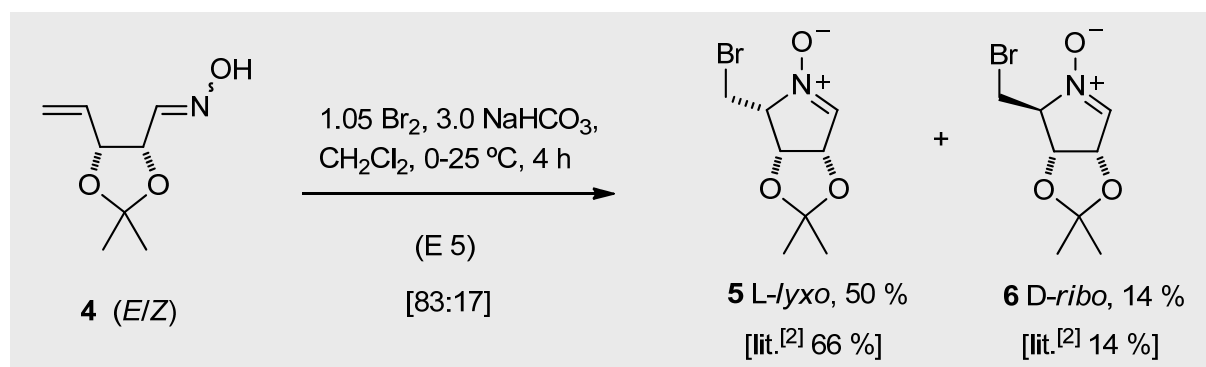


Scheme 13: Synthesis of unsaturated  $\omega$ -oxime **4** from D-ribose (4 steps,  $\Sigma$  67 %): (i) DMP, acetone, MeOH, HCl (gas), 4 h, r. t., 91 % (lit.<sup>[156]</sup> 95 %); (ii) I<sub>2</sub>, PPh<sub>3</sub>, 70 °C, imidazole, toluene, 84 % (lit.<sup>[2]</sup> 90 %); (iii) n-BuLi, THF, -80 °C, (iv) NH<sub>2</sub>OH·HCl, Na<sub>2</sub>CO<sub>3</sub>, EtOH/H<sub>2</sub>O, r. t. 16 h, 2 steps,  $\Sigma$  87 % (lit.<sup>[2]</sup>  $\Sigma$  90 %).

Treatment of the iodofuranose **2** with n-butyllithium at -78 °C induced a reductive elimination (*Boord* reaction)<sup>[115]</sup> to afford protected pentenose **3**, followed immediately by an *in situ* condensation with the free base of hydroxylamine hydrochloride to obtain unsaturated oxime **4** (2 steps,  $\Sigma$  87 %; lit.<sup>[2]</sup> 90 %; *E:Z* product mixture = 2:1). For the transformation of **2** to **3**, which is analogous to the ring-opening of related 6-deoxy-6-halopyranosides (cf. Scheme 2), the reagent choice is not restricted to n-butyllithium.<sup>[2,3,4,110a]</sup> Zinc is most commonly taken, conducted in various alcoholic solvent as done by Bennett and Vasella<sup>[110]</sup> (cf. Jäger and Grund<sup>[109b]</sup>; related review from Madsen<sup>[162]</sup>). An improvement on this has been developed in the Jäger group by Kleban<sup>[163,164,165,166]</sup> by combining zinc with catalytic amounts of vitamin B<sub>12</sub>. This methodology is the basis for the efficient synthesis of hexenose derivatives elaborated from D-glucose,<sup>[4,120,163,164,167,168,169]</sup> D-mannose,<sup>[120,122,164,167,169,170,171,172]</sup> D-galactose,<sup>[120,164,169,173,174]</sup> L-galactose<sup>[102,122]</sup> as well as D-glucosamine.<sup>[164,165]</sup> Apparently, by using vitamin B<sub>12</sub>, the formation of by-products due to competing reduction of 6-deoxy-6-iodo-sugars, known to afflict other zinc reagents,<sup>[175]</sup> can largely be circumvented.<sup>[164]</sup> Also, competing reductive elimination of O-benzyl protecting groups of certain D-*gluco*-pyranosides<sup>[110]</sup> is not observed, as has been reported elsewhere.<sup>[164]</sup> However, it has been noted recently that the efficiency of the vitamin B<sub>12</sub>-catalysed process can be perturbed by reaction scale-up, resulting in less than satisfactory product yields.<sup>[176]</sup> Zinc and zinc/vit. B<sub>12</sub> reagent combinations were investigated by Palmer<sup>[4a]</sup> with the substrate in question, 5-deoxy-5-iodosugar **2**, followed by condensation with *N*-benzyl hydroxylamine. Reactions with the zinc reagents, however, gave lower yields than n-butyllithium over these two steps.

### 2.2.1.2 Bromocyclisation of pentenose oxime **4**

Treatment of pentenose oxime **4** with elemental bromine and sodium hydrogencarbonate led to a mixture of diastereomeric nitrones (L-*lyxo* **5** = 50 %; D-*ribo* **6** = 14 %; d. r. **5:6** = 83:17 from <sup>13</sup>C NMR). Recently, Schmidt<sup>[177]</sup> also recorded a combined yield of 67 % for this step, which is somewhat lower than Bierer's<sup>[2]</sup> reported yield of 80 % for reactions carried out on a small scale (25 mmol) (cf. Scheme 3). Although the yield for this step amounted to 64 % in this thesis, if one takes into account the improved yield for the isopropylideneation (i.e. protection of D-ribose to yield **2**), the overall yield for the synthesis of L-*lyxo* nitrone **5** still amounts to 33 % (Bierer: 37 %) while the yield of D-*ribo* nitrone **6** is actually improved slightly to 9.3 % (Bierer: 7.9 %) for the five synthetic steps. This is quite useful, since the D-*ribo* nitrone has proved *also* of utility in the synthesis of new nitrone building blocks (see oxidation of 2-bromomethyl-1-hydroxypyrrolidines from Section 4 onwards).



Scheme 14: Bromocyclisation of pentenose oxime **4** affording the nitrones, L-lyxo **5** and D-ribo **6** (IUPAC: 2-bromomethyl-dihydro-2H-pyrrole-1-oxide).

### 2.2.1.3 Reaction pathway of the bromocyclisation of oxime **4**

The favoured *cis*-stereoselectivity (i.e. at substituents C-2/C-3) for the bromocyclisation of oxime **4** is in accordance with literature studies from Chamberlin, Hehre<sup>[178]</sup> and others<sup>[179]</sup> which describe the directing effect of an allylic hydroxyl or ether functionality during the halocyclisations. This model (scaled down for clarity using allyl alcohols below)<sup>[178b]</sup> states a kinetically controlled addition and assumes a reactant-like (early) transition state. The nucleophile is thought to cyclise onto a “ $\pi$ -complex” before it has chance to form an “onium ion” (although, this can be temperature dependent, *see below*). The model predicts electrophile attack preferentially at the face of the  $\pi$ -bond which is *syn* to the allylic hydrogen (i.e. “OH in plane” conformation) to afford the *cis* (*erthyro*) diastereoisomer **CG**.

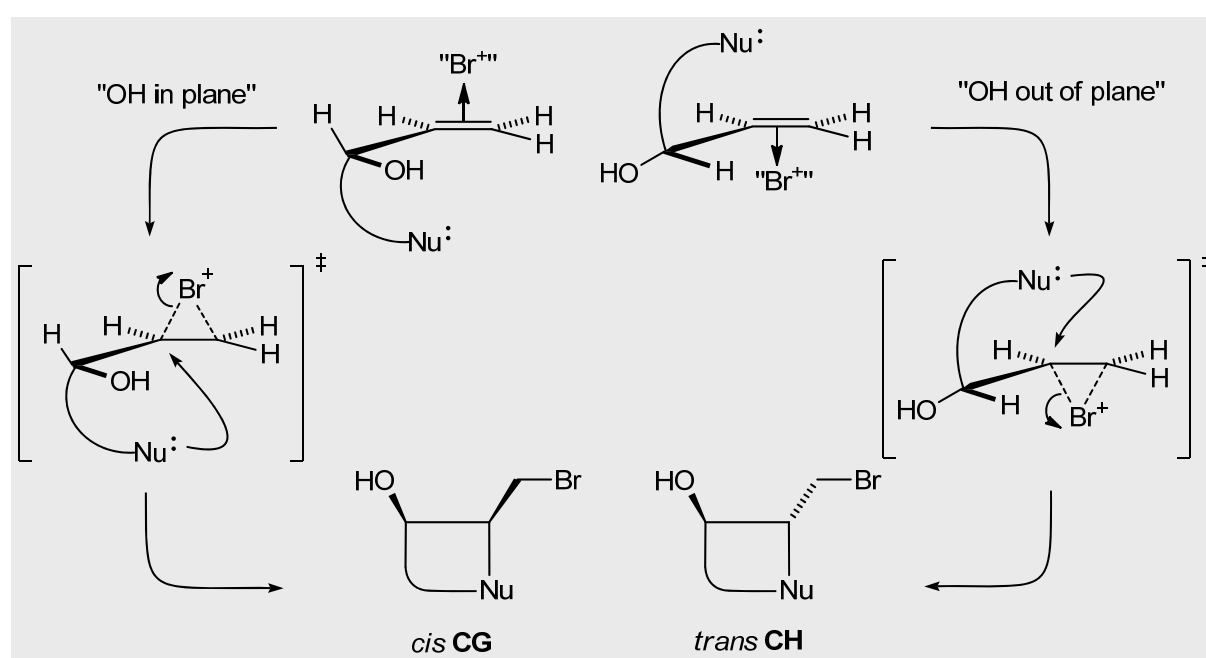


Diagram 13: Model representation of the electrophile induced cyclisation of allyl alcohols

However, in the “OH out-of-plane” conformation, where the allylic hydrogen is planar to the  $\pi$ -bond, electrophilic attack proceeds from the opposite face to yield the minor product, that is, *trans* (*threo*) diastereoisomer **CH**. An extension of this, reported by Houk, Jäger and co-workers,<sup>[180]</sup> relates to the selectivity of 1,3-dipolar cycloadditions with (electrophilic !) nitrile oxides bearing  $\alpha$ -alkoxy substituents. Houk and Jäger termed the favoured pathway as the “OR-inside” conformation or described it as an “alkoxy-inside effect”: During the attack of an electrophile on to an allyl ether, for example through halogen, the double bond becomes “electron poor”. The “inside” conformation places the allylic C-O bond approximately in the same plane as the double bond –*in an analogous way to that illustrated above in Diagram 13*. In this conformation, the overlap between the bonding  $\sigma_{\text{CH}}$ - and  $\sigma_{\text{CR}}$ -orbitals on C-3 with the  $\pi$ -orbital of the double bond is maximised (electron-donating effect); concurrently, this orbital has only minimal overlap with the anti-bonding  $\sigma^*_{\text{CO}}$ -orbital. This situation increases the nucleophilic character/role of the C=C bond (cf. Bierer’s Thesis, lit.<sup>[2]</sup>, Diagram p. 33).

Essentially the same reasoning can be applied for the bromocyclisation of pentenose oxime (Diagram 14). Again, in analogy to the model described by Chamberlin and Hehre<sup>[178]</sup> above, the double bond of the oxime **4** should be preferably in the same plane as the dioxolane ring of the neighbouring acetonide-protecting group. This would explain the predominate formation of the L-lyxo-configured nitrone **5** (cf. Thesis, Bierer<sup>[2]</sup>, p. 32).

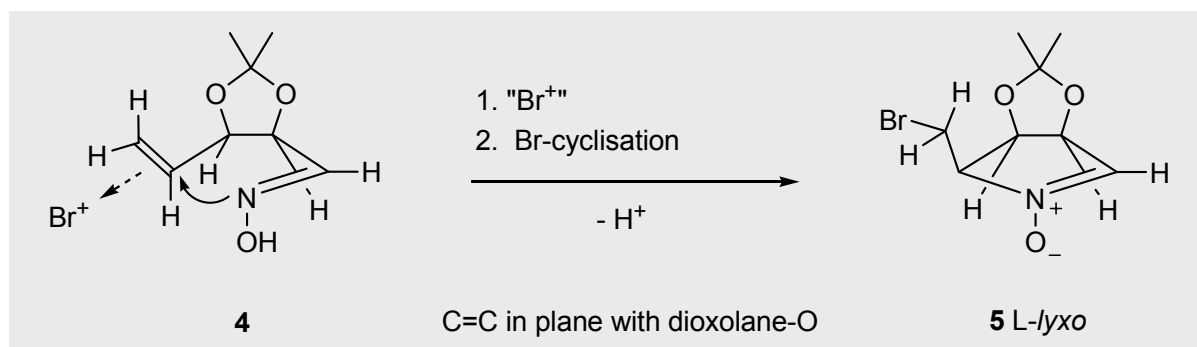
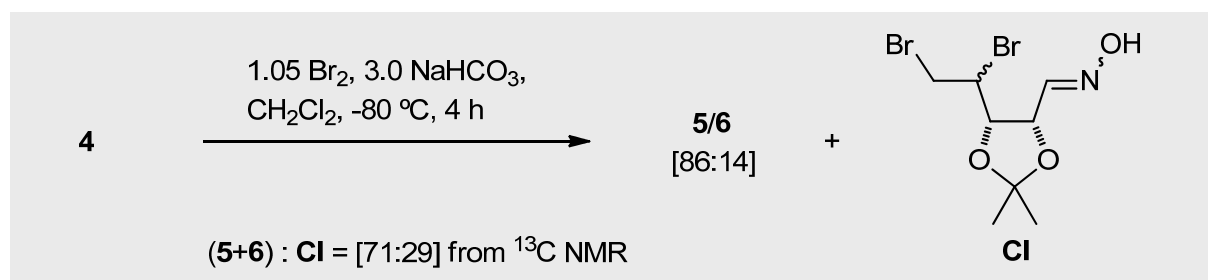


Diagram 14: Preferred pathway for the cyclisation of oxime **4**. Adopted from lit.<sup>[2]</sup> (L. Bierer)

Schmidt<sup>[177]</sup> has shown that the rate of cyclisation decreases at low temperatures favouring the competing reaction path, i.e. *erythro* addition of bromine to the double bond, to provide the dibromide **CI** (Diagram 15). The ratio of the nitrone products was only slightly attenuated at low temperatures, and the application of pure (*E*)- or (*Z*)-oxime **4** bore no effect on the observed diastereoselectivity (note: for an example of the directing effect of an allylic hydroxy group vs. the directing effect of N-substituents in the Hg(II)-mediated intramolecular amidomercuration of 5-alkenyl-4-alkoxy-amides, refer to lit.<sup>[181]</sup>).



Scheme 15: Low temperature reaction of the oxime **4** with bromine leading to the dibromide co-product<sup>[177]</sup>

### 2.2.1.4 NMR and solid state properties of D-ribo-nitronone **6**

Note: an extensive account of the spectroscopic and solid state properties<sup>[182]</sup> of the L-lyxo nitronone **5** has been given by Bierer.<sup>[2]</sup> The <sup>1</sup>H NMR  $J_{4,5}$  value for the D-ribo nitronone **6** was equal to 1.7 Hz. Seeing as there is an angular dependence of vicinal coupling constants (i.e. Karplus curve/equation<sup>[102,183,184,185]</sup>), the 4-H/C-4/C-5/5-H dihedral angle ( $\phi$ ) can be estimated to be ca. 60-70°. In tune with L-lyxo nitronone **5**, the  $J_{3,4}$  value was found to be 6.4 Hz (3-H/C-3/C-4/4-H  $\phi =$  ca. 25-30°), which indicates a *syn-clinal* relationship for protons 3-H and 4-H. For  $J_{2,3}$ , however, a much smaller coupling constant of 1.4 Hz is observed (i.e. 2-H/C-2/C-3/3-H,  $\phi =$  ca. 90-100°), suggesting that 2-H and 3-H should be standing *trans* to each other. In contrast, the corresponding coupling in L-lyxo nitronone **5** measures 4.8 Hz (2-H/C-2/C-3/3-H,  $\phi =$  ca. 35-45°), indicating that the hydrogens in question are standing *syn* to each other.

**Table 1:** Comparison of the conformations of the nitrones **5** and **6** in solution and solid state

Coupling partners	Solution		Crystal		Solution		Crystal	
	<sup>3</sup> J [Hz]	$\phi$ [°] <sup>[a]</sup>	$\phi$ [°]	<sup>3</sup> J [Hz] <sup>[a]</sup>	<sup>3</sup> J [Hz]	$\phi$ [°] <sup>[a]</sup>	$\phi$ [°]	<sup>3</sup> J [Hz] <sup>[a]</sup>
4-H, 5-H	2.0	60-70	71	1-2	1.7	60-70	62	2-3
3-H, 4-H	6.1	25-30	18	7-8	6.4	25-30	11	6-7
2-H, 3-H	4.8	35-45	22	7-8	1.4	90-100	110	2-3
2-H, 1'-H <sub>A</sub>	11.3	170-180	179	9-11	2.9	50-60	61	2-3
2-H, 1'-H <sub>B</sub>	3.6	50-60	62	2-3	3.6	50-60	56	2-3

[a] Through estimation using Karplus curve/equation<sup>[183]</sup>

The use of the Karplus curve can allow deductions to be made for the preferred ring conformation as well as the orientation of the bromomethyl group with respect to 2-H in solution. The C=N double bond imposes a planarity on the adjacent atoms at C-2 and C-4 which explains why the dihedral angle for C-2/N-1/C-5/C-4 of **6** in the solid state amounts to only 1.6°. The planarity of the dihydro-2*H*-pyrrole-1-oxide ring can clearly be observed in the solid state by referring to Diagram 15.<sup>[186]</sup> However, from the coupling constants observed in solution, C-3 probably points out of the plane giving a  $E_3$  (envelope)-like conformation (like that in Diagram 15; cf discussion concerning **5** in Bierer's Thesis, lit.<sup>[2]</sup> Diagram on p. 25).

Returning to L-*lyxo* nitrone **5**, the preferred orientation of the bromomethyl group to 2-H has been estimated by consideration of  $^3J$  values.<sup>[2]</sup> In the L-*lyxo* nitrone **5**, the bromine atom was found to reside in one of two equivalent *syn-clinal* conformations with respect to 2-H. This means that one of the methylene protons (1'-H<sub>A</sub>) is positioned *anti-periplanar* to 2-H (i.e. 1'-H<sub>A</sub>/C-1'/C-2/2-H,  $\phi = 160-180^\circ$ ). This explains the large  $^3J_{2,1'A}$  value of 11.3 Hz. In comparison, for the D-*ribo* nitrone **6**, the relative position of bromine and 1-H<sub>A</sub> must be swapped so that *both* protons take up a *syn-clinal* conformation with respect to 2-H. This is reflected by the smaller  $^3J_{2,1'A}$  value (2.9 Hz) of 1'-H<sub>A</sub> which is complemented by the  $J$  value of the other *syn-clinal* standing proton, 1'-H<sub>B</sub> ( $^3J_{2,1'B} = 3.6$  Hz). The estimated dihedral angle is then ca. 50-60° for each. This assumption is backed up by the actual dihedral angles found in the solid state for 1'-H<sub>A</sub>/C-1'/C-2/2-H and 1'-H<sub>B</sub>/C-1'/C-2/2-H (61 and 56°, respectively, see Table 1). Furthermore, the dihedral angle for Br-1B/C5B/C1B/H1B (crystal numbering, see Section 7.1 for full details) in the solid state was found to be 177° which confirms the *anti-periplanar* orientation of bromine to 2-H (Diagram 15).

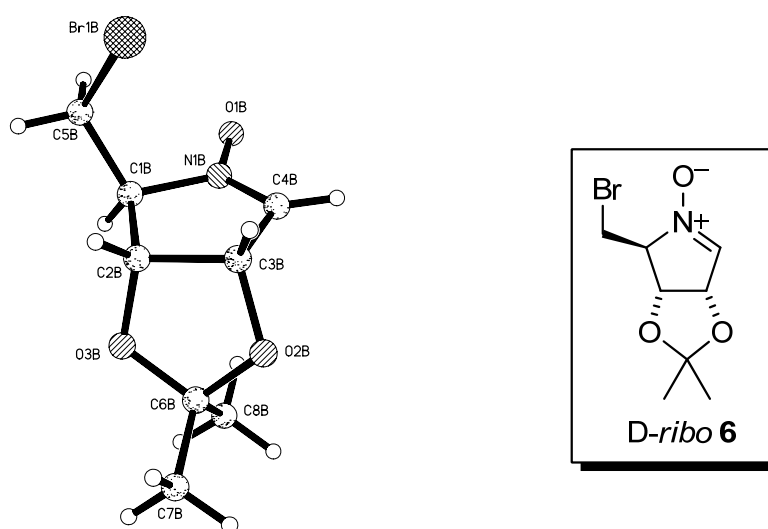
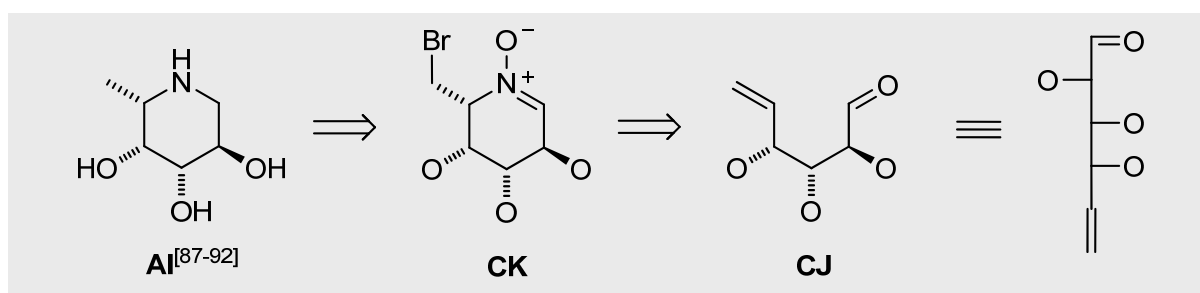


Diagram 15: X-Ray structure of D-*ribo* nitrone **6**<sup>[186]</sup>

## 2.2.2 Synthesis of L-*fuco*-nitrones 27, 28, and D-*altro*-nitrone 29

### 2.2.2.1 Initial investigations with non-carbohydrate-derived precursors

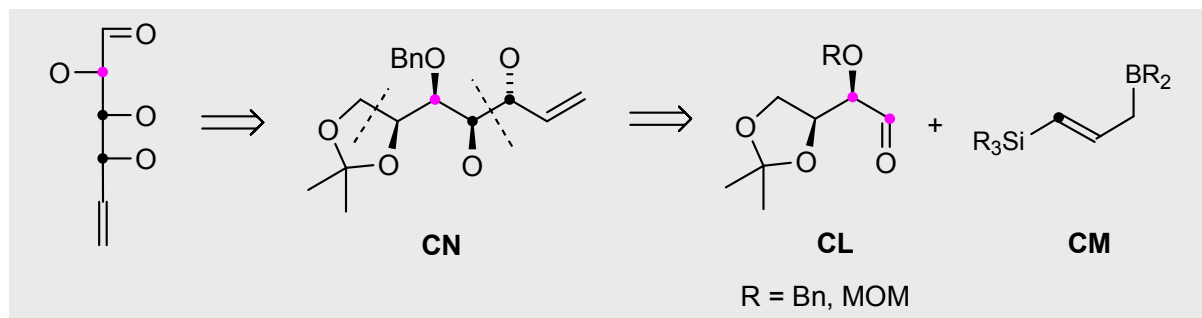
We have seen from the Introduction and Sections 1.3.1-1.3.3, that there are many analogues of deoxynojirimycin (**L**, “DNJ”) with biological activities. Numerous reviews on the synthesis of DNJ and its analogues exist,<sup>[187]</sup> however synthetic procedures towards the synthesis of 1,6-dideoxy-DNJ analogues such as deoxyfuconojirimycin **AI**<sup>[87-92]</sup> have scarcely been described. The bromocyclisation of a suitably configured hexenose oxime would give access to this class of compounds in the L-*fuco* series. Of course, the deciding factor is the synthesis of the required D-*arabino*-configured *aldehyde* **CJ**, which following oximation and cyclisation should predominately lead to the L-*fuco*-configured six-membered nitrone **CK**. The retrosynthetic pathway is shown in Scheme 16.



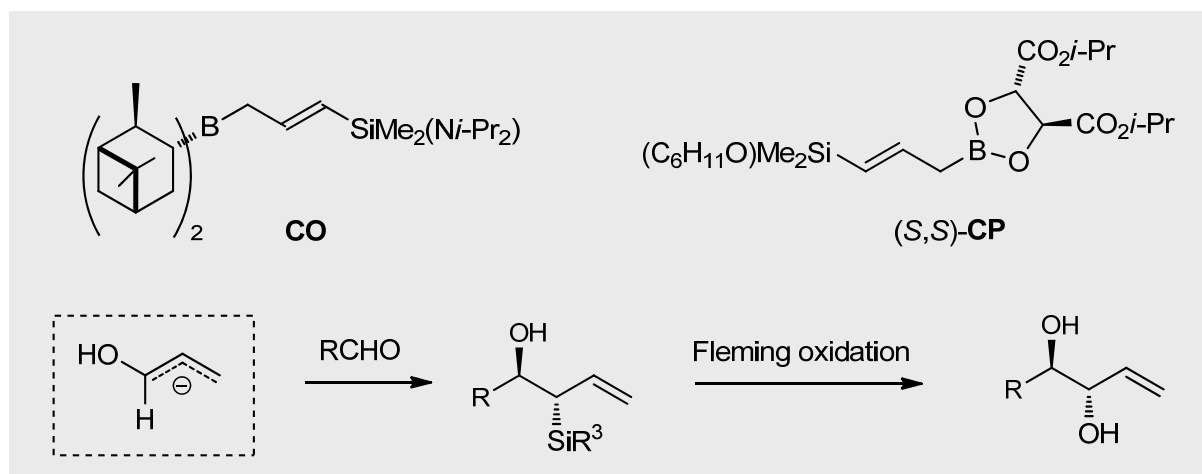
Scheme 16: Planned entry into the L-*fuco* nitrone series requires a D-*arabino* hexenose **CJ**

The planned key-step to aldehyde **CJ** could be the  $\alpha$ -hydroxyallylation of 2-O-“protected”-3,4-isopropylidene-L-threose **CL** using a suitable (*E*)-(trialkylsilyl)allylborane **CM** (cf. similar route discussed in Li Feng’s Thesis, lit.<sup>[188]</sup>). This is an attractive route, in principle, as a carbon-carbon bond and the installation of an *erythro* vicinal-diol are generated simultaneously with double stereodifferentiation.<sup>[189]</sup> Further protecting group modifications followed by cleavage of the acetonide moiety in **CN** using periodic acid<sup>[188a]</sup> were envisaged to be a robust route to the D-*arabino* hexenose (for clarity, the origin of the relevant stereocenters in the target product are highlighted with dark grey/black points, Scheme 17). In this thesis, the L-threose derivatives **CL** were made available through co-operation with J. Sayago,<sup>[190]</sup> who expertly produced the 2-O-benzylated compound in four steps from diethyl L-tartrate (using a “quicker” modification of our group’s procedure from Steuer<sup>[191]</sup>) and a 2-O-methoxymethyl (‘MOM’) ether derivative in five steps beginning from L-ascorbic acid.<sup>[192]</sup>



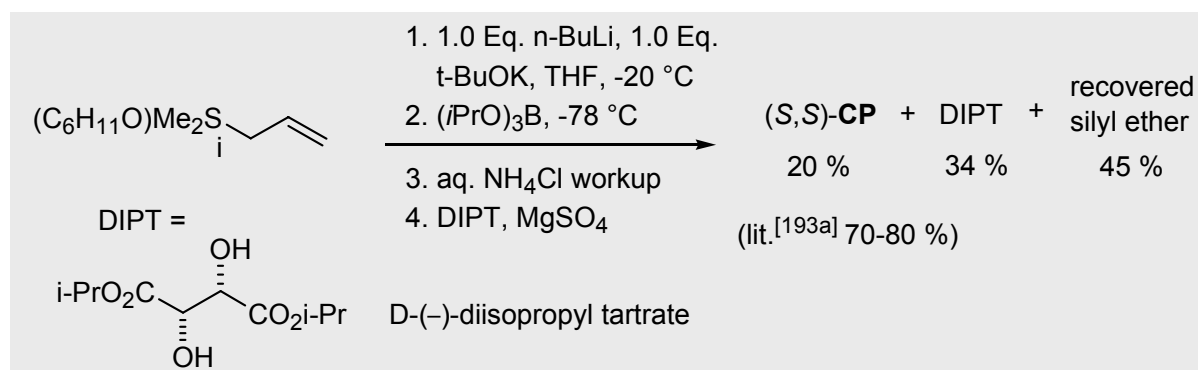
Scheme 17: Original retrosynthetic pathway for *D-arabino* hexenose

A range of (*E*)- $\gamma$ -silylallylboranes are available as surrogates for the synthesis of *erythro*-vicinal diols: Barrett and Malecha<sup>[193]</sup> introduced the terpene-derived *B*-[(*E*)-3-(diphenylamino)-allyl]diisopinocampheyl reagent **CO**, based on an adaptation of Brown's [(*Z*)- $\gamma$ -alkoxyallyl]diisopinocampheylborane (for the enantioselective synthesis of *threo*-vicinal diols),<sup>[188,194]</sup> while Roush and Glover<sup>[195]</sup> have reported (*E*)- $\gamma$ -[(cyclohexyloxy)dimethylsilyl]allylboronates **CP** as chiral allylic alcohol  $\alpha$ -carbanion equivalents, outlined in Diagram 16. The term "surrogate" is in reference to the silyl component which, ultimately, acts as a masked hydroxyl group ('Fleming oxidation'<sup>[196]</sup>) and, firstly, itself needs to be quite bulky to disfavour the competing Peterson olefination under the alkylation conditions.

Diagram 16: *Erythro*-selective  $\alpha$ -hydroxyallylation reagents

Roush's reagent **CQ** has seen application with chiral aldehydes similar to "our" **CL**, and a decision was made to go down this route. The (cyclohexyloxy)-dimethylallylsilane was required, prepared from allyldimethylchlorosilane (71 %),<sup>[197]</sup> and followed by treatment with *n*-butyllithium and potassium *tert*-butoxide ('Schlosser's base'<sup>[198]</sup>) at -20 °C for 20 min. Triisopropoxyborane was added at -78 °C and ca. 15 min later poured into aqueous NH<sub>4</sub>Cl

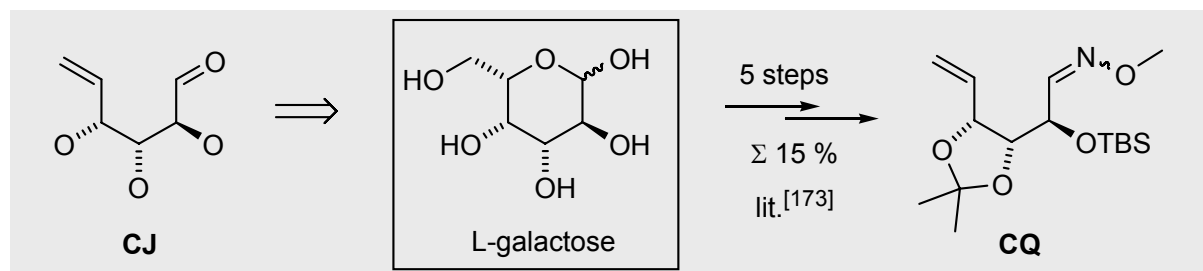
solution, extracted with diethyl ether and treated with D-(–)-diisopropyl tartrate. In spite of careful preparations (fresh n-butyllithium, sublimed potassium tert-butoxide, etc.), a best yield of ca. 20 % for (S,S)-**CP** (lit.<sup>[195a]</sup> 70-80 %) was obtained, along with ca. 34 % DIPT and ca. 45 % unreacted silyl ether (Scheme 18). Due to the poor yield and (un)reliability problems, further investigations on this or related chemistry were not carried out.



Scheme 18: Problematic synthesis of Roush's boronate reagent (S,S)-**CP**

### 2.2.2.2 Use of L-galactose as a carbohydrate starting material precursor?

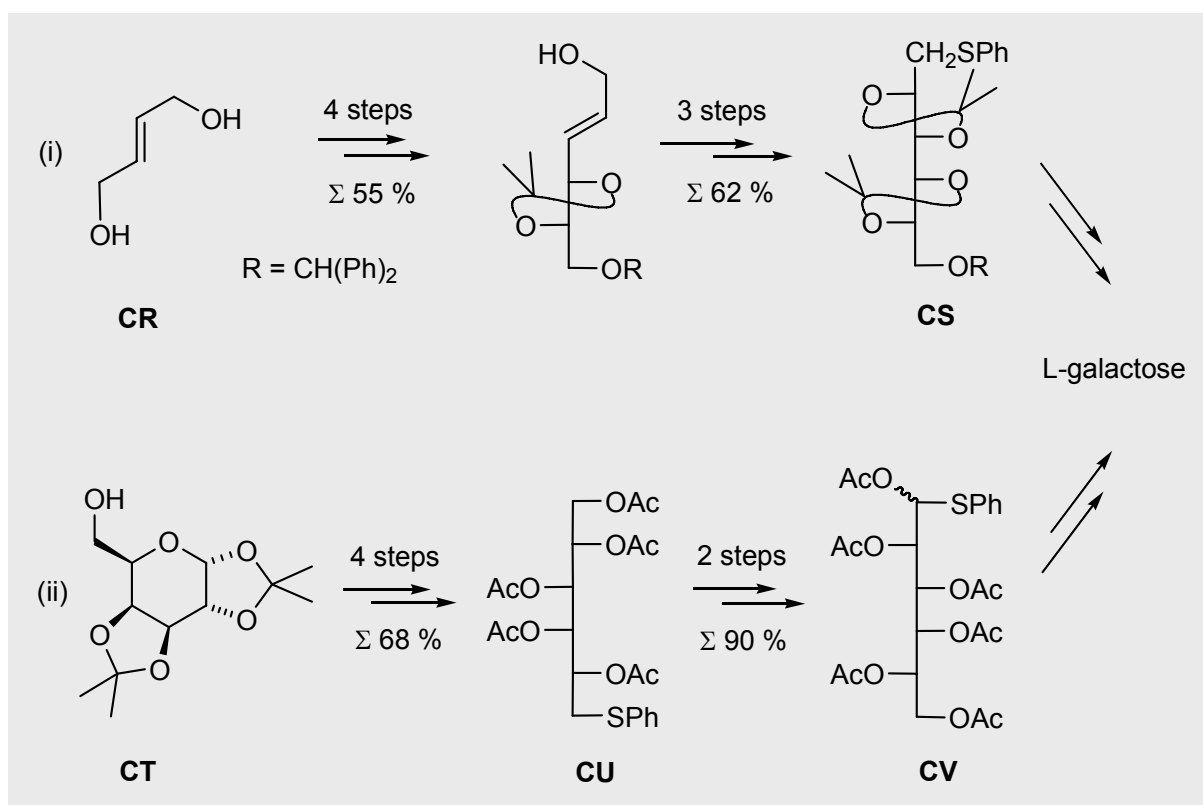
The alternative use of L-galactose as starting material required the D-*arabino*-configured aldehyde **CJ**, which can be prepared through a Vitamin B<sub>12</sub>-catalysed fragmentation of the corresponding 6-iodoglucoside (cf. Section 2.1.2). Indeed, Greul<sup>[102]</sup> has demonstrated the viability of this route by synthesising the D-*arabino* O-methyl-oxime derivative **CQ** in 5 steps (Σ 15 %) from L-galactose (for bromocyclisation, **CQ** would also have to be selectively demethylated first). This method relies on L-galactose, an incredibly expensive starting material (1 g, € 716; Sigma-Aldrich, 2009),\* which raises issues for the preparative useful synthesis of **CQ**-derivatives *via* this method.



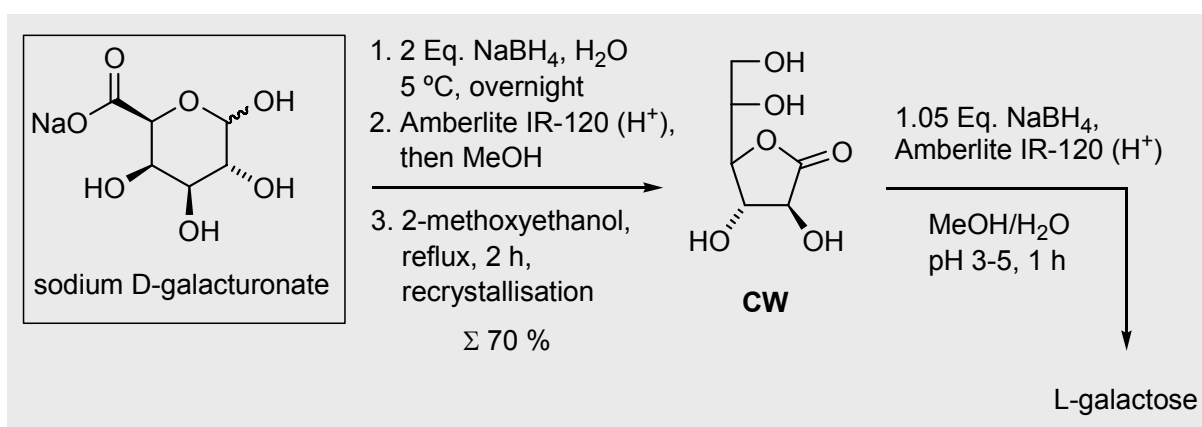
Scheme 19: Direct route to D-*arabino* hexenose **CJ** and oxime **CQ**<sup>[173]</sup> from L-galactose

\* A gift of 100 g of L-galactose from Dr. B. Ernst/Dr. R. Öhrlein, then in the carbohydrate group of Ciba-Geigy, had enabled this; the sample was not prepared there, but bought from Fluka (?).

There are several literature reports, however, for the synthesis of L-galactose starting from bulk chemicals. For example, the total synthesis of all L-hexoses was reported by Ko, Masamune, Sharpless and co-workers<sup>[199]</sup> beginning from 4-benzhydryloxy-(*E*)-but-2-en-1-ol **CR**, using a “double-cycle”, iterative two-carbon extension strategy. This route to L-galactose (7 steps,  $\Sigma$  25 %), was invariably meant to be a showcase for Sharpless’ own method for asymmetric epoxidation, which constitutes the key-step for diol-formation. The penultimate steps make use of the Pummerer reaction,<sup>[200]</sup> beginning with sulphide **CS** to generate an  $\alpha$ -acyloxy-thioether which collapses to the aldehyde to give L-galactose [case (i), Scheme 20]. Elsewhere, the Pummerer reaction was also used by González and Baer in their synthesis of L-galactose (7 steps,  $\Sigma$  46 %), starting from the 1,2:3,4-diacetonide-protected galactose derivative **CT** [case (ii), Scheme 20].<sup>[201]</sup> After transformation of the aforementioned galactose derivative to 6-phenylthio-D-galactitol **CU**, the Pummerer reaction is initiated by oxidation to the sulfoxide and treatment with acetic anhydride. The  $\alpha$ -acyloxy-thioether **CV** converts to the aldehyde under conditions of concomitant global transesterification to afford L-galactose. Recently, L-galactose syntheses have been reported by Kim, Cho and Shin<sup>[202]</sup> (from L-ascorbic acid; 9 steps, ca  $\Sigma$  45 %), while White and co-workers<sup>[203]</sup> have communicated the synthesis of a useful 2,3,4-protected L-galactose intermediate from (*Z*)-2-butene-1,4-diol (10 steps,  $\Sigma$  22 %)

Scheme 20: Examples of synthetic routes to L-galactose<sup>[199,201]</sup>

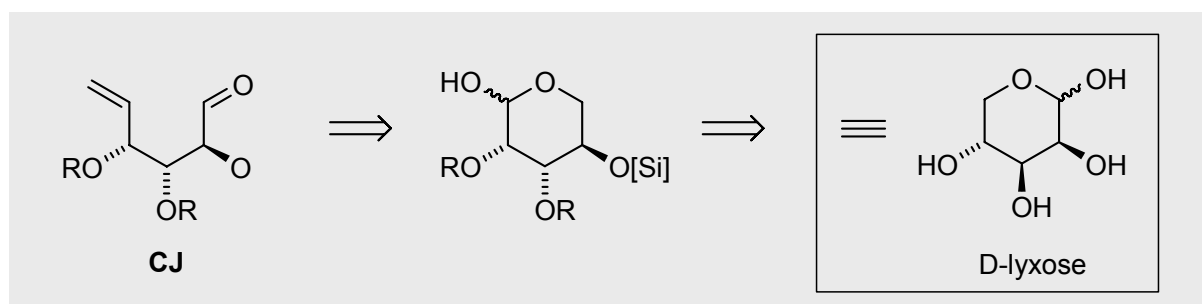
However, perhaps the simplest synthesis of L-galactose has been reported by Frush,<sup>[204]</sup> Binch and co-workers (Scheme 21).<sup>[205]</sup> This (tedious) “two-step” sequence commenced from sodium D-galacturonate, which is firstly reduced under aqueous conditions. Filtration through acid-activated Amberlite liberates the free acid, while methanol is added to remove boric acid as trimethyl borate through evaporation. Refluxing in 2-methoxyethanol drives lactonisation to yield the L-galactono-1,4-lactone **CW**. The lactone is reduced with sodium borohydride under acidic conditions (i.e. Amberlite IR-120, H<sup>+</sup> form, pH 3-5), to yield a mixture of L-galactose and over-reduced L-galactitol. Under basic conditions, the over-reduction to the galactitol would be the main product.<sup>[206]</sup>



Scheme 21: “Two step” L-galactose synthesis (isolated as penta-acetate, cf. lit.<sup>[205]</sup>)

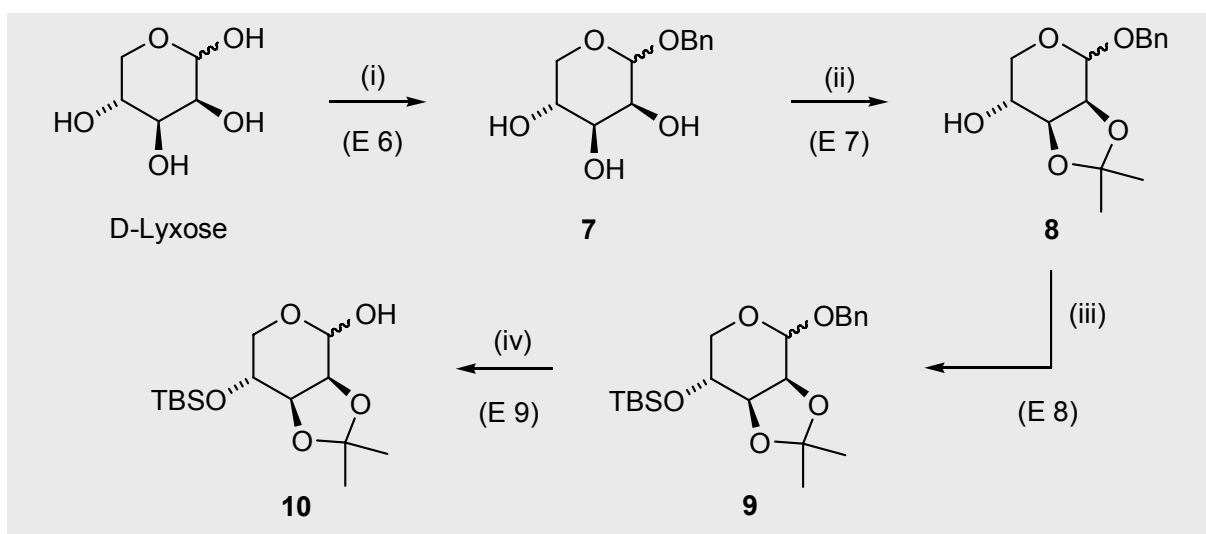
### 2.2.2.3 Synthesis of D-arabino hexenose oximes **18** and **22** from D-lyxose

In this Thesis, after the previous efforts the use of L-galactose or a derivative thereof was not deemed necessary anymore for the synthesis of D-arabino hexenoses and oximes. Instead, D-lyxose was employed – which exhibits the correct hydroxyl group conformation corresponding to C-2, C-3, and C-4 in L-galactose – to synthesise the required D-arabino-configured hexenose **CJ**, using a Wittig reaction/oxidation sequence (Scheme 22).



Scheme 22: Proposed route to D-arabino-configured hexenose from D-lyxose

Following a procedure of Keck and co-workers,<sup>[207,208]</sup> D-lyxose was firstly converted into the benzyl D-lyxopyranoside **7**, followed by acetonide formation to produce the alcohol **8**. The free hydroxyl group was silylated in high yield to form the *O-tert*-butyldimethylsilyl ('TBS') ether **9**, which following reduction with lithium in liquid ammonia provided the hemi-acetal **10**, as exemplified in Scheme 23. Crystals of sufficient quality for X-ray structural analysis of compound **10** could be grown from methylene chloride, displayed in Diagram 17. The compound crystallises as the  $\alpha$ -anomer in a truncated  ${}^4C_1$  conformation; hydrogen bonding exists between the anomeric hydroxyl group (as acceptor) and the acetonide oxygen on C-4 (H2A...O4 = 1.98 Å; O2/H2A/O4 = 169°; crystallographic numbering, cf. Section 9.2).



Scheme 23: Synthesis of the 4-*O*-silylether pyranose **10**: (i) BnOH, H<sub>2</sub>SO<sub>4</sub>, *p*-TsOH cat., 60 °C, 48 h, 86 % (lit.<sup>[207]</sup> 82 %),  $\alpha/\beta$  = 83:17. (ii) 2,2-Dimethoxypropane, *p*-TsOH (cat.), acetone, 16 h, r. t., 71 %, (lit.<sup>[207]</sup> 91 %),  $\alpha/\beta$  = 88:12. (iii) TBSCl, imidazole, DMF, 3 h, r. t., 94 % [lit.<sup>[207]</sup> 95 %], (iv) Li, NH<sub>3</sub>, -40 °C, 0.5 h, then NH<sub>4</sub>Cl, r. t., 2 h, 83 % (lit.<sup>[207]</sup> "100 %"),  $\alpha/\beta$  = 95:5.

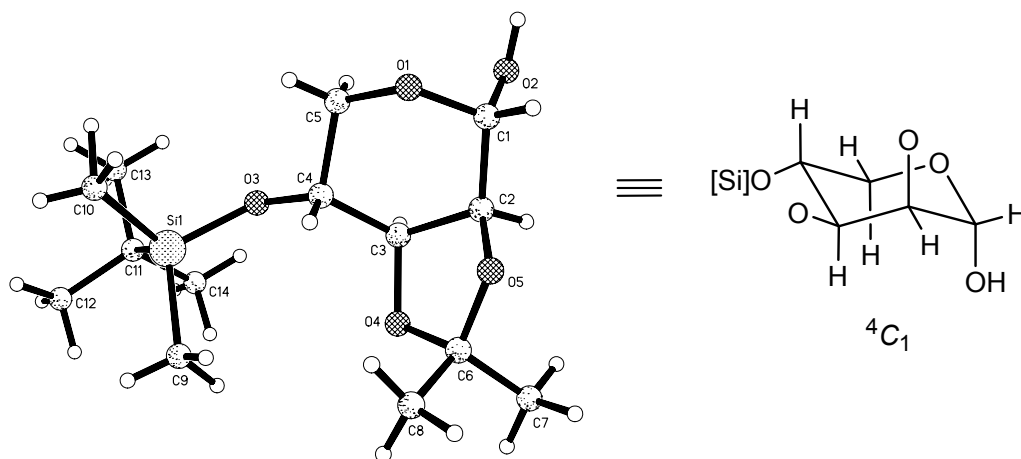
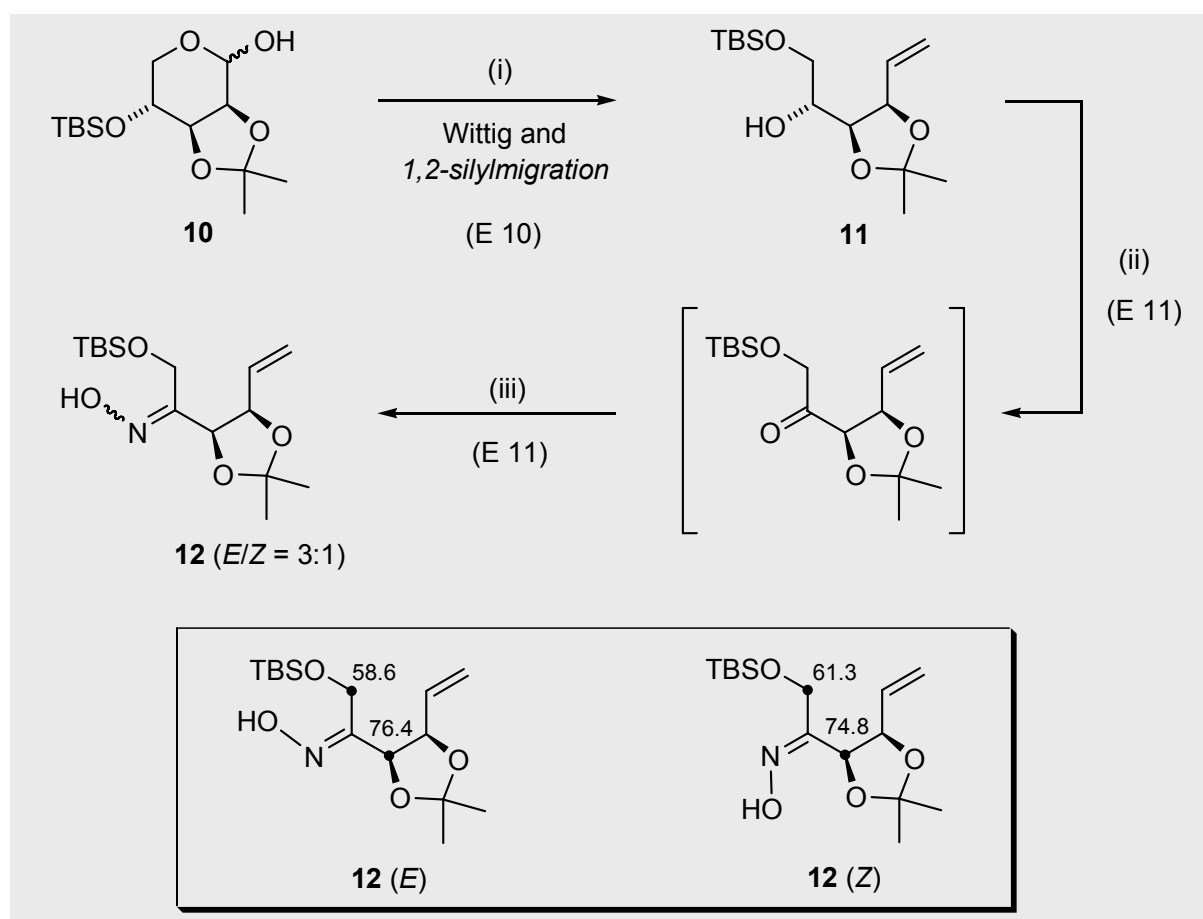


Diagram 17: X-Ray crystal structure of the  $\alpha$ -D-lyxopyranose derivative **10**

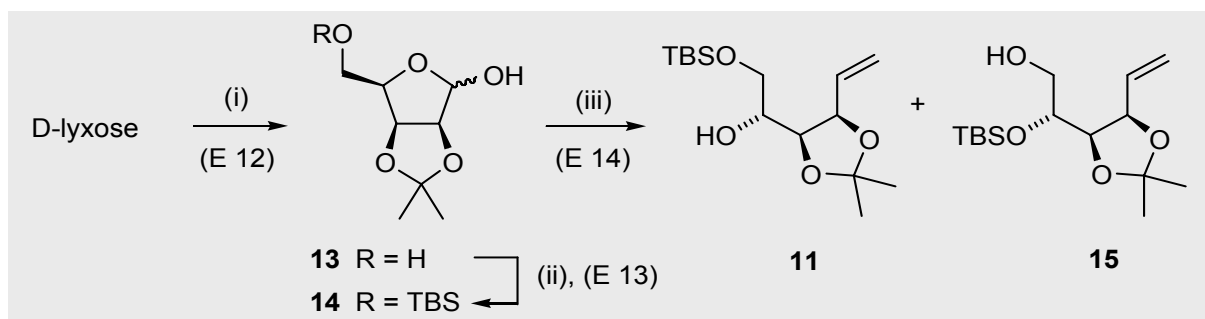
The hemi-acetal **10** was subjected to a Wittig reaction with lithium bis(trimethylsilyl)amide ('LiHMDS') and methytri-phenylphosponium bromide<sup>[209]</sup> to provide the 1-*O*-*tert*-butyldimethylsilyl ether olefin **11** in 80 % yield (Scheme 24) and not, as to be expected, the 2-*O*-silylated olefin **15** (cf. Scheme 25). Other bases for the Wittig reaction were tested (i.e. potassium *tert*-butoxide,<sup>[210]</sup> *n*-butyllithium<sup>[211]</sup>), however the 1,2-silyl migration could not be prevented. Unfortunately, the migratory aptitude of the TBS group to adjacent hydroxyl groups under basic conditions is well-known,<sup>[212,213,214]</sup> to which, according to Fleet,<sup>[215]</sup> diols like **11** are particularly prone. This rearrangement was confirmed by oxidation of **11** under Ley's<sup>[216,217]</sup> conditions leading to the intermediary ketone which upon condensation with hydroxylamine provided the *keto*-oxime **12** (<sup>1</sup>H NMR, *E/Z* = 3:1) – adjudged to have formed after <sup>1</sup>H NMR revealed the missing *aldo*-oxime proton resonances, which would otherwise have been observed at 6.8 to 7.1 ppm.<sup>[218]</sup> The assignment of *E* and *Z* diastereoisomers was rationalised on the basis of <sup>13</sup>C chemical shifts of C-1 and C-3 (see insert, Scheme 24).



Scheme 24: Wittig reaction and base-induced, undesired 1,2-silyl migration to yield **11**: (i) 2.2 Eq. LiHMDS, 2.5 Eq. Ph<sub>3</sub>PCH<sub>2</sub>Br, THF, 0 to 60 °C, 2 h, 80 %. (ii) 2.0 Eq. *N*-morpholine-*N*-oxide, 0.07 Eq. *tetra-n*-propylammonium perruthenate(VII), MS 4 Å, CH<sub>2</sub>Cl<sub>2</sub>, r. t., 1 h. (iii) NH<sub>2</sub>OH·HCl, pyridine, r. t., 8 h, Σ 75 % (2 steps), *E/Z* = 3:1.

According to Wehrli *et al.*<sup>[219]</sup>, the (*E*) oxime should be in a position to induce a degree of C-H bond polarisation on carbon C-1, *syn* relative to the N-OH group; this “steric perturbation” leads to a drift of charge along the bond towards C-1 to increase the shielding. The (*Z*) oxime should then have a shielding influence on C-3, while C-1 should be deshielded, which, indeed, is the case. In practice, this relationship between steric compression and chemical shift is an example of an angular  $\gamma$ -*gauche effect*,<sup>[219,220]</sup> and allows the two keto-oximes to be distinguished from each other. Apparently, the effect is also well documented for other *E/Z*-keto-imine systems (imines, hydrazones, ketazines, etc; cf. Kalinowski *et al.*<sup>[221]</sup>, Levy *et al.*<sup>[222]</sup>) and from  $\alpha$ -enoximes, as studied in our group (cf. Jäger and Grund<sup>[109b]</sup>).

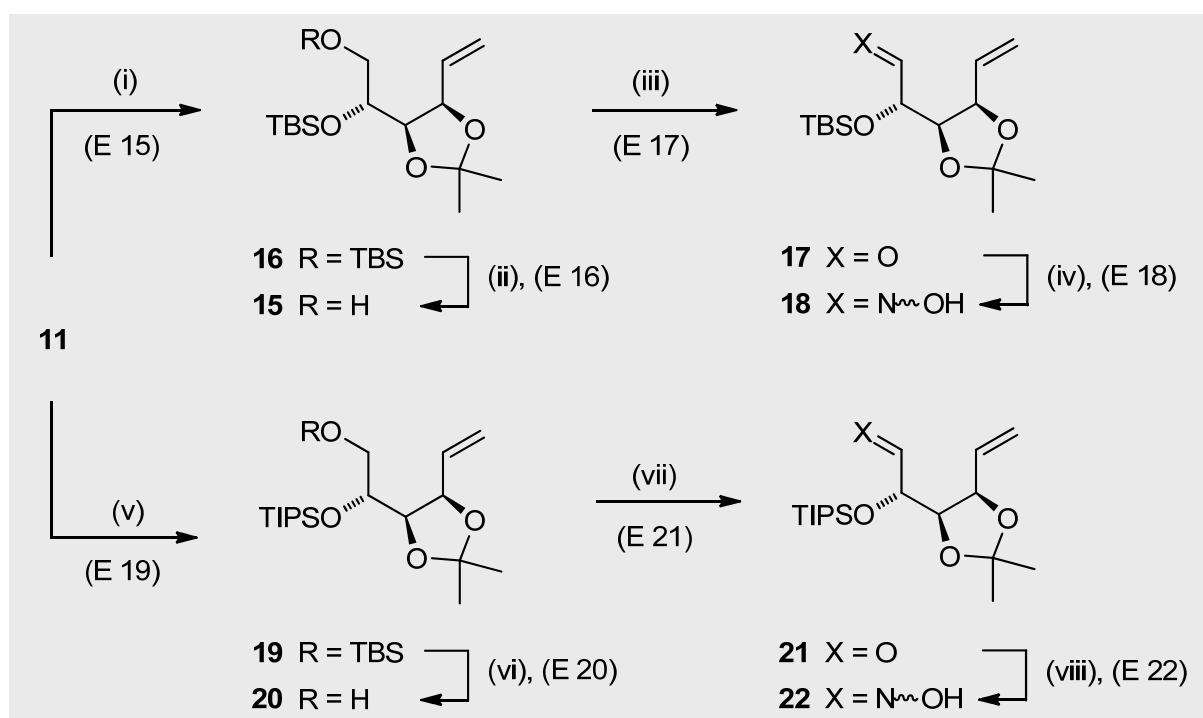
In retrospect of the unexpected and unwanted 1,2-O-silyl migration, the idea was now to deliberately make 1-O-silylated hexenitols using a shorter route from the D-lyxofuranose **13** followed by masking of the secondary alcohol to provide an orthogonal set of protecting groups. Selective deprotection of the primary hydroxyl group and oxidation would then provide the required hexenose of D-*arabino*-configuration (Scheme 25). Treatment of D-lyxose with acetone and H<sub>2</sub>SO<sub>4</sub> (cat.),<sup>[223]</sup> as with D-ribose above (cf. Scheme 13), led to the introduction of the 1,3-dioxolane system with quantitative formation of 2,3-O-isopropylidene-D-lyxofuranose **13** bearing two fused five-membered rings. Selective protection of the C-5 hydroxyl group with *tert*-butyldimethylsilylchloride ('TBSCl') in dichloromethane in the presence of imidazole<sup>[224]</sup> provided 5-O-silylated derivative **14** in 85 %. The low temperature (-30 °C) and gradual addition of TBSCl was needed to circumvent competing formation of a 1,5-O-disilylated side-product (under these conditions<sup>[224a]</sup> limited to ca. 5 %). The hemi-acetal was subjected to a Wittig reaction using an excess of ylide to yield the expected 1-O-silylated hexenitol **11** (86 %) and, again this time through 1,2-silyl migration in the 'other' direction, a useful amount of 2-O-silylated hexenitol **15** (10 %) (Scheme 25).



Scheme 25: Synthesis of **11** and **15** through partial 1,2-silyl migration, from D-lyxose: (i) acetone, H<sub>2</sub>SO<sub>4</sub> (cat.), 16 h, “100 %” (lit.<sup>[223]</sup> “100 %”). (ii) 1.1 Eq. TBSCl, 2.0 Eq. imidazole, CH<sub>2</sub>Cl<sub>2</sub>, -30 °C, 4 h, 85 %. (iii) 4.0 Eq. Ph<sub>3</sub>PCH<sub>2</sub>Br, 4.0 Eq. nBuLi, THF, -20 to 55 °C, 2 h, then r. t. overnight, 86 % (**11**) and 10 % (**15**).

From  $^1\text{H}$  NMR analysis, it was quite easy to differentiate between the two regioisomers **11** and **15**. For example, the protons 1- $\text{H}_\text{A}$ , 1- $\text{H}_\text{B}$  and 2- $\text{H}$  are grouped together as a multiplet for compound **11** in deuterated chloroform. In the same solvent, for compound **15**, 1- $\text{H}_\text{A}$  and 1- $\text{H}_\text{B}$  are split into a pair of doublet of double doublets ('ddd'; 16 lines in total) resulting from  $^3J$ -*gauche* coupling to neighbouring 2- $\text{H}$  (4.4 and 3.6 Hz, resp.), to the primary OH (7.4 and 5.4 Hz, resp.), and a geminal coupling  $^2J$  of 11.5 Hz. In deuterated methanol the 'ddd' signal pair for 1- $\text{H}_\text{A}$  and 1- $\text{H}_\text{B}$  in compound **15** is simplified to 8 lines (i.e. pair of double doublets) because of the missing OH coupling due to fast H,D-exchange.<sup>[183-185]</sup>

The 1-O-silylated hexenitol **11** was converted into the required D-arabino-configured oxime as follows: Protection of the free secondary hydroxyl group using *tert*-butyldimethylsilyl trifluoroemethanesulfonate ('TBSOTf') with 2,6-lutidine<sup>[120,225]</sup> furnished the 1,2-O-TBS ether **16** in near quantitative yield.



Scheme 26: Synthesis of oximes, for **18**: (i) 1.4 Eq. TBSOTf, 2 Eq. 2,6-lutidine,  $\text{CH}_2\text{Cl}_2$ , 0 °C to r. t., 2 h, 98 %. (ii) HF-pyridine, THF/pyridine, r. t., 30 h, 55 % (**15**), 10 % (recovered **16**). (iii) 2.0 Eq. *N*-morpholine-*N*-oxide, 0.07 Eq. *tetra*-*n*-propylammonium perruthenate(VII), MS 4 Å,  $\text{CH}_2\text{Cl}_2$ , r. t., 1 h. (iv)  $\text{NH}_2\text{OH}\cdot\text{HCl}$ , EtOH/ $\text{H}_2\text{O}$ , r. t., 6 h.  $\Sigma$  68 % (2 steps), *E:Z* = 90:10 (from D-lyxose, 7 steps  $\Sigma$  30 %). For **22**: (v) 1.4 Eq. TIPSOTf, 2 Eq. 2,6-lutidine,  $\text{CH}_2\text{Cl}_2$ , 0 °C to r. t., 2 h, "100 %". (vi) HF-pyridine, THF/pyridine, r. t., 2 d, 59 % (**20**), 24 % (recovered **19**). (vii) 2.0 Eq. Dess-Martin periodinane, 4 Eq.  $\text{NaHCO}_3$ ,  $\text{CH}_2\text{Cl}_2$ , r. t., 45 min. (viii)  $\text{NH}_2\text{OH}\cdot\text{HCl}$ , EtOH/ $\text{H}_2\text{O}$ , r. t., 16 h.  $\Sigma$  86 % (2 steps), *E:Z* = 90:10 (from D-lyxose, 7 steps  $\Sigma$  37 %).

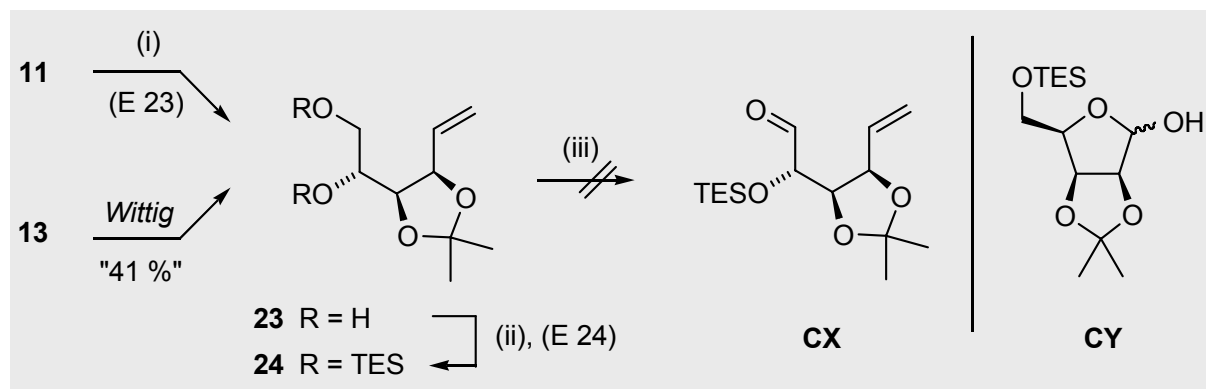


Literature reports are available for the selective deprotection of a duet of TBS protecting groups<sup>[226]</sup> and so using a modified procedure from Williams,<sup>[226a]</sup> the 2-O-TBS ether **16** was treated with five 'fluoride' equivalents using 70 % HF·pyridine complex in THF. Hydrofluoric acid ( $pK_a$  3.45) is only slightly more acidic than formic acid ( $pK_a$  3.75) and, when buffered with additional pyridine, ensures that the acetonide group remained impervious to attack. Deprotection of the less hindered TBS ether was, however, slow and incomplete even after 30 h! More worryingly, TLC analysis indicated the gradual deprotection of the secondary TBS ether which prompted a basic reaction quench to afford the required primary alcohol **15** in a moderate 55 % yield as well as 10 % starting material **15**. Other conditions for this step, such as TBAF/THF or *p*-toluenesulfonic acid (0.1 Eq.) in  $CH_2Cl_2$  or methanol, were unfruitful and mainly led to rapid, concomitant removal of both TBS ethers. With the alcohol **15** in hand, oxidation using Ley's conditions to the aldehyde **17** and condensation with hydroxylamine expediently provided the *D-arabino*-configured oxime **18** as an analytically pure oil in 68 % yield over 2 steps (from D-lyxose, 7 steps,  $\Sigma$  30 %; *E/Z* = 90:10).

With an eventual aim of examining the stability of silyl protecting groups to the conditions of bromocyclisation (see Section 2.2.2.2), the substantially bulkier and less acid-sensitive triisopropylsilyl ('TIPS') oxime **22** was synthesised in analogy to the TBS oxime **18**, also exemplified in Scheme 26. Two points from this synthesis are worth mentioning: firstly, introduction of the TIPS protecting group<sup>[227]</sup> noticeably slowed down the removal of the TBS group with HF·pyridine, requiring 2 days at room temperature to isolate 59 % of the TIPS alcohol **20** and 24 % recovered starting material **19**. Secondly, a switch to Dess-Martin periodinane (1,1,1-triacetoxy-1,1-dihydro-1,2-benziodoxol-3(1*H*)-one),<sup>[228,229,230]</sup> buffered with  $NaHCO_3$ ,<sup>[230c]</sup> gave a very clean oxidation to the hexenose **21** and oxime formation to yield **22** ( $\Sigma$  86 %, two steps, *E:Z* = 90:10) (from D-lyxose, 7 steps,  $\Sigma$  35 %).

#### 2.2.2.4 Attempted synthesis of a TES-protected *D-arabino*-hexenose oxime

In addition to the TBS and TIPS oximes, **18** and **22**, the synthesis of the analogous triethylsilyl ('TES') oxime was considered (Scheme **27**). Beginning with D-lyxofuranose **13**, Wittig olefination provided the *D-arabino*-hexenitol diol **23** in modest yield only, mainly due to purification problems concerning the near identical  $R_f$  values of triphenylphosphine oxide and the diol **23**. Thus, for spectroscopic purposes, a portion of compound **11** was treated with tetrabutylammonium fluoride ('TBAF'), which provided the diol **23** in analytically pure form. After persilylation (TESCl, pyridine<sup>[231]</sup>), the resulting silyl ether could be oxidized directly with an adaptation of the Swern oxidation<sup>[231a]</sup> to the hexenose **CX** which, however, could not be isolated after silica gel filtration on account of decomposition/acid-catalysed TES removal.

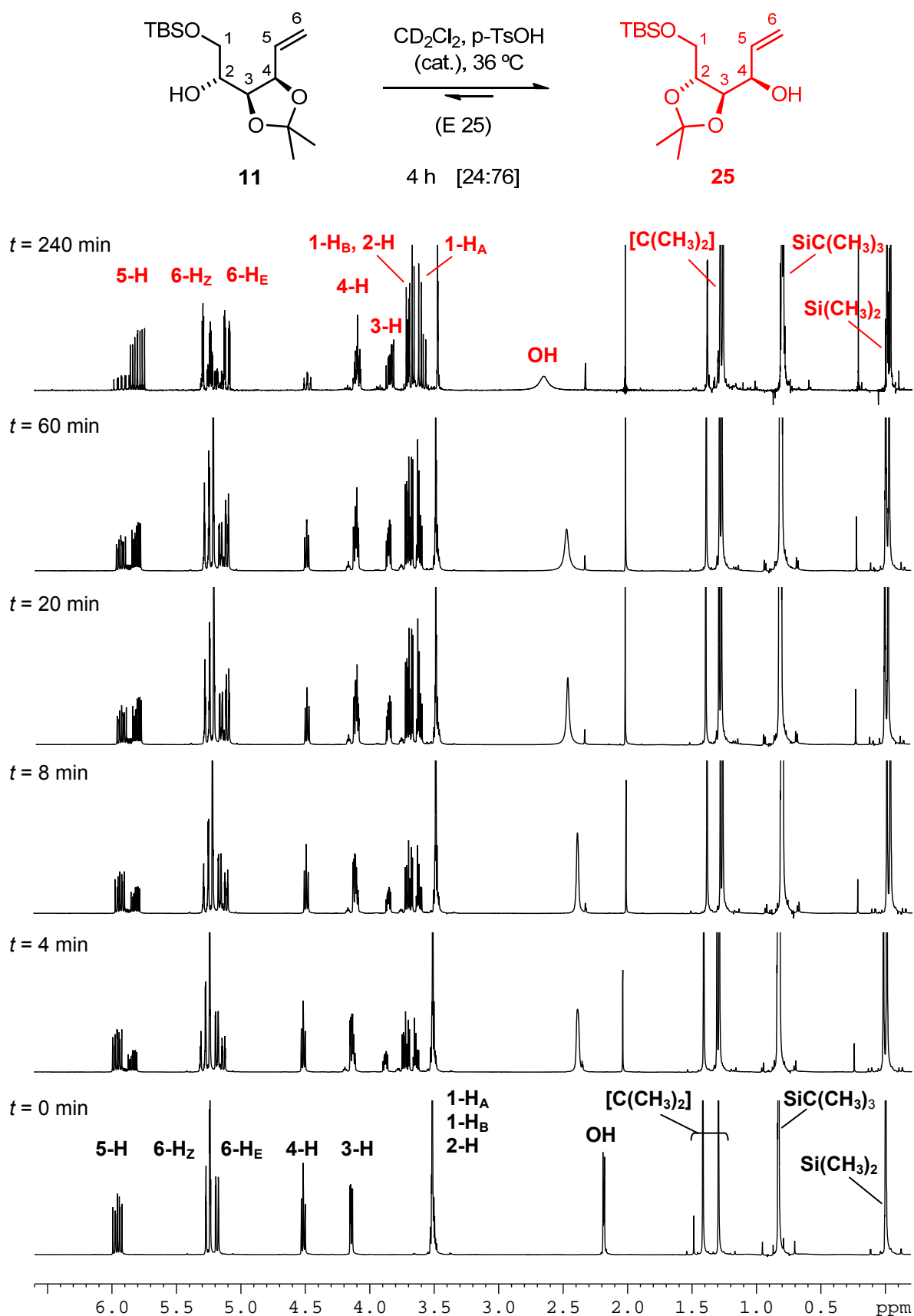


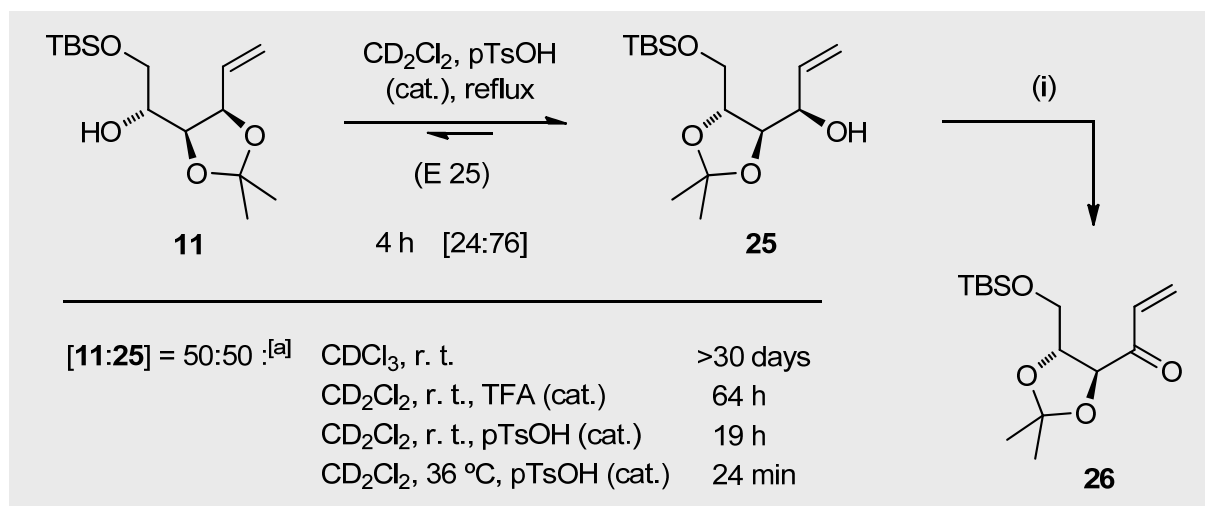
Scheme 27: Attempted synthesis of a TES-protected hexenose (oxime): (i) 3 Eq. TBAF, THF, 2 h, 89 %. (ii) 2.9 Eq. TESCl, pyridine, r. t. 16 h, 86 %. (iii) 5 Eq.  $(\text{CO})_2\text{Cl}_2$ , 10 Eq. DMSO, 18.5 Eq.  $\text{Et}_3\text{N}$ ,  $-78\text{ }^\circ\text{C}$  to r. t. then work-up, purification (on  $\text{SiO}_2$  led to decomposition).

This result was in stark contrast to the behaviour of TBS- and TIPS-protected aldehydes, **17** and **21** (cf. Scheme 26), which are stable to column chromatography. The questionable stability of the TES group to acidic conditions has been mentioned by Kocieński,<sup>[232]</sup> who states that the rate of cleavage depends on the steric and electronic environment. For example, the steric bulk of two neighbouring TES groups in diol **24** provided enough stability to silica gel chromatography whereas the exposed primary TES ether in the lyxofuranose derivative **CY**, on the other hand, did not survive purification. As the TES group would therefore probably not survive the conditions of bromocyclisation (see Section 2.2.2.6), the TES oxime synthesis was aborted.

### 2.2.2.5 Stability of acetonide **11** under acidic conditions

The re-examination of the alcohol **11** after several weeks in  $\text{CDCl}_3$  solution revealed the existence of a second product later determined to be the allylic alcohol **25**, which was judged to have formed after acid-catalysed equilibration of the *cis*-3,4-acetonide with the more stable *trans*-2,3-acetonide. The migration reflects the more favoured case where the substituents on the resultant five-membered ring will be *trans*.<sup>[233]</sup> Other acid catalysts and higher temperatures accelerated the conversion of **11** to **25** considerably (Scheme **28**). For example, in Diagram 18 the reaction of alcohol **11** with pTsOH (cat.) was followed periodically by  $^1\text{H}$  NMR at 309 K ( $36\text{ }^\circ\text{C}$ ) which led to rapid equilibration ( $[\mathbf{11}:\mathbf{25}] = 50:50$  after ca. 24 min). For preparative purposes (E 25), the alcohol **11** was allowed to react at reflux with pTsOH (cat.) for 4 h to give a (final) equilibrium mixture of **11** to **25** of 24:76. The allylic alcohol **25** then underwent rapid oxidation to afford the vinyl ketone **26** ( $^{13}\text{C}$  NMR: C-3 = 198.4 ppm) as an analytically pure, colourless oil.

Diagram 18: Progress of acid-catalysed acetal migration followed by  $^1\text{H}$  NMR at 500 MHz<sup>[a]</sup>[a]  $t = 240$  min spectrum recorded on 300 MHz machine (parallel reaction; preparative scale).

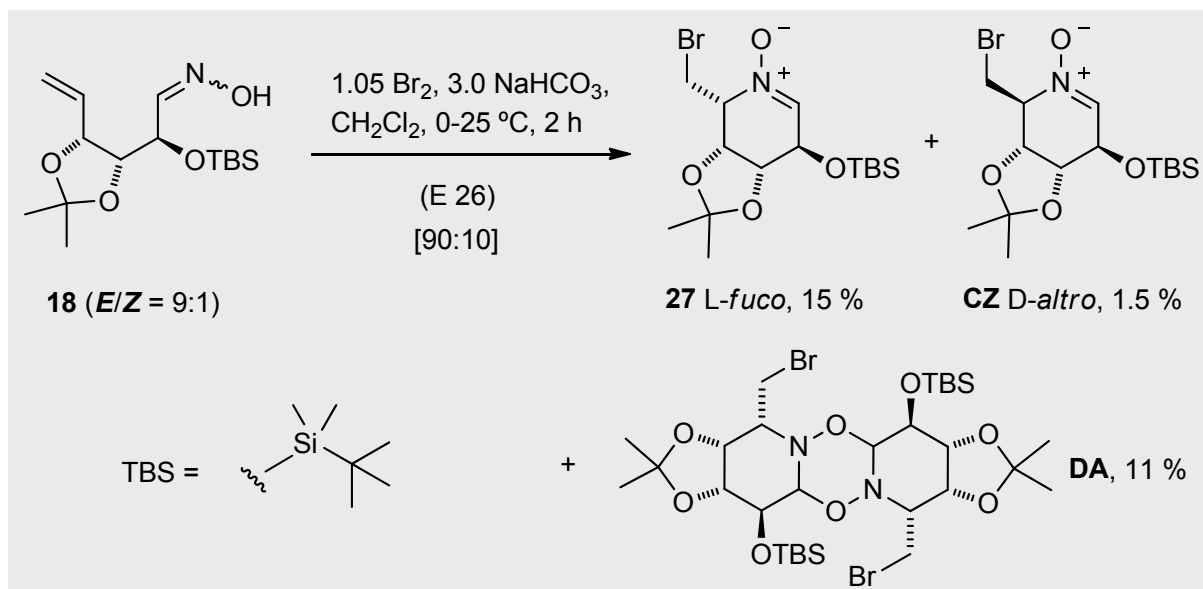


Scheme 28: *Cis*- to *trans*-acetonide migration: (i) Dess-Martin periodinane, CH<sub>2</sub>Cl<sub>2</sub>, r. t., 30 min, 60 %. [a] Periodic <sup>1</sup>H NMR measurements using sealed 0.18 M solutions of **11**.

The migration of acetonide groups under acidic conditions is, of course, nothing new: numerous reports are known of triols that have formed *cis*-acetonides, i.e. from the diol entity in the *erythro* configuration, that subsequently convert to *trans*-acetonides in which the hydroxyl groups of the diol entity have the more stable *threo* configuration.<sup>[234]</sup> The order of stability *cis* < *trans* is said to reflect the destabilisation of the 1,3-dioxolane ring on account of nonbonded interactions between *cis*-1,2-substituents.<sup>[233]</sup> In the Jäger group, Häfele has observed similar migrations of acetonide groups in *D-erythro*-4-pentene-1,2,3 triol derivatives.<sup>[235,236]</sup>

### 2.2.2.6 Bromocyclisation of hexenose oximes **18** and **22**

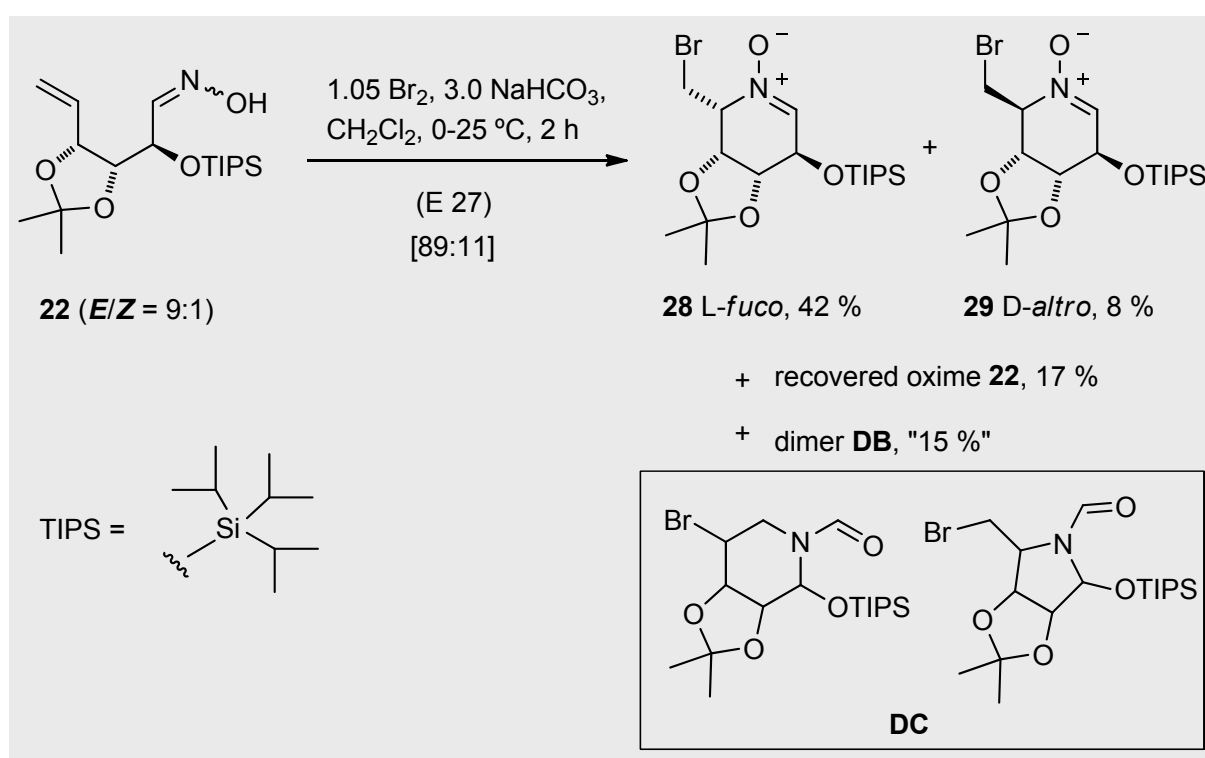
Treatment of the 2-O-TBS-protected hexenose oxime **18** with elemental bromine and sodium hydrogencarbonate under “standard conditions” (i.e. 3.0 Eq. NaHCO<sub>3</sub>, 1.05 Eq. bromine, dichloromethane, 0 °C) provided a mixture of diastereomeric nitrones (*L-fuco* nitrone **26** = 15 %; *D-altru* nitrone **DA** = 1.7 %; d.r. **27**:**CZ** = 90:10 from <sup>13</sup>C NMR) in low yield (Scheme 29). This indicates that the reaction conditions are unsuitable and lead to the formation of co-products or aid the decomposition of the intended products. The chromatographic separation yielded an impure nitrone dimer **DA** in ca. 11 % yield, evidenced by an ESI (positive ion) MS peak at *m/z* 788.2 ([M+H]<sup>+</sup>). Dissolving in CDCl<sub>3</sub> also transformed a pure sample of *L-fuco*-nitrone **27** into the dimer **DA**. The acid-catalysed dimerisation of nitrones in aprotic solvents is well precedented.<sup>[237,238]</sup> These observations are in agreement with those by Vasella et al.<sup>[151]</sup> who reported dimerisation and also gradual decomposition to “polar and apolar products” of an *L-fuco*-configured nitrone **DD** (displayed in Table 2, p. 52).

Scheme 29: Disappointing yield of the bromocyclisation of TBS-hexenose oxime **18**

The bromocyclisation proceeded more smoothly in the case of TIPS-protected oxime **22**. Under standard conditions, a moderate yield of 50 % was obtained comprising of 41 % of the *L-fuco*-nitron **28**, 9 % of *D-alto*-nitron **29** (<sup>13</sup>C NMR d. r. **28:29** = 89:11), 17 % of recovered starting material and ca. “10 %” of the corresponding dimers (Scheme 30). The reasons for the favoured formation of the *L-fuco* nitrones **27** and **28** are analogous to those concerning the formation of the five-membered *L-lyxo*-nitron **5** (cf. Section 2.2.1.3.) and will not be discussed here further. According to <sup>1</sup>H NMR and TLC analysis, the TIPS-protected nitrones dimerised and decomposed gradually at room temperature, although they can be stored indefinitely in the freezer (i.e. -28 °C) without problem. The synthesis of **28** and **29** required eight steps from *D-lyxose* and proceeded in an overall yield of 19 % (*L-fuco* **28**, Σ 16 %; *D-alto* **29**, Σ 3 %). This synthetic sequence compares favourably to the 11 steps (Σ 18 %) required by Vasella and co-workers<sup>[152]</sup> to synthesise the *L-fuco*-nitron **DD** starting from the advanced intermediate, allyl 4,6-*O*-benzylidene- $\alpha$ -*D*-glucopyranoside.<sup>[239]</sup>

The rate of nitron dimerisation was investigated by MS analyses and found, not surprisingly, to be temperature-dependent. The molecular ion peak for the *L-fuco*-nitron **28** (*m/z* 436.1 [M+H]<sup>+</sup>) dropped off sharply in abundance as the sample temperature was ramped up from 370 K to 480 K, which, in turn, accelerated the dimerisation. The dimer **DB** has an ESI (positive ion) MS peak at *m/z* 972.1 ([M+H]<sup>+</sup>). The reaction yielded additional co-products, although comprehensive identification of them proved difficult as only impure “product” fractions could be obtained, despite column chromatography, MPLC purification, etc.. Again, MS analysis provided the most useful information: an ESI (positive ion) MS peak at *m/z*

436.1 ( $[M+H]^+$ ) points to the *N*-formyl substituted piperidine/pyrrolidine **DC**. Although this molecular ion peak is equal in mass to the basis nitrones **28/29**, its abundance is only 10 % (nitrone **28**: ca. 70 %). Loss of 28 amu gives a fragment peak with 100 % abundance at  $m/z = 408.1$  (i.e.  $-C=O$ ), strongly suggesting *N*-decarbonylation. Their formation can be (very tentatively) rationalised in terms of an initial Beckman rearrangement of the starting oxime followed by either 6-*endo*-tet or 5-*exo*-tet bromocyclisation to yield the piperidine/pyrrolidine **DC**. This reaction and its side-products, however, need to be investigated further.<sup>[122]</sup>



Scheme 30: Improved yield of the synthesis of cyclic nitrones from the bromocyclisation of TIPS-hexenose oxime **22**

### 2.2.2.7 NMR and conformational analysis of the L-*fuco*-nitrones **27**, **28**, and D-*altro*-nitrone **29**

The <sup>1</sup>H and <sup>13</sup>C NMR spectra of the L-*fuco*-configured TBS nitrone **27** and TIPS nitrone **28** are essentially identical meaning that for all intents and purposes the discussion needs only to focus on a comparison of the spectral properties of the TIPS-protected nitrone pair **28** and **29** (Table 2 and Diagram 19). For guidance, the NMR data of the L-*fuco*-configured nitrone **DD**, reported by Vasella and co-workers,<sup>[152]</sup> are also given. A good point is to kick off with the configuration analysis at C-2 by considering the <sup>13</sup>C NMR absorptions at the C-2/C-3 juncture: in the L-*fuco*-nitrone **28**, C-2 and C-3 are found at 67.4 and 74.5 ppm while for the

D-*altro*-nitrone **29**, the corresponding signals are found at 74.4 and 75.2 ppm. Comparatively speaking, C-2 is deshielded by 7.0 ppm and suggests a *trans* orientation of substituents at C-2/C-3 and therefore a D-*altro* assignment for nitrone **29**; consequently, for L-*fuco*-nitrone **28**, *cis*-relative substituents at C-2/C-3 prevail. The downfield shift propagated by *trans*-vicinal substituents is a well documented phenomenon, usually referred to as a “ $\beta$ -effect”,<sup>[219-221]</sup> and allows the diastereoisomers to be distinguished from each other. In contrast, the  $J_{2,3}$  coupling constants from the  $^1\text{H}$  NMR (i.e. 2.4 versus 1.9 Hz for **28** and **29**, resp.) are of little diagnostic value. In Section 3.2.3.1, a further example of a “ $\beta$ -effect” concerning the piperidine diastereoisomers **48** and **49** will be illustrated.

The conformational analysis of the L-*fuco*-nitrone **28** can be undertaken on the basis of a direct comparison to Vasella’s L-*fuco*-nitrone **DD**,<sup>[152]</sup> which is suggested to have a cyclohexene-like  $^3H_4$  (half-chair) conformation in solution. However, what quickly becomes apparent is that the conformation of the L-*fuco*-nitrone **28** is certainly no half-chair, as evidenced by the disparities found between the  $J_{3,4}$  and  $J_{4,5}$  coupling constants of the two compounds in question: The tri-*O*-benzyl derivative from Vasella (**DD**), with  $^3H_4$  conformation, showed  $J_{3,4}$  and  $J_{4,5}$  values (1.9 and 6.8 Hz) compatible with staggered (*gauche*) and *anti-periplanar* dispositions, respectively. This can be excluded for L-*fuco*-nitrone **28** since  $J_{3,4} = 6.9$  Hz (i.e. 3-H and 4-H are standing *syn*), while  $J_{4,5}$  equates to 2.5 Hz, thus indicating a *gauche* disposition for 4-H and 5-H. Based on this, a  $^{2,5}B$  boat-like conformation is more fitting for the L-*fuco*-nitrone **28** rather than the half-chair observed for the benzylated derivative **DD**. This is corroborated by the  $J_{2,3}$  value = 2.4 Hz (i.e. *gauche* disposition for 2-H and 3-H). Force-field calculations (MM2/MOPAC, ChemDraw 3-D, Version 8.0) of the L-*fuco* nitrone **28** confirmed a  $^{2,5}B$  conformation (Diagram 19).

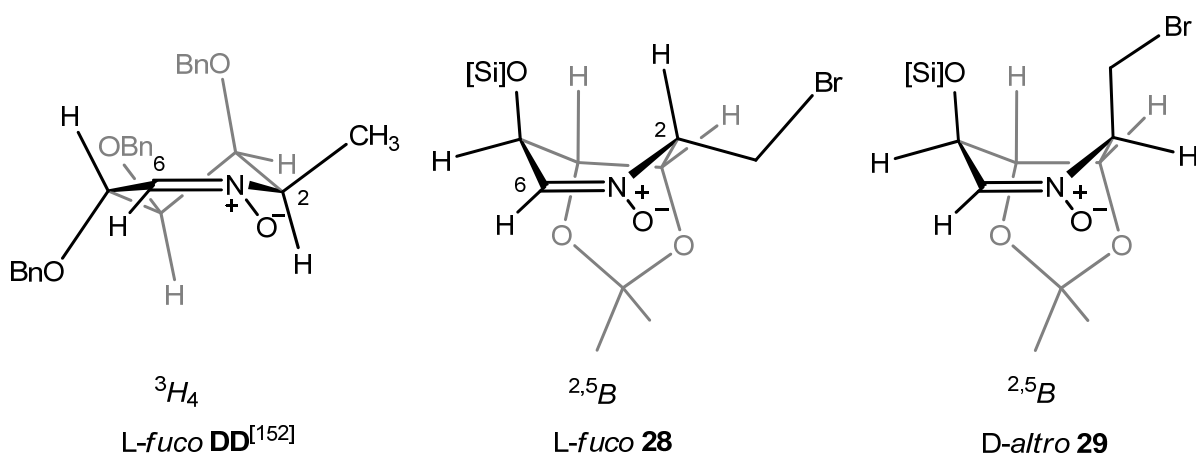


Diagram 19: Suggested  $^{2,5}B$  boat-like solution conformations of L-*fuco* **29** and D-*altro* **30** configured nitrones; comparison with Vasella’s “half-chair” L-*fuco*-nitronate derivative **DE**.

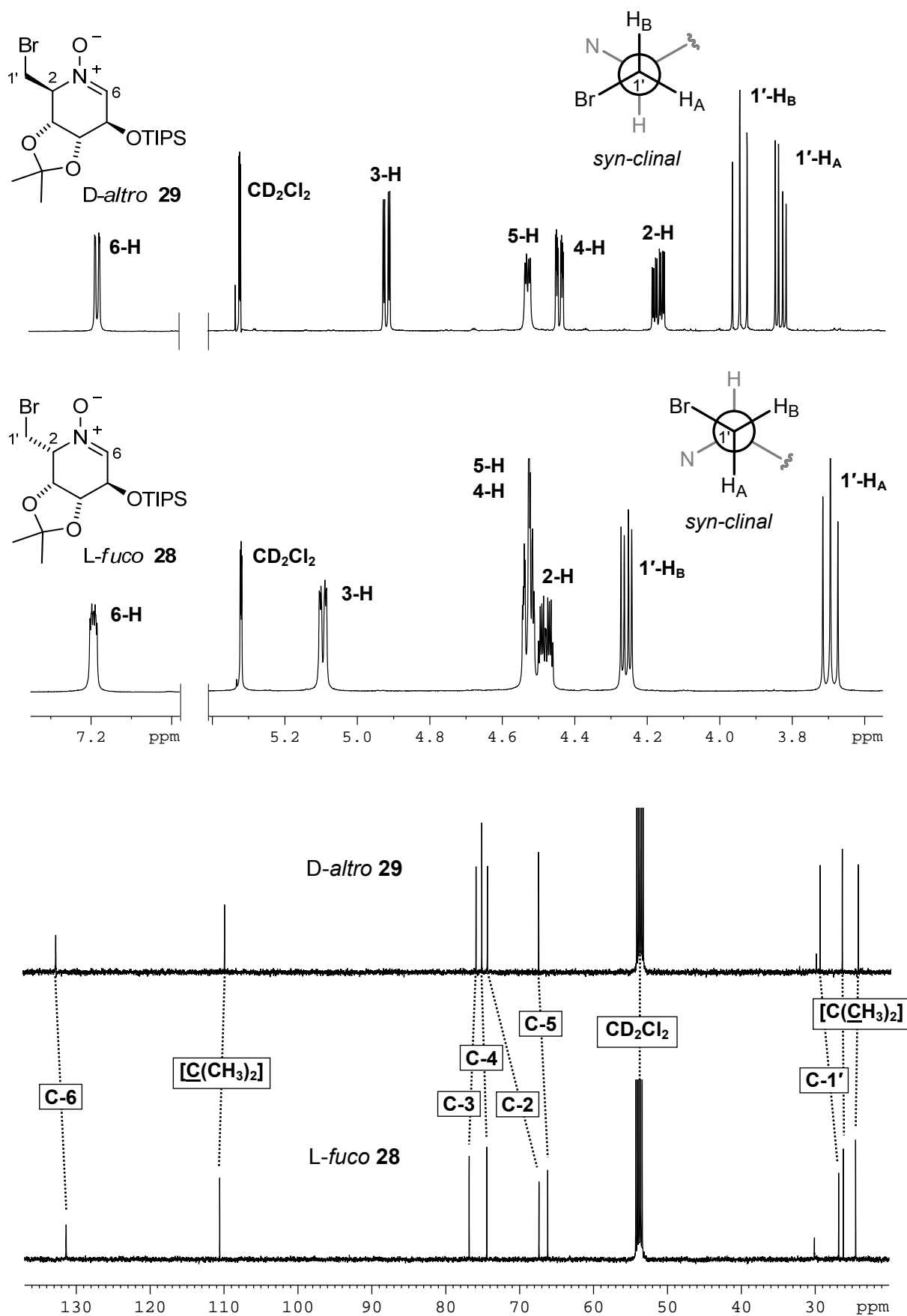
The alternative  $B_{2,5}$  conformation of L-*fuco* **28** — obtainable by “flipping” the flagpole substituents at C-2 and C-5 (not shown) — was ca. 3.2 kcal/mole higher in energy. In other words,  $\Delta G$  is positive for an equatorial to axial conformational change at C-2. Interestingly, the difference in energy is larger than the “A value” alone would suggest, i.e. the estimated energy needed for the bromomethyl substituent (on a cyclohexane ring) to go from an equatorial position to the axial (for  $\text{CH}_2\text{Br}$  = ca. 1.9 kcal/mol; cf. A values for  $\text{CH}_3$ ,  $\text{C}_2\text{H}_5$  are 1.74, 1.8 kcal/mol, respectively).<sup>[240,277]</sup> Presumably, there are additional energy costs resulting from repulsive *gauche* interactions of the axial C-2 substituent with the acetonide moiety. The  $^1\text{H}$  NMR data does not support the  $B_{2,5}$  conformation either, since the requirement for diaxial hydrogens at C-4 and C-5 is not met on the basis of  $J_{4,5} = 2.5$  Hz.

**Table 2:** Selected  $^1\text{H}$  and  $^{13}\text{C}$  NMR data from L-*fuco* and D-*altro* configured nitrones<sup>[a]</sup>

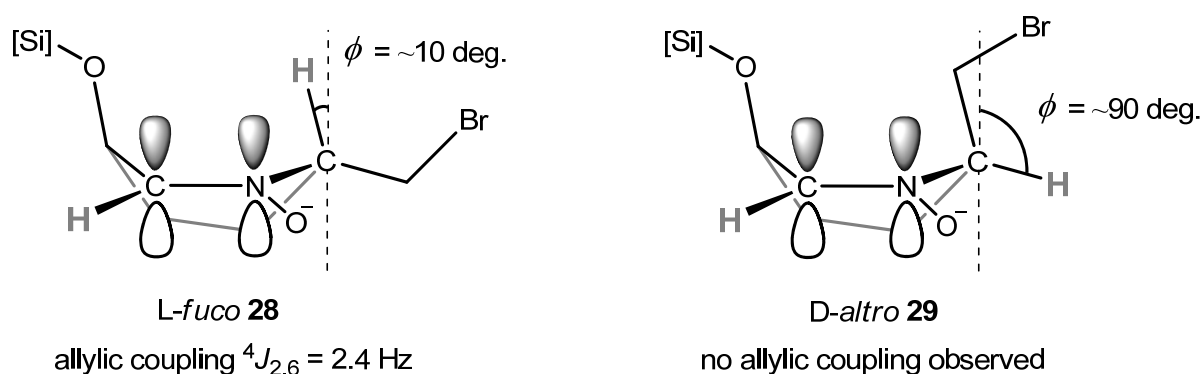
	DD L- <i>fuco</i> <sup>[b]</sup>	<b>27</b> L- <i>fuco</i>	<b>28</b> L- <i>fuco</i>	<b>29</b> D- <i>altro</i>
2-H	3.90-4.02	4.51 <sup>[c]</sup>	4.48	4.17
3-H	4.00	5.10	5.09	4.92
4-H	3.87	4.58	4.53 <sup>[d]</sup>	4.44
5-H	4.51	4.54 <sup>[c]</sup>	4.52 <sup>[d]</sup>	4.53
6-H	7.05	7.19	7.20	7.18
1'-H <sub>A</sub>	1.55 (CH <sub>3</sub> )	3.80	3.70	3.83
1'-H <sub>B</sub>		4.36	4.26	3.95
$J_{2,3}$	3.7	2.4	2.4	1.9
$J_{3,4}$	1.9	7.2	6.9	7.1
$J_{4,5}$	6.8	2.5	2.5	2.2
$J_{5,6}$	2.5	5.4	n/d	5.0
$J_{2,1A}$	n/a	10.4	10.4	4.7
$J_{2,1B}$	n/a	4.6	4.7	10.3
$^2J_{1A,1B}$	n/a	9.9	9.9	9.7
C-2	66.9	67.3	67.4	74.4
C-3	75.2	74.4	74.5	75.2
C-4	78.6	76.7	76.8	76.0
C-5	73.1	66.1	66.2	67.5
C-6	133.7	132.0	131.4	132.6
C-1'	14.5	26.8	26.8	29.6

[a] Spectra recorded at 500 MHz. [b] Data taken from Vasella and Peer, lit.<sup>[152]</sup>. [c] 2-H and 5-H signals overlapping. [d] 4-H and 5-H signals overlapping. n/a = not applicable. n/d = not determined.



Diagram 20: Comparison of parts of the  $^1\text{H}$  and  $^{13}\text{C}$  NMR spectra of the six-membered nitrones, L-fuco **28** and D-altro **29** ( $\text{CD}_2\text{Cl}_2$ , 500 MHz)

Surprisingly, the ring conformation of the *D-altro*-nitrone **29** is roughly the same as that preferred by *L-fuco*-nitrone **28**, i.e. a  $^{2,5}B$  (boat) conformation (Diagram 19). Owing to the sensitivity of  $^{13}\text{C}$  shieldings to minor structural changes, significant chemical shift differences should be evident in the case of a change in conformation. However, from  $^{13}\text{C}$  NMR only negligible chemical shift differences for C-3, C-4 and C-5 (i.e.  $<1$  ppm), compared to the respective signals for the *L-fuco*-configured nitrone, are observed. The absorption of C-2 for the *D-altro* **29** is found at lower field ( $\Delta = +7.0$  ppm) as a direct consequence of a configurational “ $\beta$ -effect”. Although the  $^{2,5}B$  boat conformation places C-2 and C-5 substituents in an unfavourable-looking 2,5-*syn*-diaxial relationship, several findings support this: The  $^1\text{H}$  NMR  $J_{2,3}$  and  $J_{4,5}$  values indicate a *gauche* disposition for the hydrogens in question; if the alternative  $B_{2,5}$  conformation were preferred, we should expect two large *axial,axial* coupling constants for  $J_{2,3}$  and  $J_{4,5}$  in the region of 7-9 Hz. More interesting, however, is a comparison of the peak-splitting of 2-H in the *L-fuco*-nitrone **28** to its congener in *D-altro*-nitrone **29**. In the former, 2-H absorbs at 4.48 ppm as a four spin system in the form of a “double quintet”, comprising of vicinal couplings to methylene hydrogens, to 3-H and, tellingly, a long range  $^4J$ -allyl coupling of 2.4 Hz to 6-H. In contrast, for *D-altro* nitrone **29**, 2-H absorbs at 4.18 ppm as a *three* spin system (‘ddd’); the difference being that the allyl-coupling is no longer observed. The diagrams shown below visualise this situation:



Essentially, the diagram shows that the magnitude of the allylic coupling is *torsional angle*-dependent. According to Günther,<sup>[184]</sup> the best chance of observing allylic couplings is when the allylic  $\sigma\text{C}-\text{H}$  bond is standing *co-planar* to the neighbouring  $\pi$ -system, since the “ $\pi$ -contribution” to the  $^4J$  coupling is large when  $\phi = 0^\circ$  or  $\phi = 180^\circ$ . On the other hand, the  $\pi$ -contribution disappears when  $\phi = 90^\circ$  or  $\phi = 270^\circ$  because the  $\sigma\text{C}-\text{H}$  bond projects along the axis of the *nodal plane* of the neighbouring  $\pi$ -system. This explains why the  $^4J$  coupling is augmented in *L-fuco*-nitrone **28** and not observable in *D-altro* **29**. The corollary of this is that a  $B_{2,5}$  conformation for *D-altro*-nitrone **29** can, again, be ruled out, since 2-H would be *co-planar* to the  $\pi$ -system and, consequently, an allylic coupling would have been observed.

# 3

## Reactions of Cyclic Nitrones

### 3.1 General Introduction

Nitrones are a well-known class of compounds that have been reviewed on several occasions<sup>[123-125,241,242]</sup> The term “nitrone”, a contraction of nitrogen ketone, was first coined by Pfeiffer<sup>[243]</sup> in 1916 in order to emphasise their similarity to ketones. The analogy rests on the mesomeric effect [**DE**↔**DF** and **DG**↔**DH**] making the nitrone or azomethine *N*-oxide group (**DE**) behave as an extended carbonyl function (Diagram 21). The term “nitrone” is usually restricted to compounds in which the canonical forms (**DE**) and (**DF**) contribute most to the structure and excludes all azomethine *N*-oxides in which considerable delocalisation of the positive charge occurs. Pyridine (**DI**) and quinoline *N*-oxides (**DJ**) would thus be excluded since their C=N bond forms part of an aromatic ring, as is the case with 2-isoxazoline *N*-oxide (**DK**), cyclic nitronates, in which nitrogen is attached to an atom with unshared electron pairs that can exert an electronic shift to diminish the contribution of canonical form **DF**. Silyl nitronates (**DL**), introduced by Kashutina<sup>[244]</sup> and Torssell,<sup>[245]</sup> are a special case and may be considered as synthetic equivalents of nitrile oxides. One final note: If R' = H, the group **DE** would represent the unstable thermal tautomer of an oxime, a so called “N-H nitrone”. Jäger and co-workers,<sup>[163-167]</sup> among others, exploited the utility of this tautomerisation in the oxime-alkene 1,2-prototropy-cycloaddition.<sup>[246]</sup> However, this will not be discussed here further.

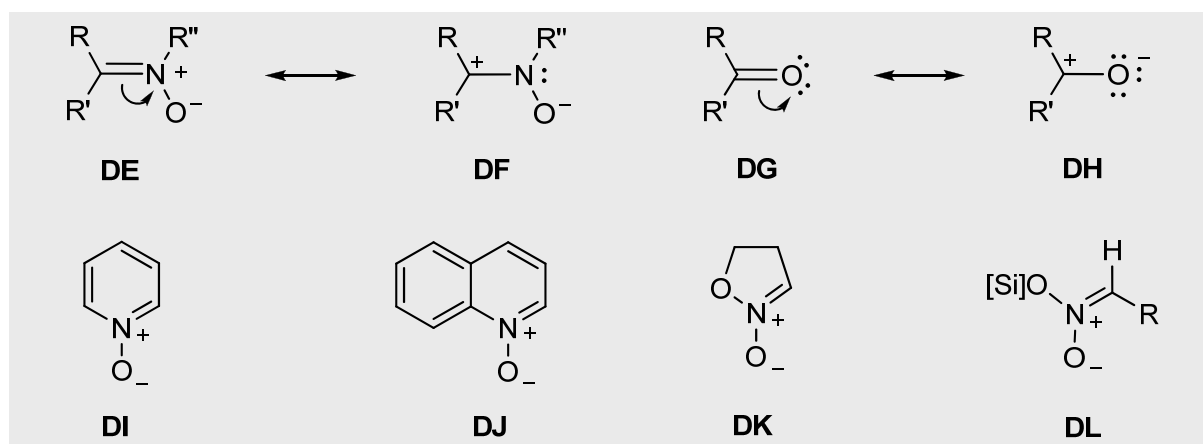


Diagram 21: Comparison between nitrone and carbonyl functionalities; nitrone types

### 3.1.1 Quick overview of common nitrone reactions

Since reviewed already in detail in the literature<sup>[123-125,241,242,245]</sup>, only a condensed account of the most common nitrone reactions will be addressed here. These reactions are characterised below and accompanied by diagrams on the following pages:

- (a) The high oxidation state of nitrones predictably allows for chemioselective reduction by judicious choice of reagent.<sup>[123]</sup> This can be directed to selective deoxygenation with the formation of imines (**DM**), double bond reduction to give N-substituted hydroxylamines (**DN**), or complete reduction to yield amines (**DO**). Deoxygenation is accomplished readily with phosphines or phosphites.<sup>[247]</sup> Metal hydrides (e.g. LiAlH<sub>4</sub> or NaBH<sub>4</sub>)<sup>[2]</sup> are used for the reduction of nitrones to hydroxylamines and the reduction stops usually at this level. For the complete reduction to the amine, catalytic hydrogenation (using palladium on carbon<sup>[2]</sup> or Raney-Ni<sup>[248]</sup>) is the best method.
- (b) The positive charge on the azomethine carbon atom dictates the pathway of their susceptibility to nucleophilic attack. Organometallic reagents add 1,3 across the nitrone system and give hydroxylamines of type **DP** after hydrolytic work-up. The addition of organometallic reagents (i.e. usually Grignard or organolithium/-zinc reagents) to nitrones has recently been reviewed by Trombini<sup>[249]</sup> and has been widely reported in our group<sup>[2-4,101,121-122,188]</sup> and elsewhere.<sup>[123-126,129b,130a,132,141,145,250,251,252,253]</sup> The addition of nucleophiles to nitrones can be promoted by 'precomplexation' with Lewis acids,<sup>[3-4,254]</sup> although no detailed discussion of this will be given here. Nitrones also add trimethylsilyl cyanide (or 'metal cyanides', i.e. Et<sub>2</sub>AlCN) to give  $\alpha$ -cyanohydroxylamines (**DQ**)<sup>[2,251,255]</sup> which, in certain cases, under acidic hydrolysis can further be transformed into  $\alpha$ -amino acids.<sup>[256]</sup> Related to this, although at first not obvious, is the nitroaldol type addition of nitronates to nitrones to afford  $\beta$ -nitrohydroxylamines (**DR**): Both structural types, **DQ** and **DR**, can be reduced further which, from a practical point of view, essentially amounts to a novel, convergent synthesis of 1,2-diamines.<sup>[2,5,177,257]</sup> The synthesis of  $\beta$ -amino acids represents another important structural class. This can be achieved through the addition of ester-derived lithium enolates or silyl ketene acetals to nitrones (Diagram 23).<sup>[249,258]</sup> The factors governing the mechanism of the addition have been the source of some consternation.<sup>[259]</sup> lithium enolates add step-wise to nitrones (cf. Mannich type reaction) to yield  $\beta$ -amino esters (**DS**) directly. Silylated ketene acetals, on the other hand, are poorer nucleophiles which require activation for reaction to take place with nitrones. Activation is usually done in the form of a prior treatment of the nitrone with

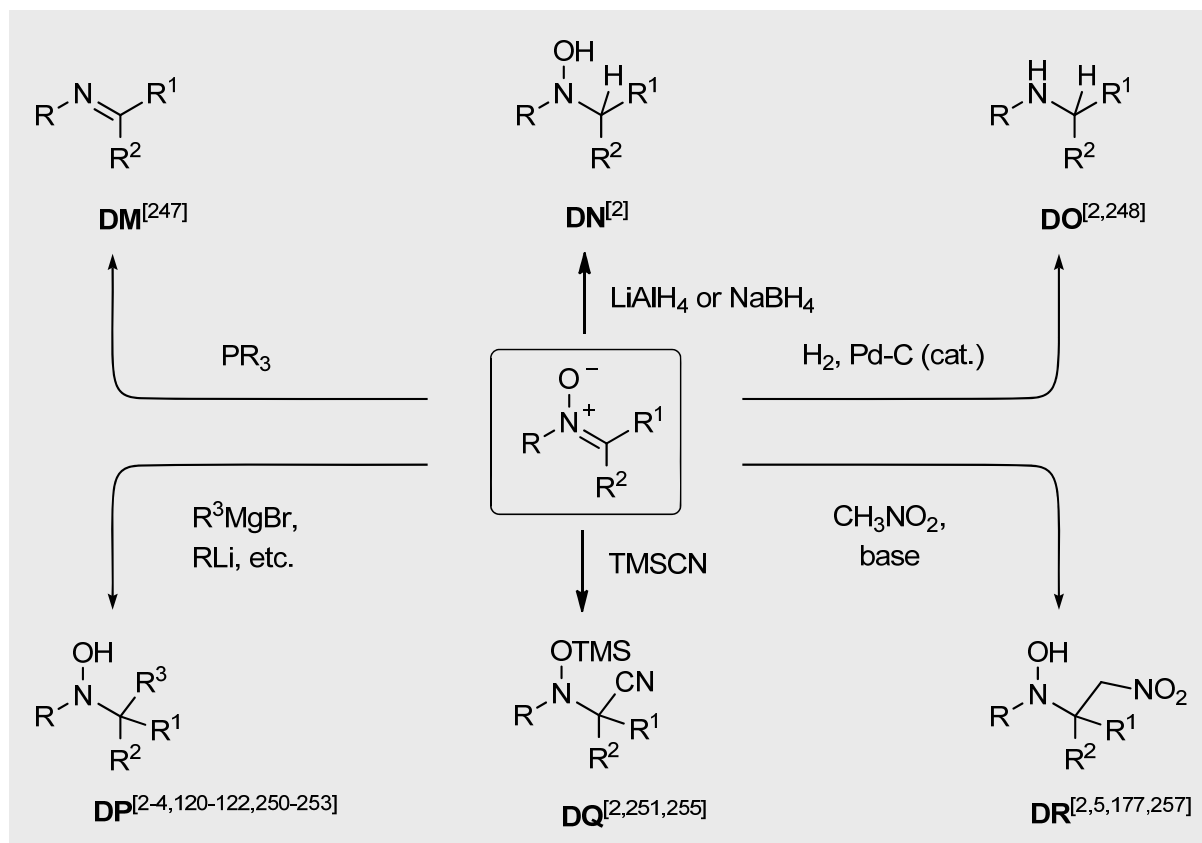


Diagram 22: The chemoselective reduction of nitrones and examples of possible types of nucleophiles that readily add to nitrones to produce  $\alpha$ -substituted hydroxylamines

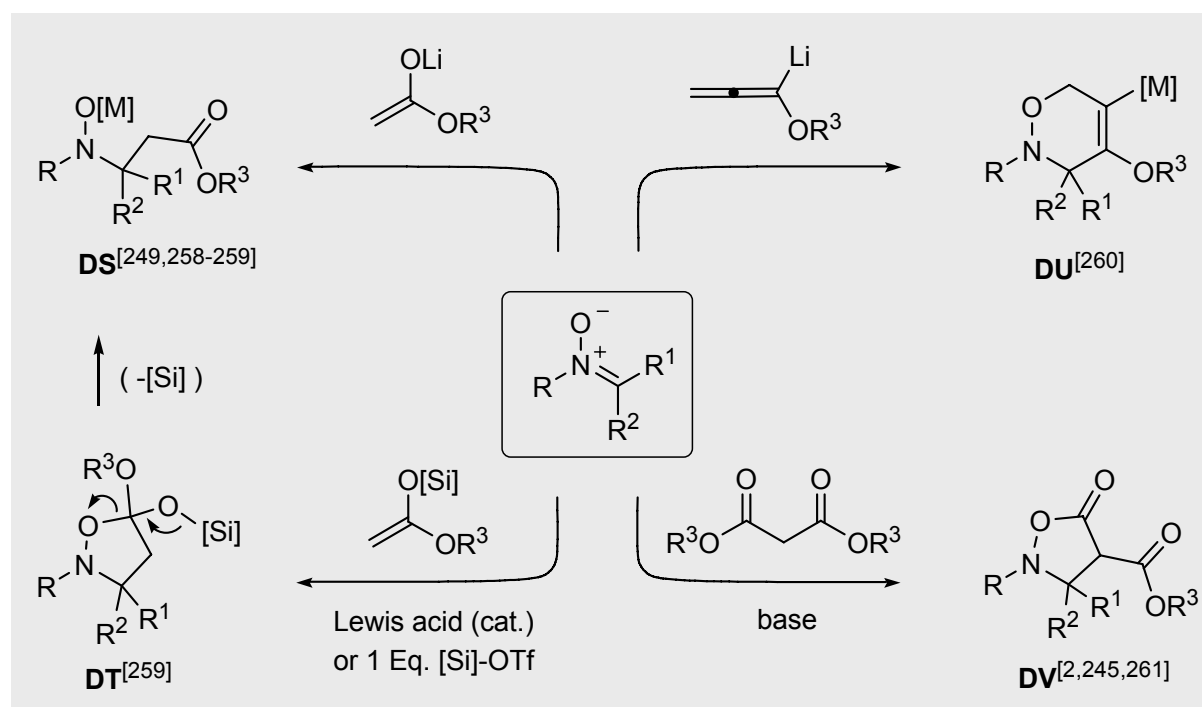


Diagram 23: Further types of nucleophiles that react readily with nitrones to generate intermediates of synthetic utility

Lewis acids or by applying O-silylation using stoichiometric amounts of silylating reagents (e.g. 'TBSOTf') to further enhance the electrophilicity of the azomethine carbon. Experimental evidence indicates that a step-wise or concerted 1,3-dipolar cycloaddition mechanism is operative,<sup>[259]</sup> which in the latter case can lead to cycloadducts of type **DT**. This suggests that activation can alter the relative energies of the molecular orbitals and therefore influence the mechanistic pathway dramatically. Further silyl migration/deprotection steps offer a plausible rationale of the subsequent transformations in order to arrive at the open-chain product (**DS**).

Related to the usage of lithium enolates is the application of lithiated methoxyallenes, as introduced by Reissig et al.<sup>[260]</sup> Addition to nitrones provides entry to 3,6-dihydro-2*H*-1,2-oxazines (**DU**). Further elaboration of **DU** usually comprises hydroxylation of the enol ether double bond followed by reductive N-O bond cleavage; this protocol leads to heavily-substituted 1,4-amino alcohols which have been utilised as intermediates *en route* to a variety of iminopolyol structures. The addition of active methylene compounds is also possible: The reaction, for example, of nitrones with the carbanion from malonate proceeds to the isoxazolidinones **DV**.<sup>[2,245,261]</sup>

- (c) The 1,3-dipolar cycloaddition with nitrones allows the formation of five-membered heterocycles using alkene and alkyne dipolarophiles, although other multiply bonded systems may be used (allenes, isocyanates, nitriles, thiocarbonyls, etc.). Olefins react with nitrones to afford isoxazolidines (**DW**) whereas symmetrically substituted acetylenes, for instance, react with nitrones to produce 4-isoxazolines of type **DX** (Scheme 24). *N*-Silyloxynitrones ("nitronates"; where R = O[Si], R<sup>1</sup> = H) undergo reaction with alkenes to yield firstly *N*-silyloxyisoxazolidines (**DY**) which upon heating or treatment with acid easily eliminate to form 2-isoxazolines (**DZ**).<sup>[245,262]</sup> The alternative, indicated synthesis of isoxazolines can take place through the reaction of nitrile oxides with alkenes. This variation can be considered to be the "*synthetic hegemony*" since it leads directly to the corresponding heterocycle. This approach was investigated extensively by Jäger and co-workers<sup>[263]</sup> as part of the framework of their publication series, "Synthesis *via* Isoxazolines", which has included recent preparations of furanomycin<sup>[264]</sup> and carbafuranomycin.<sup>[265]</sup> Returning to the 1,3-dipolar cycloaddition with nitrones, a vast literary basis for this reaction exists which is built on the seminal work of Huisgen<sup>[266]</sup>, monographs from Padwa and Pearson (Eds.),<sup>[267]</sup> along with reviews of Houk<sup>[268]</sup> and others.<sup>[245,269]</sup> An adequate discussion of the characteristic features of the 1,3-dipolar cycloaddition with alkenes would be beyond the scope and context of this Thesis, though the main specifics are deserving of comment: The cycloaddition can be considered to be a concerted, although

asynchronous  $[\pi 4_s + \pi 2_s]^{(*)}$  (i.e. *syn*-addition, supra-supra), with a reactant-like early transition state (T.S.) which invokes a large negative entropy of activation, thus suggesting a highly ordered T.S. bearing resemblance to that of the Diels-Alder reaction.<sup>[245,266]</sup> For the formation of isoxazolidines of type **DW**, when 1,2-disubstituted alkenes (i.e.  $R^3 \neq R^4$ ) are involved in reaction with 1,3-dipoles, two new stereogenic centres can be created in a “stereospecific” manner due to the *syn* attack of the dipole on to the double bond (cf. example in Scheme 6). For the reaction of nitrones with mono-substituted olefins, however, regioisomers can be obtained along with diastereoisomers resulting from *exo/endo* attack to the double bond (i.e. *cis/trans* selectivity). In general, a high regioselective preference for the C-3, C-5-disubstituted isoxazolidines for both electron-donating (e.g.  $R^3 = OR$ ) and electron-withdrawing groups ( $R^3 = CO_2R$ ) is observed. Only very strong electron-withdrawing groups – e.g.  $SO_2R$  – give predominately the C-3, C-4-disubstituted derivatives (Scheme 25).

Fukui's frontier molecular orbital concept ('FMO theory')<sup>[270]</sup> provides us with a rationalisation of these experimental results and was first adopted to the reactivity of 1,3-dipolar cycloadditions by Sustmann.<sup>[271]</sup> This concept considers the magnitudes of the frontier molecular orbitals when aligning the mono-substituted alkene with the nitron, i.e. the interaction between the HOMO (highest occupied molecular orbital) of dipolarophile with the LUMO (lowest unoccupied molecular orbital) of the 1,3-dipole – or *vice versa* – through which a stabilisation of the molecular complex results. To paraphrase Sustmann, *substituents will influence the energy of the [frontier] molecular orbitals and change their relative separation. The closer these energies the higher the stabilisation [and the quicker the reaction].*<sup>[271]</sup> The HOMO-LUMO energy gap between 1,3-dipoles and alkenes is relatively small (i.e.  $<1$  e.V.),<sup>[245,268]</sup> which can complicate the situation somewhat. This means that interactions of both alignments may be important and is a reason why mixtures of regioisomers often result.

Furthermore, it is not generally possible to predict the degree of *exo/endo* selectivity, although, in the absence of *secondary orbital interactions*,<sup>[2,269]</sup> it is usual that the *exo*-isomer is formed predominately (i.e. when the N–R and C–R<sup>1</sup> substituents are in the *trans*-relationship as set out in Diagram 25). Unfortunately, a further avenue for the formation of product mixtures can stem from the *cis-trans* isomerisation of the starting nitron prior to cycloaddition. By employing cyclic nitrones as starting materials this can be avoided since, obviously, they possess a fixed nitron geometry.

---

\* *Asynchronous* in the sense that each bond undergoing change need not necessarily have been made or been broken to the same extent by the time the T.S. has been reached.

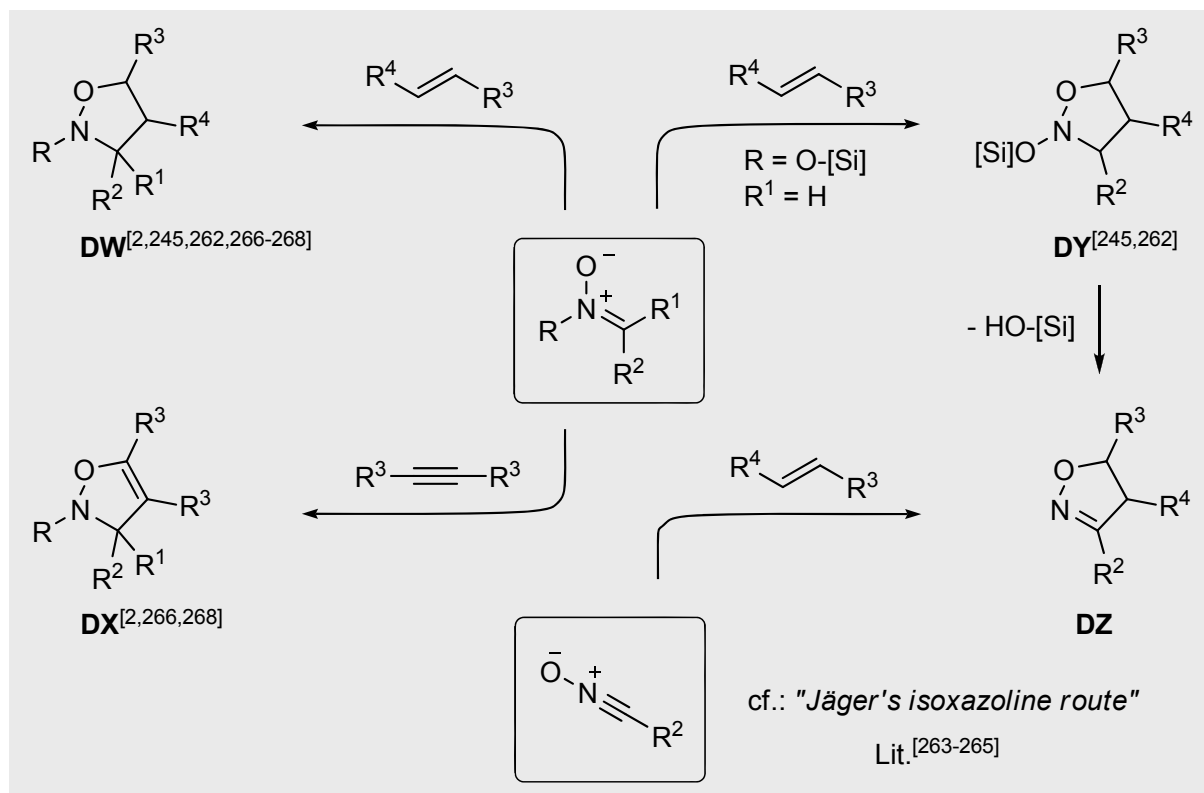


Diagram 24: The 1,3-dipolar cycloaddition of nitrones with olefins and acetylenes. Note how 2-isoxazolines (**DZ**) are *also* obtained from the reaction of nitrile oxides with alkenes.

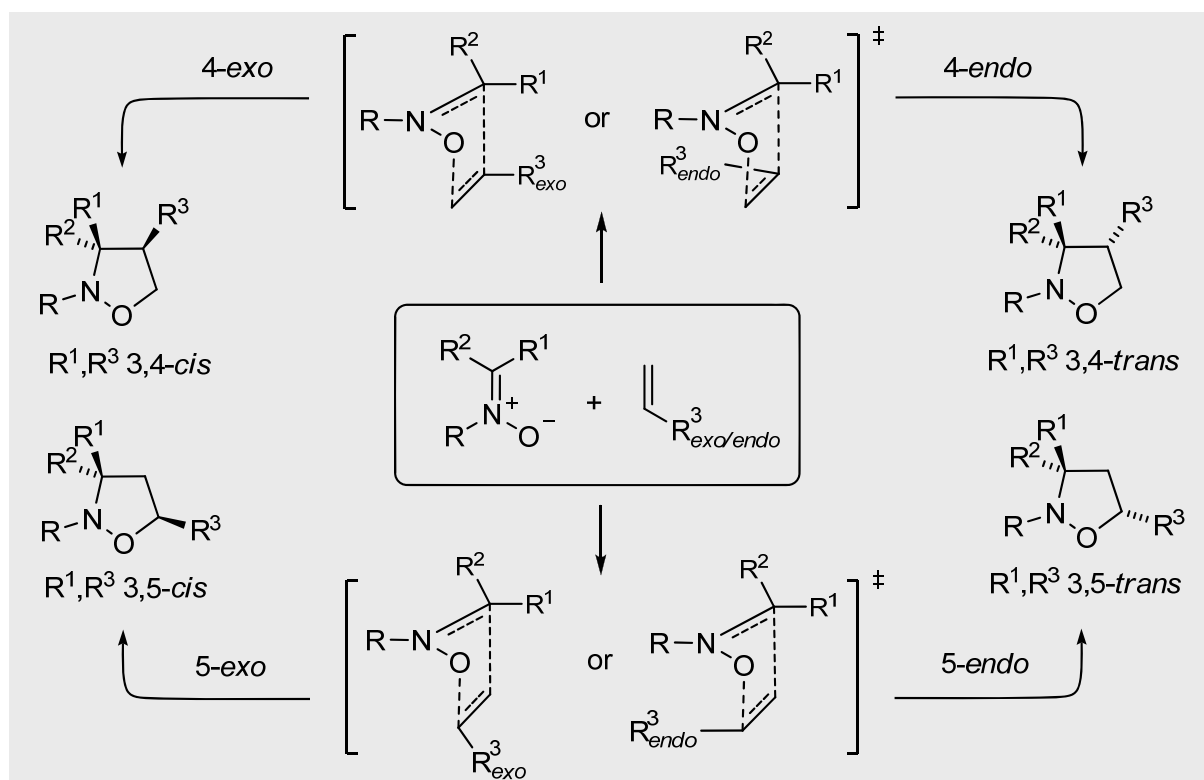


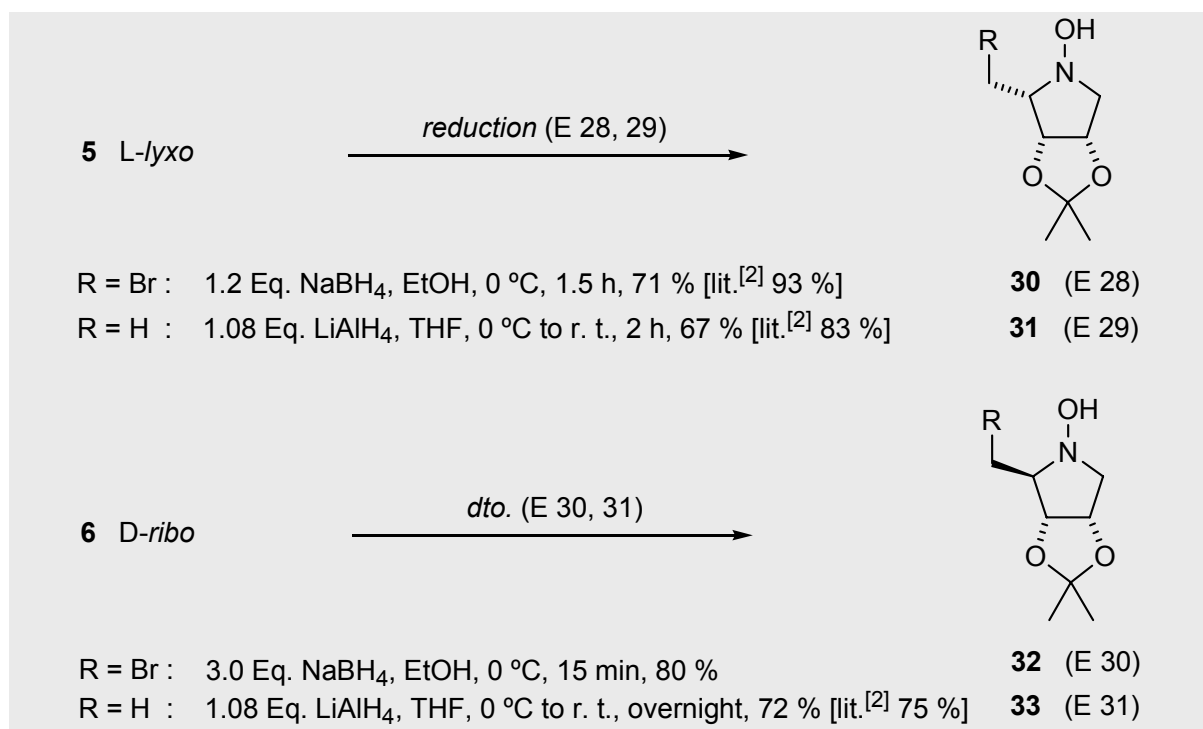
Diagram 25: Products that can arise from the nitrone and mono-substituted alkene approaching each other in either one of the two regiochemical senses, and in either an *endo*- or *exo*-fashion (assuming no intermittent (*E/Z*) nitrone isomerisation)



## 3.2 Own Results

### 3.2.1 Chemoselective reduction of L-lyxo-nitrone **5** and D-ribo-nitrone **6**

In accordance to Bierer's procedure,<sup>[2]</sup> reduction of the L-lyxo nitrone **5** with 1.2 equivalents of sodium borohydride (NaBH<sub>4</sub>) provided the bromomethyl-N-hydroxypyrrolidine **30** (71 %, lit.<sup>[2]</sup> 93 %) while reduction and simultaneous substitution of bromine was accomplished using 1.08 equiv. of lithium aluminium hydride (LiAlH<sub>4</sub>) to yield the N-hydroxypyrrolidine **31** in 67 % yield (lit.<sup>[2]</sup> 83 %). In a near identical fashion, the same round of transformations furnished the corresponding bromomethyl- and methyl-N-hydroxypyrrolidines (**32**, 80 % and **33**, 72 %, lit.<sup>[2]</sup> 75 %, respectively) in the D-ribo series, as exemplified below in Scheme 31.



Scheme 31: Chemoselective reduction of L-lyxo/D-ribo configured nitrones **5** and **6**

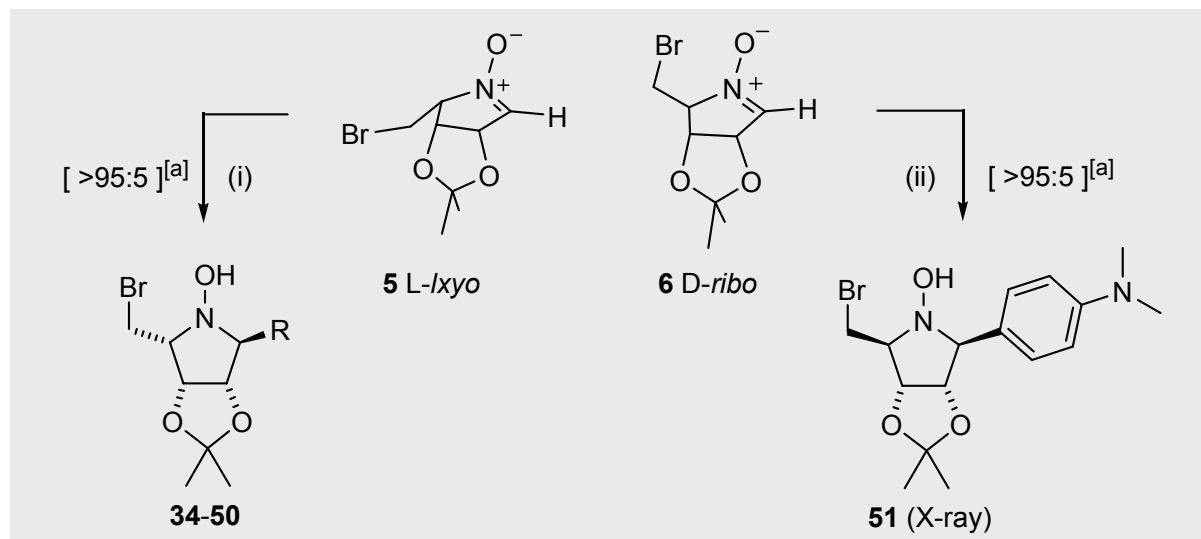
One point is worth mentioning here: For the reduction and substitution of bromine to be successful, good quality LiAlH<sub>4</sub> is required (i.e. not too old; always stored under inert atmosphere). Otherwise, as was observed, the reduction is retarded and stops at the bromomethyl stage. The synthetic utility of these pyrrolidines will be described later in Section 4 which addresses the oxidation of cyclic N-hydroxypyrrolidines to nitrones.

### 3.2.2 Addition of Grignard reagents to nitrones *L-lyxo* **5** and *D-ribo* **6**

The addition of Grignard and organolithium reagents to the *L-lyxo* nitrone **5** was examined first. Thus, the nitrone **5** was treated with 2.0 Eq. of Grignard reagent at temperatures of around -40 °C in THF. This gave the addition products **34** to **50** and **51**, as depicted in Table 2 below. The addition of 2-furyllithium (prepared according to the procedure used by Palmer<sup>[4]</sup>) to the *L-lyxo*-nitronone **5** in THF at -78 °C furnished the 2-furyl-substituted pyrrolidine **49** in 80 % yield (Entry 16). In the *D-ribo* series (Entry 18), the addition product **51**, containing the *p*-*N,N*-dimethylanilino moiety, was synthesised from the corresponding Grignard reagent and the *D-ribo* nitronone-**6**, in 79 % yield. The diastereoselectivity in all cases amounted to >95:5 and was not affected by temperature variations. The high diastereoselectivity is due to the favoured delivery of the attacking nucleophile *anti* to the dioxolane substituent, which bridges the adjacent carbons C-3 and C-4. This rationale is based on existing experimental evidence from Bierer,<sup>[2]</sup> NMR studies (see next section) and is further substantiated by literature reports<sup>[129b,132,141a,142,145,250a,251,253,272]</sup> which describe the preferential *anti*-attack of C-nucleophiles to cyclic nitrones, with respect to the facial orientation of the adjacent substituent, to give the *trans*-configured pyrrolidine. Interestingly enough, crystals could be grown from the 5-(*p*-methoxyphenyl), 5-(*p*-bromophenyl), 5-(*p*-phenoxyphenyl) and 5-(*p*-*N,N*-dimethylanilino) derivatives, **41**, **45**, **47** and **51** respectively, which proved amenable to X-ray analysis to provide additional structural proof (more in Section 3.2.2.1), also showing the extent of the large shielding of the acetonide moiety.

From Table 3, a noticeable effect of the size/bulkiness of the incoming nucleophile on the product yield can be observed. The reaction of the *L-lyxo*-nitronone **5** with isopropylmagnesium bromide or *tert*-butylmagnesium chloride furnished the respective pyrrolidine adducts, **36** and **37**, in low to moderate yields only (33-55 %; Entries 3-4). In the latter case, the reaction did not go to completion and the incumbent pyrrolidine, after isolation, was susceptible to rapid decomposition at room temperature. Similar observations (i.e. incomplete reaction, low yields) have been reported by Palmer<sup>[4]</sup> regarding the addition of neopentyl- and *tert*-butylmagnesium bromide to (*Z*)-4,5-didesoxy-2,3-O-isopropylidene-*D-erythro*-4-pentenose-*N*-benzyl nitronone. In the former case, a competing Grignard reduction was observed in approximately equal amounts.

**Table 3:** Synthesis of 2,5-disubstituted *N*-hydroxypyrrolidines through the addition of Grignard reagents or organolithium reagents (2.0 Eq. RM, THF; temp. and time see below) to (i) *L*-xylo-nitronone **5** (E 32-48) or to (ii) *D*-ribo-nitronone **6** (E 49).



Entry	Grignard reagent	Conditions		Product No.	Yield [%] <sup>[b]</sup>
		temp. [°C]	time [h]		
1 (E 32)	methyl-MgBr <sup>[c]</sup>	-40	2	<b>34</b>	94 [lit. <sup>[2]</sup> 90]
2 (E 33)	propyl-MgCl	-40	2	<b>35</b>	65
3 (E 34)	isopropyl-MgBr	-40	2	<b>36</b>	55
4 (E 35)	<i>tert</i> -butyl-MgCl <sup>[d]</sup>	-50 to -10	3	<b>37</b>	33
5 (E 36)	allyl-MgBr <sup>[e]</sup>	-40	2.5	<b>38</b>	81 [lit. <sup>[2]</sup> 90]
6 (E 37)	4-penten-1-yl-MgBr	-30 to -10	3	<b>39</b>	68
7 (E 38)	phenyl-MgBr	-40	2	<b>40</b>	72 [lit. <sup>[2]</sup> 91]
8 (E 39)	<i>p</i> -anisyl-MgBr	-40	2	<b>41 (X-ray)</b>	87
9 (E 40)	([1,1'-biphenyl]-4-yl)-MgBr	-40	2.5	<b>42</b>	80
10 (E 41)	<i>p</i> -fluorophenyl-MgBr	-40	2.5	<b>43</b>	80
11 (E 42)	<i>p</i> -chlorophenyl-MgBr	-40	3	<b>44</b>	91
12 (E 43)	<i>p</i> -bromophenyl-MgBr	-40 to -10	4	<b>45 (X-ray)</b>	55
13 (E 44)	<i>p</i> -methoxybenzyl-MgCl	-40	1.5	<b>46</b>	89
14 (E 45)	<i>p</i> -phenoxyphenyl-MgBr	-40	3	<b>47 (X-ray)</b>	75
15 (E 46)	<i>p</i> -thioanisyl-MgBr	-40	2	<b>48</b>	80
16 (E 47)	2-furyl-Li <sup>[f]</sup>	-78	1.5	<b>49</b>	80
17 (E 48)	<i>p</i> - <i>N,N</i> -dimethylanilino-MgBr	-40	2	<b>50</b>	87
18 (E 49)	<i>p</i> - <i>N,N</i> -dimethylanilino-MgBr	-40	2	<b>51 (X-ray)</b>	79

[a] Determined through <sup>1</sup>H NMR spectroscopy. [b] Yield of pure stereoisomer isolated after silica gel chromatography. [c] 2.5 Eq. RM, 3.0 M in Et<sub>2</sub>O solution (Aldrich). [d] RM 2.0 M in THF solution (Aldrich). [e] 1.5 Eq. RM, 1.0 M in THF solution (Aldrich). [f] 2-Furyl-Li, 3.0 Eq. used.

### 3.2.2.1 Configuration and conformational analysis of addition products **34-51** according to NMR spectroscopic data and comparison with the X-ray structures of pyrrolidines **41** and **51**

The  $^1\text{H}$  NMR chemical shifts and coupling constants of the *N*-hydroxypyrrolidine addition products, **35** to **51** are presented in Tables 4 and 5 (for 5-methyl, **34**, see Experimental). The  $^{13}\text{C}$  NMR chemical shifts are given in Table 6.

Turning first to the addition products **34** to **50** originating from the *L-lyxo* series, a chemical shift of 3.25 to 3.55 ppm is observed for 2-H. The corresponding vicinal coupling to 3-H,  $J_{2,3}$ , is between 4.1 and 5.2 Hz, suggesting a *cis*-orientation for substituents at C-2 and C-3 (for 2-H/C-2/C-3/3-H,  $\phi$  = approx. 35 to 45°) according to the Karplus relationship<sup>[102,183-185]</sup> The same is true for the substituents at C-3 and C-4 where  $J_{3,4}$  = 6.0 to 6.7 Hz, that is, 3-H/C-3/C-4/C-5  $\phi$  = approx. 25°. For 5-H, a substituent dependent chemical shift region for non-aromatic (i.e. 3.10 to 3.48 ppm) and aromatic (4.10 to 4.65 ppm) side-chains is evident. There is also a dramatic decrease in the value  $J_{4,5}$  which, with the exception of the pyrrolidines **32** and **33**, was in all cases ~0 Hz. The singlet for the 4-H signal thus implies a *trans* relationship for substituents at the C-4/C-5 juncture (4-H/C-4/C-5/5-H approx. 80 to 100°). This is in agreement with the discussion in the previous section regarding the *anti*-addition of the incoming nucleophile to the acetonide moiety.

The preferred orientation of the bromomethyl group in pyrrolidines **34-50** is the same as that found in the *L-lyxo* nitrone **5** as evidenced by near-identical  $J_{2,1A}$  and  $J_{2,1B}$  coupling constants. On this footing, the bromine atom is spacially *syn*-clinal with respect to 2-H.

The  $^1\text{H}$  NMR coupling constants from the addition products **34-50** provide some insight into the preferred conformation of the five-membered ring in solution.<sup>[273,274,275,276,277]</sup> A planar pyrrolidine ring – although free of valence angle strain (108°) – can be ruled out, as it would have several eclipsed bonds. It is better on the whole to distribute the strain by adding deformation out of the plane. In our pyrrolidine system, this deformation results in conformations where there is an optimum interplay between substituent staggering and *pseudo*-equatorial positioning of substituents to avoid 1,3-*syn*-axial interactions. The C—N bond is shorter than the C—C bond (1.48 Å and 1.53 Å, respectively) and so any unfavourable *syn-pentane*-like 1,3-relationships will involve the substituents adjoining the heteroatom, i.e. at carbons C-2 and C-5, the most. One of these substituents, the bromomethyl at C-2 or the branched-alkyl/aromatic side chain at C-5, should then preferably occupy a *pseudo*-equatorial position. One conformation consistent with  $^1\text{H}$  NMR is the

puckered envelope conformation  ${}^1E$  (Diagram 26). Here, C-2, C-3, C-4 and C-5 are coplanar while nitrogen is at the envelope flap above the plane with the hydroxyl group *equatorial*. The notation  ${}^1E$ , valid as depicted, implies a pyrrolidine ring with  $C_s$  symmetry.

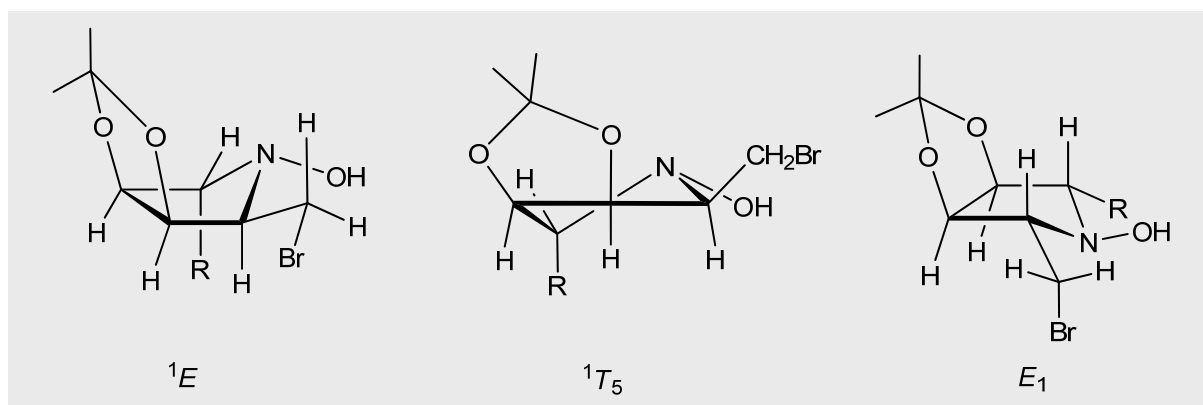


Diagram 26: Possible conformations of the pyrrolidine addition products in solution

It should be noted that the  ${}^1E$  envelope presents only an instantaneous “picture” of the pyrrolidine ring in solution. Strictly speaking, the ring is not fixed but possesses a degree of *conformational flux* meaning that additional conformations can be populated also. By rotating the ring to a distinct point of view, the pyrrolidine ring appears to adopt  $C_2$  symmetry. This is termed a “twist”, where  ${}^1T_2$  (not shown) or  ${}^1T_5$  conformations are probable.<sup>[278]</sup> For a pyrrolidine ring to have a true half-chair conformation only three atoms are deemed to adopt coplanarity while the remaining two atoms are deflected at equal distances, right angles to either side of the plane.<sup>(1)</sup> In solution, the interchange between  $C_s$  to  $C_2$  conformations, i. e.  $E$  to  $T$ , is part of the pseudorotational itinerary. In a *pseudorotation* the atoms themselves do not rotate, it is the phase of the puckering that rotates around the ring.<sup>[279]</sup> This explains why multiple conformations for the synthesised pyrrolidines need to be considered. The energy barrier to interchange is low, since in a *pseudorotation* the ring is not required to pass through a planar intermediate, i. e. the inversion barrier of nitrogen is not an issue.<sup>[275,276]</sup>

Since we have both diastereoisomers of the *p-N,N*-dimethylanilino substituted pyrrolidines, a fruitful comparison of  ${}^1H$  and  ${}^{13}C$  NMR spectroscopic data in the  $\alpha$ -L-*lyxo* **50** and the  $\beta$ -D-*ribo* **51** series can be made (Diagrams 27, 28, 29). The  ${}^1H$  NMR data from the  $\beta$ -D-*ribo* pyrrolidine **51** reveals the 2-H resonance at 3.25 ppm, very close to the 2-H chemical shift of 3.34 ppm in the diastereoisomer, pyrrolidine  $\alpha$ -L-*lyxo* **50**. The  $J_{2,3} = 5.0$  Hz and is fitting for a *trans*-configuration of the substituents at C-2/C-3 (2-H/C-2/C-3/3-H,  $\phi =$  approx. 130 to 135°).

<sup>1</sup> The reader is encouraged to construct his own model to “see” this!

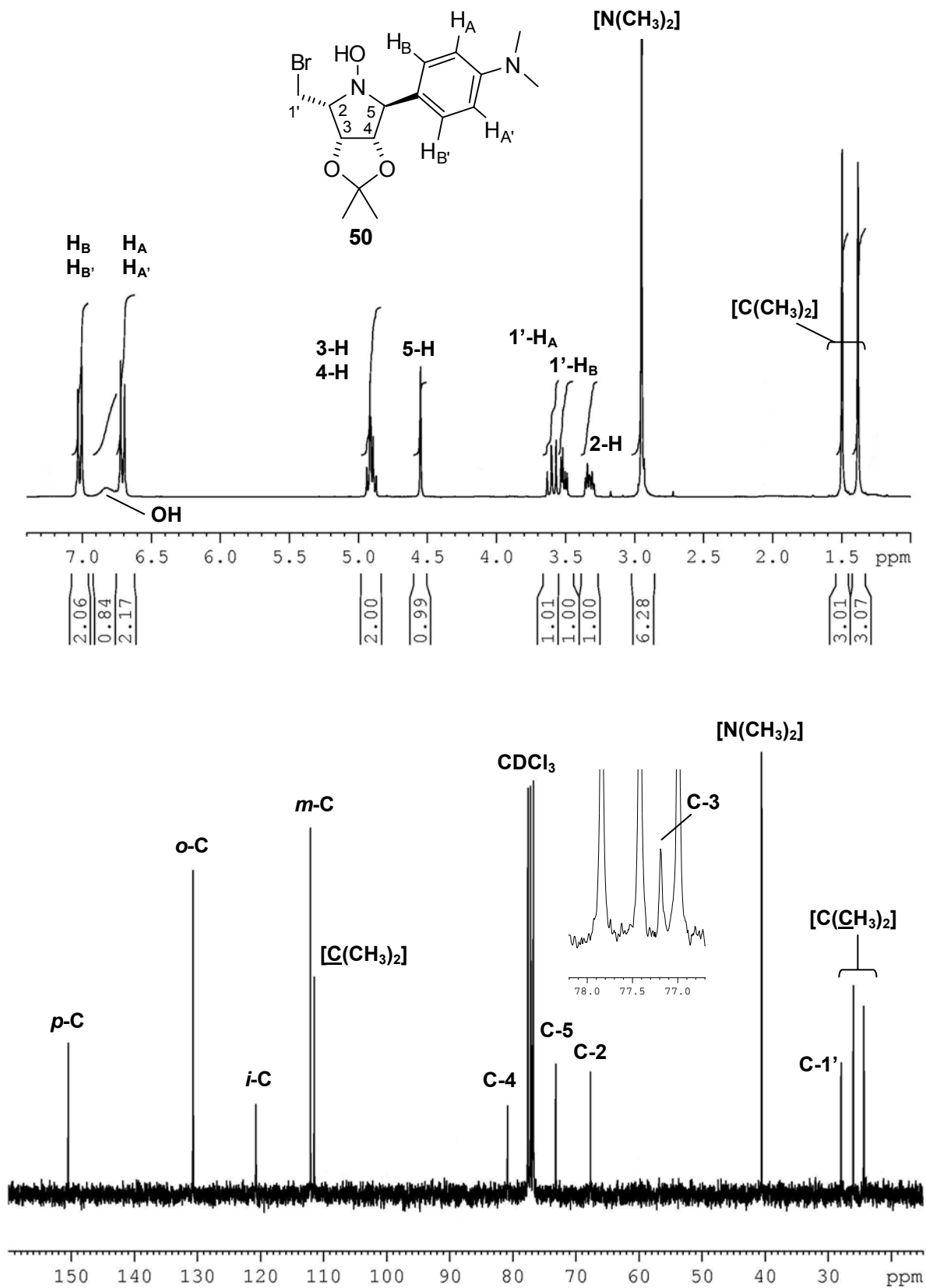
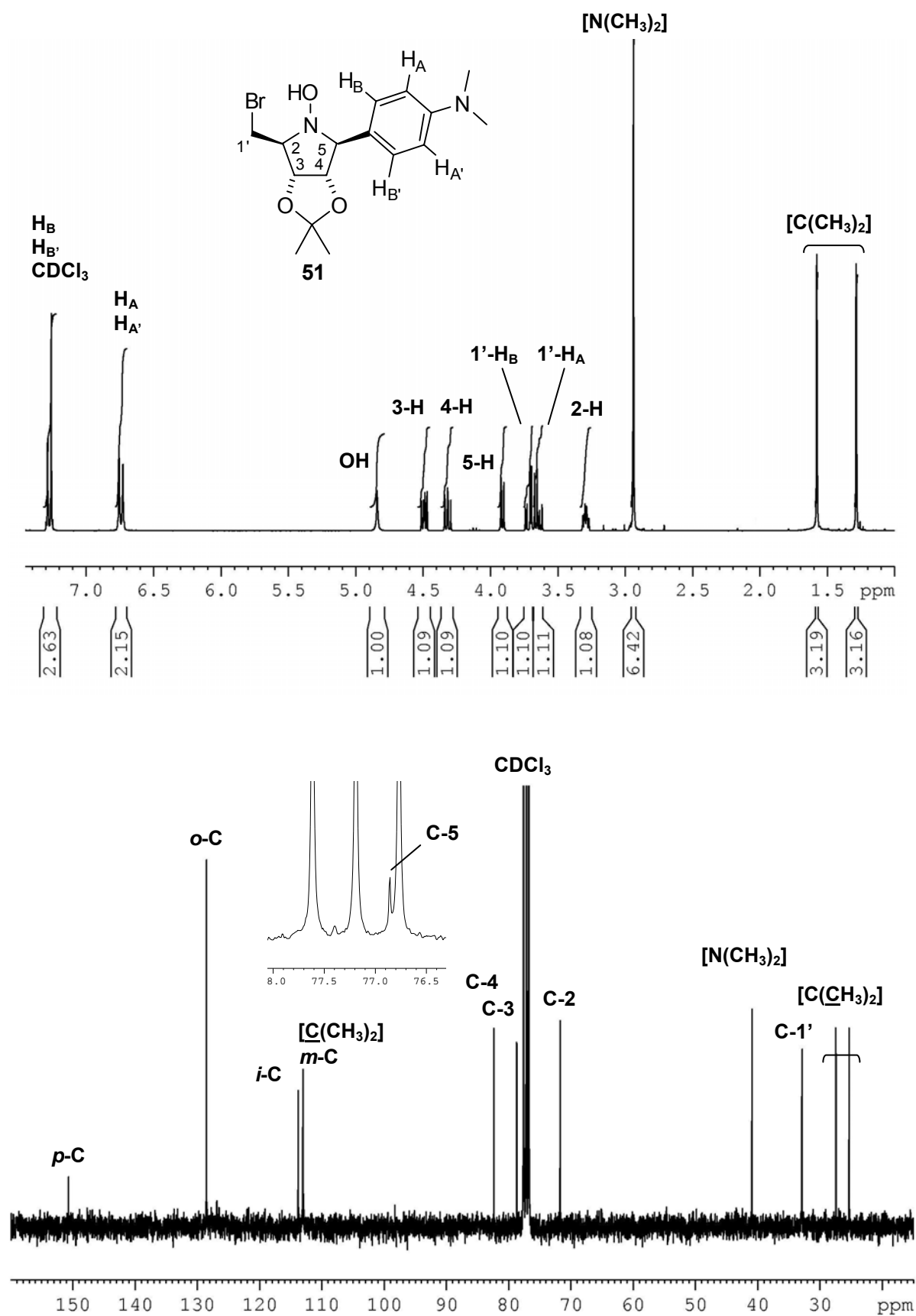
Diagram 27:  $^1\text{H}$  and  $^{13}\text{C}$  NMR spectra of the pyrrolidine,  $\alpha\text{-L-lyxo}$  **50** (300 MHz,  $\text{CDCl}_3$ )

Diagram 28:  $^1\text{H}$  and  $^{13}\text{C}$  NMR spectra of the pyrrolidine,  $\beta$ -D-ribo **51** (300 MHz,  $\text{CDCl}_3$ )

An inspection of the  $^{13}\text{C}$  NMR data shows a large chemical shift difference for C-2 in **50** as compared to **51** (67.8 versus 71.8 ppm). Whereas the substituents at C-2 and C-3 are *cis* in **50**, they are *trans* in **51**. The 4.0 ppm downfield shift for the signal of this carbon in  $\beta$ -D-ribo **51** is in keeping with the observations of Moffat *et al.*<sup>[280]</sup> who reported the same trend for substituents standing *trans* to the dioxolane ring in 2,3-O-isopropylidene furanose derivatives when compared to the data of the *cis* isomer. This is an example of a “ $\beta$ -effect”, as seen already (cf. p. 51). The *trans* assignment for the configuration of C-2/C-3 in **51** is then justified, and is further corroborated by the corresponding X-ray solid state structure (below).

The 3-H and 4-H chemical shifts as well as the  $J_{3,4}$  coupling constant in **51** are of the same order as found in the diastereoisomer **50**. In contrast, the signal for 5-H in the  $\beta$ -D-ribo pyrrolidine **51** is found at 3.98 ppm which constitutes an upfield shift of 0.57 ppm as compared to the 5-H resonance in the diastereoisomer **50**. The  $J_{4,5}$  value has also increased substantially to 6.1 Hz. Although it can be inferred from this that there is now a *trans*-orientation of substituents at C-4/C-5 (4-H/C-4/C-5/5-H approx.  $140$ - $145^\circ$ ), the configurational assignment at C-5 by NMR remains ambiguous due to the inherent flexibility of the pyrrolidine ring.

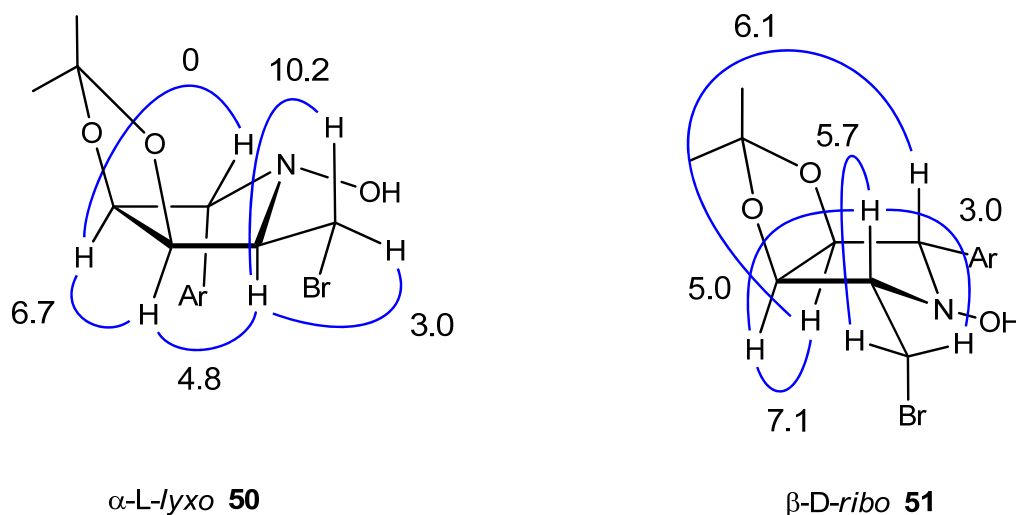


Diagram 29: Stereo-formulas and vicinal couplings constants for the pyrrolidine diastereoisomers,  $\alpha$ -L-lyxo **50** and  $\beta$ -D-ribo **51**

A possible explanation for the increased shielding of 5-H in pyrrolidine **51** manifests itself in the aromatic substituent relocating from *pseudo*-axial to a *pseudo*-equatorial orientation, whereas the only marginal chemical shift change for 2-H indicates that the *pseudo*-equatorial orientation of the bromomethyl group is retained.<sup>[281,282]</sup> Taken together, the preferred ring conformation of the pyrrolidine **51** would appear to hold for an  $E_1$  envelope rather than the



<sup>1</sup>E. This distinction places C-2 and C-5 substituents in a favourable *pseudo-equatorial* orientation so that the 1,3-diaxial steric interactions, which would afflict the pyrrolidine **51** in the case of an <sup>1</sup>E envelope, are avoided. There is also the possibility for additional half-chair or “twist” conformations for pyrrolidine **51**, as has been discussed above. Lastly, on the basis of  $J_{2,1'A} = 3.0$  Hz and  $J_{2,1'B} = 5.7$  Hz, the bromine atom in the pyrrolidine **51** is assigned an *anti-periplanar* orientation to 2-H (cf. in *D-ribo-nitron* **6**, p. 35).

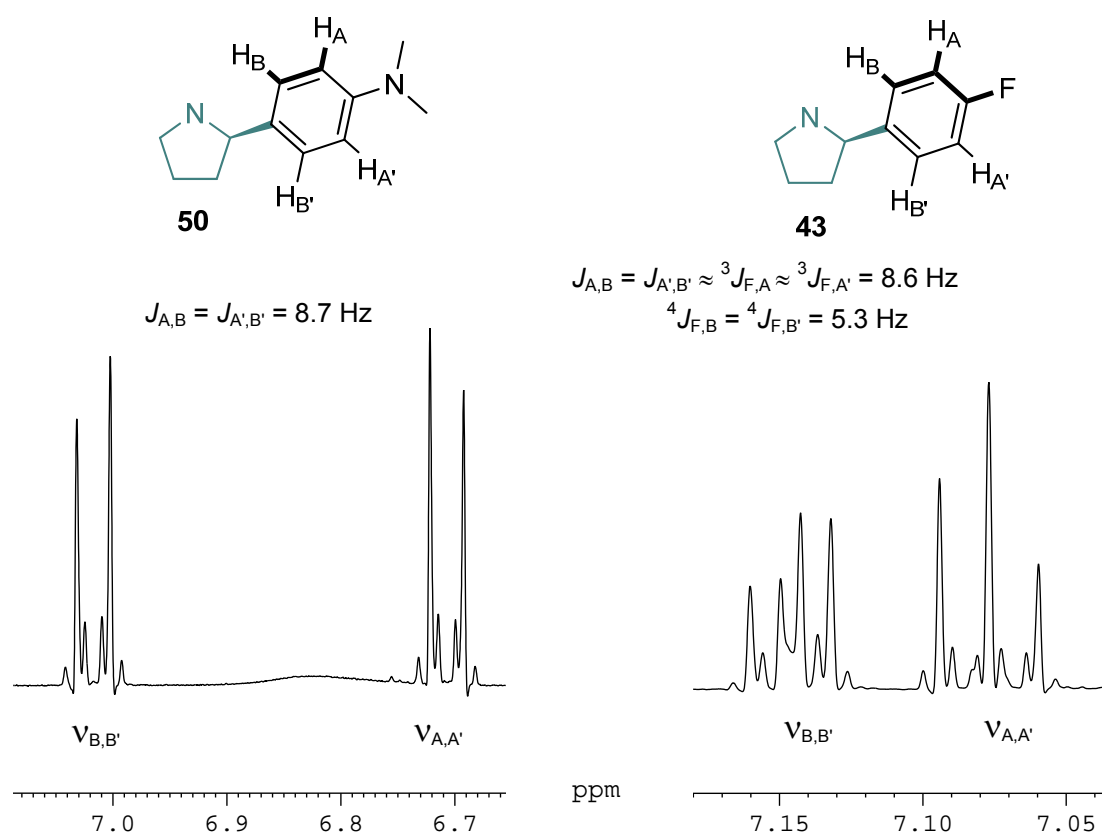
*<sup>1</sup>H NMR splitting patterns of the aromatic region of para-disubstituted benzenes in p-N,N-dimethylanilino- and p-fluorophenyl substituted pyrrolidines, 50 and 43 resp.*

The left part of Diagram 30 shows the 300 MHz <sup>1</sup>H NMR spectrum of the aromatic signals of *p*-*N*-dimethylanilino-substituted pyrrolidine **50** which are characteristic of a spectrum of the AA'BB' type. This four spin system consists of only two resonance frequencies from two sets of chemically equivalent protons (i.e.  $\nu_A = \nu_{A'}$ ,  $\nu_B = \nu_{B'}$ ), symmetric about the centre  $\frac{1}{2}(\nu_A + \nu_B)$ . The A and B nuclei are not *magnetically* equivalent (i.e.  $J_{A,B} \neq J_{A,B'}$ ;  $J_{A,A'} \neq J_{B,B'}$ ), and lead to theoretically four coupling constants meaning that first-order rules cannot be used for the analysis of the spectrum. The system is also sensitive to the chemical shift difference between the A and B nuclei so, consequently, a strong *roof effect* (i.e. when  $\Delta\delta/J \approx 0.1$ ) is observed. This is a further indication of a *spectrum of higher order*. The spectrum is not particularly well resolved either, since the AA'BB' system can show up to 24 lines, 12 each for AA' and BB' parts. Since as we have already noted the spectrum is symmetric, we can limit the discussion to a consideration of one half of the spectrum: By conducting an *on-spec* analysis, the two most intense lines, according to Günther<sup>[184,283]</sup> correspond to the  $a_2$  subspectra separated by 8.7 Hz, which from a *pseudo-first order* point of view<sup>[284]</sup> approximates to the large *ortho* coupling (perhaps, misleadingly, denoted as ' $J_{A,B}$ ').

A further quartet-like ab sub spectrum can be discerned from the spectrum. In this case, only limited information can be extracted since the signals coincide with the  $a_2$  system. Thus, no direct assignment of the smaller *meta* or *para*-coupling is made (or, apparently, possible: see discussion in lit.<sup>[184]</sup>). The coupling constant data taken in the accompanying <sup>1</sup>H NMR Tables reflects this. The dissymmetric nature of the *p*-fluorophenyl substituted pyrrolidine **43** spectrum seems daunting in comparison. Nevertheless, by assuming a degree of chemical naivety and working to the *pseudo-first order* approximation, assignment becomes straightforward: Coupling of <sup>1</sup>H with fluorine (<sup>19</sup>F,  $I = \frac{1}{2}$ , abundance = 100 %) gives rise to the primary line splittings in the form of their characteristic  ${}^3J_{H,F}$ ,  ${}^4J_{H,F}$ <sup>[220,285]</sup> coupling constants, clearly extractable from Diagram 30. Incidentally, the <sup>13</sup>C NMR signals of the aromatic

component permitted the measurement of  $^1J_{C,F}$ ,  $^2J_{C,F}$  and  $^3J_{C,F}$  coupling constants, i.e. -248.0, 21.4 and 8.1 Hz, respectively, which were all in good agreement to literature known values.<sup>[221]</sup>

Diagram 30: Detailed  $^1H$  NMR sketch of the aromatic spin system pattern ('Gaused') of *p*-*N,N*-dimethylanilino **50** and *p*-fluorophenyl-pyrrolidine **43** (300 MHz,  $CDCl_3$ )



### Discussion of the X-ray crystal structures of pyrrolidines **41** and **51**<sup>[286,287,288]</sup>

The pyrrolidine **41**, bearing the *p*-methoxyphenyl substituent, crystallises in the orthorhombic space group  $P2_12_12_1$  with two independent molecules in the asymmetric unit. The X-ray analysis of **41** firmly establishes that the pyrrolidine ring is in an envelope conformation (cf. Section 9.3 for additional diagrams). The two independent molecules form a hydrogen-bonded dimer, which is comprised of two O1-H proton donors and N1 atoms as acceptors. In this arrangement, illustrated in Diagram 31, the four atoms are in approximately the same plane; interestingly, the two hydrogen bond lengths differ appreciably – as do the corresponding angles (which contrasts sharply with, for example, the X-ray structure of Bierer's<sup>[2]</sup> very similar phenyl-pyrrolidine adduct).

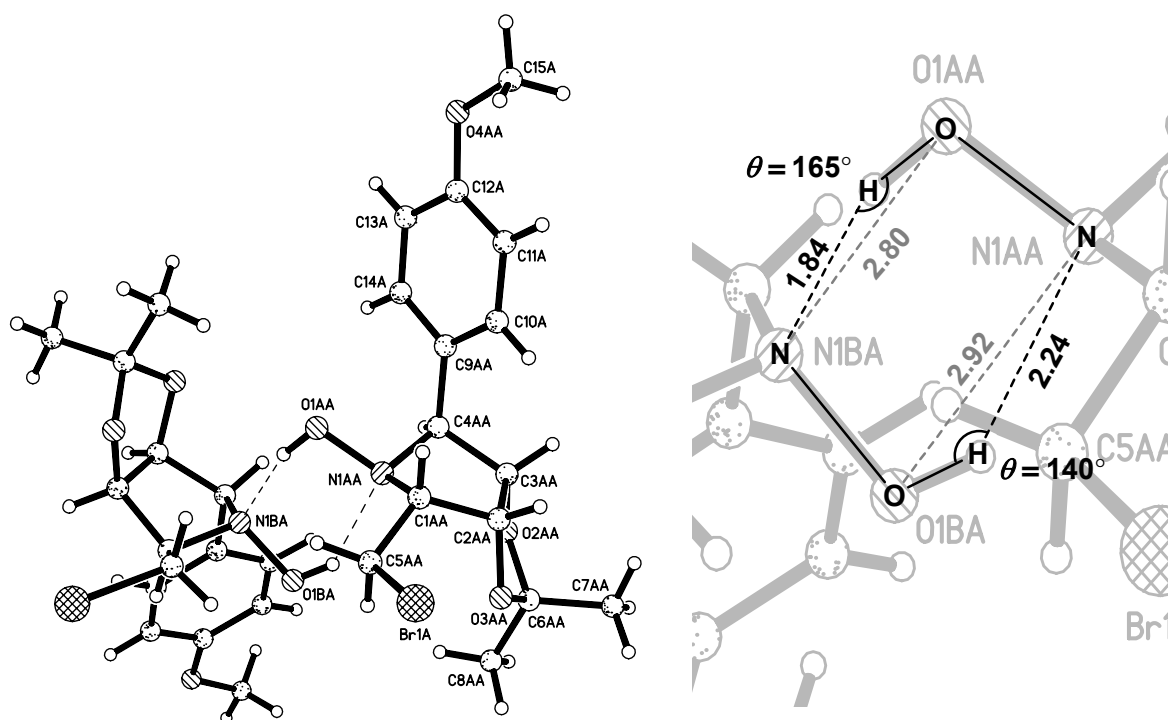


Diagram 31: Crystal dimer and detailed view of the hydrogen-bonding network found in the pyrrolidine **41**. Hydrogen bonds are represented by darker dashed lines, interatomic distances by lighter dashed ones. Lengths in Angstroms ( $1 \text{ \AA} = 1 \times 10^{-10} \text{ m}$ ).

Although omitted here to save space, the hydrogen-bonding arrangement of *p*-bromophenyl and *p*-phenoxyphenyl pyrrolidines, **45** and **47**, is nearly identical to that in **41** above, but appears in the less-symmetrical monoclinic space group  $P2_1$ . The crystal structure data and full diagrams are presented for these in Sections 9.4 & 9.5).

In the *D-ribo* series, the bilayer arrangement of the pyrrolidine **51**, bearing the *p*-*N,N*-dimethylanilino substituent, incorporates a hydrogen-bonding motif different to those described so far (Diagram 32). Here, a singular O1-H proton donor to an O2 acceptor on the isopropylidene link the adjacent layers into a “T”-shaped-hydrogen bonded bilayer set across a two-fold screw axis parallel to the *b*-axis. This aids the nesting of the two independent molecules in the asymmetric unit (monoclinic,  $P2_1$ ). Evidently, the inverted envelope conformation and/or *trans*-orientation of the bulky  $-\text{CH}_2\text{Br}$  moiety in the pyrrolidine **51** has hindered the intimate electrostatic interaction of the juxtaposed hydroxylamine groups, and has resulted in the marked difference to the array of hydrogen bonds.

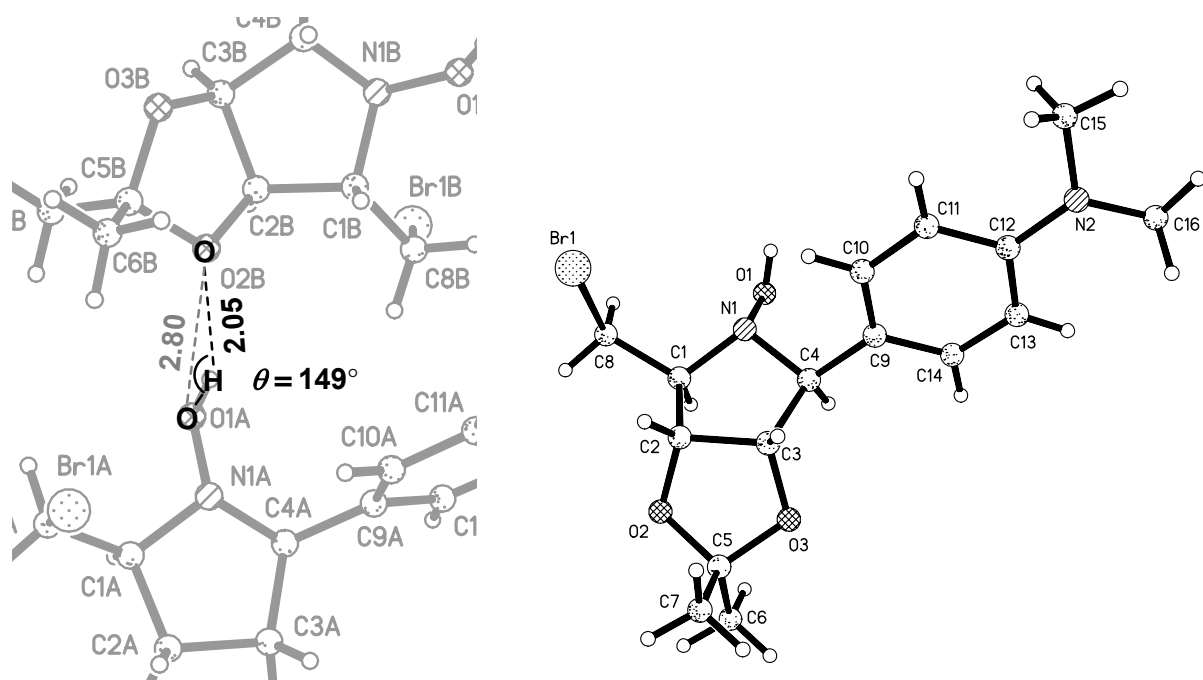


Diagram 32: Close-up of the hydrogen bond in the molecular bilayer and the asymmetric unit of the pyrrolidine **51**. Lengths in Angstroms ( $1 \text{ \AA} = 1 \times 10^{-10} \text{ m}$ ).

Inspection of the solid state structure of the pyrrolidine **51** shows that the envelope ring conformation is in good agreement with the  $^1\text{H}$  NMR, the  $J$ -values and the  $^{13}\text{C}$  NMR data discussed above. Lastly, no conformational discrepancy for the conformation of the bromomethyl group can be observed either, which is found – just as in solution, and for the crystal structure of the *D-ribo*-configured nitrone **6** (cf. p. 35) – to be standing clearly *anti*-periplanar with respect to 2-H.

**Table 4:**  $^1\text{H}$  NMR Chemical shifts of *N*-hydroxypyrrolidines **35–51** ( $\delta$  [ppm], 300.1 MHz or 500.1 MHz,  $\text{CDCl}_3$ )

Nr.	2-H	3-H	4-H	5-H	1'-H <sub>A</sub>	1'-H <sub>B</sub>	C(CH <sub>3</sub> ) <sub>2</sub>	<i>p</i> -C <sub>6</sub> H <sub>4</sub> and/or other 5-R; OH
<b>35</b>	3.25	4.60	4.35	3.20	3.48	3.55	1.23, 1.36	0.90 (CH <sub>2</sub> CH <sub>2</sub> CH <sub>3</sub> ), 1.20—1.45 (CH <sub>2</sub> CH <sub>2</sub> CH <sub>3</sub> & CH <sub>a</sub> H <sub>b</sub> CH <sub>2</sub> CH <sub>3</sub> ), 1.90 (CH <sub>a</sub> H <sub>b</sub> CH <sub>2</sub> CH <sub>3</sub> )
<b>36</b>	3.50	4.66	4.66	3.10	3.60—3.64		1.33, 1.47	0.96 (CH <sub>3</sub> ), 0.96 (CH <sub>3</sub> ), 2.00 (CH(CH <sub>3</sub> ) <sub>2</sub> )
<b>37</b>	3.40	4.75	4.68	3.35	3.75	3.85	1.36, 1.55	0.99 [9 H, C(CH <sub>3</sub> ) <sub>3</sub> ], 5.49 (OH)
<b>38</b>	3.30	4.68	4.46	3.48	3.55	3.60	1.35, 1.47	1.85 (CH <sub>a</sub> H <sub>b</sub> ), 2.80 (CH <sub>a</sub> H <sub>b</sub> ), 5.14 (CH <sub>E</sub> H <sub>Z</sub> ), 5.15 (CH <sub>E</sub> H <sub>Z</sub> ), 5.78 (CH)
<b>39</b>	3.30	4.70	4.42	3.24	3.51	3.55	1.28, 1.39	1.02, 1.37—1.48 (CH <sub>a</sub> H <sub>b</sub> CH <sub>2</sub> CH <sub>2</sub> CH=CH <sub>2</sub> ), 2.00—2.15 (CH <sub>a</sub> H <sub>b</sub> CH <sub>2</sub> CH <sub>2</sub> CH=CH <sub>2</sub> ), 4.97 (CH <sub>E</sub> H <sub>Z</sub> ), 5.03 (CH <sub>E</sub> H <sub>Z</sub> ), 5.81 (CH)
<b>40</b>	3.41	4.93	4.96	4.60	3.53	3.61	1.39, 1.50	7.10—7.40 [5 H, C <sub>6</sub> H <sub>5</sub> ]
<b>41</b>	3.35	4.89	4.91	4.54	3.50	3.55	1.38, 1.47	6.85 [2 H, H <sub>A</sub> , H <sub>A'</sub> ], 7.18 [2 H, H <sub>B</sub> , H <sub>B'</sub> ], 3.80 (OCH <sub>3</sub> )
<b>42</b>	3.41	4.97	4.93	4.65	3.56	3.64	1.38, 1.47	7.10—7.70 [9 H, C <sub>12</sub> H <sub>9</sub> ]
<b>43</b>	3.37	4.89—4.92		4.55	3.52	3.60	1.38, 1.49	7.08 [2 H, H <sub>A</sub> , H <sub>A'</sub> ], 7.15 [2 H, H <sub>B</sub> , H <sub>B'</sub> ]
<b>44</b>	3.35	4.90—4.92		4.65	3.53	3.60	1.38, 1.49	6.80 [2 H, H <sub>A</sub> , H <sub>A'</sub> ], 7.10 [2 H, H <sub>B</sub> , H <sub>B'</sub> ]
<b>45</b>	3.35	4.85—4.92		4.50	3.49	3.58	1.37, 1.46	7.00 [2 H, H <sub>A</sub> , H <sub>A'</sub> ], 7.20 [2 H, H <sub>B</sub> , H <sub>B'</sub> ]
<b>46</b>	3.30	4.73	4.45	3.35	3.59	3.65	1.26, 1.42	2.33 (CH <sub>a</sub> H <sub>b</sub> C <sub>6</sub> H <sub>4</sub> ), 3.40 (CH <sub>a</sub> H <sub>b</sub> C <sub>6</sub> H <sub>4</sub> ), 3.80 (OCH <sub>3</sub> ), 6.80 [2 H, H <sub>α</sub> , H <sub>α'</sub> ], 7.10 [2 H, H <sub>β</sub> , H <sub>β'</sub> ]
<b>47</b>	3.40	4.92	4.93	4.55	3.54	3.62	1.37, 1.49	7.00—7.33 [9 H, C <sub>6</sub> H <sub>4</sub> , C <sub>6</sub> H <sub>5</sub> ]
<b>48</b>	3.35	4.85—4.95		4.54	3.51	3.60	1.38, 1.48	7.08 [2 H, H <sub>A</sub> , H <sub>A'</sub> ], 7.25 [2 H, H <sub>B</sub> , H <sub>B'</sub> ], 2.47 (SCH <sub>3</sub> )
<b>49</b>	3.45—3.55	4.87	4.80	4.55	3.45—3.55	3.60	1.35, 1.47	6.30 (3'-H), 6.35 (2'-H), 7.40 (4'-H)

**Table 4** (continued):  $^1\text{H}$  NMR Chemical shifts of *N*-hydroxypyrrolidines **35–51** ( $\delta$  [ppm], 300.1 MHz or 500.1 MHz,  $\text{CDCl}_3$ )

Nr.	2-H	3-H	4-H	5-H	1'-H <sub>A</sub>	1'-H <sub>B</sub>	C(CH <sub>3</sub> ) <sub>2</sub>	<i>p</i> -C <sub>6</sub> H <sub>4</sub> and/or other 5-R; OH
<b>50</b>	3.34	4.92	4.90	4.55	3.55	3.60	1.37, 1.50	2.90 [6 H, N(CH <sub>3</sub> ) <sub>2</sub> ] 6.72 [2 H, H <sub>A</sub> ,H <sub>A'</sub> ], 7.00 [2 H, H <sub>B</sub> ,H <sub>B'</sub> ]
<b>51</b>	3.25	4.46	4.30	3.98	3.60	3.67	1.25, 1.55	2.90 [6 H, N(CH <sub>3</sub> ) <sub>2</sub> ] 6.70 [2 H, H <sub>A</sub> ,H <sub>A'</sub> ], 7.20 [2 H, H <sub>B</sub> ,H <sub>B'</sub> ]

**Table 5:**  $^1\text{H}$ ,  $^1\text{H}$  Coupling constants of *N*-Hydroxypyrrolidines **35–51** ( $J$  [Hz],  $\text{CDCl}_3$ )

Nr.	$J_{2,3}$	$J_{3,4}$	$J_{4,5}$	$J_{2,1'A}$	$J_{2,1'B}$	$^2J_{1'A,1'B}$	Other (5-R; AA'BB')
<b>35</b>	5.0	6.7	—	9.8	4.5	9.1	—
<b>36</b>	5.2	6.5	1.8	—	—	—	$J(\text{CHCH}_3) = J(5\text{-H,CH}) = 6.8$
<b>37</b>	4.3	6.0	2.2	6.3	7.8	10.0	—
<b>38</b>	5.0	6.7	—	10.2	4.1	9.0	$J(2\text{-H,CH}) = 8.7$ , $J(\text{CH}=\text{CH}_E\text{H}_Z) = 10.2$ , $J(\text{CH}=\text{CH}_E\text{H}_Z) = 18.7$ , $^2J(\text{CH}_E\text{H}_Z) = 1.8$
<b>39</b>	5.1	6.7	—	9.8	4.3	9.3	$J(\text{CH}_a\text{H}_b\text{CH}=\text{CH}_2) = 6.7$ , $J(\text{CH}_a\text{H}_b\text{CH}=\text{CH}_2) = 3.2$ , $J(\text{CH}=\text{CH}_E\text{H}_Z) = 10.2$ , $J(\text{CH}=\text{CH}_E\text{H}_Z) = 17.2$ , $^2J(\text{CH}_E\text{H}_Z) = 1.6$
<b>40</b>	4.9	6.7	—	10.1	4.2	9.2	—
<b>41</b>	4.7	6.7	—	10.0	4.0	9.2	$J(\text{H}_A, \text{H}_B) = J(\text{H}_{A'}, \text{H}_{B'}) = 8.7$
<b>42</b>	4.5	6.7	—	10.0	4.2	9.2	—
<b>43</b>	—	—	—	9.8	4.3	9.2	$J(\text{H}_A, \text{H}_B) = J(\text{H}_{A'}, \text{H}_{B'}) \approx ^3J(\text{F}, \text{H}_A) = ^3J(\text{F}, \text{H}_{A'}) = 8.6$ $^4J(\text{F}, \text{H}_B) = ^4J(\text{F}, \text{H}_{B'}) = 5.3$

**Table 5** (continued):  $^1\text{H}$ ,  $^1\text{H}$  Coupling constants of *N*-Hydroxypyrrolidines **35–51** ( $J$  [Hz],  $\text{CDCl}_3$ )

Nr.	$J_{2,3}$	$J_{3,4}$	$J_{4,5}$	$J_{2,1'A}$	$J_{2,1'B}$	$^2J_{1'A,1'B}$	Other (5-R; AA'BB')
<b>44</b>	5.1	6.7	—	9.9	4.4	9.2	$J(\text{H}_A, \text{H}_B) = J(\text{H}_{A'}, \text{H}_{B'}) = 8.6$
<b>45</b>	4.1	6.8	—	9.9	4.3	9.2	$J(\text{H}_A, \text{H}_B) = J(\text{H}_{A'}, \text{H}_{B'}) = 8.5$
<b>46</b>	5.0	6.7	—	—	—	—	$J(5\text{-H}, \text{CH}_a, \text{CH}_b) = 11.7 = 11.7$ , $^2J(\text{CH}_a, \text{CH}_b) = 13.9$ , $J(\text{H}_A, \text{H}_B) = J(\text{H}_{A'}, \text{H}_{B'}) = 8.6$
<b>47</b>	4.7	6.7	—	9.7	4.3	9.2	—
<b>48</b>	5.0	—	—	9.8	4.3	9.3	$J(\text{H}_A, \text{H}_B) = J(\text{H}_{A'}, \text{H}_{B'}) = 8.3$
<b>49</b>	4.3	6.6	—	10.9	4.1	9.0	$J(3'\text{-H}, 5'\text{-H}) = 0.9$ , $J(4'\text{-H}, 5'\text{-H}) = 2.1$ , $J(3'\text{-H}, 4'\text{-H}) = 3.3$
<b>50</b>	4.8	6.7	—	10.2	4.0	9.2	$J(\text{H}_A, \text{H}_B) = J(\text{H}_{A'}, \text{H}_{B'}) = 8.7$
<b>51</b>	5.0	7.1	6.1	3.0	5.7	10.7	$J(\text{H}_A, \text{H}_B) = J(\text{H}_{A'}, \text{H}_{B'}) = 8.5$

**Table 6:**  $^{13}\text{C}$  NMR Shifts of *N*-hydroxypyrrolidines **35–51** ( $\delta$  [ppm], 125.8 MHz,  $\text{CDCl}_3$ )

Nr.	C-2	C-3	C-4	C-5	C-1'	C(CH <sub>3</sub> ) <sub>2</sub>	Other (5-R; Ar-C of <i>p</i> -C <sub>6</sub> H <sub>4</sub> )
<b>35</b>	70.1	75.9	79.8	67.8	27.5	24.0, 25.6, 111.1	9.3 (CH <sub>2</sub> CH <sub>2</sub> <u>CH</u> <sub>3</sub> ), 19.9 (CH <sub>2</sub> <u>CH</u> <sub>2</sub> CH <sub>3</sub> ), 25.1 ( <u>CH</u> <sub>2</sub> CH <sub>2</sub> CH <sub>3</sub> )
<b>36</b>	69.3	77.7	80.2	75.5	26.8	23.1, 25.1, 111.2	18.7, 19.7 (CH( <u>CH</u> <sub>3</sub> ) <sub>2</sub> ), 25.5 ( <u>CH</u> (CH <sub>3</sub> ) <sub>2</sub> )
<b>37</b>	71.5	81.8	82.5	86.5	27.3	24.5, 26.9, 112.9	27.6 (C( <u>CH</u> <sub>3</sub> ) <sub>3</sub> ), 33.2 ( <u>C</u> (CH <sub>3</sub> ) <sub>3</sub> )
<b>38</b>	68.0	75.8	79.0	69.4	27.7	24.1, 25.7, 111.2	28.0 ( <u>CH</u> <sub>2</sub> CH=CH <sub>2</sub> ), 118.0 (CH <sub>2</sub> CH <sub>2</sub> CH= <u>CH</u> <sub>2</sub> ), 134.5 (CH <sub>2</sub> CH <sub>2</sub> <u>CH</u> =CH <sub>2</sub> )

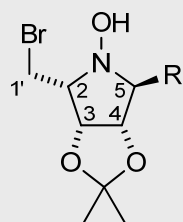
**Table 6** (continued):  $^{13}\text{C}$  NMR Shifts of *N*-hydroxypyrrolidines **35–51** ( $\delta$  [ppm], 125.8 MHz,  $\text{CDCl}_3$ )

Nr.	C-2	C-3	C-4	C-5	C-1'	C(CH <sub>3</sub> ) <sub>2</sub>	Other (5-R, Ar-C of <i>p</i> -C <sub>6</sub> H <sub>4</sub> )
<b>39</b>	70.7	76.5	80.4	68.3	28.1	24.5, 26.1, 111.7	24.5, 26.4, 34.0 ( <u>CH</u> <sub>2</sub> CH <sub>2</sub> CH <sub>2</sub> CH=CH <sub>2</sub> ), 115.4 (CH <sub>2</sub> CH <sub>2</sub> CH <sub>2</sub> CH= <u>C</u> H <sub>2</sub> ), 138.4 (CH <sub>2</sub> CH <sub>2</sub> CH <sub>2</sub> <u>C</u> H=CH <sub>2</sub> )
<b>40</b>	67.9	77.0	80.9	73.8	27.5	24.1, 25.8, 111.7	128.3, 128.4, 129.7, (3 d; <i>o</i> -, <i>m</i> -, <i>p</i> -C of C <sub>6</sub> H <sub>5</sub> ), 133.8 (s, <i>i</i> -C of C <sub>6</sub> H <sub>5</sub> )
<b>41</b>	67.5	76.6	80.4	73.0	27.5	24.1, 25.8, 111.6	55.3 (O <u>C</u> H <sub>3</sub> ), 113.7 (d, <i>m</i> -C), 125.5 (s, <i>i</i> -C), 131.0 (d, <i>o</i> -C), 159.6 (s, <i>p</i> -C)
<b>42</b>	67.7	77.5	80.9	73.2	27.4	21.0, 24.1, 111.7	127.1, 127.4, 128.8, 130.2, 132.6, 140.4, 141.2 [C <sub>6</sub> H <sub>4</sub> , C <sub>6</sub> H <sub>5</sub> ; signals overlapping]
<b>43</b>	67.8	76.7	80.8	73.0	27.3	24.1, 25.8, 111.8	115.18, 115.36 (d, <i>m</i> -C, <sup>2</sup> J <sub>C,F</sub> = 21.4 Hz), 129.6 (s, <i>i</i> -C), 131.24, 131.31 (d, <i>o</i> -C, <sup>3</sup> J <sub>C,F</sub> = 8.1 Hz), 161.65, 163.62 (s, <i>p</i> -C, <sup>1</sup> J <sub>C,F</sub> = -248.1 Hz)
<b>44</b>	68.0	77.6	80.9	73.2	27.4	24.2, 25.9, 111.9	128.6 (d, <i>m</i> -C), 130.9 (s, <i>i</i> -C), 132.4 (d, <i>o</i> -C), 134.5 (s, <i>p</i> -C)
<b>45</b>	67.7	77.7	80.5	73.1	27.3	24.2, 25.8, 111.9	128.4 (s, <i>i</i> -C), 129.9 (d, <i>o</i> -C), 131.5, 132.6 (2 d, <i>m</i> -C), 133.6 (s, <i>p</i> -C)
<b>46</b>	67.9	75.7	78.8	72.0	28.5	24.1, 25.7, 111.2	28.5 ( <u>C</u> H <sub>2</sub> C <sub>6</sub> H <sub>4</sub> ), 55.3 (O <u>C</u> H <sub>3</sub> ), 114.3 (d, <i>m</i> -C), 130.0 (s, <i>i</i> -C), 130.1 (d, <i>o</i> -C), 158.3 (s, <i>p</i> -C)
<b>47</b>	67.9	77.5	80.9	73.1	27.4	24.1, 25.8, 111.7	118.1, 119.4, 123.7, 128.1, 129.8, 131.1 [C <sub>6</sub> H <sub>4</sub> , C <sub>6</sub> H <sub>5</sub> ; signals overlapping]
<b>48</b>	67.8	77.5	80.8	73.3	27.7	24.1, 25.8, 111.6	14.6 (SCH <sub>3</sub> ), 126.1 (d, <i>m</i> -C), 130.1 (s, <i>i</i> -C), 130.3 (d, <i>o</i> -C), 138.9 (s, <i>p</i> -C)

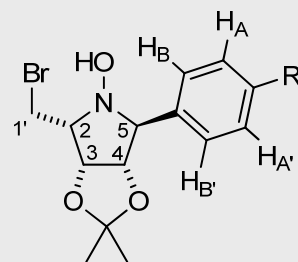
**Table 6** (continued):  $^{13}\text{C}$  NMR Shifts of *N*-hydroxypyrrolidines **35–51** ( $\delta$  [ppm], 125.8 MHz,  $\text{CDCl}_3$ )



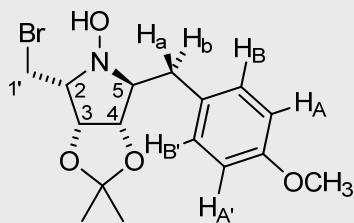
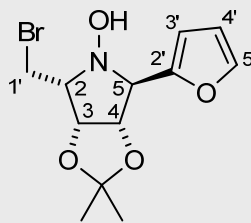
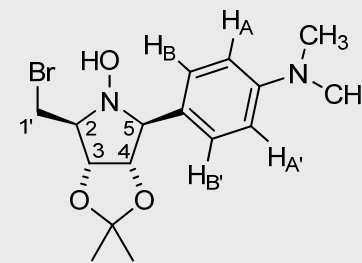
Nr.	C-2	C-3	C-4	C-5	C-1'	C(CH <sub>3</sub> ) <sub>2</sub>	Other (5-R, Ar-C of <i>p</i> -C <sub>6</sub> H <sub>4</sub> )
<b>49</b>	68.5	76.8	79.4	67.8	27.6	24.3, 25.8, 111.7	111.4 [2', 3'], 142.7 (4'), 150.4 (5')
<b>50</b>	67.8	77.2	80.7	73.1	27.7	24.2, 25.8, 111.4	40.5 [N(CH <sub>3</sub> ) <sub>2</sub> ], 111.9 (d, <i>m</i> -C), 120.6 (s, <i>i</i> -C), 130.6 (d, <i>o</i> -C), 150.3 (s, <i>p</i> -C)
<b>51</b>	71.6	78.6	82.2	76.7	32.8	25.2, 27.3, 112.9	40.8 [N(CH <sub>3</sub> ) <sub>2</sub> ], 113.0 (d, <i>m</i> -C), 113.6 (s, <i>i</i> -C), 128.4 (d, <i>o</i> -C), 150.6 (s, <i>p</i> -C)

**35-40**

<b>35</b>	R =	CH <sub>2</sub> CH <sub>2</sub> CH <sub>3</sub>
<b>36</b>		CH(CH <sub>3</sub> ) <sub>2</sub>
<b>37</b>		C(CH <sub>3</sub> ) <sub>3</sub>
<b>38</b>		CH <sub>2</sub> CH=CH <sub>2</sub>
<b>39</b>		CH <sub>2</sub> CH <sub>2</sub> CH <sub>2</sub> CH=CH <sub>2</sub>
<b>40</b>		Ph

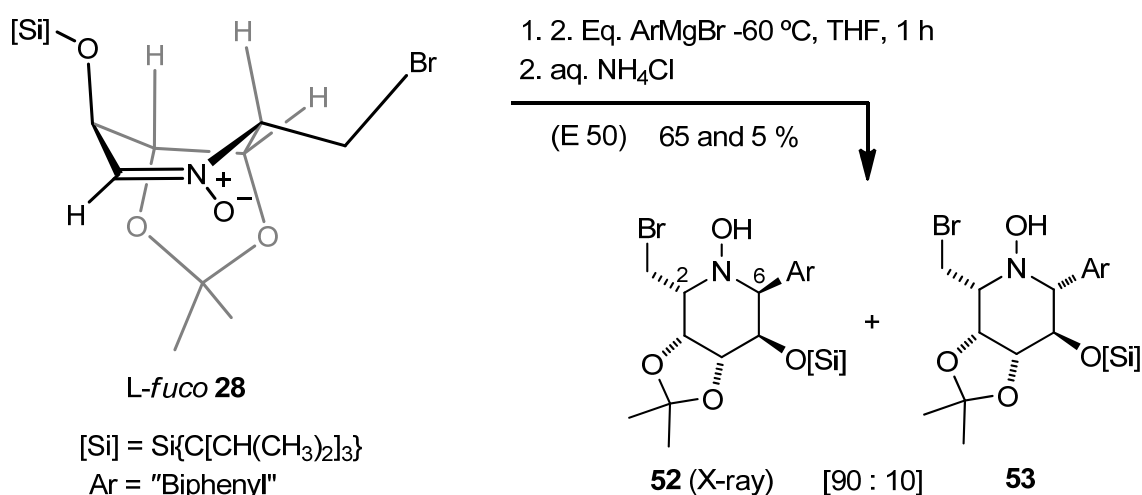
**41-45, 47, 48, 50**

<b>41</b>	R' =	OCH <sub>3</sub>	<b>48</b>	SCH <sub>3</sub>
<b>42</b>		C <sub>6</sub> H <sub>5</sub>	<b>50</b>	N(CH <sub>3</sub> ) <sub>2</sub>
<b>43</b>		F		
<b>44</b>		Cl		
<b>45</b>		Br		
<b>47</b>		OC <sub>6</sub> H <sub>5</sub>		

**46****49****51**

### 3.2.3 Grignard addition to TIPS-protected L-fuco-nitrone **28**

The addition of ([1,1'-biphenyl]-4-yl)-magnesium bromide in THF at low temperature to the six-membered L-fuco-nitrone **28** generated the pair of diastereoisomeric piperidines **52** and **53** in a ratio of 90:10 (from  $^{13}\text{C}$  NMR) in a yield of 70 % after column chromatography and MPLC separation of the diastereoisomers. The channel of attack of the Grignard reagent took place through preferential addition to the *Si*-face to predominately afford the  $\alpha$ -anomer **52** in 65 %, besides 5 % of the  $\beta$ -anomer **53** (Scheme 32). The structure of **52** was subsequently confirmed by X-ray crystal structure analysis (see below).



Scheme 32: Stereoselective addition of a Grignard reagent to L-fuco-configured nitrone **28**

#### 3.2.3.1 Analysis of the NMR spectroscopic data of the addition products and a discussion of the X-ray crystal structure of piperidine **52**

A good starting point is to kick off with the determination of the relative configuration of the diastereoisomers **52** and **53** by dealing with the dispersion of chemical shifts at the 6-H/C-6 and 5-H/C-5 juncture (spectra of **52** and **53** in Diagrams 34, 35, resp.). On the reasonable assumption that in the major isomer the C-6 substituent is *cis* relative to the one at C-5 (from attack at the *Si*-face on the L-fuco-nitrone **28**; cf. attack on L-fuco nitrone **EA**, lit.<sup>[152]</sup>), two sets of lines can be assigned: The chemical shifts for C-5/C-6 in **52** are 73.6 and 67.9 ppm whereas for **53** they are 77.1 and 77.2 ppm (Table 7). The large down-field chemical shift for C-6 ( $\Delta = +9.3$  ppm) in **53** as compared to **52** is indicative of a change to a *trans*-orientation of substituents at C-5/C-6. This is unambiguously in-line with the deshielding influence observed for *trans*-configured vicinal substituents as a result of "inductive  $\beta$ -effects"<sup>[219-221]</sup> (cf. C-2/C-3 shifts of pyrrolidine diastereoisomers in Section 3.2.2.1, p. 68).

The *cis/trans* determination of substituents at the C-5/C-6 juncture was further confirmed by  $^1\text{H}$  NMR through a comparison of  $J_{5,6} = 2.6$  Hz for 6-H at 4.55 ppm in *cis*-**52**, to  $J_{5,6} = 8.6$  Hz for 6-H at 3.52 ppm in the *trans*-piperidine **53** (i.e. 5-H/C-5/C-6/6-H,  $\phi = \text{ca. } 30\text{-}60^\circ$  in **52**; ca.  $150\text{-}170^\circ$  in **53**). Aside from the configuration at C-6, the  $^1\text{H}$  NMR data provided, to a certain extent, reliable information for the determination of ring conformation in solution. For the piperidine **52**, a normal *gauche* dihedral angle is found between the vicinal protons 4-H/5-H from  $J_{4,5} = 2.5$  Hz. This value excludes the 4,5-*trans*-diaxial arrangement and, consequently, a  $^1\text{C}_4$  ring conformation ( $^3\text{C}_6$  numbering for **52**). For acetonide bound protons, 3-H/4-H,  $J_{3,4} = 7.6$  Hz which is evidence that they are standing *syn* to each other (i.e. 3-H/C-3/C-4/4-H,  $\phi = \text{ca. } 20\text{-}30^\circ$ ); this goes against the alternative  $^4\text{C}_1$  conformation ( $^6\text{C}_3$ ) on account of the flattening of the piperidine ring that would result. A further *contra*-chair argument is thrown up by the small  $J_{2,3}$  coupling constant of 1.4 Hz. At first sight, a more obtuse than normal *gauche* dihedral angle or substituent effects would appear as plausible rationalisations. However, the Karplus relationship<sup>[102,183-185]</sup> cannot confidently be taken to explain the latter as it does not compensate for electronegative substituents. Nevertheless, electronegative substituents can reduce the *gauche*  $J$ -value, the effect being at a maximum when a substituent is standing *anti-periplanar* to one of the coupled protons (cf. Günther<sup>[184]</sup>, p. 119-121; for hexoses, see Forrest<sup>[289]</sup>). The Newman projections below highlight the relevant *anti-periplanar* arrangements that have possibly contributed to the small  $J_{2,3}$  value and, at the same time, lend additional support for a non-chair conformation in solution.\* The piperidine **52** is most likely a boat (i.e.  $^{2,5}\text{B}$ ) or some weak twist-boat conformation. The strain arising from the biphenyl substituent is relieved when put, as shown, *pseudo-equatorially* (Diagram 33).

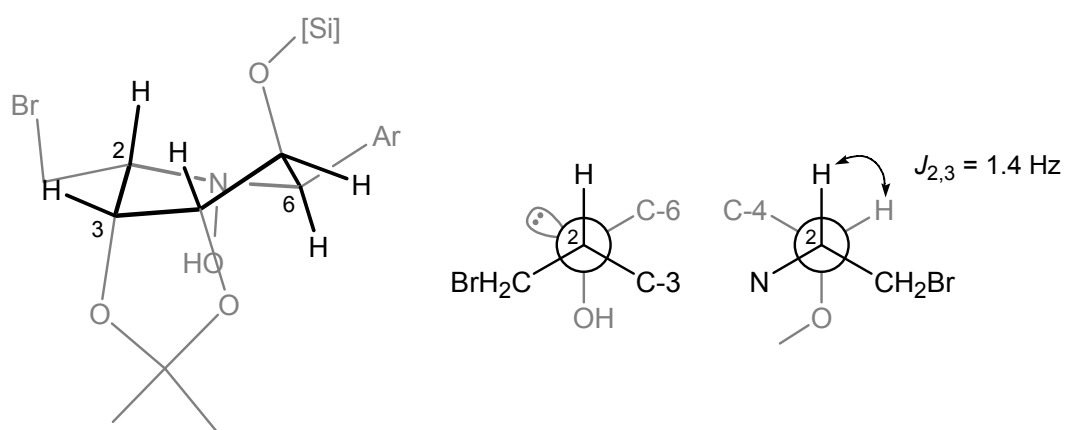


Diagram 33: A solution  $^{2,5}\text{B}$  conformation for the piperidine **52** according to  $^1\text{H}$  NMR

\* Molecular Modelling (MM2/MOPAC, ChemDraw 3-D, Version 8.0) indicated that the N-OH bond was most stable when *pseudo-axial*, as depicted. An upwards orientation of N-OH incurred an energy penalty of  $-1.84$  kcal/mol (i.e. relative free energy,  $\Delta G^0 = -106.43$  versus  $-104.59$  kcal/mol) and gave rise to an alternative, distorted "flipped"  $B_{2,5}$  conformation.

For the minor diastereoisomer, piperidine **53**, the conformational analysis is handicapped by the unresolved  $J_{4,5}$  coupling constant (4-H and 5-H form a multiplet at 4.06–4.10 ppm). According to  $J_{3,4} = 5.1$  Hz, the protons adjoining the isopropylidene unit have become largely staggered compared to **52**; staggering also exists between 2-H and 3-H ( $J_{2,3} = 3.6$  Hz). Looking elsewhere, the implications of the bulky biphenyl substituent on the conformational analysis are twofold. One stems from the  $J_{5,6}$  value equating to 8.6 Hz which confirms that an equatorial biphenyl substituent prevails (i.e. 5-H and 6-H are approx. *trans*-diaxial). This eliminates the  ${}^4C_1$  conformation, since a rather ominous looking *syn*-pentane interaction with C-2 would result. Comparison of the data of **52** with those of **53** show that the shielding effect of a change in configuration at C-6 on 2-H and 6-H amounts to -0.71 and -1.03 ppm, respectively. While the latter is attributable to  $\alpha$ -effects and to the adjacent polar silyl ether substituent, the former must represent the net change in ring conformation. This is corroborated by a 6.7 ppm down-field shift for C-2 in the  ${}^{13}\text{C}$  NMR spectrum. Furthermore, the down-field shift of the aromatic *ipso* C-4'' signal from **52** to **53** is consistent for a C-5/C-6 *trans*-configuration in piperidine **53**. Although so far so good, attempting to explain remaining differences on the basis of the  ${}^1\text{H}$  and  ${}^{13}\text{C}$  NMR chemical shifts becomes a more speculative exercise: for example, it could be argued that the enhanced shielding of 2-H in **53** in the  ${}^1\text{H}$  NMR is *perhaps* down to a removal of the proximate electrostatic interactions with the silyl ether substituent at C-5, on account of the  ${}^{2,5}B$  conformation (i.e. that of the diastereoisomer **52**, see previous page) no longer prevailing. Also difficult to explain is that the  ${}^1\text{H}$  and  ${}^{13}\text{C}$  NMR shifts for 3-H and C-3 remain unchanged – an unlikely event for a pair of diastereoisomers. On the other hand, this could be an indication that two effects are working in opposite directions (i.e. electrostatic *versus* compression:  $\beta$ - or  $\gamma$ -*gauche* effects). To sum up, the conformation of **53** – chair or non-chair – remains open to interpretation.

Nr.	2-H	3-H	4-H	5-H	6-H	1'-H <sub>A</sub>	1'-H <sub>B</sub>	$J_{2,3}$	$J_{3,4}$	$J_{4,5}$	$J_{5,6}$	$J_{2,1A}$	$J_{2,1B}$
<b>52</b>	3.97	4.72	4.39	4.18	4.55	3.78	4.03	1.4	7.6	2.6	2.6	7.7	6.6
<b>53</b>	3.26	4.72	4.06–4.10		3.52	3.71	4.02	3.2	5.1	n/d	8.6	10.5	3.5
$\Delta\delta$	-0.71	0.0	n/d	n/d	-1.03	-0.07	-0.01						

	C-2	C-3	C-4	C-5	C-6	C-4''
<b>52</b>	59.6	73.5	76.1	73.6	67.9	140.7
<b>53</b>	66.3	73.1	79.4	77.1	77.2	142.0
$\Delta\delta$	6.7	-0.4	3.3	3.5	9.3	1.3

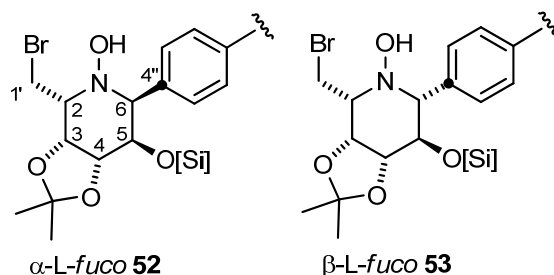


**Table 7:** Selected  ${}^1\text{H}$  and  ${}^{13}\text{C}$  NMR data for diastereoisomers **52** and **53**

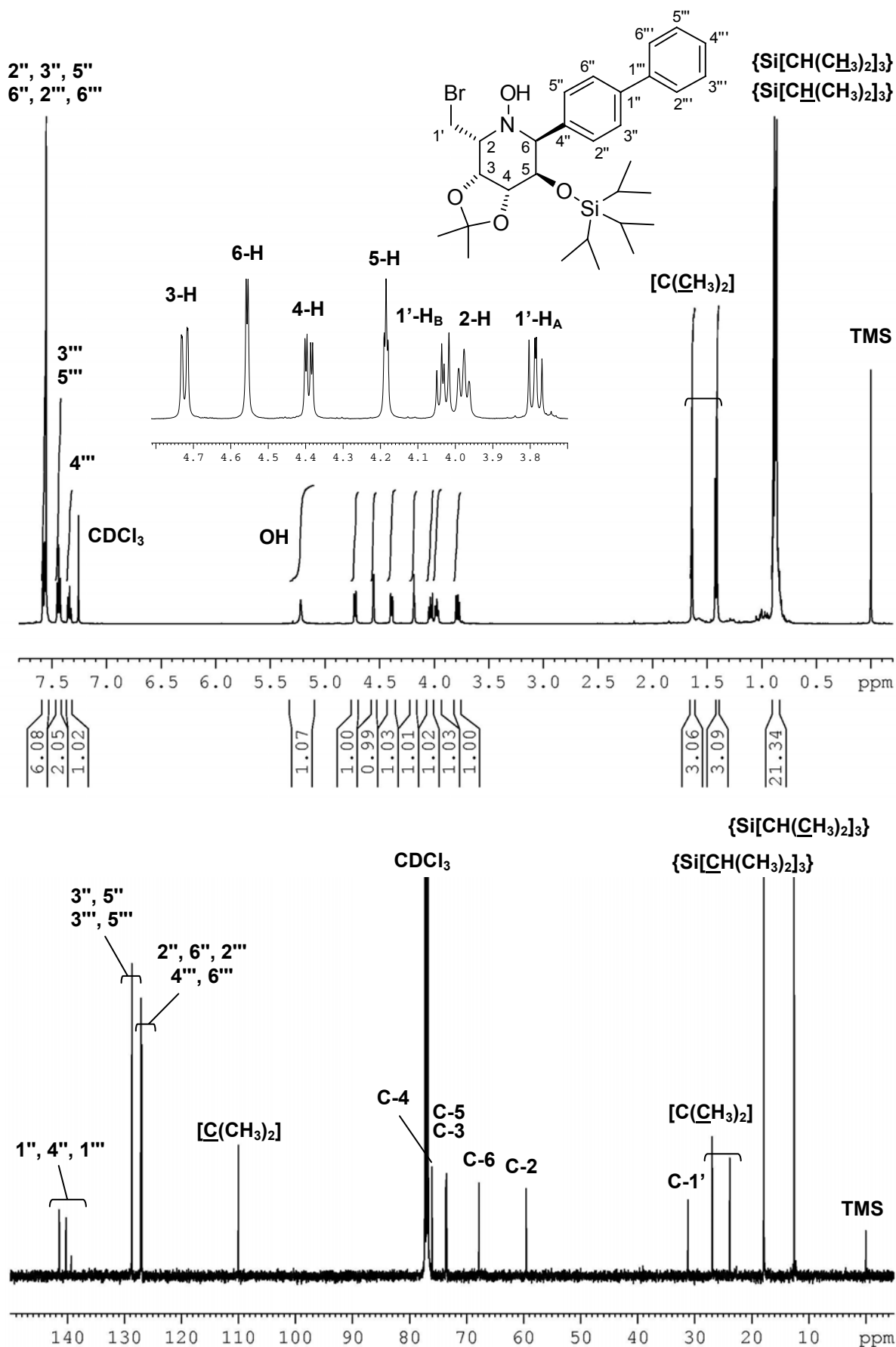
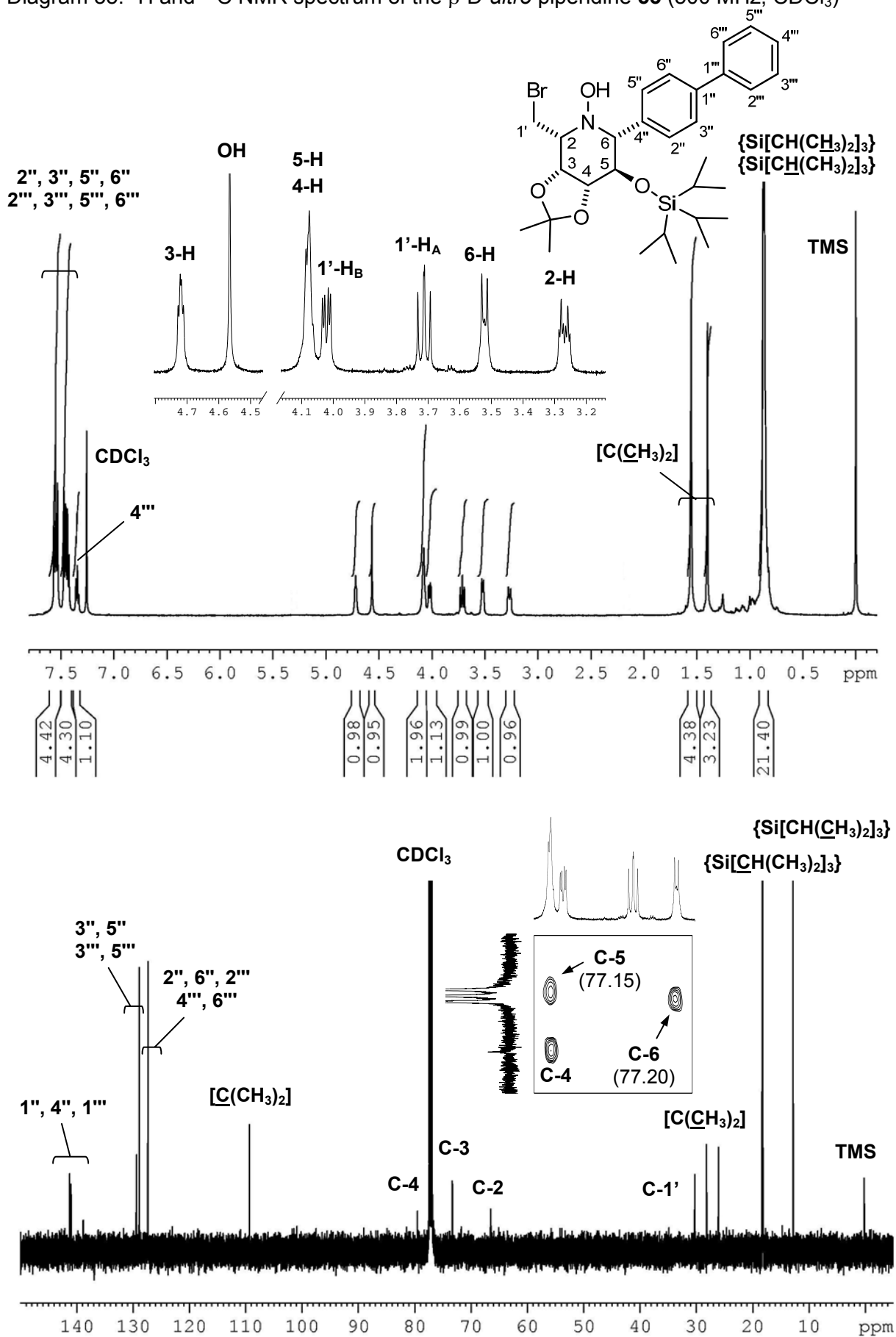
Diagram 34:  $^1\text{H}$  and  $^{13}\text{C}$  NMR spectrum of the  $\alpha$ -L-*fuco* piperidine **52** (500 MHz,  $\text{CDCl}_3$ )

Diagram 35:  $^1\text{H}$  and  $^{13}\text{C}$  NMR spectrum of the  $\beta$ -D-*altro* piperidine **53** (500 MHz,  $\text{CDCl}_3$ )

*Discussion of the X-ray crystal structure of piperidine 52*<sup>[286-288]</sup>

The solid state structure of piperidine **52** is interesting in several ways. Apart from confirming the path of stereofacial nucleophilic attack, it firmly establishes the absolute configuration of the starting material, the *L-fuco*-nitrone **28**. The piperidine **52** co-crystallises with dichloromethane in the hexagonal space group, R3. The crystalline solvate functions as a “filler” molecule with piperidine **52** although, surprisingly, it itself engineers no hydrogen bonds (in contrast to methanol as co-solvent, cf. Section 5.1.7.2). Hydrogen bonding exists between the *N*-hydroxyl group as hydrogen bond donor to a neighbouring molecule’s acetonide oxygen on C-3 as hydrogen bond acceptor ( $H1B \cdots O3 = 2.19 \text{ \AA}$ ;  $O1B/H1B/O3A = 153.4^\circ$ ; crystal numbering; diagrams omitted here, refer to Section 9.7). The biphenyl units undergo stacking in a face-to-face orientation, perpendicular to the *a/b* plane, thereby resembling the packing situation found in the biphenyl-substituted pyrrolidine **97·HCl** (discussed on p. 120, Section 5.1.7.3). However, the most intriguing aspect of the solid state structure concerns the ring’s non-chair conformation: the <sup>2,5</sup>*B* boat conformation presumably found in solution has been supplanted by a “twist-boat” conformation in the solid state (Diagram 36). This conformation might be favourably supported by the hydrogen bond between the OH group to the acetonide oxygen at C-3, which in turn has induced a rotation about the C-3/C-4 bond to permit the ring to twist to a marginally more stable “skew boat” conformation. The added stability could be comprised of reduced torsional strain between the *syn*-standing 3-H and 4-H (although, admittedly, worth only ca. 0.5 kcal/mol<sup>[277]</sup>) and the weakening of interactions between the flagpole substituents on C-2 and C-5.

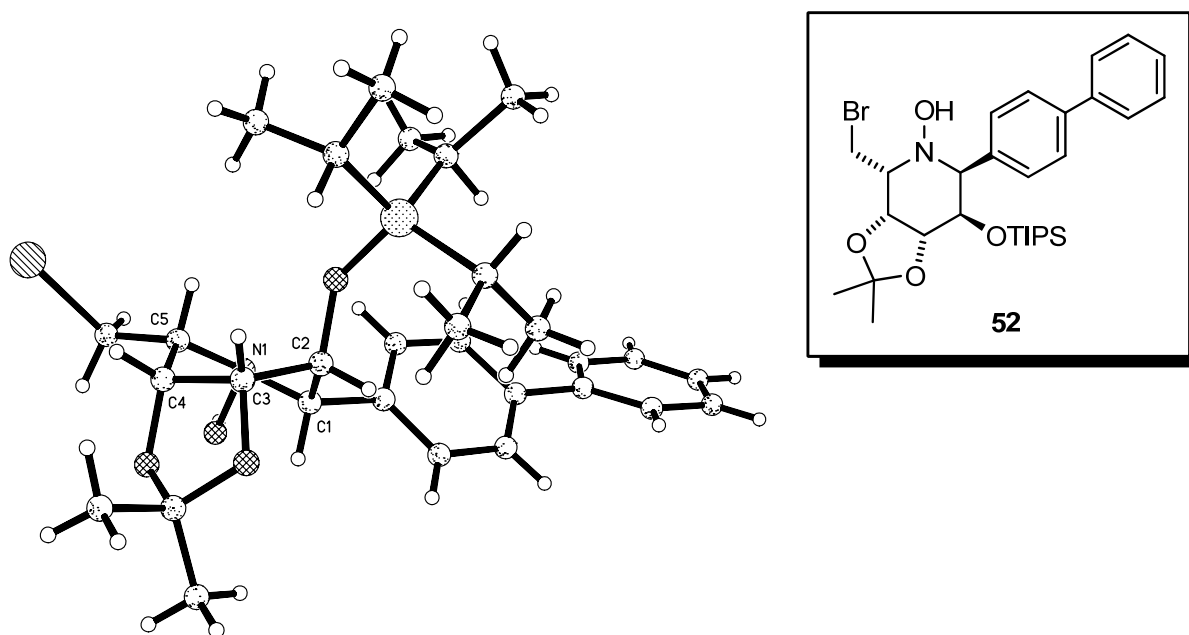


Diagram 36: Representation of the X-ray crystal structure of piperidine **52**





# 4 Oxidation of *N*-Hydroxypyrrolidines

## 4.1 Introduction

The oxidation of *N,N*-disubstituted hydroxylamines is an efficient method to prepare nitrones. However, in the course of the oxidation, if each carbon attached to the nitrogen carries an extractable  $\alpha$ -hydrogen, a mixture of regioisomeric nitrones will normally result due to subtle steric and electronic effects. A vast variety of reagents can be used for the oxidation of *N,N*-disubstituted hydroxylamines (Diagram 37). In certain cases, it merely suffices to pass oxygen (or air) into an aqueous solution of the hydroxylamine, provided a suitable (heterogeneous) catalyst is present to accelerate the uptake of oxygen (usually copper(II) acetate).<sup>[132,290]</sup> Unfortunately, the majority of reactions require stoichiometric amounts of transition metals for an efficient oxidation to occur, such as (roughly in chronological order of publication) potassium hexacyanoferrate(III),<sup>[291]</sup> lead(IV) oxide (or lead(IV) acetate),<sup>[292]</sup> and

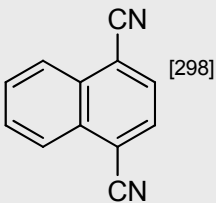
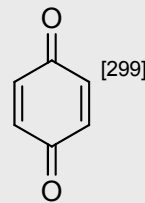
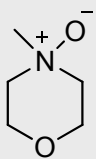
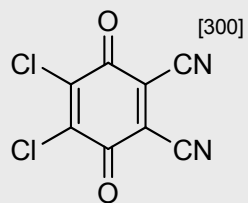
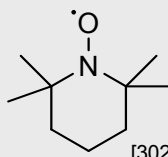
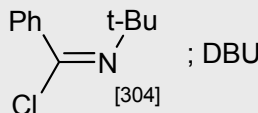
<i>metallic</i>	<i>catalytic systems</i>	<i>organic</i>
$K_3[Fe(CN)_6]$ <sup>[291]</sup>	$O_2$ (air), $Cu(OAc)_2$ <sup>[132,290]</sup>	 <sup>[298]</sup>  <sup>[299]</sup>
$PbO_2$ ; $Pb(OAc)_4$ <sup>[292]</sup>	$Pd$ (black) <sup>[130,296]</sup>	
$Ni_2O_3$ <sup>[293]</sup>	 , $(n-C_3H_7)_4N^+$ <sup>[294,308b]</sup> $RuO_4^-$ <sup>[294,308b]</sup>	 <sup>[300]</sup>
$NaClO$ <sup>[297]</sup>		$SO_2Cl_2$ <sup>[301]</sup>
$HgO$ <sup>[292,303,306-310]</sup>	$H_2O_2$ , $H_3C-ReO_3$ <sup>[295]</sup>	 <sup>[302,303]</sup>  <sup>[304]</sup> ; DBU
$MnO_2$ <sup>[251,303,311-313]</sup>		

Diagram 37: Literature-known reagents for the oxidation of *N,N*-disubstituted hydroxylamines

nickel(III) oxide.<sup>[293]</sup> The usage of these reagents has lessened through the development of catalytic systems such as *N*-morpholine-*N*-oxide/tetra-*n*-propylammonium perruthenate (cat.)<sup>[294]</sup> or hydrogen peroxide/methylrhenium trioxide (cat.)<sup>[295]</sup> In this respect, a somewhat overlooked oxidant is palladium black, shown by Murahashi<sup>[130,296]</sup> to be an efficient oxidant at 10 mol % for several *N,N*-disubstituted hydroxylamines. Bleach (NaClO) can be considered to be a “green chemistry” oxidant, since the reaction produces only NaCl as a byproduct.<sup>[297]</sup> Organic oxidants have literature precedents too: 1,4-dicyanonaphthalene (an electron acceptor; under photolysis conditions);<sup>[298]</sup> benzoquinone<sup>[241,299]</sup> or, even stronger, 2,3-dichloro-4,5-dicyanobenzoquinone (DDQ);<sup>[300]</sup> sulfuryl chloride (admittedly, not very “green”!),<sup>[301]</sup> tetramethylpiperidine-*N*-oxide (TEMPO);<sup>[302,303]</sup> *N*-*t*-butylbenzene-sulfinimidoyl chloride (*sic.*) with 1,8-diazabicyclo[5.4.0]-undec-7-ene (DBU).<sup>[304]</sup> As a reminder, most of the reagents listed here have been covered in the review articles cited above (lit.<sup>[124,125,241-242]</sup>) and particularly by Döpp<sup>[123]</sup> and Rundel<sup>[305]</sup> which include several experimental procedures.

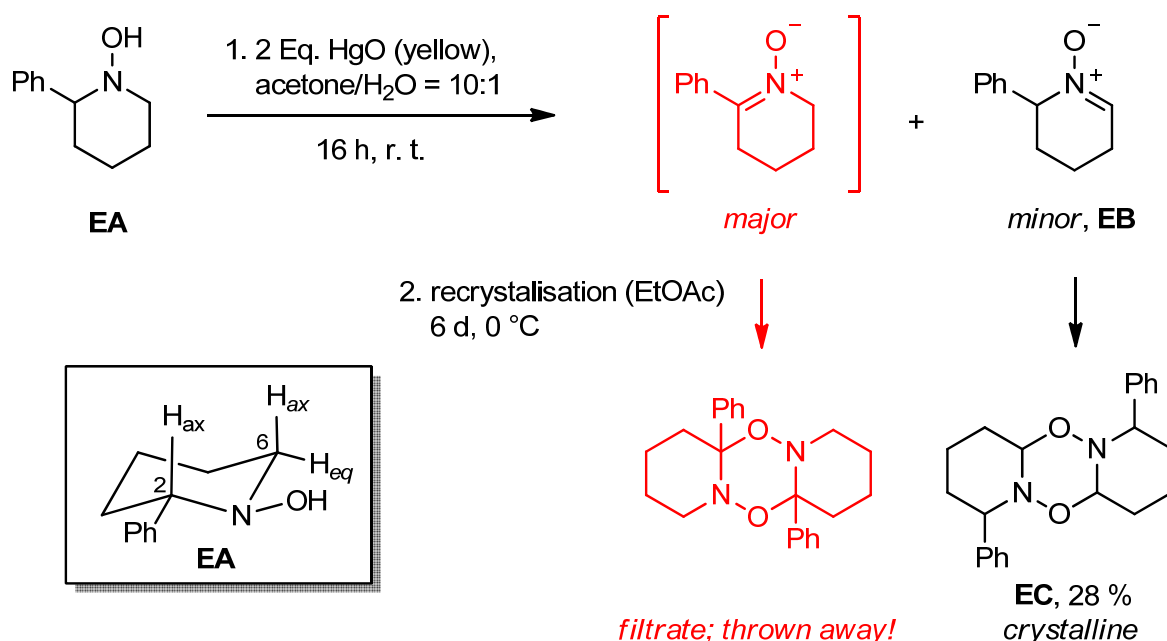
The list, however, contains two noticeable exceptions: mercury(II) oxide (HgO) and manganese(IV) oxide (MnO<sub>2</sub>). They deserve extra mention since the number of publications attributed to their usage far outstrips the cumulative total of those above. HgO, until recently, has been the first choice reagent for the oxidation of hydroxylamines (refer to lit.<sup>[292,303,306,307,308,309,310]</sup>). However, MnO<sub>2</sub> is finding broader appeal due to its relative non-toxicity and on-par oxidation regioselectivity (lit.<sup>[251,303,311,312,313]</sup>).

## 4.2 Regioselectivity of Oxidation

### 4.2.1 Oxidation of *N*-hydroxypiperidines. Earlier work of Thesing, Ali, Tufariello, and Pothier and Jäger

The regioselectivity of the oxidation of *N*-hydroxypiperidines is, just as with *N*-hydroxypyrrolidines, generally steered by substituents and not by reagent. The oxidation of 2-substituted *N*-hydroxypiperidines provides keto-nitrones, not aldo-nitrones as the major products, since the reaction is dominated by thermodynamic control. Of course, what this means is that it would be very useful to have a way of synthesizing aldo-nitrones selectively. In 1957, Thesing and Mayer<sup>[306]</sup> published what at first appeared to be a selective synthesis of the aldo-nitrone **EB**. In doing so, the authors claimed they had seemingly circumvented

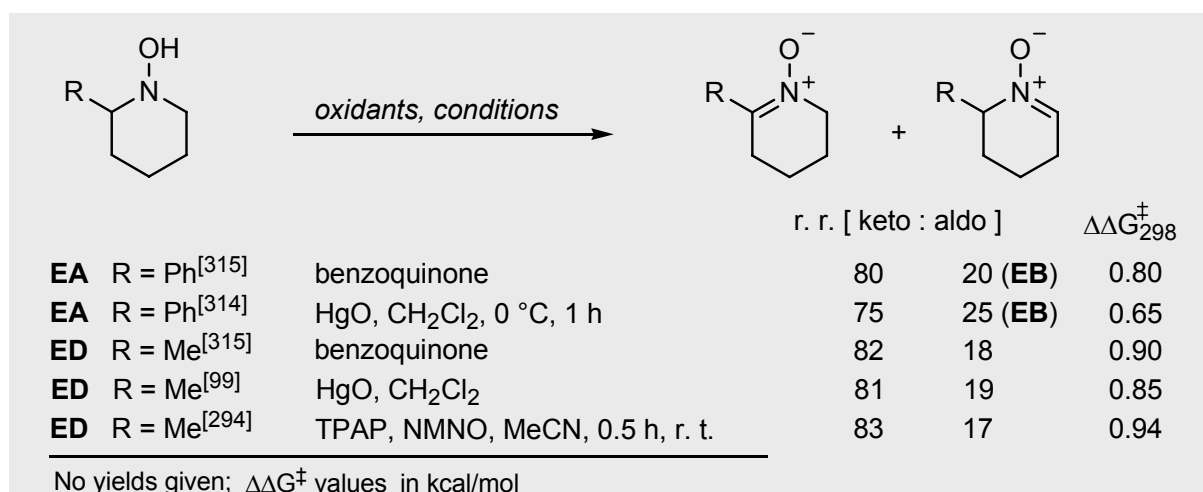
the non-trivial problem of the favoured extraction of the benzylic  $\alpha$ -hydrogen, which leads to the keto-nitrone as the major product. Starting from 2-phenyl-*N*-hydroxypiperidine **EA**, the protagonists were themselves surprised by the “sole” formation of the kinetically-favoured aldo-nitrone **EB**. However, the authors never isolated the aldo-nitrone **EB**. Instead, after oxidation with HgO, the crude reaction mixture was filtered, suspended in ethyl acetate and refrigerated for 6 days to invoke dimerisation (cf. method of Todd et al.<sup>[127]</sup>) to provide crystals of a dimer pertaining to have the structure **EC**, though interestingly, only in a low yield of 28 %. The structural assignment of **EC** and thus “sole” formation of **EB** was inferred after treatment of the dimer with phenyl magnesium bromide yielded the known 2,6-diphenyl-*N*-hydroxypiperidine (not shown).



Scheme 33: Thesing's claim to the selective formation of an aldo-nitrone (i.e. nitrone **EB**) arising from the oxidation of 2-phenyl-*N*-hydroxypiperidine with mercury(II) oxide.<sup>[306]</sup>

Of course, the oxidation of **EA** had certainly provided the keto-nitrone as the major product. The non-crystalline keto-nitrone-dimer was probably a part of the filtrate, inadvertently discarded by Thesing or at least one of his co-workers! Some years later, Ali<sup>[314,315]</sup> was able to rebut Thesing's erroneous claims concerning the oxidation regioselectivity: Re-examination of the oxidation, and also of 2-methyl-*N*-hydroxypiperidine **ED** for comparison, revealed in each case the formation of both isomeric nitrone, with predominance for the conjugated or “keto” isomer. Pothier and Jäger<sup>[99]</sup> reaffirmed this result (Scheme 34). These set of experiments highlight also that, (i) the hydrogen at the benzylic position is not “activated” and

did not control the regioselection (i.e. only small differences  $\Delta\Delta G^\ddagger$ , compare R = Ph to R = Me) and, (ii) neither did the choice of oxidant (cf. discussion in Section 4.2.2).

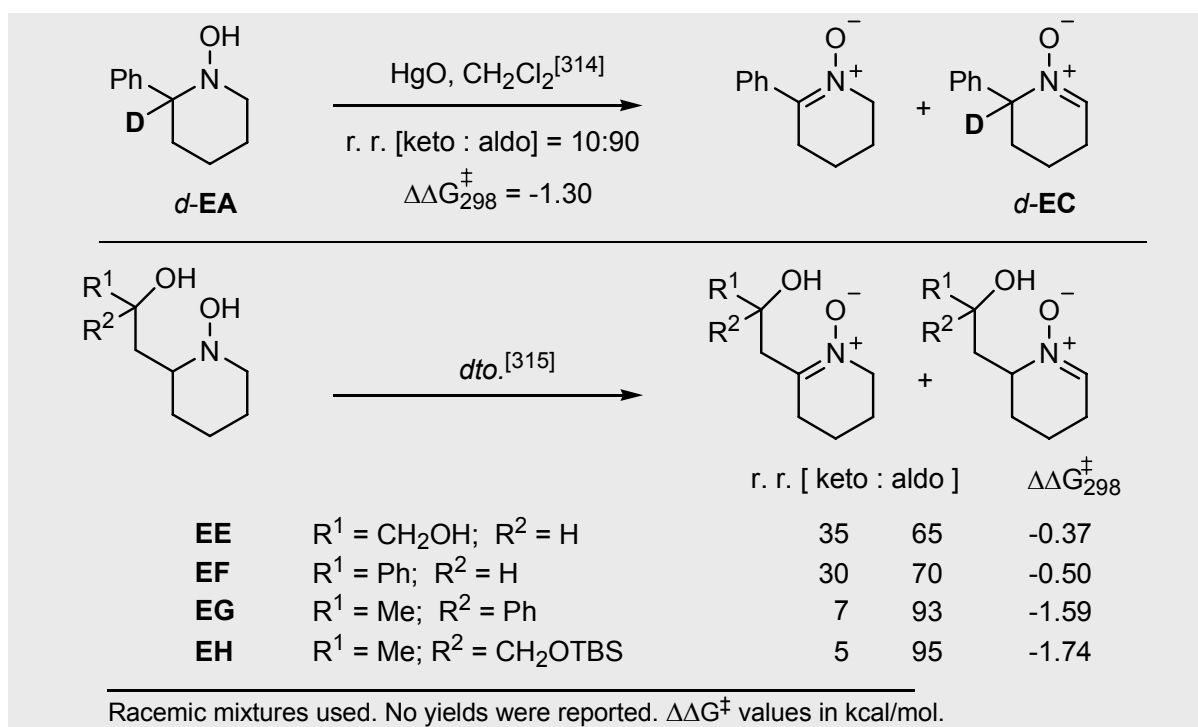


Scheme 34: Oxidation of non-symmetric *N*-hydroxypiperidines under thermodynamic control

Returning to Thesing,<sup>[306]</sup> in trying to provide an alibi for the formation of the kinetically-favoured aldo-nitrone **EB**, the authors explained that the rate-determining step of the oxidation involved abstraction by the reagent of the less-hindered *equatorial*  $\alpha$ -hydrogen at C—6 or, as they put it, “the cleavage of the less-polarisable C—H bond”, on the basis that the piperidine ring adopted the chair conformation shown in Scheme 33 (i.e. *equatorial* and *trans* N—OH and phenyl substituents). Although, as we know now, Thesing’s judgement was swayed by poor experimental practice, credit is due to him since he was in effect one of the first to imply that *stereodynamics* and *steric effects* in a six-membered ring may influence the oxidation regioselectivity. If the abstraction of the thermodynamically-favoured  $\alpha$ -hydrogen can be impeded, the formation of the kinetically-favoured aldo-nitrone will be favoured.

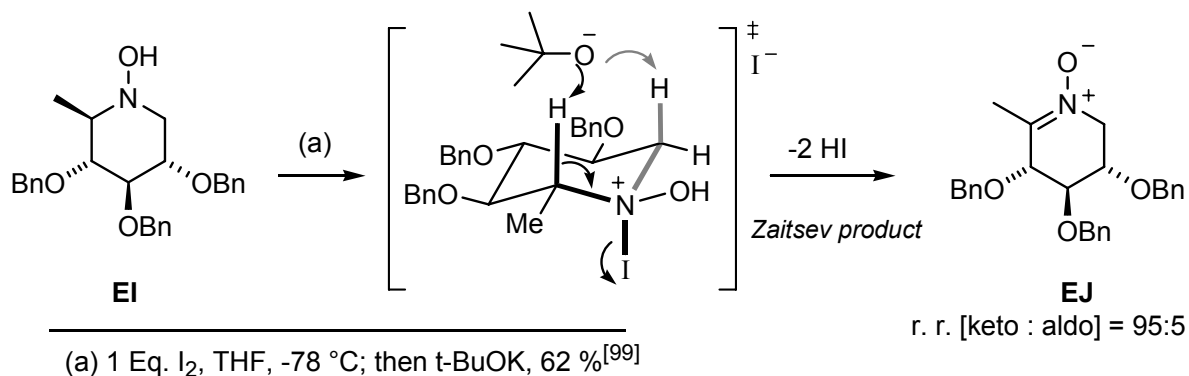
Indeed, there are cases where the oxidation has yielded the aldo-nitrone as the major product, though “tricks” are usually required. For example, Ali et al.<sup>[314]</sup> were able to exploit a primary kinetic isotope effect in *d*-**EA** (i.e. deuterated analogue of **EA**) to effect a sharp reversal in the regioselective outcome. This led to the aldo-nitrone *d*-**EC** as the major product (Scheme 35). Here, the swing in activation energy of the transition state,  $\Delta G^\ddagger$ , is a reflection of the larger  $\Delta H^\ddagger$  term required for the dissociation of the stronger C—D bond. This is enough to “tip the balance” towards the favoured formation of aldo-nitrone *d*-**EC**. Increasing the steric demand at the  $\beta$ -carbon had a similar effect.<sup>[314]</sup> The selectivity of aldo-nitrone formation followed the trend of secondary alcohols (i.e. hydroxylamines **EE**, **EF**) < tertiary alcohols (i.e. **EG**, **EH**), and reflects the relative obstruction to the abstraction of the  $\alpha$ -hydrogen at the “keto” side.<sup>[315]</sup> In describing these findings, Ali notes his “delight” and “overwhelming

surprise” at the sudden, though logical, “aldo” selectivity. His wording is here unfortunate, however, since the relationship between bulky substituents at the  $\beta$ -position and “aldo” selectivity was documented already by Tufariello<sup>[316,317]</sup> on the subject of the oxidative opening of isoxazolidines (cf. “nitron/cycloaddition approach to *dl*-cocaine”, lit.<sup>[317]</sup>), where Ali, himself, had been a co-worker, some 15 years earlier!



Scheme 35: Tricks used by Ali et al.<sup>[314,315]</sup> to favour the formation of the aldo-nitrones

In contrast, Pothier and Jäger<sup>[99]</sup> thought about exploiting the stereodynamics of the chair-conformation to study the selectivity of nitron formation. However, the oxidation of iminoglucitol **EI**<sup>[4a]</sup> using iodine followed by quenching with a base at  $-78^\circ\text{C}$  led to the near exclusive formation of keto-nitron **EJ** in 62 % yield (Scheme 36).

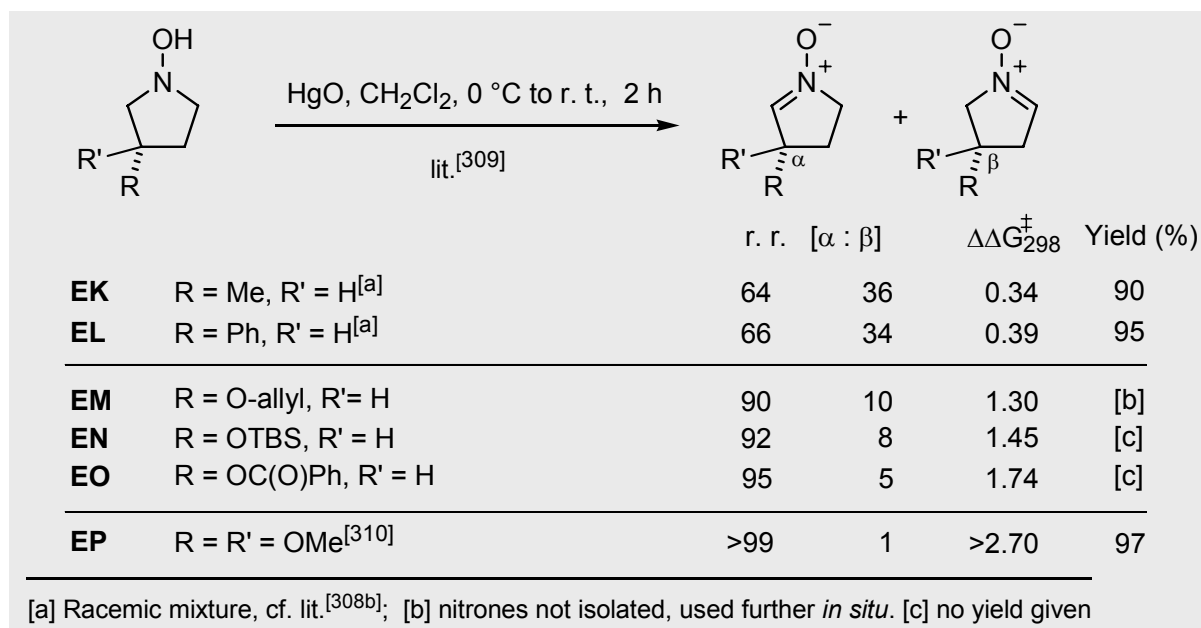


Scheme 36: Iodine oxidation of iminoglucitol **EI** undergoing Zaitsev elimination to yield **EJ**<sup>[99]</sup>

Although Pothier was presumably fully aware that these conditions are typical for a Zaitsev, E2 elimination (cf. March, Chapter 17<sup>[240]</sup>) there may be other conditions to favour the Hoffmann product (i.e. the aldo-nitrone) predominately. Further investigation of the reaction parameters (steric/electronic properties of the nucleofuge, base strength, size, etc.) would be of considerable interest.

#### 4.2.2 Oxidation of *N*-hydroxypyrrolidines. Electronic effects and mechanism

Several Italian groups including those led by Goti and Brandi,<sup>[308b,309]</sup> looked at the synthesis of pyrrole-1-oxides with substituents at the 3-position (with respect to starting hydroxylamine). In all cases, the oxidation with mercury(II) oxide afforded the  $\alpha$ -nitrone as the main product, where the C—4 substituent is vicinally situated to the newly created C=N double bond (Scheme 37). The minor product is termed consequently as the  $\beta$ -nitrone.

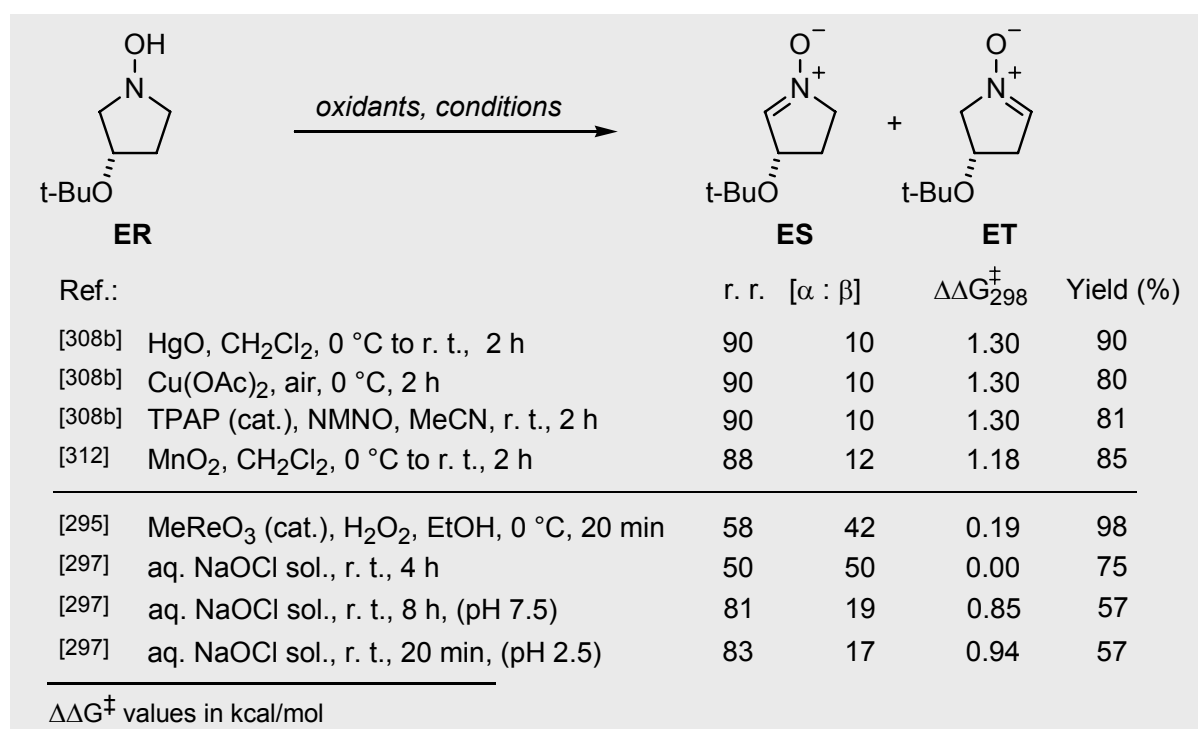


Scheme 37: The 3-substituent influence on the regioselective outcome of oxidation<sup>[308b,309,310]</sup>

Again, for a semi-quantitative explanation of the regioselection, a useful barometer is the free energy difference  $\Delta\Delta G^\ddagger$  (i.e.  $|\Delta G_{\alpha}^\ddagger - \Delta G_{\beta}^\ddagger|$ ) of the isomeric nitrone products. In terms of the regioselectivities listed in Scheme 37, hydroxylamines **EK** to **EP** can be split into three groups: The introduction of an O-substituent at C—3 in the hydroxylamines **EM**, **EN** and **EO** (O-allyl, O-silyl ether, O-benzoyl, resp.) led to an increase in the selectivity towards the formation of their respective  $\alpha$ -nitrones by ca. 1.0 to 1.3 kcal/mol over hydroxylamines **EK**

and **EL** which feature only alkyl or aryl substituents at C—3. For the *gem*-dimethoxy hydroxylamine **EP**, reported by Tufariello et al.<sup>[310]</sup>, the  $\Delta\Delta G^\ddagger$  difference opened up further by the same margin (i.e. ca. 1.0 to 1.4 kcal/mol) in favour of the  $\alpha$ -nitron. This was a direct consequence of the second alkoxy functionality at C—3. Interestingly, these results imply a degree of additivity in  $\Delta\Delta G^\ddagger$  values with regard to the alkoxy moiety which, in this series at least, equates to approx. 1.0 kcal/mol gain in regioselectivity per alkoxy unit present.

The oxidation of the malic acid-derived 3-*O-tert*-butyl-*N*-hydroxypyrrolidine **ER** illustrates a rare occurrence, namely that the experiment conditions can influence the regioselectivity of the reaction (Scheme 38). While the oxidation with the mercury(II), copper(II), TPAP and manganese(IV) reagents produced near-identical regioselectivities, a dramatic drop in selectivity was observed for the oxidation of 3-alkoxyhydroxylamine **ER** with the rhenium and sodium hypochlorite (bleach, at basic pH) reagents.



Scheme 38: Influence of the reagent on the regioselective outcome of oxidation

The question that arises is this: is there a common mechanism for oxidation? Since they produce similar selectivities, the first four reagents in Scheme 38 according to Goti, Brandi and co-workers<sup>[251,303,308,309,312,313]</sup> share a common oxidation mechanism. In Diagram 38 below, a graphical representation of Goti, Brandi and co-workers' proposed oxidation mechanism is shown. Though the intermediary nitrosonium cation is reasonable (step-wise loss of two electrons, *via* N—O radical intermediate), the mechanism or species responsible

for the extraction of the proton attached to the neighbouring carbon is less clear. The exact mechanism of this step is open to debate. Goti et al.<sup>[297]</sup> argues that the different selectivities from the rhenium and bleach reagents for the oxidation of **ER**, compared to the others, is evidence that a different mechanism operates. The loss of regioselectivity with the bleach reagent at basic pH is interesting, since the “electronic induction” of the alkoxy substituent (ca. 1.0 kcal/mol, cf. Scheme 37) is not felt. Further, as the pH of the bleach solution became acidic (through addition of a 0.5 M solution of KHSO<sub>4</sub>), selectivity for **ES** increased and generally shorter reaction times were observed. Goti attributed this to the higher reduction potentials of HClO ( $E^\circ = 1.63$  V) and Cl<sub>2</sub> ( $E^\circ = 1.36$  V), i.e. the actual oxidants at acidic pH values, compared to the hyperchlorite anion, ClO<sup>-</sup> ( $E^\circ = 0.89$  V), in basic medium. It would be interesting to just bubble chlorine gas into the solution to see if a similar result is obtained.

In contrast, the reduction potentials for Hg<sub>2</sub><sup>2+</sup>/2Hg and MnO<sub>2</sub>/Mn<sup>2+</sup> are  $E^\circ = 0.80$  and 1.23 V, respectively. Between the bleach and manganese reagents, only a very small difference in regioselectivity is observed – an indication that a similar mechanism is operative? A word of caution with regard to manganese dioxide: The performance of the reagent is linked intrinsically to its method of preparation, since this influences directly the oxygen stoichiometry of the resulting oxide. Several methods for the preparation<sup>[318,319,320,321,322]</sup> of “activated manganese dioxide” and standardization<sup>[319]</sup> have been reported. It seems that for the bleach reagent at basic pH, the reaction is maybe the subject of a genuine competition between kinetic and thermodynamic product formation. In comparison, the oxidation with HgO and MnO<sub>2</sub>, the product of kinetic control is also the product of thermodynamic control.

The mechanism referred to above that involves a nitrosonium cation, initial breakage of the more polarisable O—H bond and loss of two electrons was suggested by Goti and co-workers.<sup>[308b]</sup> The mechanism also attempts to account for the high regioselectivity of the mercury(II) oxide oxidation of the 3-alkoxy-substituted *N*-hydroxypyrrolidines, i.e. such as **EM** to **EO** and **ER**, featured above, as follows to paraphrase Goti:

*...an electronegative substituent on C—3 favours the C—H bond cleavage by stabilising the incipient negative charge. More specifically, as Goti goes on to describe, dehydrogenation [...] with HgO arises from a kinetic preference for the cleavage of the C—H bond anti to the tert-butoxy group (i.e. the alkoxy substituent at C—3), caused by a possible  $\sigma_{C-H} \rightarrow \sigma_{C-O}^*$  interaction that polarises specifically the anti C—H bond  $\alpha$  to nitrogen...*



In other words, the developing negative charge at the  $\alpha$ -carbon can be stabilised through hyperconjugation with the neighbouring, empty  $\sigma^*_{C-O}$  orbital. The presence of *anti-periplanar* disposition between the C—H and C—O bonds is then the deciding factor (Diagram 38).

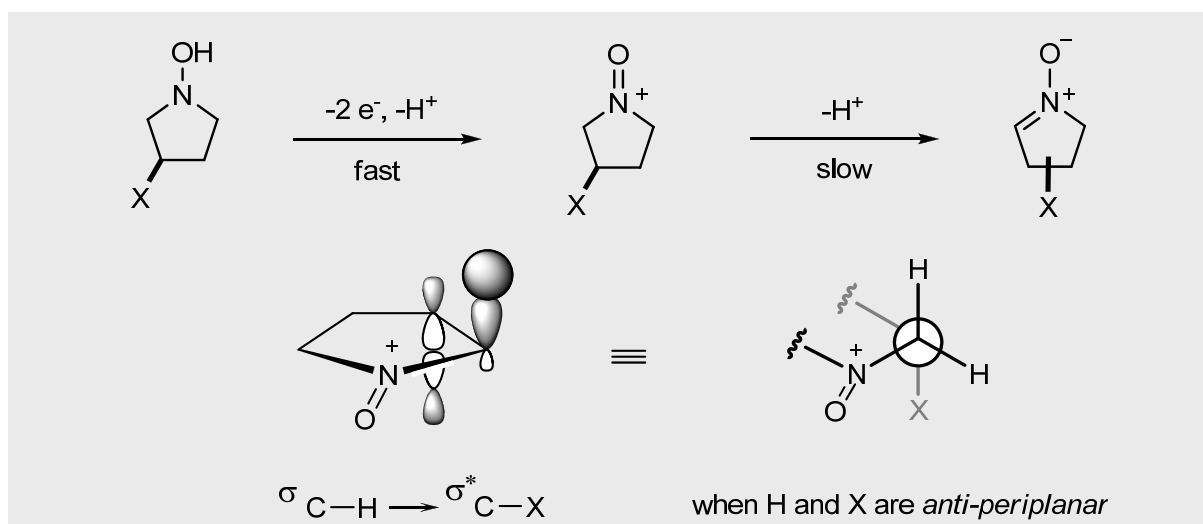


Diagram 38: A suggested mechanism for the oxidation of *N*-hydroxypyrrolidines with electron withdrawing vicinal substituents (to the C—H bond broken), adopted from Goti et al.<sup>[313]</sup>

The electronic “induction” is augmented when a second vicinal alkoxy substituent is present. This was seen for Tufariello’s *gem*-dialkoxy derivative **EP**, shown in Scheme 37. As alluded to in Diagram 39, an “exocyclic” alkoxy group<sup>[303]</sup> may have the same effect (i.e. 2<sup>nd</sup> structure, left to right). Another mode is a combination with a second alkoxy substituent at the  $\beta$ -position to the ring nitrogen (4<sup>th</sup> structure). We have mentioned that the substituents labelled as “X” are mostly of the “alkoxy” type. However, at the exocyclic position, “X” is more commonly a cyano<sup>[303]</sup>, amide or ester group<sup>[294b]</sup> or halogen substituent (cf. next section).

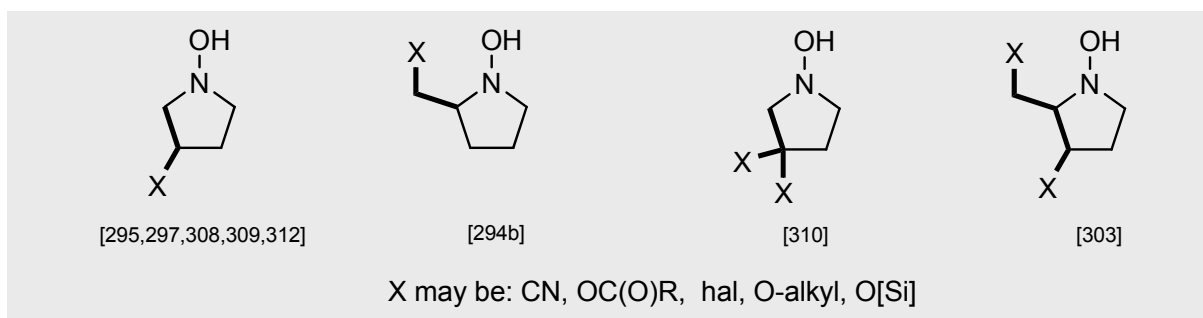


Diagram 39: Substitution modes for pyrrolidine systems where good regioselectivity has been reported due to the electronic effect of the vicinal substituents.

Nonetheless, with more complex polysubstituted *N*-hydroxypyrrolidines, the likelihood of acquiring an optimal *anti-periplanar* arrangement is, as always, at the mercy of the conformational flux of the pyrrolidine ring. Though certainly of considerable interest, this aspect will not be discussed here further.

## 4.3 Own Results

### 4.3.1 General notes

To avoid endless repetition later on, a few points are worthy of mention here. All oxidations carried out with mercury(II) oxide (yellow) were done using 3.0 equivalents of reagent, common to the procedure of Palmer and Jäger,<sup>[4a]</sup> and several other literature precedents.<sup>[308,309]</sup> Manganese(IV) oxide oxidations were accomplished using 1.3 equivalents of the “oxidation active” substance of 90 % purity procured from Fluka, the same as that employed by Goti and co-workers.<sup>[312]</sup>

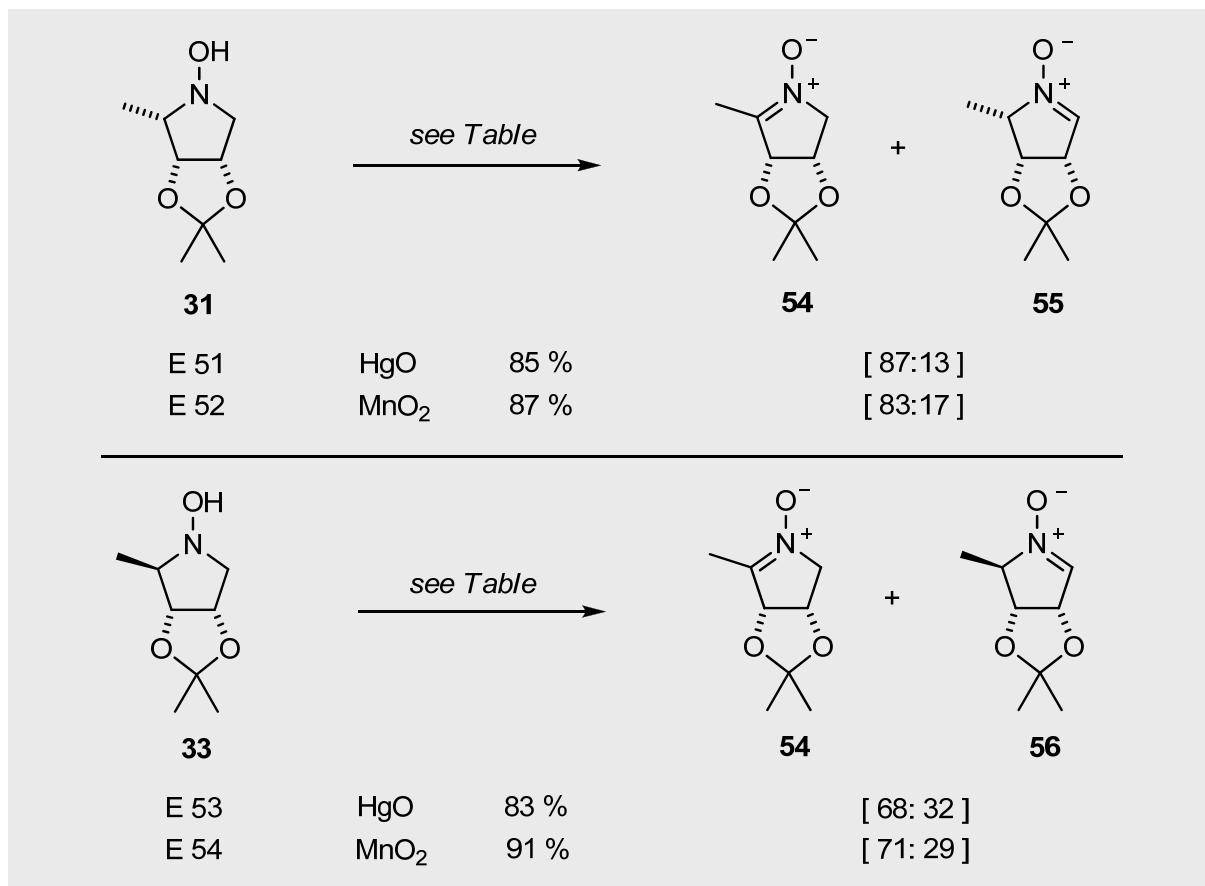
### 4.3.2 Oxidation of 2-methyl *N*-hydroxypyrrolidines **31** and **33**

Consider first the substrates with *cis* and *trans* substituents at C—2/C—3 and the influence of this on the oxidation regioselectivity. We are looking therefore at the reagent’s ability to extract a proton in two distinct steric environments:

The oxidation of the *cis*-*L*-*lyxo*-configured pyrrolidine **31** with HgO or MnO<sub>2</sub> furnished the cyclic nitrones **54** and **55** in 85-87 % yield (i.e. E 51, E 52). The oxidants gave near-identical selectivities. This compares well to results obtained from experiments using these reagents reported by Goti and co-workers<sup>[308b,312]</sup> (cf. Scheme 38).

The oxidation of the *trans*-*D*-*ribo*-configured pyrrolidine **33** provided the cyclic nitrones **54** and **56** in 83 to 91 % yield. The oxidation selectivities for HgO and MnO<sub>2</sub> were again very similar, though lower than those resulting from the oxidation of the *cis*-*L*-*lyxo*-pyrrolidine **31**. The oxidation with HgO gave **54** and **56** with a r. r. of 68:32 (cf. Palmer:<sup>[4a]</sup> **54**:**56** = 68:32,  $\Sigma$  = 75 %). As also seen in the literature,<sup>[308b,312]</sup> the oxidation of all substrates with MnO<sub>2</sub> was approximately an order of magnitude quicker than with HgO.

**Table 8:** The *cis/trans* oxidation of 2-methyl *N*-hydroxypyrrolidines, L-lyxo **31** and D-ribo **33**, to obtain keto-nitron **54** and aldo-nitrones **55** and **56**; mercury(II) oxide (HgO, yellow, Fluka, 99 %; 3 Eq., CH<sub>2</sub>Cl<sub>2</sub>, 7-8 h, r. t.); manganese(IV) oxide (MnO<sub>2</sub>, Fluka, techn. 90 %; 'oxidation active', 1.3 Eq., CH<sub>2</sub>Cl<sub>2</sub>, 30 min to 1 h, 0 °C to r. t.).



Exp.	Educt	Oxidant	Time [h]	Product r. r.	Product r. r.			Yield [%] <sup>[d]</sup>
					HPLC <sup>[a]</sup>	<sup>13</sup> C NMR <sup>[b]</sup>	$\Delta\Delta G_{298}^{\ddagger}$ <sup>[c]</sup>	
E 51	<b>31</b>	HgO	8	<b>54</b> : <b>55</b>	[79 : 21]	[87 : 13]	1.13	73 ( <b>54</b> ); 12 ( <b>55</b> )
E 52	<b>31</b>	MnO <sub>2</sub>	0.5		[78 : 22]	[83 : 17]	0.94	75 ( <b>54</b> ); 12 ( <b>55</b> )
<hr/>								
E 53	<b>33</b>	HgO	7	<b>54</b> : <b>56</b>	[67 : 33]	[68 : 32]	0.45	54 ( <b>54</b> ); 29 ( <b>56</b> )
E 54	<b>33</b>	MnO <sub>2</sub>	1		[71 : 29]	[71 : 29]	0.53	71 ( <b>54</b> ); 20 ( <b>56</b> )

[a] Determined by peak integration of the regioisomeric mixture at  $\lambda_{\max} = 242$  nm (solvent: CH<sub>2</sub>Cl<sub>2</sub>/MeOH = 95:5) from the crude product; [b] Measured from the isopropylidene methyl signal pairs intensities (i.e. [C(CH<sub>3</sub>)<sub>2</sub>]); [c] Refers to <sup>13</sup>C NMR ratio, in kcal/mol; [d] After celite filtration and separation by MPLC purification.

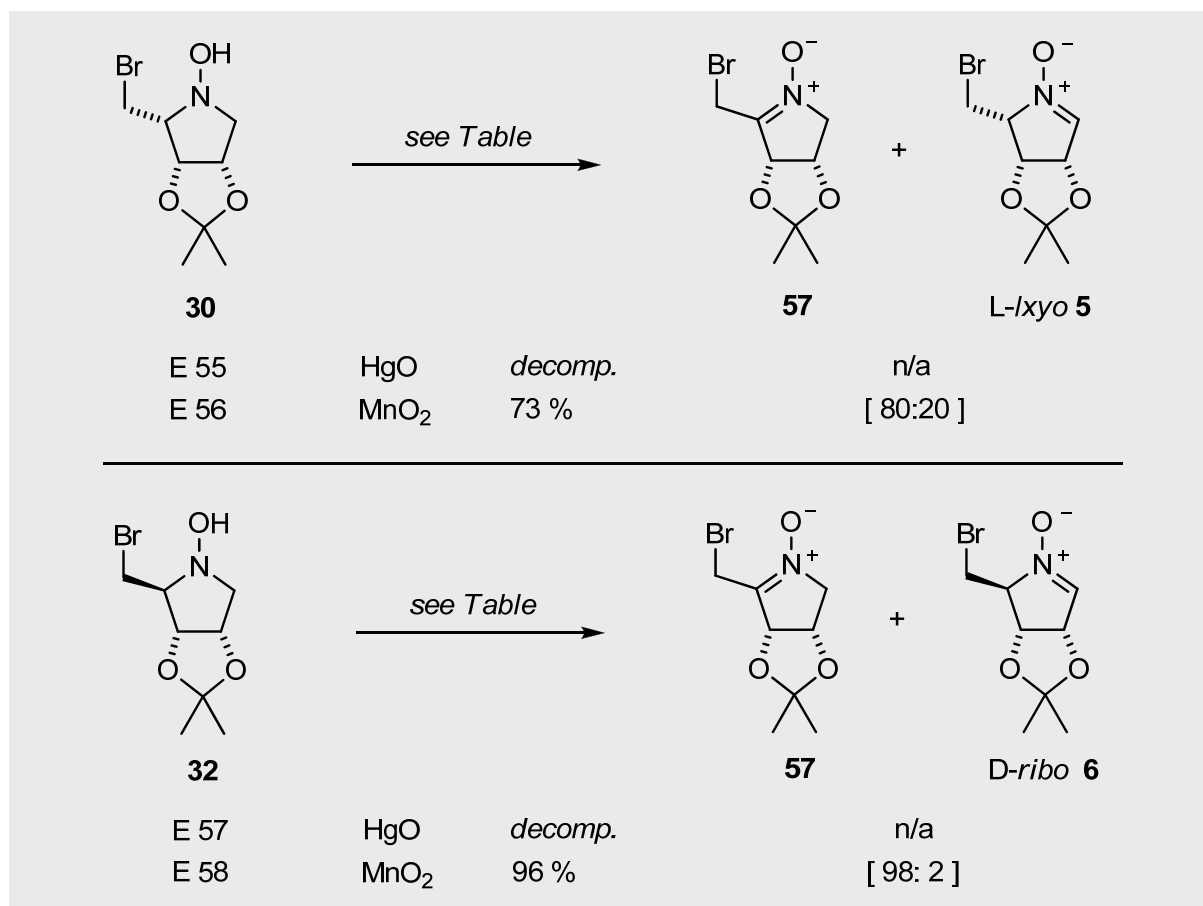
From the regioselectivities tabulated above, it can be suggested that the 2—H proton in *trans*-D-*ribo* **33** is slightly more difficult to extract than the 2—H in *cis*-L-*lyxo* **31**. This “steric hindernace” is, if any, a negligible factor, worth at most ca. 0.5 kcal/mol in terms of the lower barrier presented to the abstraction of the less-hindered 2—H in the *cis*-L-*lyxo* pyrrolidine **31**. The value of 0.5 kcal/mol is arrived at by first averaging the  $\Delta\Delta G^\ddagger$  values of the HgO and MnO<sub>2</sub> oxidations for L-*lyxo* **31** and D-*ribo* **33** (i.e. 1.03 and 0.50 kcal/mol), and then subtracting them. For the *cis*-L-*lyxo* **31**, there are the stabilising effects of the oxygen substituents at C—3 and C—4, i.e. on the incipient negative charge that develops during the abstraction of their *anti*-protons on C—2 and C—5, which cancel each other out (more on this in Section 4.2.2, cf. regioselectivities in Section 38).

The nitrones **54-56** displayed the expected NMR absorptions. For example, the azomethine carbon in the aldo-nitrones **55** and **56** resonated at  $\delta$  131 ppm; for keto-nitrone **54**, the corresponding signal absorbed down-field at  $\delta$  142.8 ppm. The aldo- and keto-nitrones could also be distinguished by IR; for the aldo-nitrones **55** and **56**, a C=N stretch could be found at ca.  $\tilde{\nu} = 1573 \text{ cm}^{-1}$ , while with the keto-nitrone **54**, this stretching mode was observed at  $\tilde{\nu} = 1604 \text{ cm}^{-1}$ . This spread of signal differences for “aldo” compared to keto-nitrones is in good agreement to the data published by Döpp<sup>[123]</sup> and Delpierre.<sup>[242]</sup>

### 4.3.3 Influence of bromine substituent. Oxidation of 2-bromomethyl *N*-hydroxypyrrolidines **30** and **32**

The next subset of pyrrolidines contains the bromomethyl moiety so that the effect of an electron-withdrawing substituent can be investigated (Table 9). Unfortunately, employing the same oxidation protocols as above led to isolation problems in the case of HgO as oxidant. The extended reaction times required for the oxidation of the L-*lyxo*- and D-*ribo*-configured substrates, **30** and **32**, respectively, resulted in intractable mixtures and considerable decomposition. This precluded the measurement of r. r. from <sup>13</sup>C NMR (i.e. E 55, 57). On the other hand, the oxidation using MnO<sub>2</sub> proceeded much quicker: The L-*lyxo*-configured substrate **30** afforded the new bromo-ketonitrone **57** in a moderate yield of 62 % along with 11 % of the original L-*lyxo*-nitrone **5** (r. r. **57**:**5** = 80:20; E 56). Surprisingly, in contrast, the D-*ribo* derivative **32** underwent oxidation with MnO<sub>2</sub> in near-perfect regiocontrol to afford the bromo-ketonitrone **57** in a yield of 96 %; only traces of the other regioisomer, the D-*ribo*-nitrone **6**, could be detected by HPLC and <sup>13</sup>C NMR. To avoid decomposition, the bromo-ketonitrone **57** should be stored in the freezer when not required.

**Table 9:** Influence of the bromine substituent on the regioselectivity of oxidation; synthesis of bromo-ketonitrone **57** and *L*-lyxo and *D*-ribo nitrones, **5** & **6**; mercury(II) oxide (HgO, yellow, Fluka, 99 %; 3 Eq., CH<sub>2</sub>Cl<sub>2</sub>, 6-18 h, r. t.); manganese(IV) oxide (MnO<sub>2</sub>, Fluka, techn. 90 %; 'oxidation active', 1.3 Eq., CH<sub>2</sub>Cl<sub>2</sub>, 20 min to 1 h, 0 °C to r. t.).



Exp.	Educt	Oxidant	Time	Product r. r.	Product			Yield
					HPLC	<sup>13</sup> C NMR <sup>[a]</sup>	$\Delta\Delta G_{298}^{\ddagger}$ <sup>[b]</sup>	
E 55	<b>30</b>	HgO	16	<b>57</b> : <b>5</b>	n/d	— <sup>[d]</sup>	n/a	n/a
E 56	<b>30</b>	MnO <sub>2</sub>	0.5		n/d	[80 : 20]	0.80	62 ( <b>57</b> ); 11 ( <b>5</b> )
E 57	<b>32</b>	HgO	20	<b>57</b> : <b>6</b>	n/d	— <sup>[d]</sup>	n/a	n/a
E 58	<b>32</b>	MnO <sub>2</sub>	0.5		[97 : 3] <sup>[e]</sup>	[98 : 2]	2.30	96 ( <b>57</b> )

[a] Measured from the intensities of the isopropylidene methyl signal pairs [i.e. C(CH<sub>3</sub>)<sub>2</sub>]; [b] Refers to <sup>13</sup>C NMR ratio, in kcal/mol; [c] After Celite filtration and separation by MPLC purification. [d] Due to decomposition, the spectrum could not be integrated. [e] Given as a guideline only since the  $\lambda_{\max}$  values for **57** and **6** differed substantially (262 nm and 240 nm, respectively; PE/EE = 85:15) for the crude products. n/d = not determined, n/a = not applicable.

Incidentally, this time it was not possible to measure the r. r. by integration of the nitron products by HPLC. The inclusion of the bromine substituent makes the UV spectra of the keto-nitrone no longer comparable to that of the aldo-nitrone: for the *L*-lyxo/*D*-ribo-nitrones **5** and **6**  $\lambda_{\max} = 240$  nm, whereas for bromo-ketonitrone **57**  $\lambda_{\max} = 262$  nm. In other words, the bromine appendage results in a significant bathochromic shift (“redshift”, i. e. shift to longer wavelength) for the  $n \rightarrow \pi^*$  transition of the C=N chromophore (note: the 2-methyl substituent by itself had only a negligible effect, cf. Zeeh,<sup>[220]</sup> Jaffé and Orchin<sup>[323]</sup>).

According to the discussion in the last section, the oxidation of the *cis* *L*-lyxo-configured bromomethyl pyrrolidine **30**, should be *slightly* more regioselective than that of the *trans* *D*-ribo diastereoisomer **32**, on the grounds of 2—H in the *cis*-configured substrate being less sterically hindered. However, the opposite is true and, furthermore, a large gap has opened up between the  $\Delta\Delta G^\ddagger$  values for the  $\text{MnO}_2$  oxidation of the two diastereoisomers (cf. E 56 and E 58; r. r. 80:20 and 98:2, or 0.80 against 2.30 kcal/mol). This suggests that the barrier to the abstraction of the 2—H proton in the *trans* *D*-ribo **32** is, in relative terms, ca. 1.50 kcal/mol lower than in *cis*-*L*-lyxo **30**. From this, it is obvious that the observed regioselectivity is rather linked to the electronic effects arising from the disposition of the bromine atom with respect to the neighbouring 2—H proton (Diagram 40).

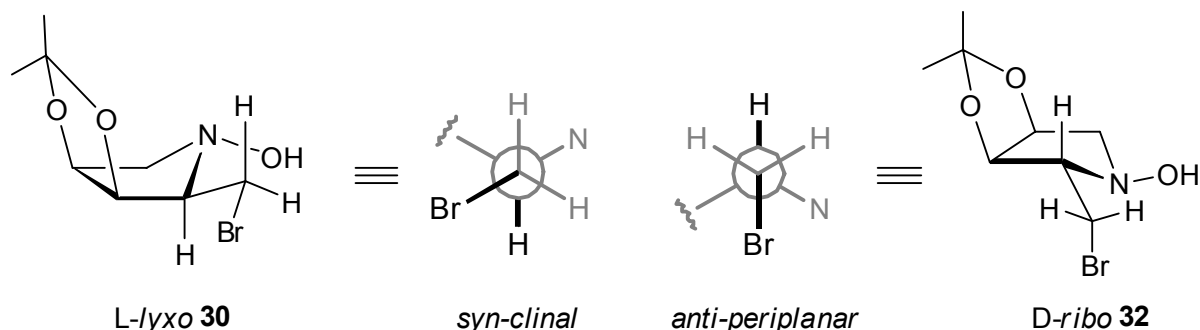


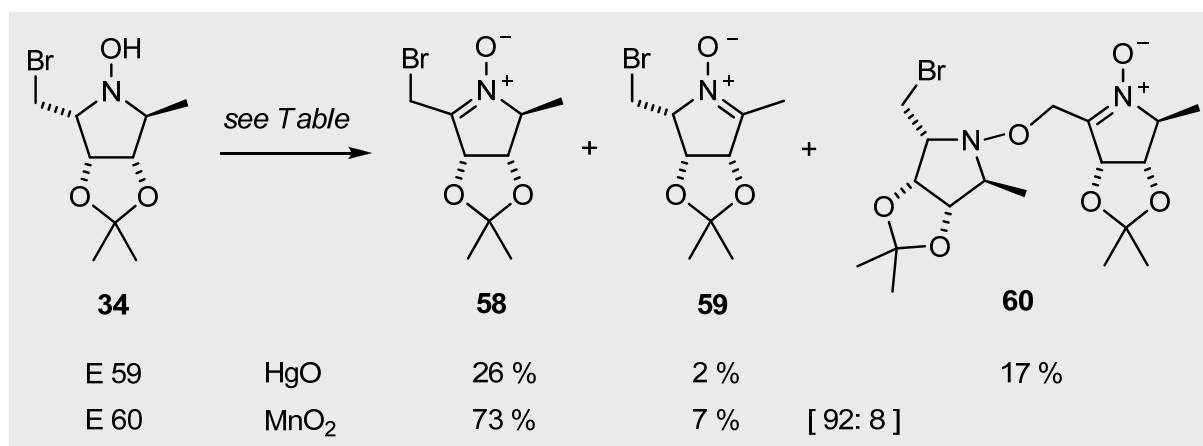
Diagram 40: Disposition of the bromomethyl group in oxidation substrates **30** and **32**

In Sections 2.2.1.4 and 3.2.2.1, the orientation of the bromomethyl substituent was determined to be *syn-clinal* to 2—H in *L*-lyxo **30**. For *D*-ribo **32**, bromine stands *anti-periplanar* to 2—H. Thus, the *D*-ribo substrate can invoke the  $\sigma_{\text{C-H}} \rightarrow \sigma_{\text{C-Br}}^*$  interactions in order to favour the cleavage of the *anti* C—H bond at C—2 (cf. Diagram 38).<sup>[303,308b,313]</sup> This explains the very high regioselectivity found in the experiment E 58 (Table 9). For the oxidation of the *L*-lyxo compound **30** (E 56, Table 9), with a *syn-clinal* orientation of bromine, no “hyperconjugative” interactions are possible. Indeed, in this case, it seems that the effect of the bromine atom is made redundant all together: the identical regioselectivity for the oxidation of the 2-methyl derivative, *L*-lyxo **31** (E 52, Table 8), supports this.

#### 4.3.4 *Cis* or *trans* proton abstraction? Oxidation of 2,5-disubstituted *N*-hydroxypyrrolidines **34** and **68**

The oxidation regioselectivity arising from substrate **34** provided some interesting observations. The protracted oxidation time (overnight) using HgO did still, surprisingly, allow for product isolation (cf. oxidation of **30** or **32**). The onset of decomposition was evident (i.e. darkening of reaction mixture and isolated products), although less rapid than in the unsubstituted bromoketonitrone **57**. Following MPLC purification, 26 % of the bromoketonitrone **58** and 2 % of the methyl-ketonitrone **59** could be isolated, along with 17 % of the “dimeric” hydroxylamine **60**, which had formed through bromine substitution by the hydroxylamine of the starting material. In comparison, the oxidation with MnO<sub>2</sub> proceeded smoothly in an r. r. of 92:8 favouring the bromoketonitrone **58** in a combined yield 80 % (Table 10).

**Table 10:** Oxidation of 2-bromomethyl-5-methyl-*N*-hydroxypyrrolidine **34** and competing bromine substitution. Reagents and conditions: HgO (yellow, Fluka, 99 %; 3 Eq., CH<sub>2</sub>Cl<sub>2</sub>, 4-16 h, r. t.); MnO<sub>2</sub> (Fluka, techn. 90 %; ‘oxidation active’, 1.3 Eq., CH<sub>2</sub>Cl<sub>2</sub>, 30 min, 0 °C to r. t.).



Exp.	Educt	Oxidant	Time [h]	Product r. r.	r. r.			Yield [%] <sup>[d]</sup>
					HPLC <sup>[a]</sup>	<sup>13</sup> C NMR <sup>[b]</sup>	$\Delta\Delta G_{298}^{\ddagger}$ <sup>[c]</sup>	
E 59	<b>34</b>	HgO	16	<b>58</b> : <b>59</b>	n/d	n/d	n/a	26 ( <b>58</b> ); 2 ( <b>59</b> )
E 60	<b>34</b>	MnO <sub>2</sub>	0.5		n/d	[92 : 8]	1.45	73 ( <b>58</b> ); 7 ( <b>59</b> )

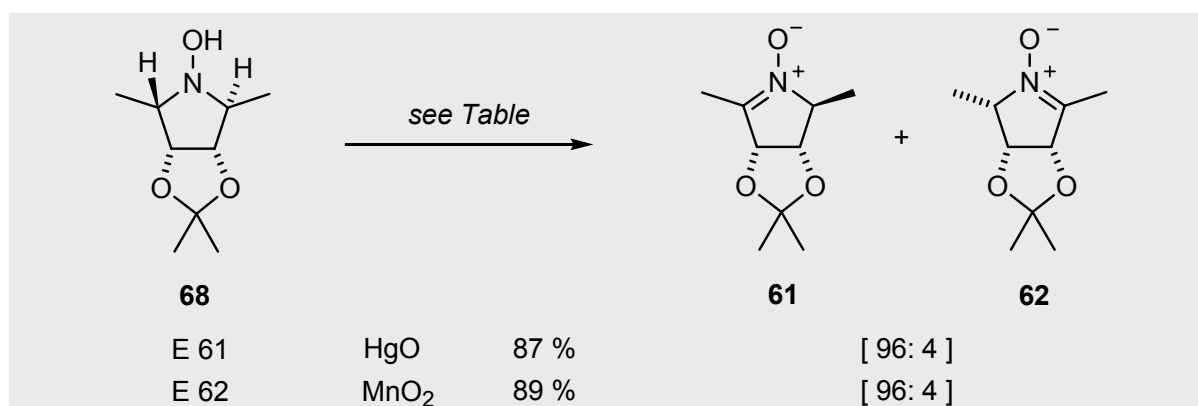
[a] The r. r. for **58** and **59** could not be determined by HPLC, since their UV spectra differed significantly – see discussion in previous section; [b] Measured from the isopropylidene methyl signal pairs intensities (i.e. [C(CH<sub>3</sub>)<sub>2</sub>]); [c] Refers to <sup>13</sup>C NMR ratio, in kcal/mol; [d] After celite filtration; MPLC purification. n/d = not determined; n/a = not applicable.

From the MS analysis (ESI, positive ion) of compound **60**, two dominant fragments resulting from demethylation (i.e.  $m/z = 435$   $[-CH_3]^+$ , 8 %) and loss of the hydroxylamine moiety after N-O bond cleavage (i.e.  $m/z = 264$   $[-C_8H_{13}NO_3]^+$ , 100 %) were observed. Nitrones **58** and **59** were easily distinguishable by their IR spectra depending upon the relative position of the C=N stretches, either side of the  $1600\text{ cm}^{-1}$  boundary: for the bromo-ketonitrone **58**  $\tilde{\nu} = 1571\text{ cm}^{-1}$ , whilst for methyl-ketonitrone **59**  $\tilde{\nu} = 1601\text{ cm}^{-1}$  was found (cf. nitrone **54**).<sup>[123,242]</sup>

The  $\Delta\Delta G^\ddagger$  value of 1.45 kcal/mol (i.e. E 60) fits nicely to the  $\Delta\Delta G^\ddagger$  scheme for the oxidations of mono-substituted bromomethyl-*N*-hydroxypyrrolidines. The higher oxidation selectivity in the oxidation of  $\alpha$ -L-lyxo **34** (E 60), for example, in comparison to the result (E 56) with substrate **30**, can be rationalised as the net effect of replacing the *anti* C—H bond (wrt. to C—3 alkoxy) with the 5-(*S*)-methyl substituent. The bromine atom, when orientated *syn-clinal* to 2—H in  $\alpha$ -L-lyxo **34**, does not aid the abstraction of 2—H (if it did, we should expect an even higher r. r. of at least 98:2, or  $\Delta\Delta G^\ddagger = 2.30$  kcal/mol; cf. E 58 in Table 9).

Turning to 2,5-dimethyl *N*-hydroxypyrrolidine **68** (formation and numbering from Section 5.1.1), the oxidation favoured the near-exclusive abstraction of the proton less hindered by the *cis*-standing methyl and isopropylidene substituents (Table 11).

**Table 11:** The question of *cis/trans* proton extraction in the oxidation of 2,5-dimethyl *N*-hydroxypyrrolidine **68**. Reagents and conditions: see preceding table.



Exp.	Educt	Oxidant	Time [h]	Product r. r.	Product		Yield
					HPLC <sup>[a]</sup>	<sup>13</sup> C NMR <sup>[b]</sup>	
E 61	<b>68</b>	HgO	4	<b>61</b> : <b>62</b>	[92 : 8]	[96 : 4]	83 ( <b>61</b> ); 4 ( <b>62</b> )
E 62	<b>68</b>	MnO <sub>2</sub>	0.5		[94 : 6]	[96 : 4]	84 ( <b>61</b> ); 5 ( <b>62</b> )

[a] Intergration at  $\lambda_{\text{max}} = 241\text{ nm}$  ( $\text{CH}_2\text{Cl}_2/\text{MeOH} = 94:6$ ). [b] From the isopropylidene methyl signal pairs intensities; [c] In kcal/mol; [d] After celite filtration; MPLC purification.